TECHNICAL REPORT S-75-11

PAVEMENT RESPONSE TO AIRCRAFT DYNAMIC LOADS

Volume II

PRESENTATION AND ANALYSIS OF DATA

by

Richard H. Ledbetter

Soils and Pavements Laboratory
U. S. Army Engineer Waterways Experiment Station
P. O. Box 631, Vicksburg, Miss. 39180

September 1975

Final Report

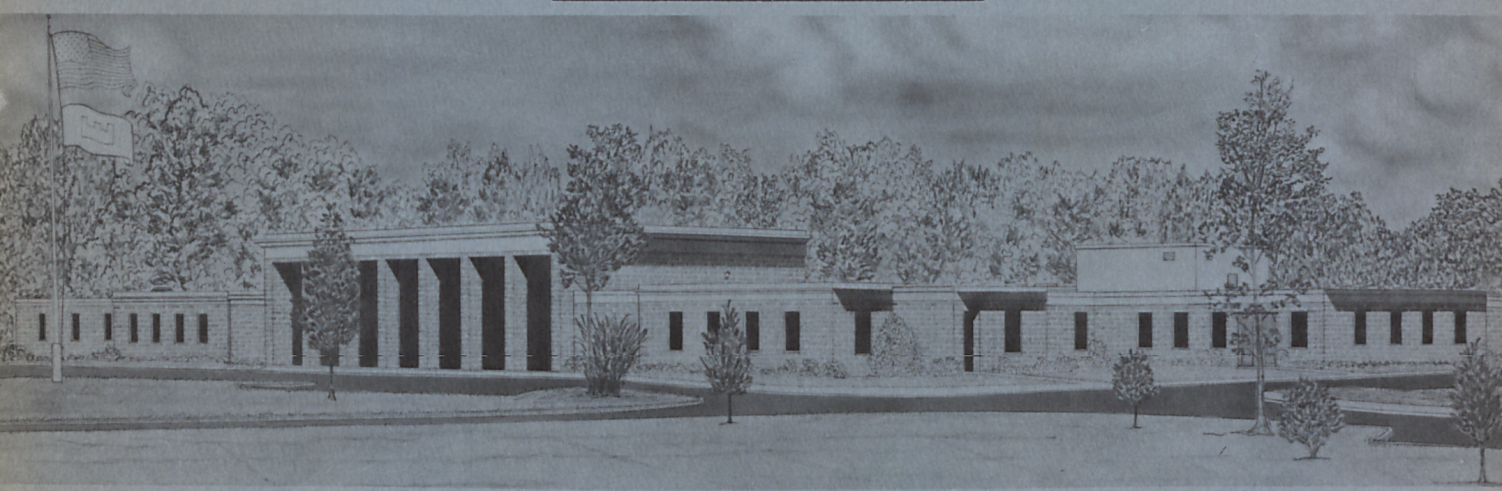

Prepared for U. S. Department of Transportation
Federal Aviation Administration
Systems Research and Development Service
Washington, D. C. 20591

Under Inter-Agency Agreement DOT FA71WA1-218

Unclassified

SECURITY CLASSIFICATION OF THIS PAGE *(When Data Entered)*

REPORT DOCUMENTATION PAGE

READ INSTRUCTIONS BEFORE COMPLETING FORM

1. REPORT NUMBER: Technical Report S-75-11	2. GOVT ACCESSION NO.
3. RECIPIENT'S CATALOG NUMBER	
4. TITLE *(and Subtitle)*: PAVEMENT RESPONSE TO AIRCRAFT DYNAMIC LOADS; Volume II: PRESENTATION AND ANALYSIS OF DATA	5. TYPE OF REPORT & PERIOD COVERED: Final Report
	6. PERFORMING ORG. REPORT NUMBER
7. AUTHOR(s): Richard H. Ledbetter	8. CONTRACT OR GRANT NUMBER(s): DOT FA71WAI-218
9. PERFORMING ORGANIZATION NAME AND ADDRESS: U. S. Army Engineer Waterways Experiment Station, Soils and Pavements Laboratory, P. O. Box 631, Vicksburg, Miss. 39180	10. PROGRAM ELEMENT, PROJECT, TASK AREA & WORK UNIT NUMBERS
11. CONTROLLING OFFICE NAME AND ADDRESS: Federal Aviation Administration, Systems Research and Development Service, Washington, D. C. 20591	12. REPORT DATE: September 1975
	13. NUMBER OF PAGES: 204
14. MONITORING AGENCY NAME & ADDRESS *(If different from Controlling Office)*	15. SECURITY CLASS. *(of this report)*: Unclassified
	15a. DECLASSIFICATION/DOWNGRADING SCHEDULE

16. DISTRIBUTION STATEMENT *(of this Report)*

Approved for public release; distribution unlimited.

17. DISTRIBUTION STATEMENT *(of the abstract entered in Block 20, if different from Report)*

18. SUPPLEMENTARY NOTES

Designated Report No. FAA-RD-74-39-II by Federal Aviation Administration, Washington, D. C.

19. KEY WORDS *(Continue on reverse side if necessary and identify by block number)*

Aircraft dynamic loads
Elastic behavior
Flexible pavement response
Inelastic behavior
Rigid pavement response

20. ABSTRACT *(Continue on reverse side if necessary and identify by block number)*

Instrumented aircraft were used to apply static and dynamic loads to instrumented pavement structures (both flexible and rigid) at the National Aviation Facilities Experimental Center (NAFEC), Atlantic City, N. J. Volume I of this report describes the testing program and instrumentation systems. This volume and Appendixes A and B present the reduction and analysis of data and the test results. Volume III contains a compendium of the entire study.

Measurements of relative displacement, velocity, pressure, and temperatures

(Continued)

DD FORM 1 JAN 73 1473 EDITION OF 1 NOV 65 IS OBSOLETE

Unclassified

SECURITY CLASSIFICATION OF THIS PAGE *(When Data Entered)*

20. ABSTRACT (Continued).

were made in the two pavement structures. Two phases of material behavior (elastic and inelastic) in both flexible and rigid pavement structures were identified. Each phase had to be treated independently for a full analysis of the static and dynamic load test results.

The tests at NAFEC showed that no basic aircraft ground operating mode induced pavement responses (elastic plus inelastic) greater than those occurring for static loading conditions. However, the test results indicate that for stiff pavement structures, such as the rigid pavement and the flexible pavement during cold weather, unusual conditions (pavement conditions rougher than those during testing at NAFEC) of dynamic loading could possibly cause responses larger than what would occur under static loading. This behavior is possible because of the inelastic behavior being of low magnitude for the stiff pavements. The test results also indicate that a reduction in the thickness of pavement structures could be allowed in the interior of the runways except at exits where aircraft side thrust is high.

THE CONTENTS OF THIS REPORT ARE NOT TO BE USED FOR ADVERTISING, PUBLICATION, OR PROMOTIONAL PURPOSES. CITATION OF TRADE NAMES DOES NOT CONSTITUTE AN OFFICIAL ENDORSEMENT OR APPROVAL OF THE USE OF SUCH COMMERCIAL PRODUCTS.

PREFACE

This project was conducted by the Soils and Pavements Laboratory (S&PL), U. S. Army Engineer Waterways Experiment Station (WES), for the Federal Aviation Administration under Inter-Agency Agreement DOT FA71WAI-218 during the period May 1971-January 1975.

The project was conducted under the general supervision of Mr. James P. Sale, Chief of the S&PL, WES. Results of the study are included in the following volumes of the report entitled "Pavement Response to Aircraft Dynamic Loads":

a. Volume I. "Instrumentation Systems and Testing Program."

b. Volume II and Appendixes A and B. "Presentation and Analysis of Data."

c. Volume III. "Compendium."

This volume (Volume II) of the report was prepared by Mr. Richard H. Ledbetter.

Because of the uniqueness of this study, WES requested and received assistance in the design of the experiment from the following consultants: Professor R. E. Fadum, North Carolina State University; Professor W. R. Hudson, University of Texas; Dr. Willard J. Turnbull, Consultant, Vicksburg, Mississippi; Professor C. L. Monismith, University of California; Professor M. E. Harr, Purdue University; Professor W. H. Goetz, Purdue University; Professor A. S. Vesic, Duke University; Professor R. K. Watkins, University of Utah; Professor K. B. Woods, Purdue University.

A concept for reduction and analysis of instrumentation data somewhat different than normally used for pavement response analysis was used for this project. Because of this, WES requested that Volume II of the report, which describes the method of analysis in detail, be thoroughly reviewed by Professors Fadum, Hudson, Vesic and Monismith. The consensus of the review was that the method of analysis was not only valid but essential to meet the stated objectives. It was the opinion of the reviewing consultants that the study has resulted in a major contribution to the understanding and knowledge of pavement response under static and dynamic loading.

Directors of WES during the conduct of the study were BG E. D. Peixotto, CE, and COL G. H. Hilt, CE. The Technical Director was Mr. F. R. Brown.

TABLE OF CONTENTS

LIST OF FIGURES

CONVERSION FACTORS, U. S. CUSTOMARY TO METRIC (SI) UNITS OF MEASUREMENT

U. S. customary units of measurement used in this report can be converted to metric (SI) units as follows:

Multiply	By	To Obtain
inches	2.54	centimetres
feet	0.3048	metres
inches per second	2.54	centimetres per second
feet per second	0.3048	metres per second
knots	0.5144444	metres per second
ounces	0.02834952	kilograms
pounds	0.45359237	kilograms
pounds per cubic foot	16.018489	kilograms per cubic metre
kips	4.448222	kilonewtons
pounds per square inch	0.6894757	kilopascals
Fahrenheit degrees	5/9	Celsius degrees or Kelvins*

* To obtain Celsius (C) temperature readings from Fahrenheit (F) readings, use the following formula: $C = (5/9)(F - 32)$. To obtain Kelvin (K) readings, use: $K = (5/9)(F - 32) + 273.15$.

INTRODUCTION

BACKGROUND

Reports of pavement distress associated with current commercial aircraft loads and growing concerns over the possibility of detrimental aircraft dynamic load effects on airport pavements persuaded the Federal Aviation Administration (FAA) to sponsor a Lockheed-California Company study described in Report No. FAA-RD-70-19, "Aircraft Dynamic Wheel Load Effects on Airport Pavements," dated May 1970.[1] The Lockheed study consisted of a literature study, computer analyses to determine aircraft loads and pavement responses, scaled pavement tests, and correlations between experimental and analytical data. In general, the Lockheed study concluded that aircraft dynamic wheel loads have a significant effect on portions of airport pavements. Specifically, the study showed that the primary effects that influence pavement response to dynamic loads are:

a. The increased magnitudes of aircraft wheel loads resulting from aircraft modes of operation, pavement unevenness, and aircraft structural characteristics during moving ground operations.

b. The dynamic load phenomena associated with the materials used in the construction of both rigid and flexible pavements.

For a given aircraft and level of pavement unevenness, the loads imposed upon a runway can be accurately defined for various ground operations. On the other hand, there is presently a serious void in information necessary to obtain an accurate description of pavement response to dynamic loads.

PURPOSE

This study was undertaken in an effort to provide experimental pavement response data so that the significance of dynamic loads on airport pavements could be evaluated. Specifically, the basic purpose of the study was to determine the relationship between the responses of typical flexible and rigid runway pavements to static and dynamic loads. The requirements to determine the magnitudes of the dynamic loads, to

determine the depths of pavement structures affected by static and dynamic loads, and to investigate the relationship between aircraft ground speeds and aircraft dynamic loads were essential elements of this study.

SCOPE

The purpose of this investigation was accomplished by conducting two series of full-scale tests using instrumented aircraft and both flexible and rigid instrumented runways. One series of tests was conducted during the cold period of the year when the average temperature of the top pavement layer was in the range of 35 to 55°F,* while the second series was conducted during the hot period of the year when the average temperature was in the range of approximately 84 to 116°F. An instrumentation system was installed aboard the aircraft to measure and record the three components of force of each of the main gear assemblies of the aircraft. Instrumentation systems were installed within the flexible and rigid pavement structures to measure the pavement responses to aircraft loads in the form of relative displacements and pressures. The key element in this experimental approach was the recording of a common time base for both the aircraft load measurements and the pavement response measurements. This control provided a means of correlating the aircraft dynamic wheel loads and the response measurements of the two pavement structures to within 1 msec. The locations of the two instrumented pavement test sites were selected so that all possible modes of aircraft ground operation could be investigated during the course of the experimental study.

The authors felt that the scope of the subject matter was too broad to be presented in a single report. Therefore, Volume I of the report[2] mainly describes the instrumentation systems and their installation and operation to collect the data required to determine the pressures and relative displacements under static and dynamic loads. Volume I also includes the history and chronology of the investigation and presents a

---

* A table of factors for converting U. S. customary units of measurement to metric (SI) units is presented on page 11.

complete description of the testing program. This report, Volume II, describes the reduction, interpretation, and analysis of instrumentation data collected during the tests. Appendix A of this report describes the automatic data processing (digital) system and techniques. Appendix B presents the data in reduced form; however, data summary plots are presented in the main text. Volume III of the report[3] contains a summary of the entire study. The computer output form of the reduced data, which is available at the U. S. Army Engineer Waterways Experiment Station (WES), makes a stack greater than 5 ft in height. Pressure data for the 1974 tests are available for only the first 40 events; the field-recorded magnetic tapes were found blank upon entering the automatic data processing system.

TEST PROGRAM

Instrumentation systems were installed in the pavement structures of runways 04-22 and 13-31 at the National Aviation Facilities Experimental Center (NAFEC) Airport, Atlantic City, N. J., at the two sites indicated in Figure 1. Instrumented aircraft were used to conduct the most common of aircraft ground operations for these test sites. Detail descriptions of the test program are presented in Volume I of this report.[2]

FLEXIBLE PAVEMENT TEST SITE

PAVEMENT STRUCTURE

An 80-ft-long segment of runway 13-31 located at its intersection with runway 8-26 was selected as the flexible pavement test site. This test site was chosen to enable the collection of typical response measurements during landing and at the point of rotation for takeoff as well as during low- and high-speed taxiing, braking, and turning operations. This particular site was in a portion of the runway which had been scheduled for reconstruction, and this factor was of great benefit during the installation of instrumentation. After reconstruction, the flexible pavement structure in this area consisted of 3 in. of bituminous surface course, 6 in. of bituminous base course, 9 in. of base course constructed from the original pavement surface and base courses, and 12 in. of subbase course constructed from the original subbase course over the compacted subgrade.

Gradation curves for the subgrade and subbase course materials are shown in Figures 2 and 3, respectively. Unified[4] and FAA[5] soil classifications for both materials were SP and E-1, respectively. For the 9-in. base course, construction specifications stated that the original pavement surface course (prior to reconstruction) was to be completely broken up such that the maximum dimension of any individual piece would not exceed 3 in. The resulting material was uniformly blended with the original base course material to form the new base course.

The bituminous base course conformed to Division 3, Section 2A,

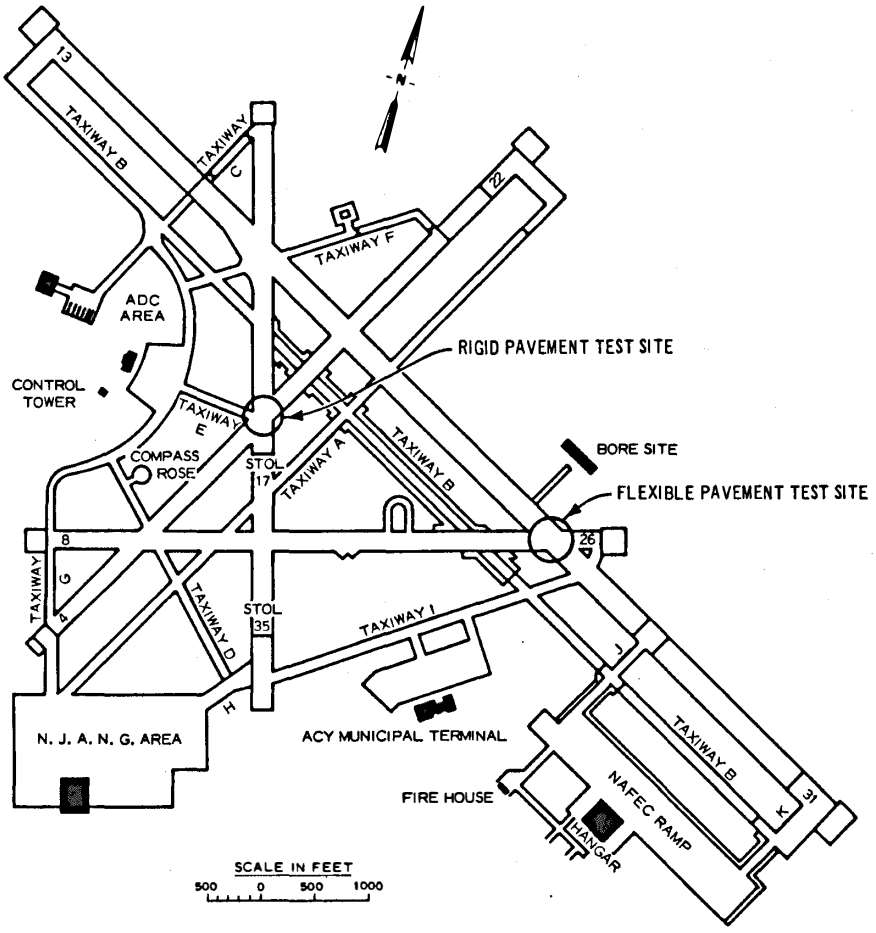

Figure 1. Locations of test sites at NAFEC airport

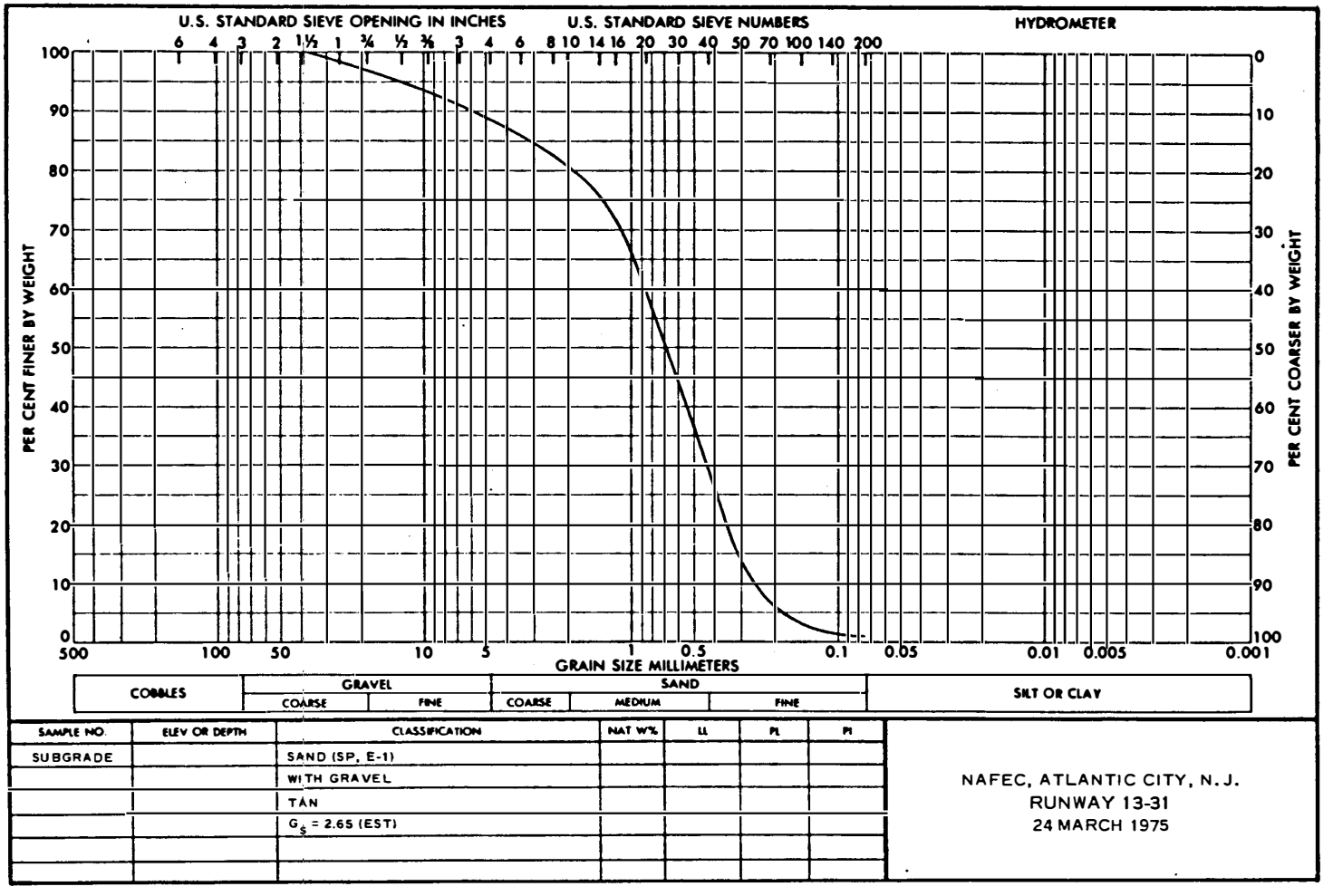

Figure 2. Gradation of subgrade material for flexible pavement test site

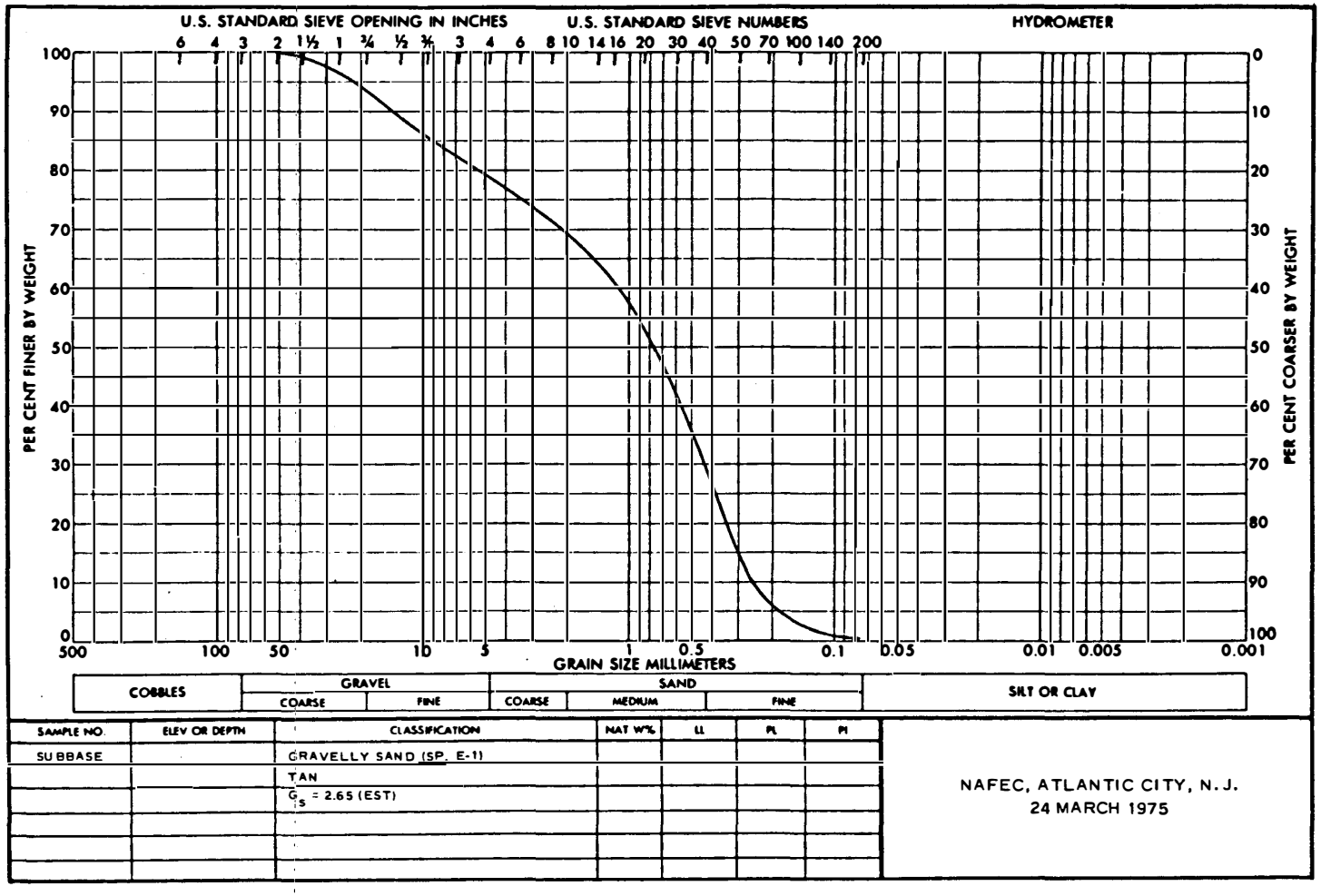

Figure 3. Gradation of subbase course material for both test sites

of the New Jersey State Highway Department "Standard Specifications for Road and Bridge Construction."[6] Aggregate was crushed hard stone mix aggregate conforming to the following gradation:

Sieve Size	Total Percent Dry Weight Passing
1-1/2 in.	100
3/4 in.	55 to 90
No. 4	25 to 60
No. 10	20 to 50
No. 40	15 to 30
No. 200	5 to 12

The mix design for the bituminous base course material conformed to mix No. 1 for hot-mixed bituminous concrete in Article 3.10.2 of the New Jersey specifications.

The bituminous surface course conformed to Item P-401 of FAA Advisory Circular AC 150/5370-1A.[7] Composition of the mixture conformed to Table 1 of Paragraph 401-3.1. Gradation of the aggregate conformed to gradation B. Asphalt cement conformed to the requirements for an 85-100 penetration grade. The bituminous surface course was designed for gross aircraft weights of more than 30,000 lb. Table 1 summarizes the material properties determined for the flexible pavement test site during and after reconstruction.

INSTRUMENTATION

A typical layout of the flexible pavement instrumentation system is shown in Figure 4. Three gage rows approximately 12 ft in length containing Bison coils, SE soil pressure cells, WES deflection gages, WES soil pressure cells, inductive probes, and velocity gages for a total of 162 instruments were installed in the pavement structure during the reconstruction of runway 13-31. Each gage row contained 12 SE soil pressure cells, 1 WES soil pressure cell, 1 WES deflection gage, and 1 velocity gage. The middle gage row contained 50 Bison coils and 5 inductive probes, and the outer two rows contained 25 Bison coils and 4 inductive probes. In addition, a thermistor was installed on the surface and at depths of 3, 6, and 9 in. within the pavement structure.

A system of laser light beam sources and detectors was installed

Table 1

Summary of Material Properties for the Flexible Pavement Test Site

Station No.	Depth Below Surface in.	Pavement Structure Element	Measurements During Construction					Measurements After Construction†			Soil Classification	
			CBR*		Water Content*	Water Content**	Dry Density**	CBR		Water Content		
			0.1 in.	0.2 in.	percent	percent	pcf	0.1 in.	0.2 in.	percent	Unified	FAA
65+20	18	Subbase course	97.0	--	4.1	8.7	130.9				SP	E-1
	30	Compacted subgrade	39.0	40.5	6.7	12.2	121.4				SP	E-1
	42	Compacted subgrade	43.5	57.0	7.0						SP	E-1
	54	Compacted subgrade	16.0	21.0	7.0						SP	E-1
65+34	11	Base course						37.0	43.0	4.1		
	20	Subbase course						25.0	26.0	5.8	SP	E-1
	32	Compacted subgrade						27.0	30.0	7.5	SP	E-1
	44	Compacted subgrade						41.0	54.0	9.1	SP	E-1
65+35	10.5	Base course						42.0	41.0	4.2		
	19.5	Subbase course						24.0	26.0	5.2	SP	E-1
	31.5	Compacted subgrade						25.0	31.0	7.6	SP	E-1
	43.5	Compacted subgrade						37.0	45.0	8.4	SP	E-1
65+50	18	Subbase course	58.5	67.5	5.5	8.6	131.1				SP	E-1
	30	Compacted subgrade	48.0	56.5	6.3	12.0	119.3				SP	E-1
	42	Compacted subgrade	34.5	44.5	7.1						SP	E-1
	54	Compacted subgrade	17.5	20.5	6.8						SP	E-1
65+80	11	Base course						33.0	35.0	6.6		
	20	Subbase course						26.0	29.0	5.1	SP	E-1
	32	Compacted subgrade						24.0	30.0	5.8	SP	E-1
	44	Compacted subgrade						44.0	44.0	6.5	SP	E-1
65+81	11.5	Base course						55.0	54.0	6.9		
	20.5	Subbase course						33.0	39.0	5.3	SP	E-1
	32.5	Compacted subgrade						40.0	46.0	5.7	SP	E-1
	44.5	Compacted subgrade						64.0	--	7.8	SP	E-1
66+00	18	Subbase course	65.0	67.0	7.5	9.3	124.2				SP	E-1
	30	Compacted subgrade	34.0	41.5	6.5	10.8	124.7				SP	E-1
	42	Compacted subgrade	32.0	42.5	6.9						SP	E-1
	54	Compacted subgrade	27.5	33.0	7.0						SP	E-1

* Average values determined from measurements in two test pits.

** Average values determined from two measurements with nuclear density device.

† Determined from small aperture testing.

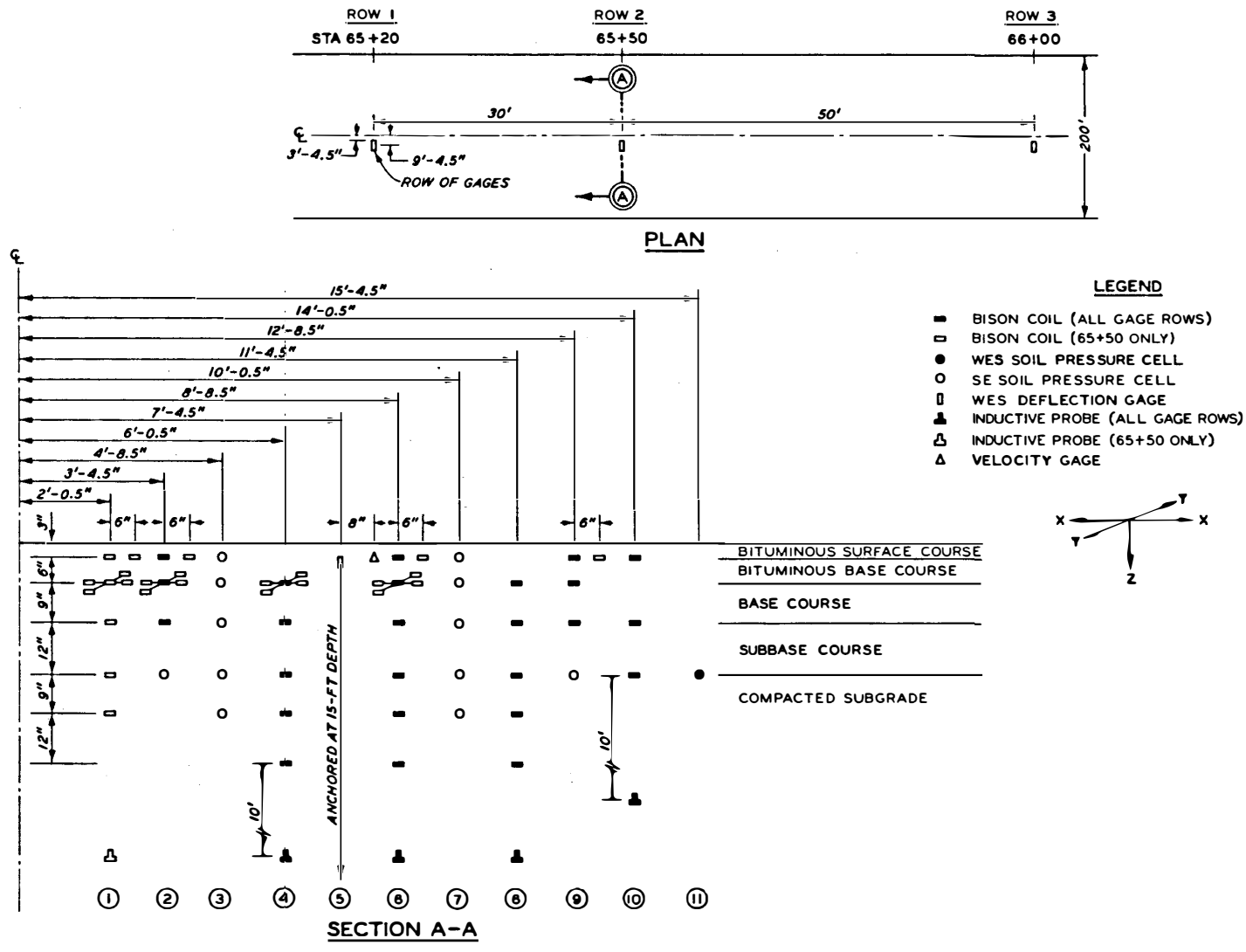

Figure 4. Typical layout of flexible pavement instrumentation

along the edge of the runway such that a light beam was projected directly above and parallel to each gage row. An electrical impulse was generated when the wheels of the instrumented aircraft passed between the source and detector, thereby signaling the instant at which the wheels were directly over the gage row. The lateral position of the aircraft was determined by visual inspection of a stripe of flour and water solution painted on the surface of the runway adjacent and parallel to each gage row.

A synchronized common time signal was recorded on both aircraft and ground data tapes. This provided the means by which the pavement response could be correlated with the corresponding aircraft load. With the exception of the thermistors, all instruments were recorded simultaneously on magnetic tapes, and all ground data tapes contained the time code and laser signals. Temperatures were recorded on paper tape.

RIGID PAVEMENT TEST SITE

PAVEMENT STRUCTURE

A 72-ft-long segment of runway 04-22 was instrumented at its intersection with runway 17-35 to form the rigid pavement test site. The pavement structure in this area consisted of 7 in. of portland cement concrete (PCC) pavement and 8 in. of subbase course over the compacted subgrade. As was the case for the flexible pavement site, this site was chosen to enable the collection of typical measurements during normal aircraft ground operations. A 12-1/2- by 25-ft slab was removed from the runway at the location of each of the gage rows, and gages were installed in holes cored through the underlying material. Since the installation of gages required the closing of the runway, it was necessary that the reconstruction of runway 13-31 be completed and the runway reopened to traffic prior to instrumenting runway 04-22.

Gradation curves for the subgrade and subbase course materials are shown in Figures 5 and 3, respectively. Unified and FAA soil classifications for the subgrade material were SM and E-1, respectively. Table 2 summarizes the materials properties determined for the rigid pavement test site. The nuclear density and water content values were

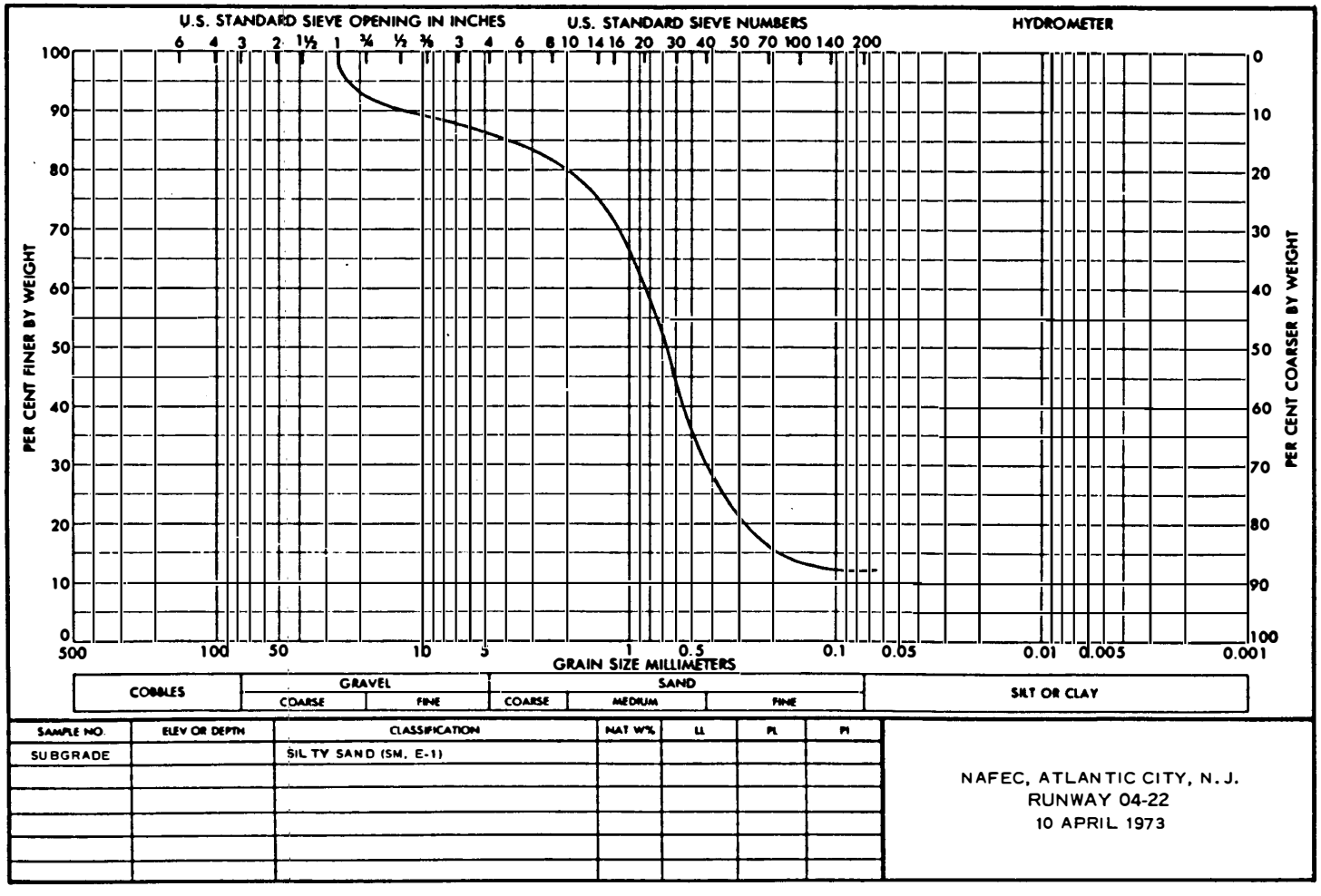

SAMPLE NO.	ELEV OR DEPTH	CLASSIFICATION	NAT W%	LL	PL	PI
SUBGRADE		SILTY SAND (SM, E-1)				

NAFEC, ATLANTIC CITY, N.J.
RUNWAY 04-22
10 APRIL 1973

Figure 5. Gradation of subgrade material for rigid pavement test site

Table 2

Summary of Material Properties for the Rigid Pavement Test Site

Station No.	Depth Below Surface in.	Pavement Structure Element	CBR 0.1 in.	CBR 0.2 in.	Water Content percent	Water Content* percent	Dry Density* pcf	Soil Classification Unified	Soil Classification FAA
26+55	8	Subbase course	9	10	9.2	13.05	114.8	SP	E-1
	16	Compacted subgrade	10	10	8.2			SM	E-1
	28	Compacted subgrade	8	9	7.4			SM	E-1
	40	Compacted subgrade	13	11	6.1			SM	E-1
26+55	8	Subbase course	10	9	9.5	13.05	114.8	SP	E-1
	16	Compacted subgrade	20	20	6.9			SM	E-1
	28	Compacted subgrade	12	12	8.1			SM	E-1
	40	Compacted subgrade	13	12	6.8			SM	E-1
26+90	8	Subbase course	10	10	13.1	13.5	122.5	SP	E-1
	16	Compacted subgrade	23	24	6.1			SM	E-1
	28	Compacted subgrade	9	8	8.6			SM	E-1
	40	Compacted subgrade	21	25	10.0			SM	E-1
26+93	8	Subbase course	11	11	8.6	13.7	123.3	SP	E-1
	16	Compacted subgrade	23	25	8.1			SM	E-1
	28	Compacted subgrade	15	14	5.0			SM	E-1
	40	Compacted subgrade	20	24	5.9			SM	E-1
27+22	8	Subbase course	16	18	9.4	11.5	125.7	SP	E-1
	16	Compacted subgrade	28	36	7.8			SM	E-1
	28	Compacted subgrade	18	19	7.4			SM	E-1
	40	Compacted subgrade	16	13	5.9			SM	E-1
27+30	8	Subbase course	14	11	9.4	12.0	125.2	SP	E-1
	16	Compacted subgrade	15	16	7.7			SM	E-1
	28	Compacted subgrade	11	12	6.7			SM	E-1
	40	Compacted subgrade	16	13	4.6			SM	E-1

* In-place measurements made with nuclear density device.

determined prior to placement of the concrete slabs, and the CBR values were determined after placement.

The PCC pavement batch plant-mix design was as follows:

a. 1950 lb of gravel aggregate per cubic yard.

b. 1265 lb of sand per cubic yard with 4 percent moisture if wet.

c. 560 lb of 3/4 high early (HE) portland cement per cubic yard with 5 oz of pozzolith per bag.

d. 2 percent entrained air per cubic yard.

e. Slump of 2.5 in.

Samples of the concrete were taken from the concrete mixtures as they were discharged from ready-mix trucks. Six- by 6- by 36-in. beams and 6-in.-diam by 12-in.-high cylinders were taken that were representative of the concrete placed for each slab and were field-cured. Tables 3 and 4 summarize the material properties.

INSTRUMENTATION

The instrumentation system installed in the rigid pavement test site was similar to that in the flexible pavement test site of runway 13-31. Figure 6 shows a typical layout of the instrumentation system. A total of 153 gages consisting of 104 Bison coils, 13 inductive probes, 3 WES deflection gages, 9 Valore strain gages, 18 SE soil pressure cells, 3 WES soil pressure cells, and 3 velocity gages were installed in three gage rows at various depths and offsets within the pavement structure. Thermistors were installed on the surface of, at the bottom of, and at a depth of 3.5 in. within two slabs of the rigid pavement test site.

The laser and time code systems used in the flexible pavement tests were also used in the rigid pavement tests. The data acquisition system was identical with that used in the flexible pavement tests.

AIRCRAFT

Instrumented aircraft were used in both the initial cold weather and the subsequent warm weather tests to provide the monitored load for the pavement structures. An instrumented B-727 was leased from United Airlines, Inc., for the cold weather testing of 1972, and a similar B-727

Table 3

Flexural Strength Data for 6- by 6- by 36-in. Field-Cured Beams of Concrete Placed in Rigid Pavement Test Site

Specimen No.	Slab No.	Slump in.	Class of Portland Cement Concrete	Curing Time days	Flexural Strength psi	Average Flexural Strength for Class and Age psi	Average Flexural Strength for Age psi
N-4	3	2.50	4000-psi HE	4	650	650	650
N-1	1,2	2.25	3000-psi HE	7	683		
N-2	1,2	2.25	3000-psi HE	7	677		
N-2	1,2	2.25	3000-psi HE	7	682	678.5	
N-1	1,2	2.25	3000-psi HE	7	672		677.75
N-4	3	2.50	4000-psi HE	7	670		
N-4	3	2.50	4000-psi HE	7	683	677	
N-4	3	2.50	4000-psi HE	7	678		
N-3	3	2.50	4000-psi HE	20	713		
N-3	3	2.50	4000-psi HE	20	722	730.75	730.75
N-3	3	2.50	4000-psi HE	20	755		
N-3	3	2.50	4000-psi HE	20	733		
N-1	1,2	2.25	3000-psi HE	21	723		
N-1	1,2	2.25	3000-psi HE	21	707	724.75	724.75
N-2	1,2	2.25	3000-psi HE	21	732		
N-2	1,2	2.25	3000-psi HE	21	737		

Table 4

Compressive Strength Data for 6-in.-Diam by 12-in.-High Field-Cured Cylinders of Concrete Placed in Rigid Pavement Test Site

Specimen No.	Slab No.	Slump in.	Class of Portland Cement Concrete	Curing Time days	Compressive Strength psi	Average Compressive Strength for Class and Age psi	Average Compressive Strength for Age psi
NAF-4	3	2.50	4000-psi HE	4	3431	3431	3431
NAF-1	1,2	2.25	3000-psi HE	7	3820	3873	4165
NAF-2	1,2	2.25	3000-psi HE	7	3926		
NAF-4	3	2.50	4000-psi HE	7	4705	4457	
NAF-4	3	2.50	4000-psi HE	7	4209		
NAF-3	3	2.50	4000-psi HE	20	4740	4797.67	4797.67
NAF-3	3	2.50	4000-psi HE	20	4809		
NAF-3	3	2.50	4000-psi HE	20	4844		
NAF-1	1,2	2.25	3000-psi HE	21	4386	4563	4563
NAF-1	1,2	2.25	3000-psi HE	21	4457		
NAF-2	1,2	2.25	3000-psi HE	21	4669		
NAF-2	1,2	2.25	3000-psi HE	21	4740		

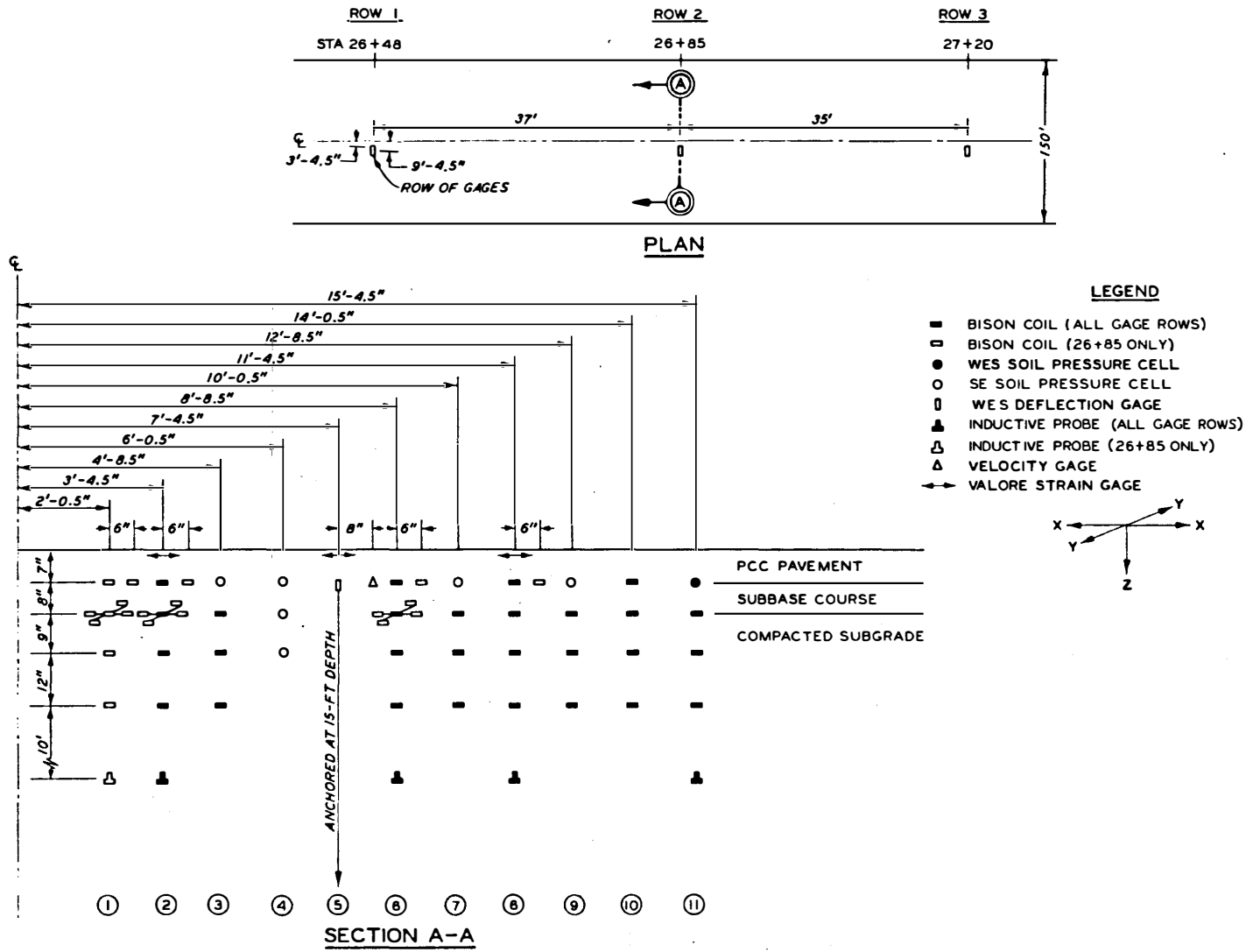

Figure 6. Typical layout of rigid pavement instrumentation

and a C-880 were obtained from the FAA and instrumented by WES for the warm weather testing of 1974. Both B-727 aircraft were equipped with strain gages installed on the drag struts, side struts, and axles of both main gears and potentiometers installed on the torsion links of both main gears to measure the three components of force transmitted to the pavement structure. Accelerometers were the only instruments installed on the C-880 and were placed at three locations to measure the aircraft acceleration response for estimating the main gear load during dynamic tests. Similar systems of accelerometers were installed on board both B-727 aircraft as backup systems for the instrumented main gears. On-board instrumentation for all three aircraft included signal conditioning equipment, a time code generator (synchronized with the ground time code generator for correlation of test results), and a 14-track analog magnetic tape recorder.

TESTING PERIODS

Two series of dynamic load tests were conducted at the NAFEC Airport to determine the nature of the pavement response to dynamic aircraft loads. The first series of tests, the cold weather tests, was conducted during the period of 12 November-11 December 1972, and the second series of tests, the warm weather tests, was conducted during the period of 8-15 July 1974. Similar testing programs were followed for each series of tests with the only significant exception being that tests were conducted on both test sites during the cold weather tests but only on the flexible pavement test site during the warm weather tests.

Data were collected for 408 aircraft operations during the cold weather tests. Of this total, 203 operations were on the flexible pavement test site and the remaining 205 were on the rigid pavement test site.

During the warm weather tests, data were collected for 281 aircraft operations on the flexible pavement test site. A B-727 was used to load the pavement for 240 of these operations, and a C-880 was used for the remaining 41 operations. The gages that had been installed in the flexible pavement test site for the 1972 test series were checked,

and approximately 94 percent of them proved to be in good condition. Ten pressure cells were not operating. With the exception of one velocity gage, no additional instruments were installed in the flexible pavement structure for the warm weather testing.

The ranges of average pavement temperatures were 35 to 55°F and 84 to 116°F for the cold and warm weather tests, respectively. Daily high, mean, and low temperatures for the four flexible pavement depths are shown in Figures 7-10 and 11-14 for the cold and warm weather tests, respectively. Daily high, mean, and low temperatures for the three rigid pavement depths are shown in Figures 15-17 for the cold weather tests. Figure 18 shows a typical 24-hour temperature cycle for the warm weather tests.

TEST MODES

The following types of tests were performed during both cold and warm weather tests:

a. Static load tests. The aircraft was positioned over each gage row and data collected. These tests provided data for comparison with data from dynamic load tests as well as a check of the capability of the instrumentation system.

b. Dynamic load tests. Various aircraft ground operations were conducted on the test sites and data collected. Pavement responses and aircraft dynamic loads were determined under the following aircraft operating modes:

(1) Creep-speed taxi (3 to 8 knots).

(2) Low-speed taxi (15 to 30 knots).

(3) Medium-speed taxi (45 to 80 knots).

(4) High-speed taxi (85 to 130 knots).

(5) High-speed braking (130 to 45 knots).

(6) Takeoff rotation (85 to 130 knots).

(7) Touchdown.

(8) High-speed braking with reverse thrust.

(9) Turning (4 to 30 knots).

Although this particular breakdown of possible aircraft operations differs slightly from that described in the Lockheed report,[1] data obtained during these operations should be directly applicable to those presented by

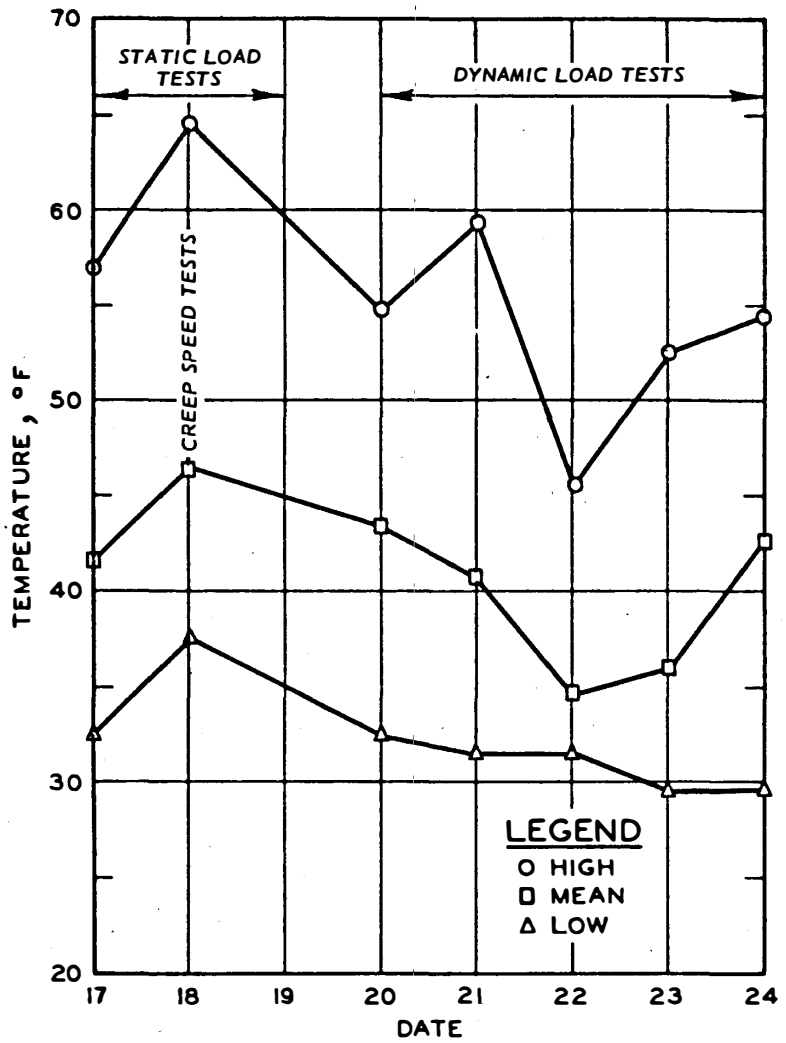

Figure 7. Flexible pavement temperatures at 1/4-in. depth , 17-24 November 1972

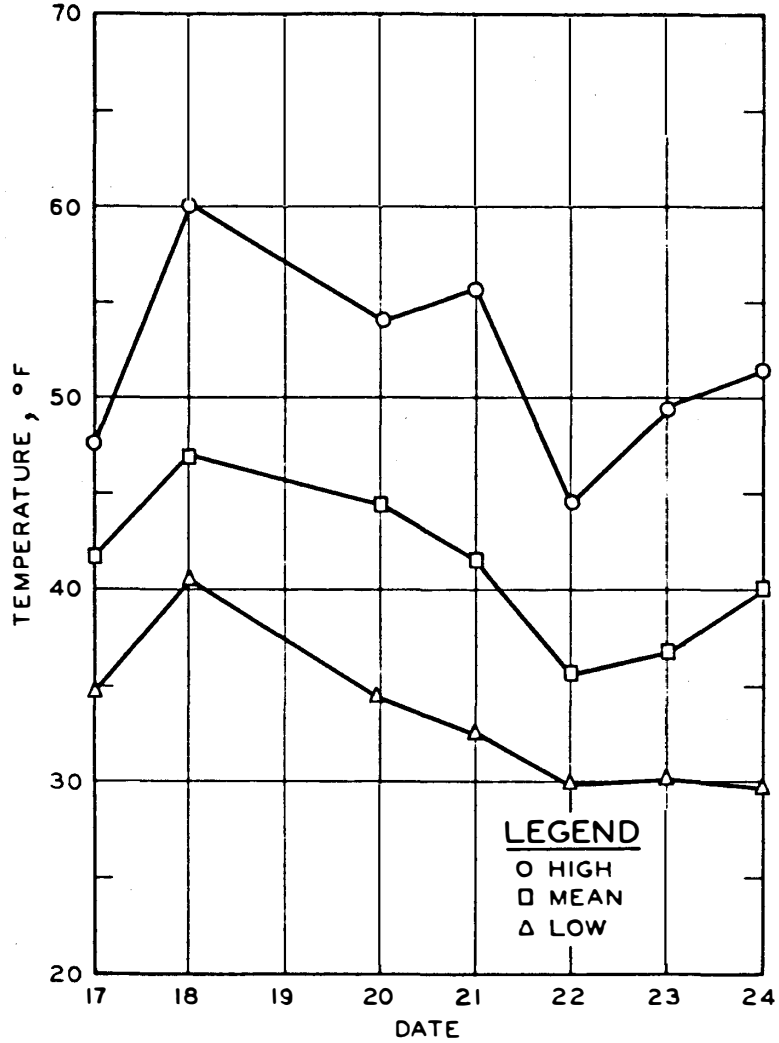

Figure 8. Flexible pavement temperatures at 3-in. depth, 17-24 November 1972

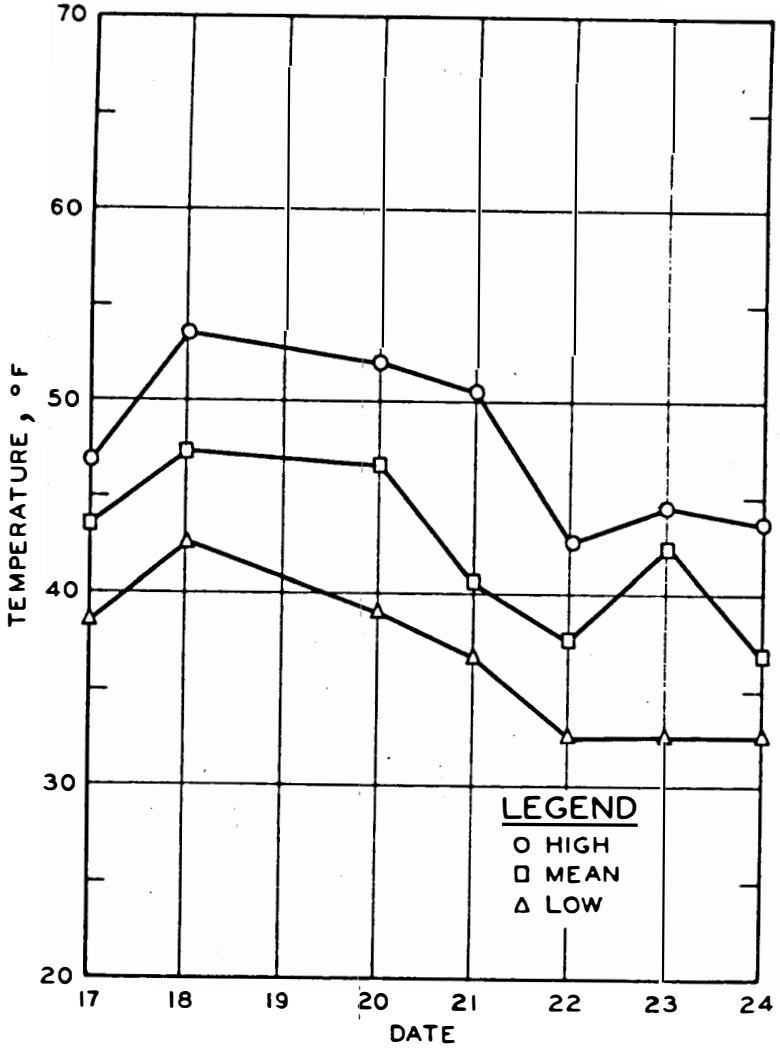

Figure 9. Flexible pavement temperatures at 6-in. depth, 17-24 November 1972

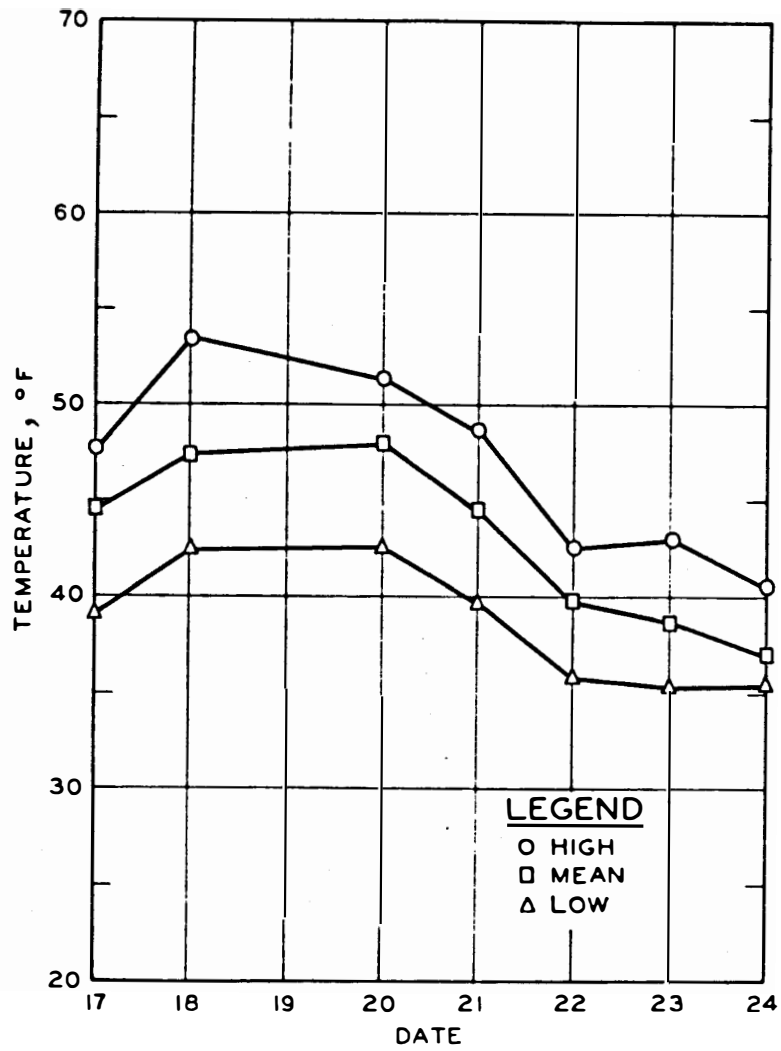

Figure 10. Flexible pavement temperatures at 9-in. depth, 17-24 November 1972

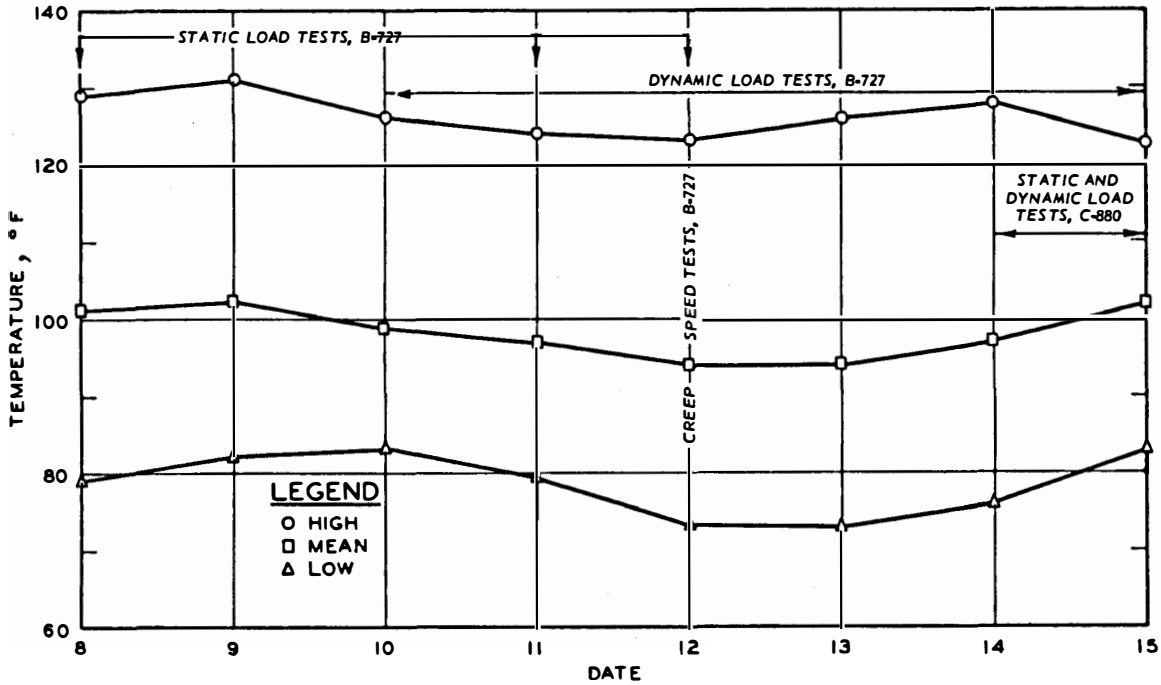

Figure 11. Flexible pavement temperatures at 1/4-in. depth, 8-15 July 1974

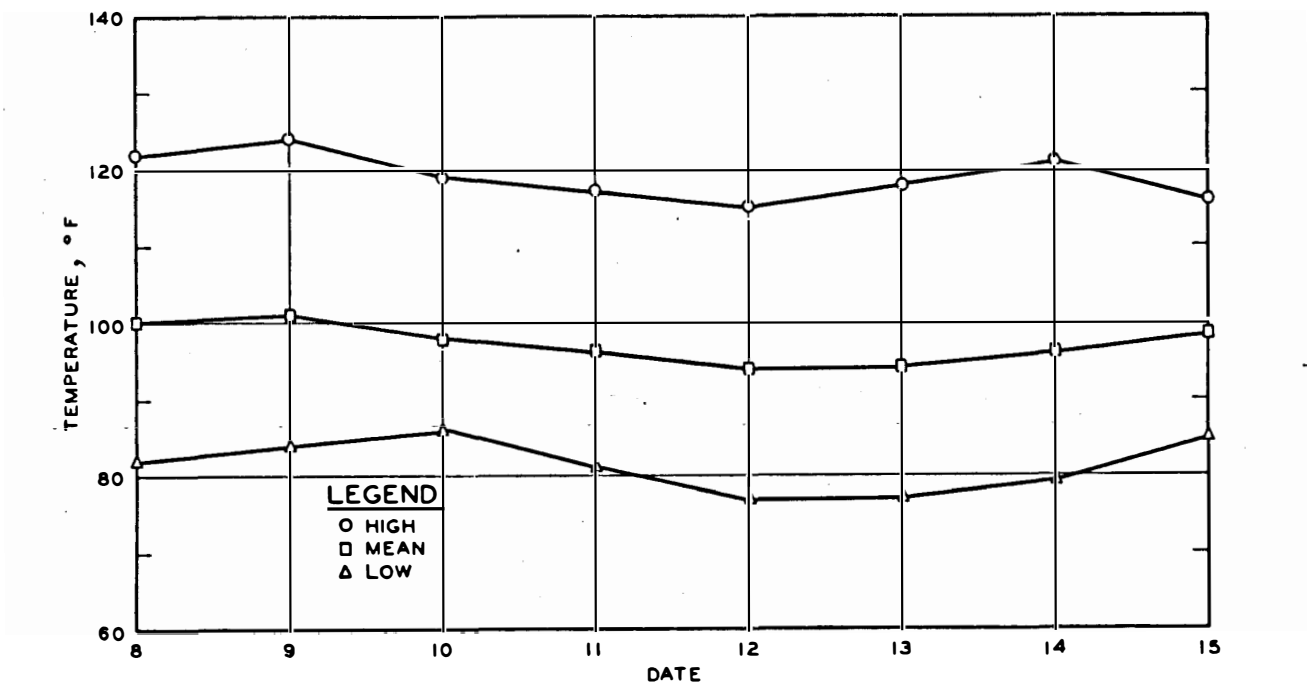

Figure 12. Flexible pavement temperatures at 3-in. depth, 8-15 July 1974

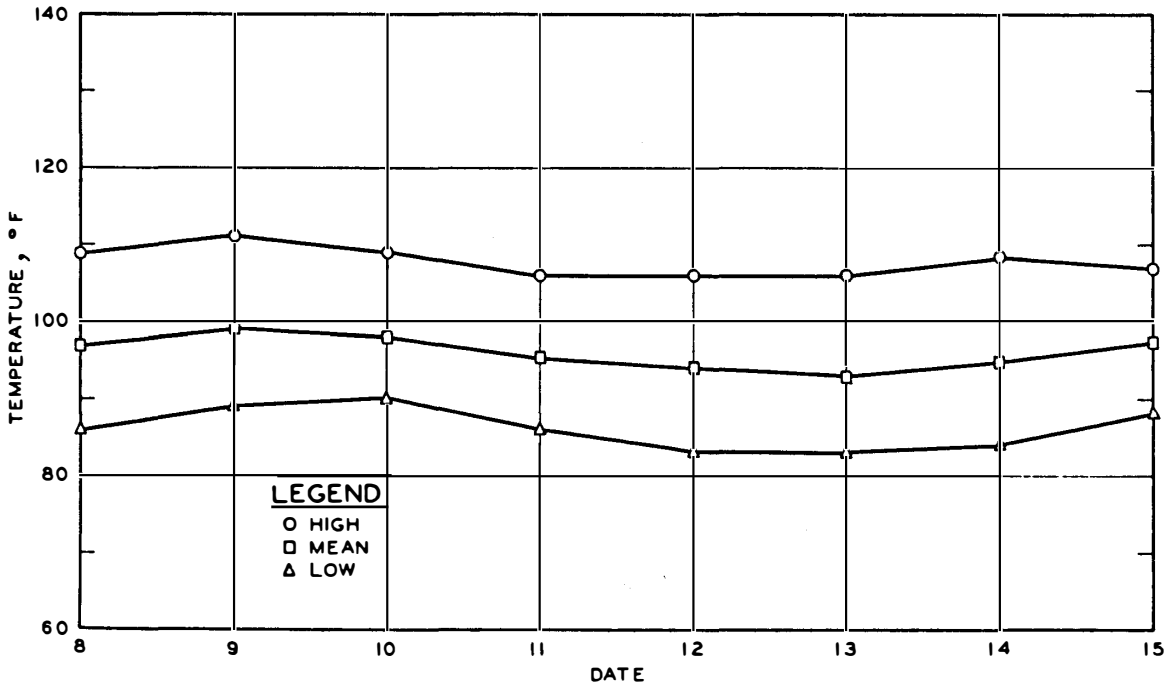

Figure 13. Flexible pavement temperatures at 6-in. depth, 8-15 July 1974

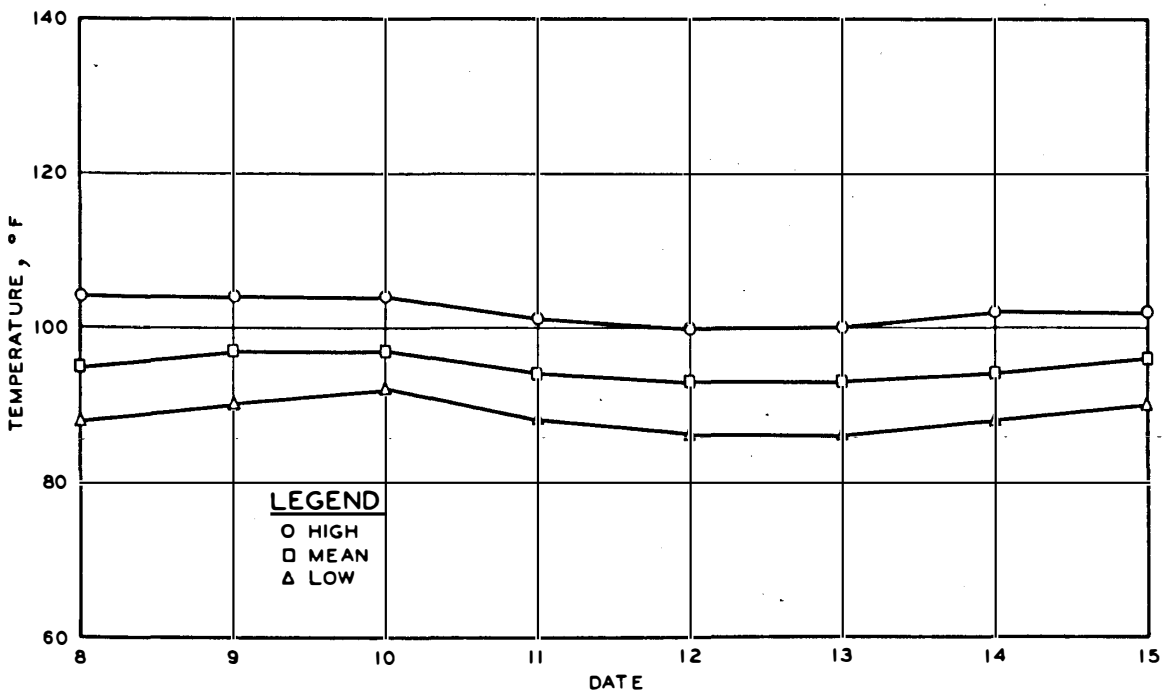

Figure 14. Flexible pavement temperatures at 9-in. depth, 8-15 July 1974

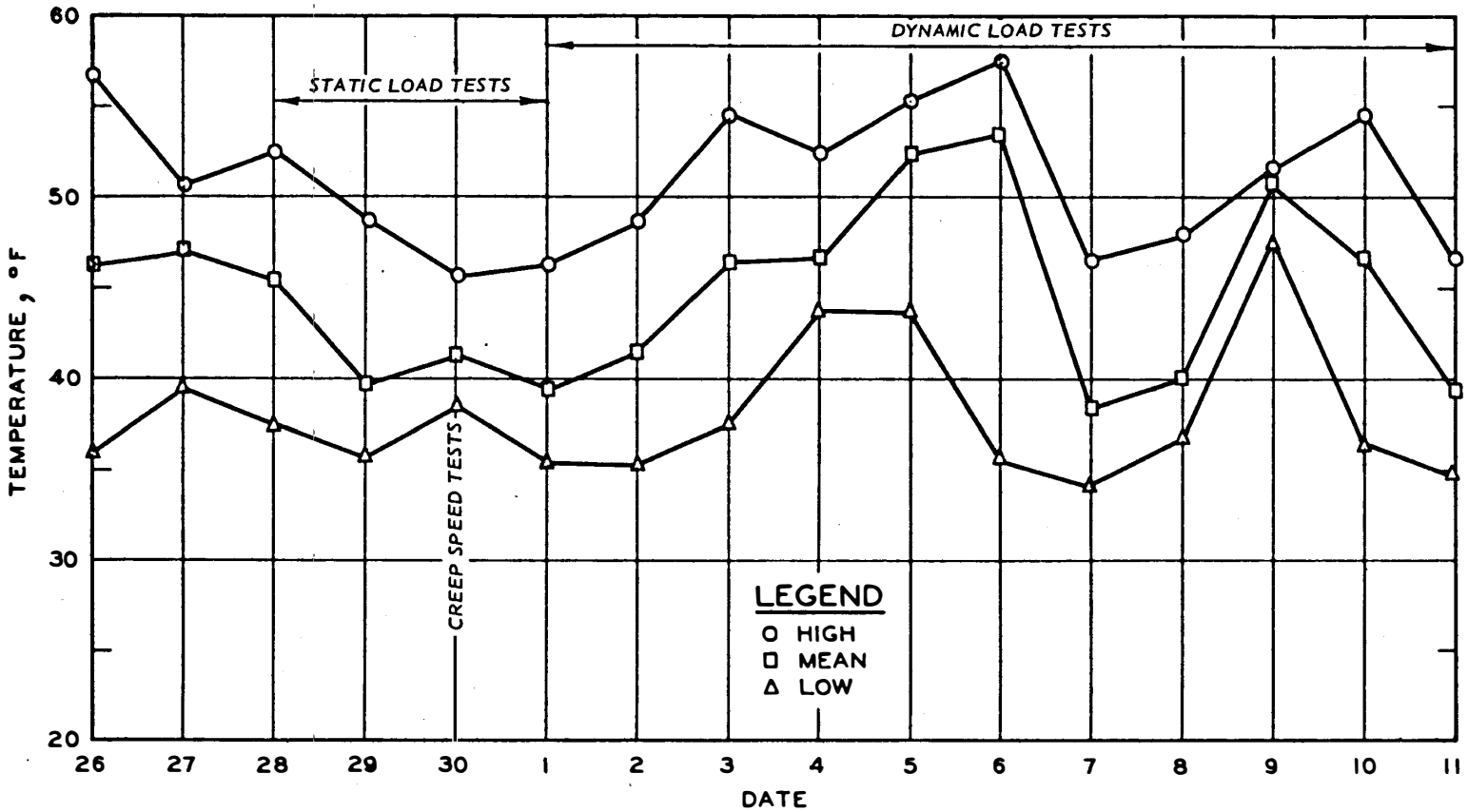

Figure 15. Rigid pavement temperatures at 1/4-in. depth, 26 November-11 December 1972

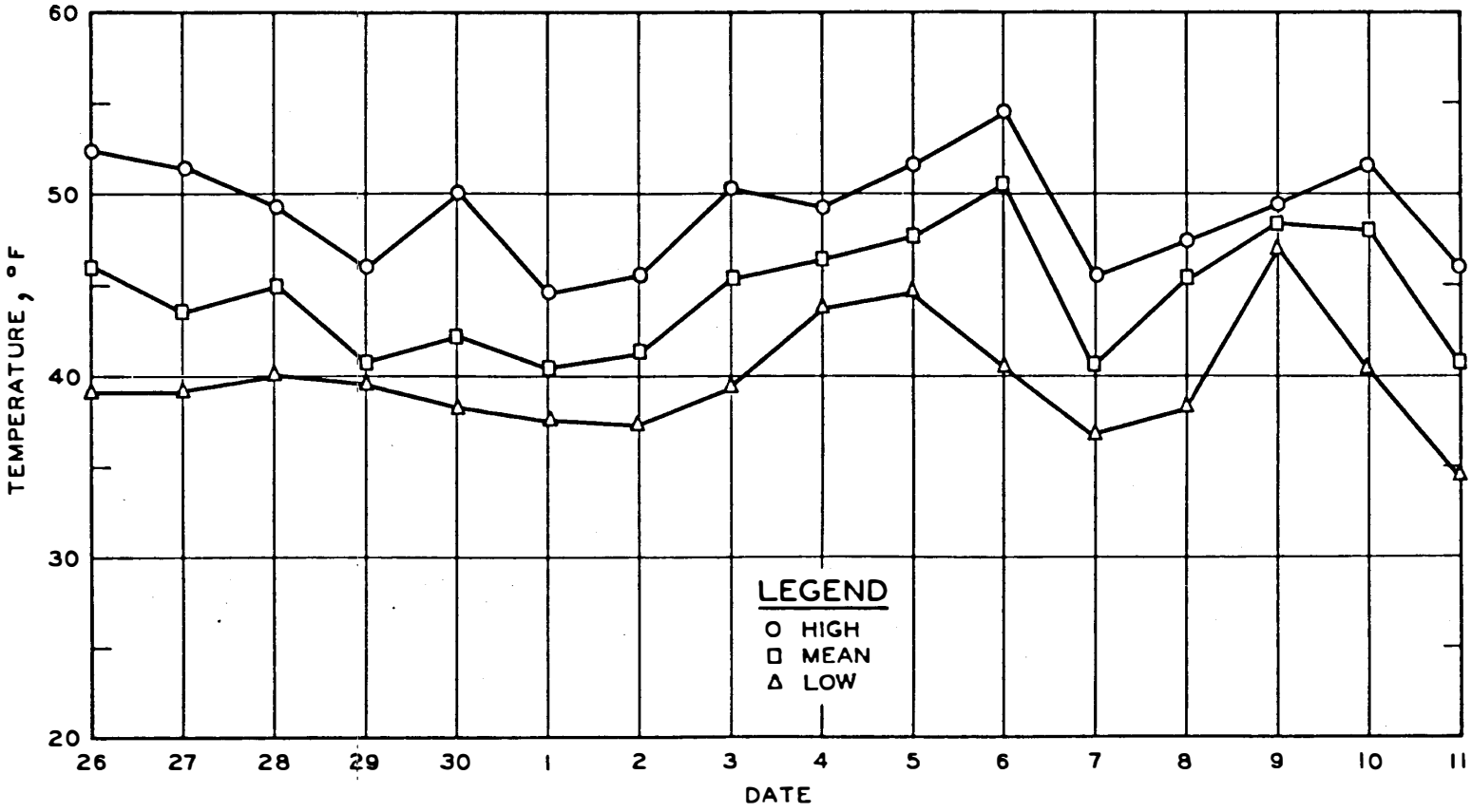

Figure 16. Rigid pavement temperatures at 3-1/2-in. depth, 26 November-11 December 1972

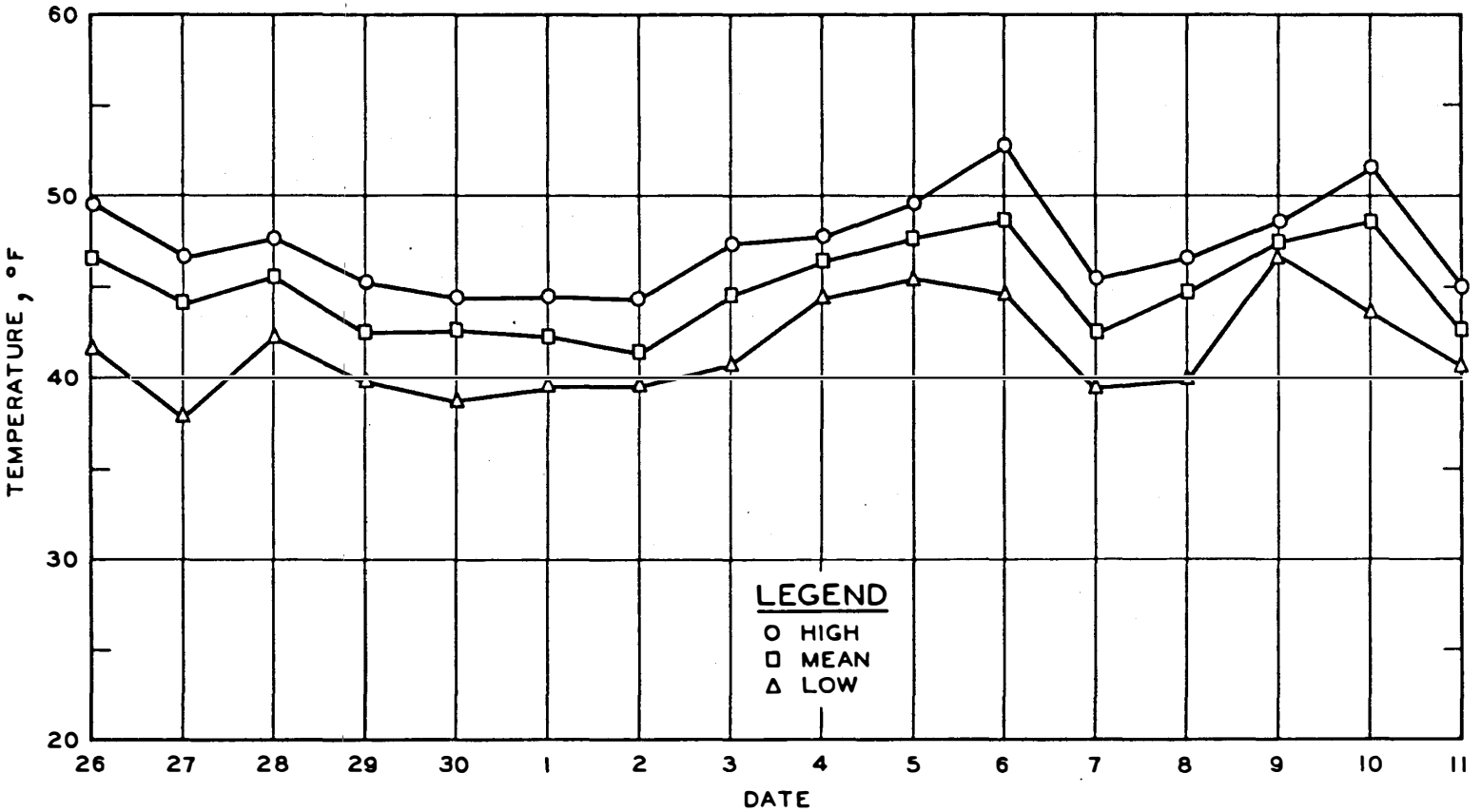

Figure 17. Rigid pavement temperatures at 7-in. depth, 26 November-11 December 1972

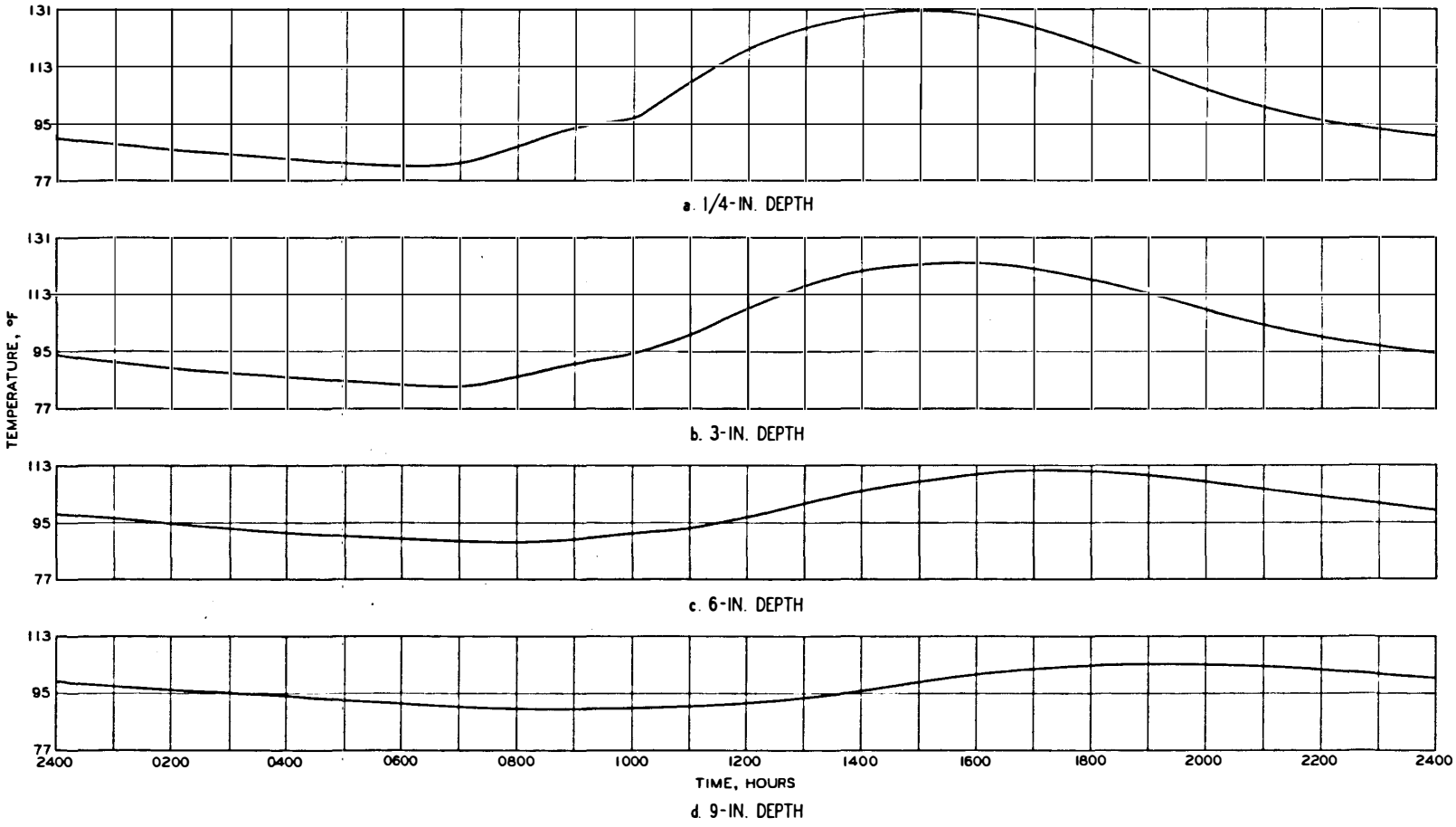

Figure 18. Twenty-four-hr temperature cycle for flexible pavement test site, 1974

Lockheed. Responses of each type of gage were recorded during tests conducted under each mode of operation. As an example of the applicability of the test modes to typical airport operations, consider a normal takeoff. At any airport, this operation involves seven of the test modes: static loading; turning; creep-, low-, medium-, and high-speed taxi; and takeoff rotation. If the takeoff was aborted, the high-speed braking modes would become applicable.

DATA ANALYSIS

AUTOMATIC DATA PROCESSING

A detailed description of the automatic data processing system is presented in Appendix A of this report. This part of the report summarizes significant sections of Appendix A concerning the data and reduction.

DATA FORM

The data were in analog form and of two basic types, static and dynamic. Data from the static load tests were in the form of straight lines or constant voltage levels. Data from the dynamic load tests were in the form of impulses at the instant a gage row was crossed and constant voltage levels before and after.

Some gages responded in the form of both upward and downward movement data peaks, while others responded in only one direction. The WES deflection gages, Valore strain gages, and pressure cells primarily registered only one data peak. Figure 19 shows typical digital computer-reproduced recordings for a WES deflection gage and an SE soil pressure cell. The Bison coils and velocity gages registered more than one data peak.

Bison coils primarily registered two data peaks in opposite directions. An upward movement peak occurred immediately before the aircraft wheels reached the center line of a gage location, and a downward movement peak occurred as the wheels were directly over a gage location. These two data peaks are referred to as the first and second peaks, and their positions were determined from correlations with the laser signals. A third peak, which was of lesser upward movement, occurred immediately after the wheels passed the center line of a gage location. Depending on the gear-to-gage offset distance, the second peak could be an upward movement and could be larger than the first peak. Figure 20 shows a typical digital computer-reproduced recording for Bison coils.

Velocity gages responded in the form of two to four peaks,

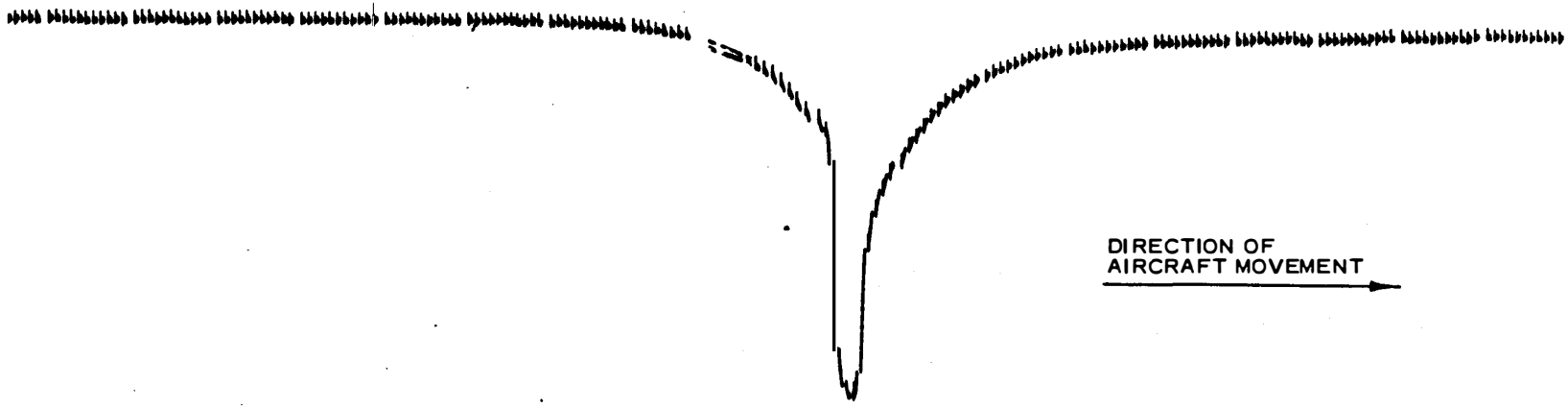

a. WES DEFLECTION GAGE

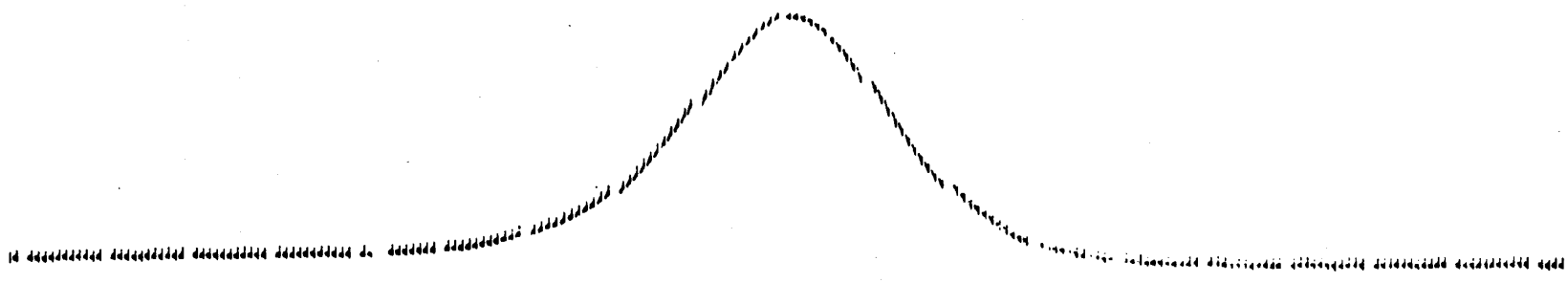

b. SE SOIL PRESSURE CELL

Figure 19. Typical recordings for WES deflection gage and SE soil pressure cell

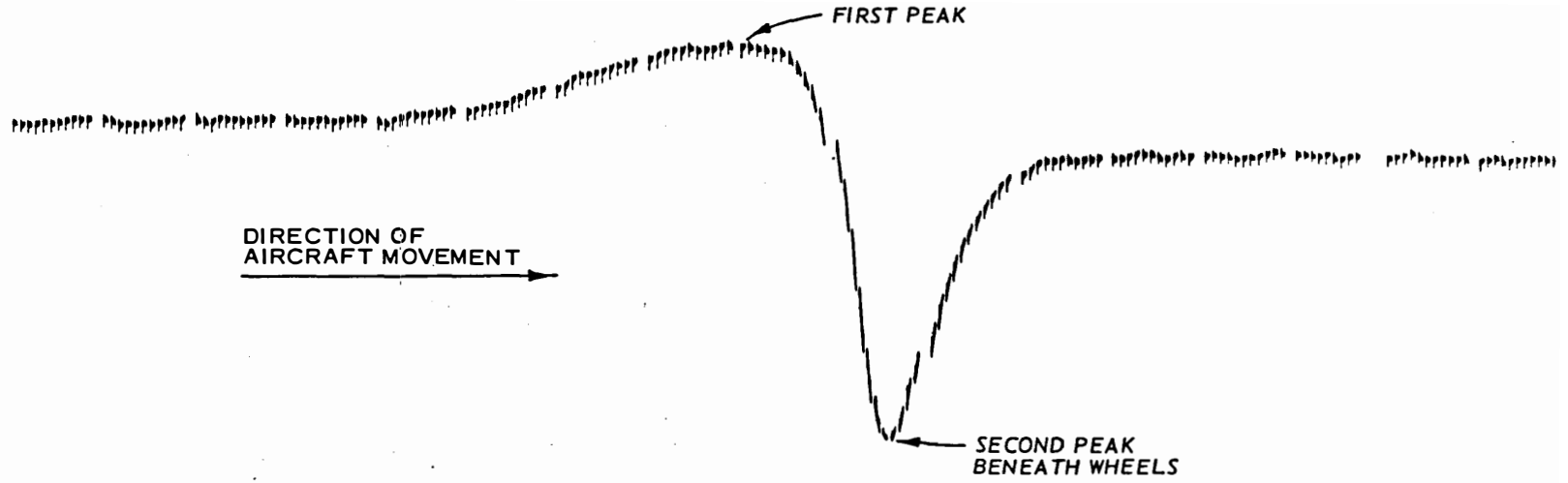

Figure 20. Typical recording for Bison coil showing first and second peaks (1972 tests)

depending on the gear-to-gage offset distance. In the immediate gage vicinity, two upward peaks occurred immediately before the wheels reached the gage center line, and one downward and then one upward peak occurred after the wheels passed. At offset distances not within the immediate gage vicinity, only a downward and then an upward peak occurred. Figure 21 shows typical digital computer-reproduced recordings for a velocity gage for 0- and 1.5-ft gear-to-gage offset distances.

DIGITIZING PROCESS

The digitizing system generally consisted of a computer-controlled analog-to-digital (A to D) converter, the computer, and output peripherals. Data tapes were played on an analog 14- or 32-track tape transport, and the signals passed through aliasing filters and through analog variable gain amplifiers. The signals were digitized by a multiplexer and the A to D converter at selected rates and stored on disc. Processing involved reading small portions of data from the disc, calibrating the data using engineering units read in from a high-speed paper tape reader, and performing operations on the data such as digital filtering and standard deviation calculations. The digitizing and processing procedures followed a basic format.

Identifying information was first entered into the computer from a teletype. Next, a calibration (cal) was located on the analog tape, digitized, and processed. Test data were then located, digitized, and processed. The digitized data were printed out on oscillograph paper (examples are Figures 19, 20, and 21), and the operator had the choice of writing the data on tape or redoing the test based on the appearance of the oscillograph record. The digitizing rates selected were approximately 2000 Hz for the dynamic load tests and 200 Hz for the static load tests.

Because noise extended beyond the folding frequency, aliasing filters were needed. The data and noise frequencies varied from channel to channel and test to test. Therefore, computer-controlled digital low-pass filters which can be easily shifted in cutoff frequency were also included in the processing program. Values selected for the aliasing

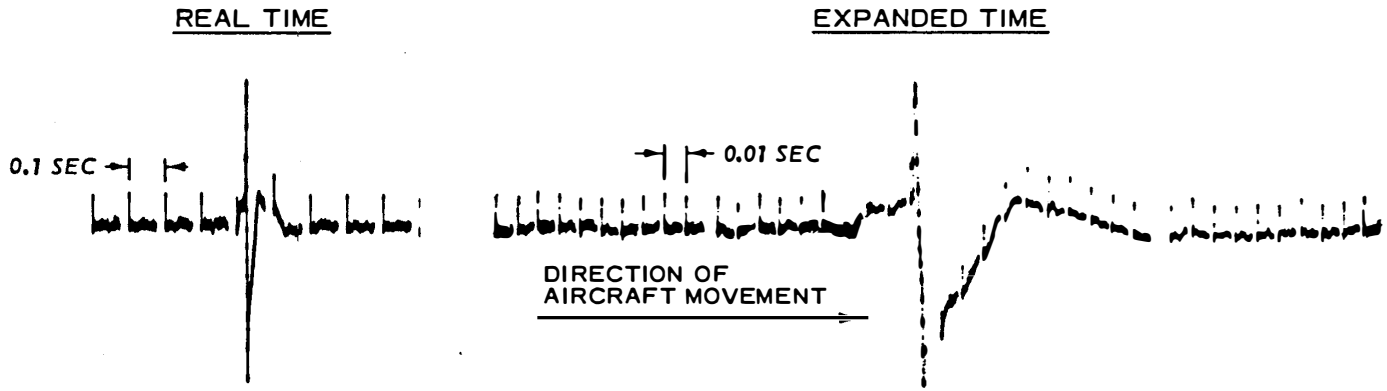

a. ZERO GEAR-TO-GAGE OFFSET

b. 1.5-FT GEAR-TO-GAGE OFFSET

Figure 21. Typical recordings for velocity gage for two different gear-to-gage offset distances

filters were 14 and 700 Hz for the static and dynamic load tests, respectively. Digital filtering was of the low-pass, single-pole recursive type. Phase shift normally introduced by this type filter was cancelled out by passing the data through the filter in the forward and reverse directions.

The standard deviation (noise level) was calculated for each data channel. Noise remaining after filtering was approximately sinusoidal around the mean level of the data; therefore, the constant by which the standard deviation was multiplied to obtain peak-to-peak noise was 2.828. This constant occurs because the root-mean-square value of a sine wave is the peak magnitude divided by the square root of two. The standard deviation value accompanied each data value in the final output.

DATA OUTPUT

The digital processed results were output on both hard copy (oscillograph records) and digital magnetic tapes in binary coded decimal (BCD) format, the most widely accepted input format for 7-track digital tapes. Digital BCD tapes provided the input media for dumping or further processing of the data on high-speed computers, and the data are available at WES in this form.

Desired data output varied with the type of test and the type of gage processed. Static load tests were more important in their relationship to one another than in themselves. Therefore, in addition to the magnitude of the static level, the change in each static level from the preceding cal and the static level was output. In addition to the cal zero level, the change from the last cal zero level was also output.

For all instruments except the velocity gages, the information that was output for the static load tests was also output for the dynamic load tests, although this was supplemented with additional information. Both data peaks were output for the Bison coils, but only one peak was output for the other gages. All data peaks were calculated from the prior-to-peak no-load level; however, the difference between the prior-to-peak and the after-peak no-load levels was also output. Another output was the change in no-load level from test to test. A description

of each test in engineering units was also output. This was made by printing (with an oscillograph) groups of points 0.01 sec in length from 0.2 sec before to 0.2 sec after the peaks and recording on magnetic tape the first point of each group. The groups on hard copy containing the peak points were marked by lines on either side of the group.

Due to the operating principle of the Bison coils (electromagnetic coupling), they are affected by metal. The metal effect is a constant for a given vehicle and can be easily determined with a pair of coils. This constant only needs to be applied to in-place measurements for affected coils. The B-727 aircraft underside was completely surveyed with a pair of Bison coils, and the only metal influence found was in the immediate vicinity of each wheel. For a wheel of the B-727 or C-880, the zone of influence for vertically spaced coils extended about 5 in. out from and around the wheel and was of a magnitude of approximately 0.003 in. of extension for 6-in.-spaced coils. For a wheel, the zone of influence for horizontally spaced coils extended about 10 in. out from and about 5 in. around the wheel and was of a magnitude of approximately 0.003 in. of compression for 6-in.-spaced coils at a 9-in. depth. These constants were applied as corrections in the wheel vicinities to the Bison coil data of the flexible pavement 3- to 9-in. depth and the 9-in. depth for horizontal coils. The horizontal coil data for the bottom of the rigid pavement slab were corrected in the same manner.

A standard procedure for reducing velocity data is integration of the signals. If data response is simple, such as downward and then upward movement, this procedure is applicable and the result is the motion (displacement) that caused the velocity. For the NAFEC velocity response data at gear-to-gage offset distances not within the immediate gage vicinity (Figure 21), integration of signals yielded the pavement displacement. However, for the velocity data in the immediate gage vicinity where multiple movement peaks occurred, direct integration was not applicable and yielded erroneous results. A description of the methodology for reduction of the velocity data to measurements of displacement is presented later in this report under "Interpretation of Pavement Structure Relative Displacements and Motion." A comparison

and check of movement computed from the velocity gage response with that measured by a WES deflection gage will also be presented in this section.

Because of the complicated behavior of the velocity data, computer treatment and integration would have been extremely complex and time-consuming. In addition, the time and cost factors were not justified because the movements computed from the velocity gage responses did check with those measured by the WES deflection gage and Bison coils.

Because velocity gages responded sharply (at very high frequencies), over a long period, and with multiple peaks, two time expansions were made by the computer, recorded, and printed of their channels as data output. The first expansion was in 0.01-sec increments from 0.2 sec before the peak to 0.2 sec afterward, and the second expansion was in 0.0005-sec increments from 0.02 sec before to 0.05 sec after (Figure 22). This is the form of the velocity data output that is available on BCD tapes at WES.

AIRCRAFT LOAD DATA

Load data for the B-727 aircraft were reduced both manually and by automatic data processing as described in Appendix A. Accelerometer data for the C-880 dynamic load tests were not reduced for the four dynamic load applications with this aircraft.

Figures 23-26 summarize the B-727 aircraft dynamic loads imposed upon the flexible and rigid pavement structures. The basic operational modes are represented in these figures. A gear load ratio, which is the ratio of dynamic to static load, is used to present the aircraft vertical loading conditions in Figures 23-25. The data for each operational mode are grouped and are presented at velocity values that are representative of a specific velocity range for each mode. Creep- and low-speed taxi data are plotted at the upper ends of their velocity ranges because the majority of these tests occurred in these ranges. High-speed taxi data are plotted at the upper end of their velocity range in order to represent the highest velocities used in the tests. All other modes are plotted about the centers of their respective velocity ranges.

The dynamic load spread at each mode is represented by mean values

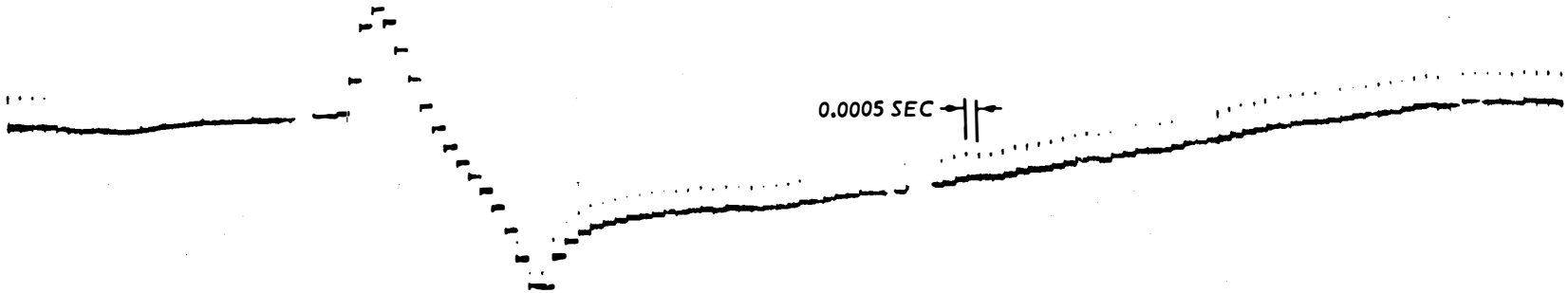

Figure 22. Reprint of Figure 21a with expanded time scale

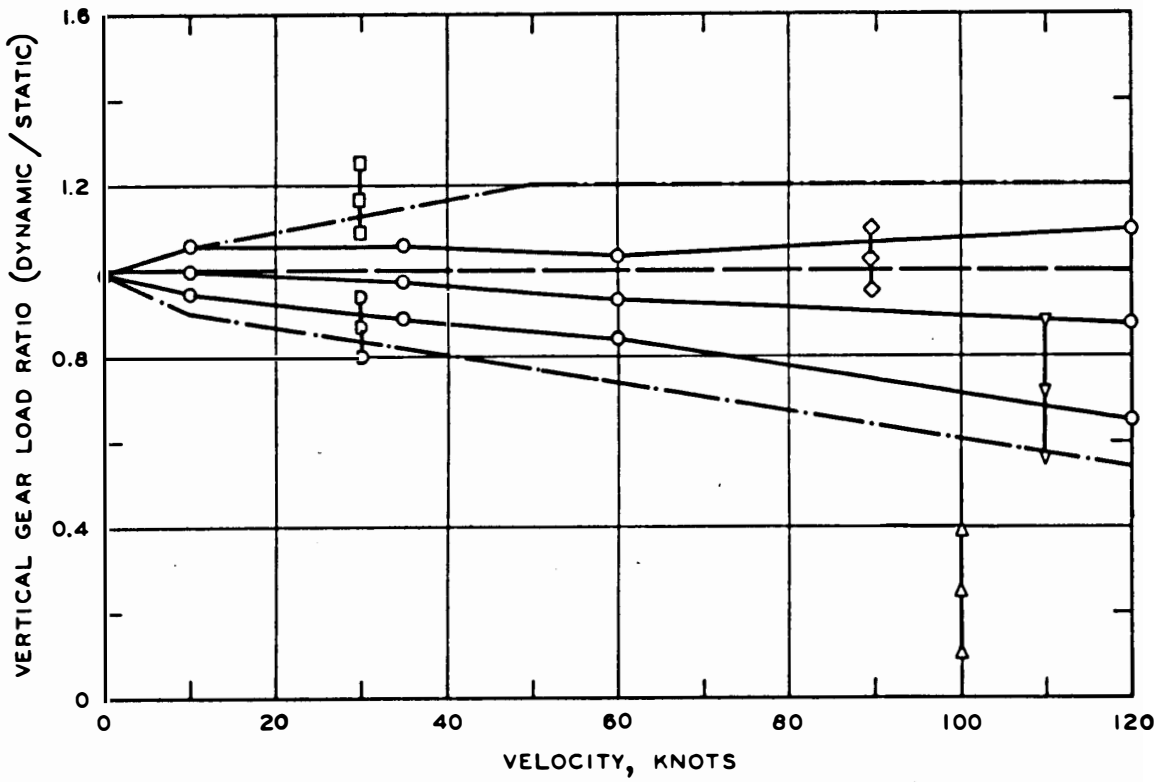

LEGEND

—·— LOAD ENVELOP FOR TAXI MODES

O STATIC LOADS AND TAXI DYNAMIC LOADS (MEAN VALUE ±1 STANDARD DEVIATION)

▽ TAKEOFF ROTATION PRIOR TO AND ON GAGES (MEAN VALUE ±1 STANDARD DEVIATION)

◇ HIGH-SPEED BRAKING WITH REVERSE THRUST (MEAN VALUE ±1 STANDARD DEVIATION)

△ TOUCHDOWN (MEAN VALUE ±1 STANDARD DEVIATION)

□ TURNING (LOAD ON GEAR ON OUTSIDE OF TURNING RADIUS ±1 STANDARD DEVIATION)

D TURNING (LOAD ON GEAR ON INSIDE OF TURNING RADIUS ±1 STANDARD DEVIATION)

Figure 23. Aircraft gear load ratios for 1972 flexible pavement tests

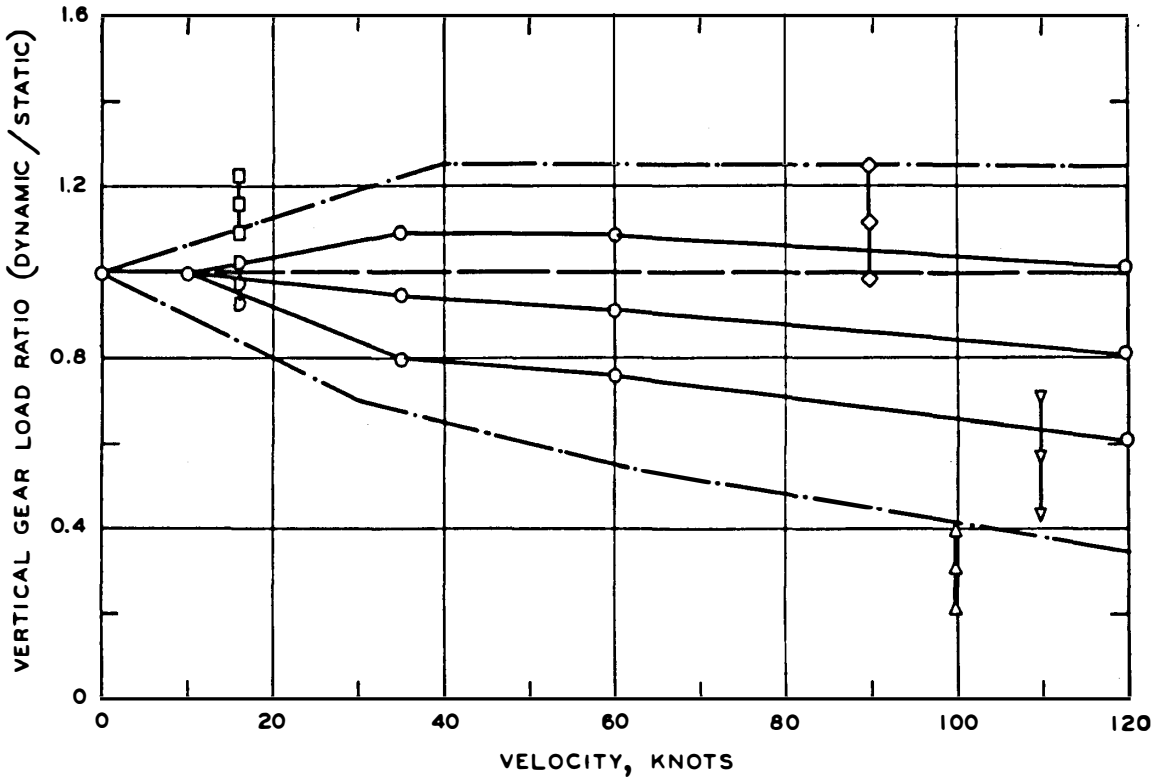

LEGEND

—·— LOAD ENVELOP FOR TAXI MODES

O STATIC LOADS AND TAXI DYNAMIC LOADS (MEAN VALUE ±1 STANDARD DEVIATION)

▽ TAKEOFF ROTATION PRIOR TO AND ON GAGES (MEAN VALUE ±1 STANDARD DEVIATION)

◇ HIGH-SPEED BRAKING WITH REVERSE THRUST (MEAN VALUE ±1 STANDARD DEVIATION)

△ TOUCHDOWN (MEAN VALUE ±1 STANDARD DEVIATION)

□ TURNING (LOAD ON GEAR ON OUTSIDE OF TURNING RADIUS ±1 STANDARD DEVIATION)

D TURNING (LOAD ON GEAR ON INSIDE OF TURNING RADIUS ±1 STANDARD DEVIATION)

Figure 24. Aircraft gear load ratios for 1972 rigid pavement tests

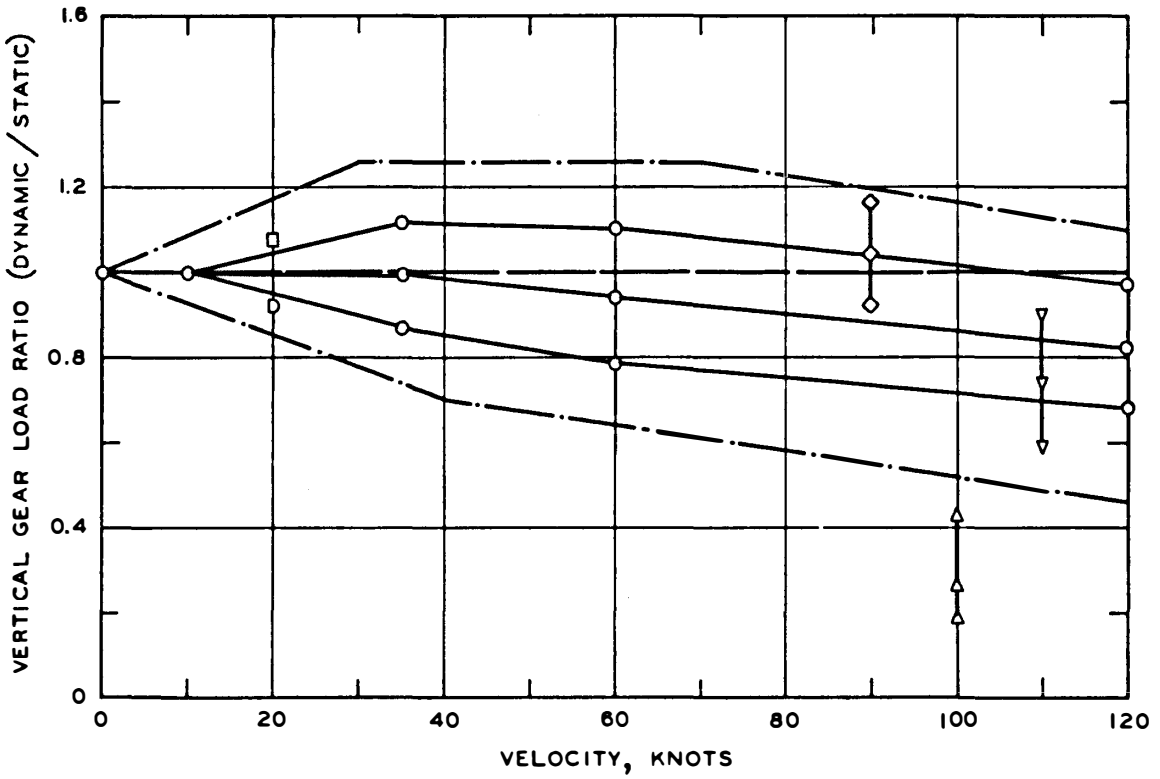

LEGEND

—·— LOAD ENVELOP FOR TAXI MODES

o STATIC LOADS AND TAXI DYNAMIC LOADS (MEAN VALUE ±1 STANDARD DEVIATION)

▽ TAKEOFF ROTATION PRIOR TO AND ON GAGES (MEAN VALUE ±1 STANDARD DEVIATION)

◇ HIGH-SPEED BRAKING WITH REVERSE THRUST (MEAN VALUE ±1 STANDARD DEVIATION)

△ TOUCHDOWN (MEAN VALUE ±1 STANDARD DEVIATION)

□ TURNING (LOAD ON GEAR ON OUTSIDE OF TURNING RADIUS ±1 STANDARD DEVIATION)

D TURNING (LOAD ON GEAR ON INSIDE OF TURNING RADIUS ±1 STANDARD DEVIATION)

Figure 25. Aircraft gear load ratios for 1974 flexible pavement tests

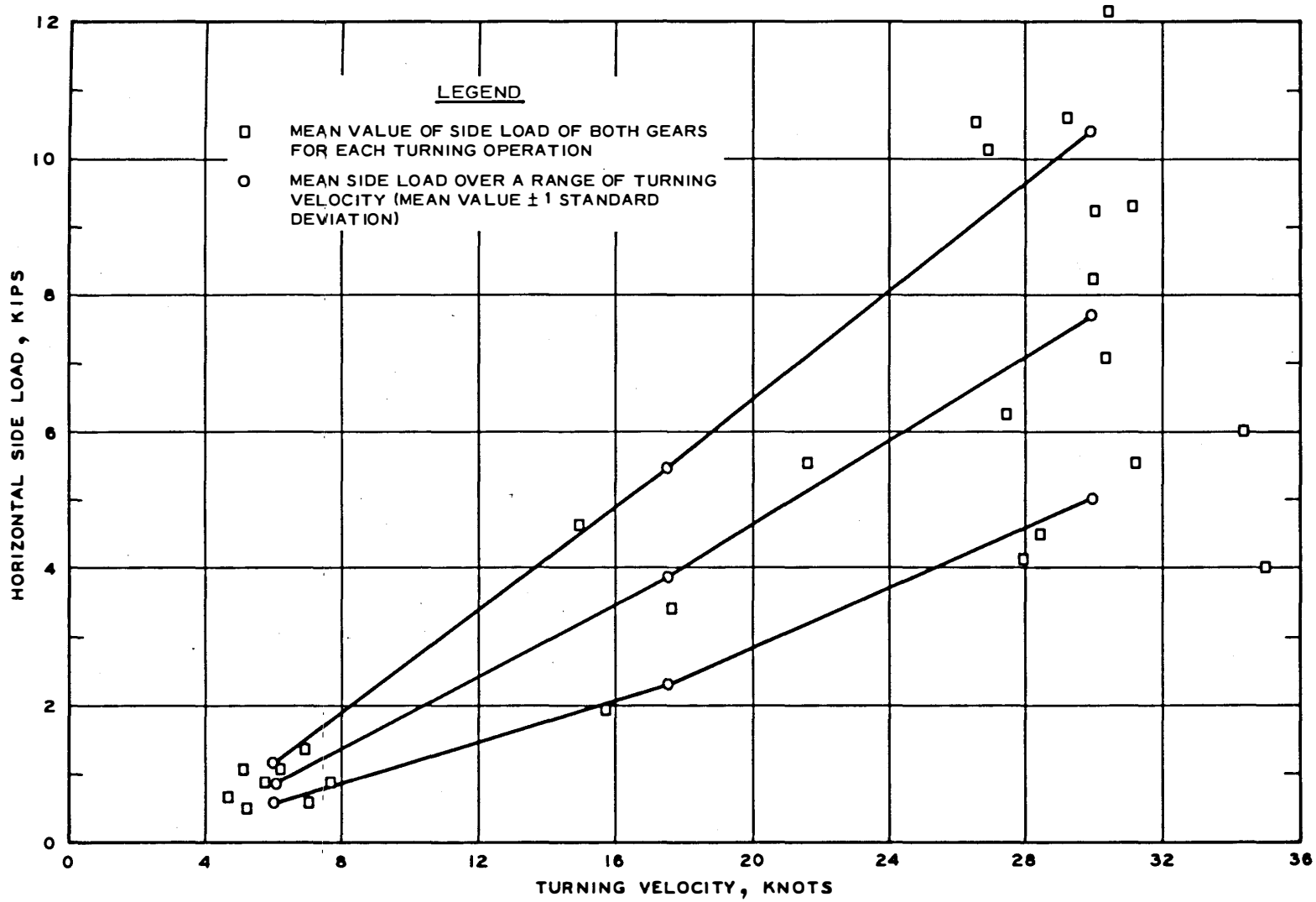

Figure 26. Horizontal load for turning operations of 1972 tests

plus or minus one standard deviation. Taxi modes are connected across the figure in order to better show their range of dynamic effects and the general decrease of the median load with an increase in taxi velocity. Also, comparisons of other operational modes with the taxi modes can be easily made with the taxi mode lines. The outer envelope represents the high and low data points for the taxi modes. The similarity between the 1972 and 1974 tests (see Figures 23 and 25) is evident.

Figure 26 shows the horizontal side thrust increase for turning operations. These results are for the 1972 tests on both the flexible and the rigid pavement test sites. Results of the 1974 tests on the flexible pavement test site are similar and within the same ranges.

For the reduction and interpretation of data described in this report, the aircraft dynamic loads were not used to normalize the pavement structure response data. Pavement structures respond nonlinearly to load changes, and preliminary studies showed that linearly normalizing the NAFEC pavement results using the aircraft data caused more variation and scatter than actually existed. In order to properly and accurately adjust the pavement structure results for the aircraft load variable, other pertinent variables (discussed in the following sections of this report) that affect the pavement structure responses and their relationships must be known and properly taken into account. If all variables and their relationships are not considered, accounting for any single one could cause erroneous results.

Table 5 presents the aircraft average wheel loads for both the 1972 and the 1974 test series. The average loads are for both static and dynamic test conditions.

INTERPRETATION OF PAVEMENT STRUCTURE RELATIVE DISPLACEMENTS AND MOTION

This section of the report presents and briefly explains a basic hypothesis of pavement and soil structure internal behavior. The hypothesis is still in its infancy, and much more work and study are necessary, particularly in the nonelastic phase (to be defined in the following discussion). Much information needed for verification and expansion was gained from the results of the tests at NAFEC. However,

Table 5

Average Aircraft Wheel Loads

Aircraft	Test	Average Vertical Wheel Load, lb	Standard Deviation, lb
B-727	1972 flexible pavement	28,073	2990
B-727	1972 rigid pavement	28,588	1971
B-727	1974 flexible pavement	30,286	2938
C-880	1974 flexible pavement	18,050	--

Note: For the 1972 and 1974 tests with the B-727 aircraft on the flexible and rigid pavement test sites, the average horizontal side load for taxiing at 45 knots was 1000 lb with a standard deviation of 100 lb.

some measure of verification of the hypothesized behavior had already been obtained on WES pavement test sections by two types of deformation measuring instruments (WES deflection gages and Bison coils) with entirely different operating principles. The NAFEC tests further verified the behavior measured by these two different instruments. Furthermore, to a certain extent, verification was obtained with a third type of instrument at NAFEC (the velocity gage) that has an entirely different operating principle.

The hypothesis may define a common characteristic that links the performance of all pavement types. In fact, inelastic behavior may be the major controlling factor of or mechanism for determining pavement performance and life since it can be the main movement (larger than elastic) occurring for static loadings and low-speed operations. Furthermore, this hypothesis explains a direct link that was observed between the behavior of WES pavement test sections under simulated aircraft loads and traffic and the behavior of actual pavements under actual aircraft loads used at NAFEC.

The NAFEC test results for relative displacement are presented in the figures in Appendix B. This appendix also details the rationale for the order in which the figures are presented. The results are discussed and summarized in this section of the report.

CHARACTERISTIC BEHAVIOR

The NAFEC test data were interpreted according to a basic hypothesis of pavement structure behavior that was conceived and derived in the WES multiple-wheel heavy gear load (MWHGL) study. The basis of the hypothesis is described in Ledbetter et al.[8]

In the MWHGL flexible pavement tests with WES deflection gages, a thorough analysis and search for a no-load reference or datum from which a gage was operating under load resulted in identification of a load- and position-dependent, moving (floating) reference for each gage. This floating reference reflects the pavement structure real behavior and is defined by the pavement rebound positions after each load application. The WES deflection gages in the MWHGL test section were located

at different depths within the pavement structure and were all anchored at a depth of 12 ft. These gages measured total pavement structure movement and not individual pavement element or layer movements.

As a simplified example of the hypothesized behavior, consider an instrumented pavement section and a loaded single wheel. The instruments measure pavement structure movement over a long gage length for a total type effect. Tests are conducted by statically loading the pavement; the following instrument responses are measured: (a) an initial no-load response (i.e., prior to loading at each gear-to-gage offset distance), (b) a load response, and (c) a final no-load response (i.e., after each loading). Now, if loads are applied sequentially, the final no-load response after loading at a given offset distance is the initial no-load response that will be measured prior to loading at the following offset distance. For each instrument, a plot of the three responses for each offset distance results in the development of three curves (an initial no-load response curve, a load response curve, and a final no-load response (rebound) curve) for the loading sequence as shown in Figure 27. (Curves of this type are presented in Ledbetter et al.[8]) A set of three curves for statically loaded offset distances can be developed following this procedure along any line at any angle to the wheel axis. Such curves can also be developed for slowly moving vehicles. If the load vehicle is moved down lines offset from and parallel to a line over an instrument, the recorded instrument responses can be broken down into initial no-load, load, and final no-load responses for each offset distance. A plot of these responses results in the three curves.

The relationships of these three response curves form the critical basis of the hypothesis of pavement structure behavior. Once the curves are obtained, they can be reduced to values of movement or displacement at the maximum and offset points. In the example curves shown in Figure 27, if the no-load reference for the sequence is taken to be the first point on the initial no-load response curve, the last point on the final no-load response curve, any point on an inclined line between the first point on the initial no-load response curve and the last point on the final no-load response curve, or the initial no-load response

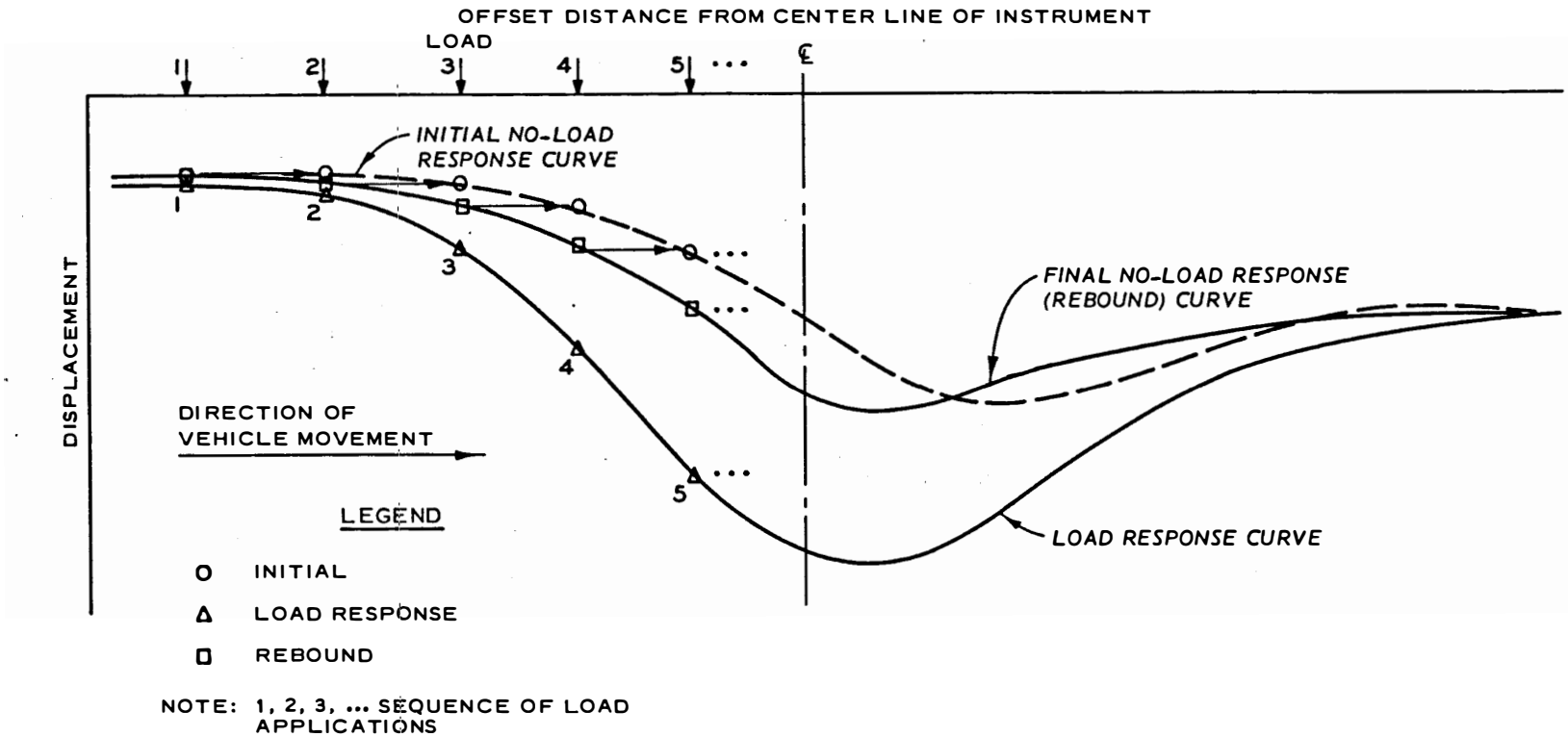

Figure 27. Typical response curves

curve itself, displacements are not symmetrical, repetitive, or equivalent at duplicate points in the pavement structure, and they are different for each reference method. Also, as can be seen in the portion of the curves to the right of the instrument center line in Figure 27 and depending on the reference method, the rebound movement can be greater than the initial movement within a given range of offset distances. In addition, the maximum displacement is not centered on the instrument.

However, if the rebound curve (the floating reference) is used as a reference for each load point, the resulting elastic displacements are symmetrical, repetitive, and equivalent at duplicate points in the pavement structure, and they are different from those obtained by any other reference method. Also, when the rebound curve is used as the reference, the maximum displacement occurs on the center of the instrument and does not lead or lag the load. For other than a single wheel when this procedure of observing the behavior is followed, duplicate elastic displacements occur on the same and duplicate instruments, at symmetrical gear load points, and under repetitive loadings.

As is obvious from the above discussion, the floating reference breaks out of the response an elastic phase of behavior. By using the rebound curve as a reference and computing the difference from the load curve, displacement values result that are entirely elastic and, in all probability, represent the total elastic phase or property of the pavement structure with respect to a given depth and load.

The initial no-load response curve is not thought to be very meaningful since it is the rebound curve shifted laterally for a sequence of loads, and reference to it causes inconsistency of data.

Static load elastic displacement in the MWHGL tests was found to remain relatively constant through thousands of load applications and with vehicle velocities up to approximately 10 knots. Indications from the MWHGL tests were that this elastic behavior should be constant up to much higher velocity values, provided no viscoelastic behavior is present, and the MWHGL tests indicated only a negligible to no amount of viscoelastic behavior.

As can be seen in Figure 27, the greatest difference between

reference methods occurs at the maximum load point (instrument center line). This difference can be as large as the elastic value calculated from the rebound curve as shown in the MWHGL tests. However, the difference is a function of the pavement structure strength, total load, number of wheels, vehicle velocity (rate of load application), and load history. (Load history means the magnitude of the previous load and the offset position with respect to a point in the pavement structure.) In the MWHGL tests, the difference in values obtained using the different reference methods increased with an increase of load and number of wheels, and it decreased with an increase of pavement structure strength and rate of load application.

The primary subject of the previous discussion has been the elastic phase of behavior, and the remaining phase has not been defined or discussed in detail. For the MWHGL flexible pavement tests, the only displacement data were from WES deflection gages. There was a possibility that the floating reference observed in these tests was a function of the instruments and not real pavement structure behavior. Thorough instrument and electrical system checks were therefore made, and they indicated the validity of the measurements. However, there were no other movement measuring instruments in the test section to verify the behavioral patterns. Even though the behavioral patterns could have been caused by the instruments, the elastic response derived from the behavioral patterns was believed to be correct. This assumption was based on the previously discussed elastic response characteristics. Results of tests of subsequent WES pavement test sections have verified the behavioral patterns.

The remaining behavioral phase will be referred to as "inelastic." This inelastic behavior is not a permanent nonrecoverable displacement; it recovers as a function of load history. Inelastic movements are upward or outward as well as downward or inward and can be larger than the elastic movements. The inelastic behavior does not appear to be related to measured total pressures but could possibly be explained by a deformation law. This behavior has not been proven to be truly plastic in the classical sense, and for this reason it is of a pseudoplastic-type nature that will become more clear in the following discussions.

This inelastic behavior has been noticed in pavement tests since the 1940's. However, the erratic behavior as indicated by instruments has always been described as an ambiguous phenomenon due possibly to unstable (varying or changing zero) instrumentation or has simply been assumed to be meaningless. This inelastic behavior has led to testing procedures in which the pavement has been loaded at a point repeatedly (conditioning) until instruments "become stable" before recording instrument responses. (Conditioning makes the inelastic response approach zero, as discussed in the following paragraphs.) While this type conditioning temporarily eliminates the inelastic movements, it is not really representative of behavior under actual traffic loading, since traffic is randomly distributed and approaches a normal distribution with time.

The nature and behavior of the inelastic phase of movement has not been defined, fully described, or utilized in the past. It is real and is believed to be an important part of pavement structure response. In analysis and interpretation of instrument response data from nonconditioned pavement structures, the inelastic behavior can be of a critical nature and should be considered. For random or distributed pavement loadings (which represent real loading conditions), instrument responses cannot be fully or correctly analyzed unless the inelastic behavior is fully recognized and utilized. The following discussions are believed essential to this report in describing the inelastic phase of movement and its behavior and considerations in the analysis of the NAFEC pavements under load tests. In investigating pavement response to dynamic loads, the inelastic behavior is at least as important as the elastic behavior.

Inelastic behavior in this report is a material response that is characterized as follows:

a. If a material is loaded so that deformation is induced which does not completely recover and the material is never loaded again, the residual deformation is permanent (never recovers).

b. However, if the material is loaded again in the same or another location, movement of the above residual deformation may occur that may change in direction and/or magnitude and result in a new residual deformation that is again subject to this definition.

Inelastic displacement can be determined for a single load application or for a sequence of load applications. In Figure 27, the difference between the initial no-load response and rebound curves at any point is the inelastic displacement for that load point. However, if the reference is taken to be the highest point occurring for a sequence (on the left side in Figure 27), the inelastic displacement at any point may be much larger that that determined as described above. As can be seen in Figure 27, inelastic displacement occurs in both upward and downward directions, depending on the load history.

Inelastic behavior includes an increment of permanent displacement. For a full sequence of load applications (from an offset of no-load influence on one side of an instrument in the pavement structure to an offset of no-load influence on the opposite side), these increments of permanent displacement accumulate and can be determined. The permanent displacement for the sequence in Figure 27 is the difference between the highest point occurring and the final rebound point of the sequence. However, according to the definition, this is the permanent displacement if and only if another load application or sequence is not applied causing an upward movement recovering part of it and changing the permanent to inelastic displacement.

In WES test section studies subsequent to the MWHGL study, movement measuring instruments (Bison coils) that operate on an entirely different principle from that of the WES deflection gage were used. Bison coil measurements verified the behavioral patterns indicated by the WES deflection gages in the MWHGL tests, and they also extended the knowledge of the character of the behavioral phases. The Bison coils gave internal responses for individual pavement structure elements or layers, whereas the WES deflection gages gave responses for the total pavement structure.

In addition to verifying the inelastic and elastic phases of behavior, the Bison coil responses to static load showed that elastic expansion or swell was occurring internally in the pavement structure elements with respect to gear-to-gage offset. Recorded vehicle traffic also showed that elastic expansion was occurring at lateral offset

distances as well as in front of the wheels. This additional elastic phase of behavior needed to be verified not only in other pavement structures but with other types of instruments, and verification was obtained in the NAFEC tests.

Additional information was also gained concerning the inelastic phase of behavior in the subsequent WES test section studies. Bison coils were recorded for a majority of the applied traffic, and these recordings showed that, for a given sequence of load applications with a given wheel configuration and load, the inelastic response had a specific form or pattern and was cyclic with the traffic pattern. The inelastic response was nearly constant under traffic until failure (as defined by WES for its test sections), at which point it increased drastically. However, the elastic response remained nearly constant even past failure. Similar behavior had also been observed in the static load tests of the MWHGL study before, during, and after traffic. Information concerning this behavior at failure, however, is very limited and not conclusive, and much more information needs to be obtained in this subject area. This trend at failure has been discussed because it concerns the inelastic behavior specifically, has been indicated by data, and could be very important in defining a mechanism or mechanisms of failure.

Inelastic behavior is dependent on magnitude of load, number of wheels, pavement structure strength, and rate of load application. It shows the effects of temperature in highly plastic, temperature-dependent materials, and it is also highly dependent on the load history. For repeated loadings at the same point on a pavement structure not near failure (same as conditioning), the inelastic response approaches zero after only a single or a few load applications, whereas the elastic response remains constant with load applications at the same point. For a sequential static or dynamic loading pattern, the inelastic behavior is consistent. However, if loading is random, the inelastic behavior may be erratic, depending on the load history and structure strength. Also depending on load history and structure strength, the inelastic phase at a given point may require more than one load application for completion.

Under relatively constant conditions, an elastic response is obtained by separating displacements into elastic and inelastic that is independent of inelastic behavior, no matter what it is, and that is symmetrical, repetitive, and equivalent at duplicate points in the pavement structure. Inelastic displacement may range from a magnitude of zero to many times the elastic response, depending on the load history and rate of load application. Now, as can be seen from the above discussion, a specific total (elastic plus inelastic) movement or displacement is impossible to define except for a single load application in the load history of a pavement structure or for high rates of loading at which the inelastic response is essentially zero and only elastic response is occurring. At any point in time of the load history, the magnitude of total movement can range from the elastic response value to many times this value. Because of this behavior, a total displacement value is completely meaningless and in fact incorrect for the conditions under which inelastic behavior is active. Due to the nature of inelastic behavior coupled with the influence of random and distributed traffic or static loads acting over a pavement surface, a pavement structure is continuously pulsating upward, downward, and laterally. (Liken the behavior to that of a ball of putty being molded.) The pavement structure is plastic to the extent that it is stable at various levels to which it might be worked under loaded conditions, and it exhibits elastic behavior at each of its changing states of inelasticity with the elastic behavior operating from the floating reference.

The response of a pavement structure to a loaded vehicle moving on its surface, therefore, can now be defined. Three-dimensional wave forms of the type shown in Figure 27 move through the structure. Along an axis in the direction of vehicle motion, a wave form moves with the vehicle; along a perpendicular axis, another wave form sweeps through the structure. A given point in the pavement structure responds to both of these wave forms, and the magnitude of the effect is a function of the offset distance perpendicular to the direction of vehicle motion. As the vehicle applies distributed or random traffic, a given point rides both of these wave forms from one end to the other. The point

completely rides a parallel wave with each passage, but the perpendicular wave takes longer to ride depending on the pattern of traffic. If a normal distribution of traffic is applied, the perpendicular wave form is continuously repeated at a given point in a cyclic manner. Repetitive loading along a traffic line results in repetition of elastic but not inelastic response of a point at the place on the wave forms. The wave forms and curves in Figure 27 are the ones that move continuously through the structure for a single wheel; however, the behavior is exactly the same for multiple wheels, though much more complicated due to interaction of the wheels and the effect of having more than one gear maximum load point.

The relationships of various vehicle loads, number of wheels, and structure behavioral patterns are not linear. In fact, they are very nonlinear, increasing with both load and number of wheels. Work concerned with the characteristics of the elastic phase of behavior, as derived from the hypothesis, can be found in References 8-10. These reports include specific work with the principle of superposition and test section data.

This general discussion of a behavioral hypothesis has now led to the point that the NAFEC tests need to be considered. Based on the WES test section results, the following various behaviors would have to be studied to determine the dynamic load test results:

a. Inelastic phase: Can the response measured in previous studies be verified? How does inelastic response vary with the rate of load application and temperature?

b. Inelastic wave form: Can its presence be verified? How does it behave?

c. Elastic (including viscoelastic) phase: Can the response measured in previous studies be verified? What is the nature of its constancy with changes in the rate of load application and traffic?

d. Elastic expansion or swell: Can its presence be verified? How does it behave?

e. Differences in total structure and layer responses: Can they be verified?

NAFEC Total Pavement Structure Behavior. Figure 28 shows typical static load test results for a WES deflection gage measuring vertical

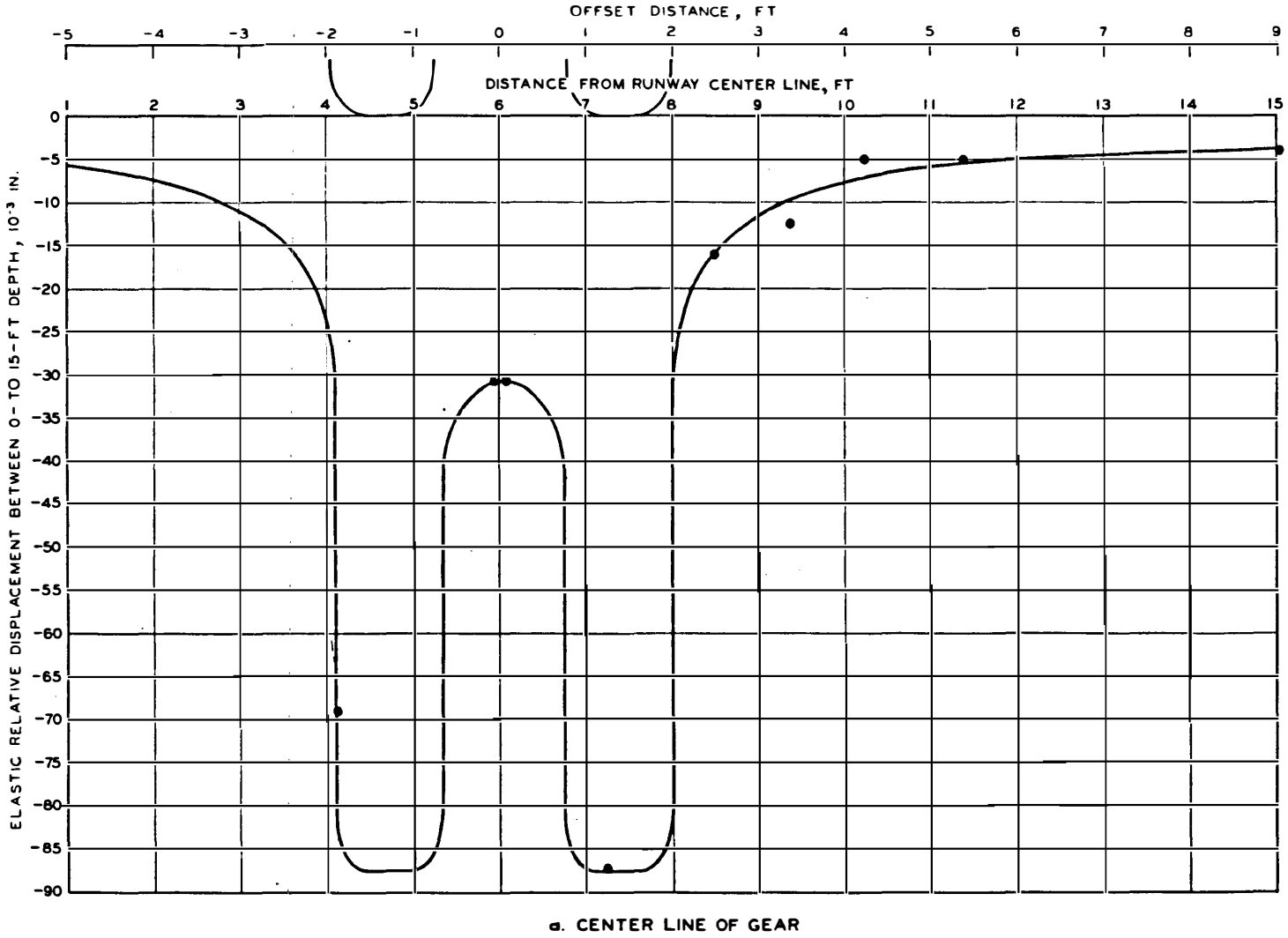

Figure 28. Typical static load test results measured with WES deflection gage (0- to 15-ft depth)

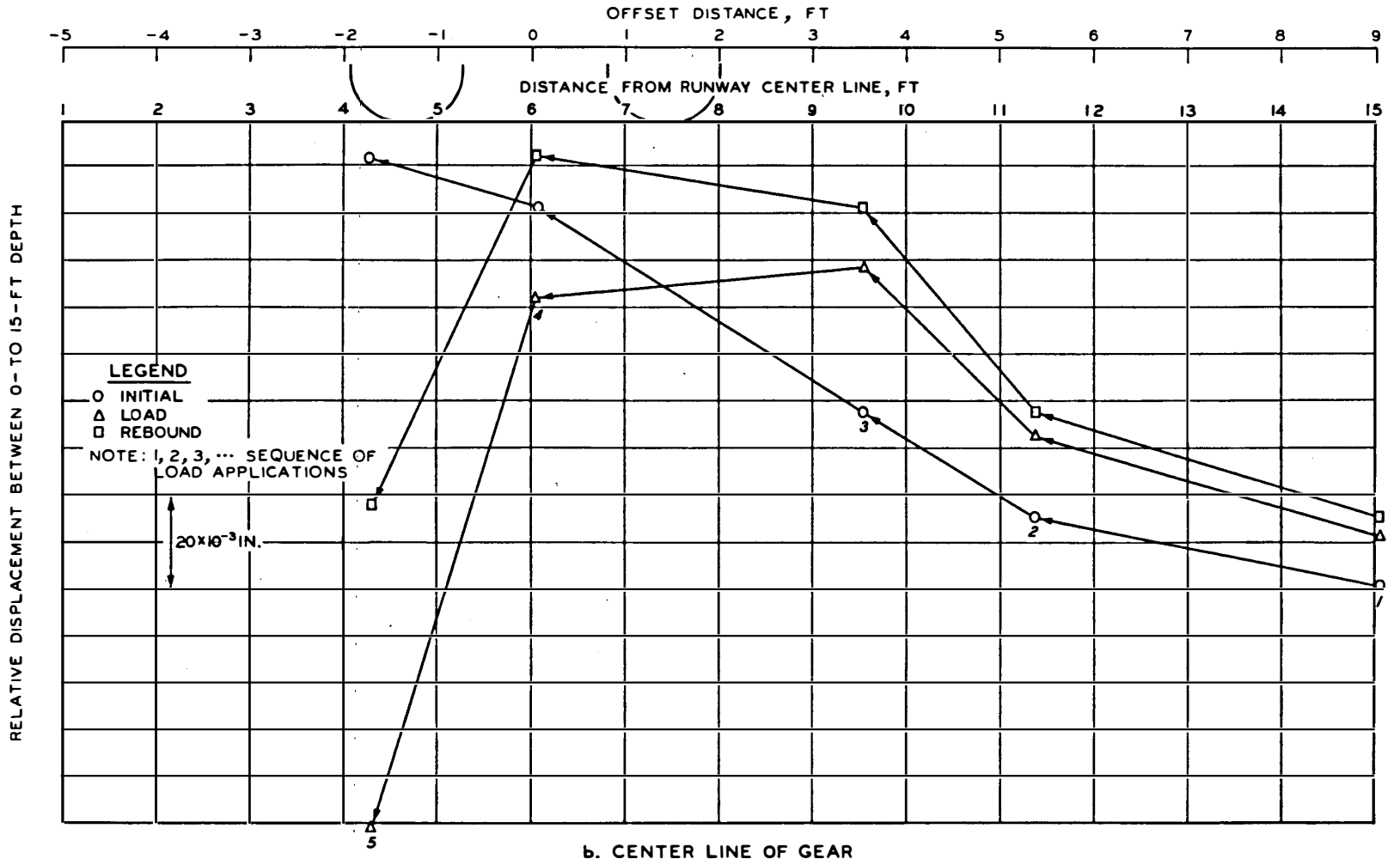

Figure 28. (Continued)

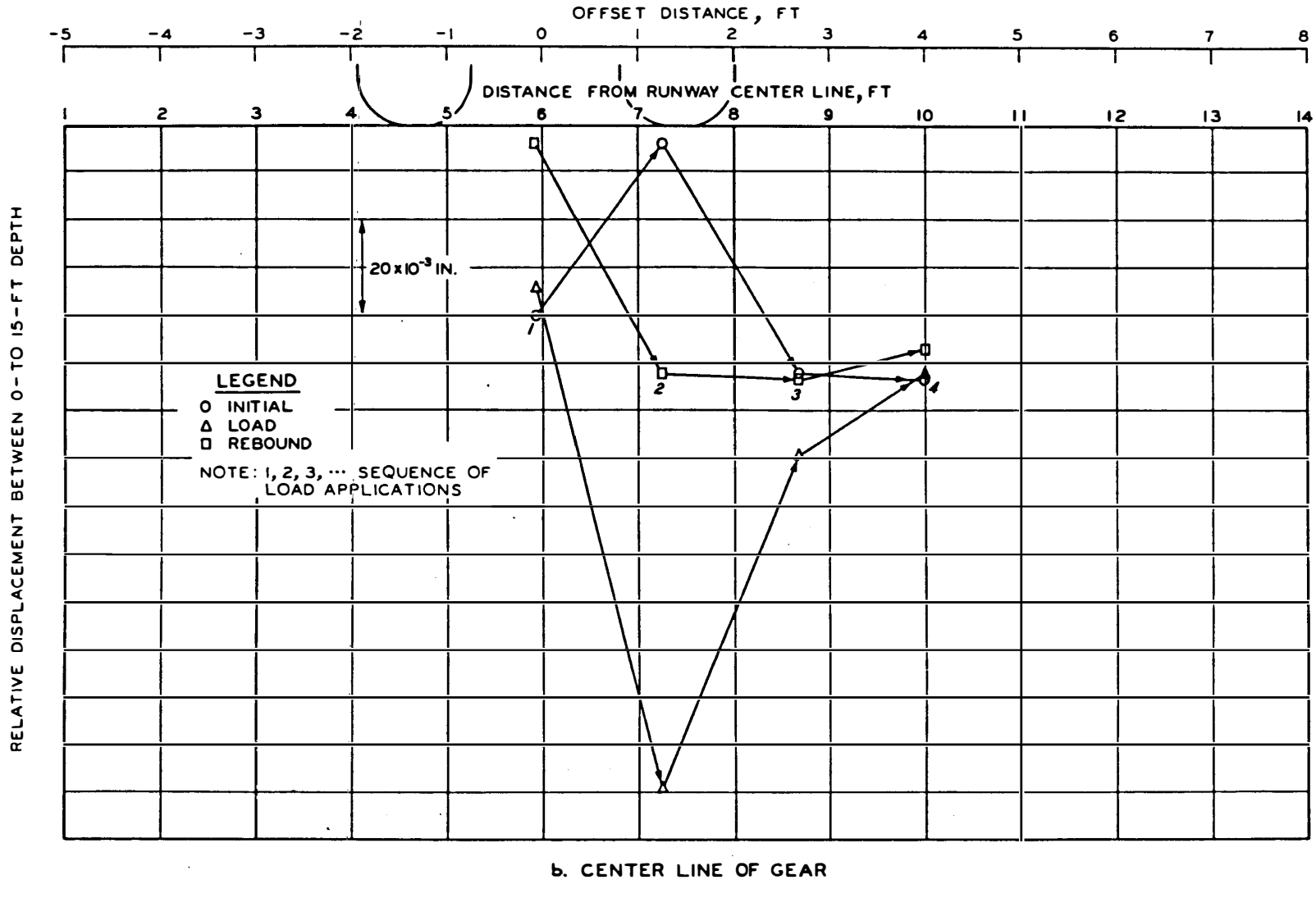

Figure 28. (Continued)

movement between the surface and a depth of 15 ft. These tests were conducted on the flexible pavement test site in 1974 with the B-727 aircraft. Offset distances were determined visually. Because the time allowed on the runway during dynamic tests normally was not sufficient to make precise measurements, offset distances consequently have a variation of about ±2 and ±3 in. for all static and dynamic load tests, respectively. In the static load tests, the aircraft was left in place for at least 5 min prior to recording measurements for the 1972 tests and for at least 10 min prior to recording those for the 1974 tests. These time periods also elapsed for rebound (final no-load) recordings. The times were determined prior to testing by timing static loads and ascertaining the time for approximately 95 percent of the movement or deformation to occur.

Figure 28 has two parts, a and b. The results shown in this figure are plotted along a line through the gear center point and perpendicular to the longitudinal axis of the aircraft. The manner of presentation gives the appearance that the aircraft was stationary and the gage itself was moving to various offset distances from it; however, this is not the case. Figure 28a shows the elastic response (derived from Figure 28b) as determined by the previously discussed hypothesis. Figure 28b shows two sets of results, one for each of two separate sequences of loadings. These load sequences were conducted with about a day of elapsed time and 23 dynamic load operations (including creep-speed taxies) occurring between them. For each load application, the measured responses in terms of initial, load, and rebound values are plotted. All like points are connected by arrows across this part of the figure in order to show the sequence of loading. No zero point is shown on the displacement axis in Figure 28b because, according to the hypothesis, the reference is floating. However, the scale of movement is given. Two scales are given on the abscissa axis for clarity.

In Figure 28b, the behavioral patterns of upward and downward movement are obvious. Also obvious is the upward and then downward movement of the load curve. The floating reference is defined by the rebound points and lines. By computing for both sequences the differences

between the load and rebound values and by following the directions of movement, the elastic responses for Figure 28a are obtained. Notice the consistency of the elastic responses regardless of the loading sequence, of the loads between sequences, or of the upward and downward movement. A small amount of variation in the static load results was caused by offset distances not being exactly determined, by variations in the pavement structure, by responses being affected by the load history, and by variations in the electronic system.

Now, by computing for both sequences the differences between the initial and rebound values, the inelastic response for each applied load is obtained. Notice that the inelastic response goes in both upward and downward directions and varies between the two sequences. For a given load sequence, the inelastic response can be calculated by taking a reference value anywhere that appears appropriate. As can be seen in Figure 28b, the largest inelastic response for an individual point is approximately equal in magnitude to the corresponding elastic response.

Figure 28b presents the actual measured movements as if they were plotted in instrument voltage output with the conversion factor given. The load sequence is specified; therefore, any desired method of movement reference and data interpretation can be chosen. The rebound points represent the actual positions of the pavement surface at the gage center line after each applied load. If surveying instruments had the required accuracy and precision, they would show the same patterns as those in Figure 28b at a given point for a load sequence. In other words, the surveying instruments would show changing elevations at a given point as a function of the load sequence. Another important fact that is obvious is that measuring techniques external to the pavement structure cannot possibly determine the patterns shown in Figure 28 in the vicinity of the wheels. External measuring techniques can determine the offset basin shape, but an extrapolation of the shape beneath the wheels would certainly be in error.

Figure 29 shows typical creep-speed taxi test results of the same WES deflection gage as above for the 1974 tests. The results are presented in the same manner as previously discussed. The static load

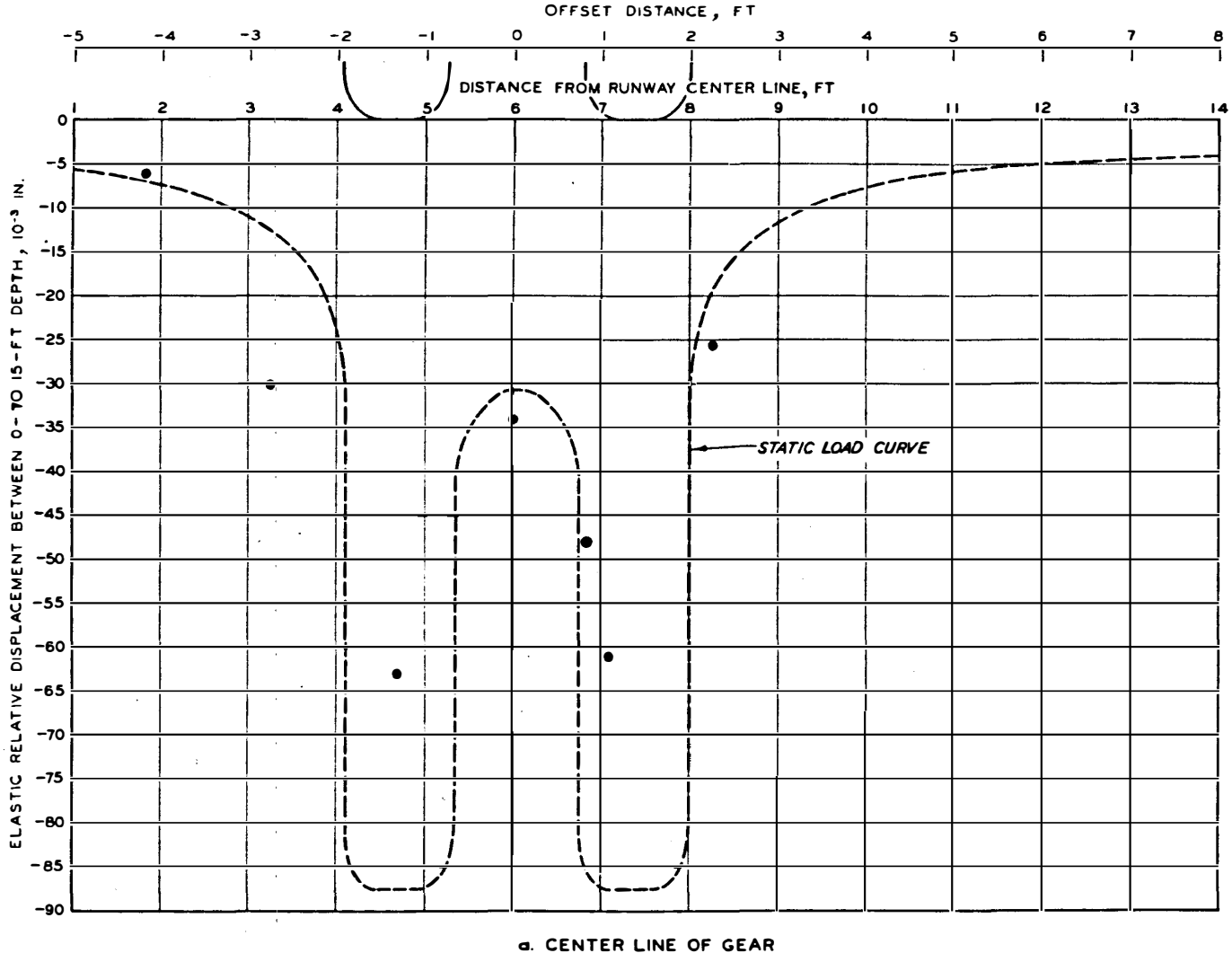

Figure 29. Typical creep-speed taxi test results measured with WES deflection gage (0- to 15-ft depth)

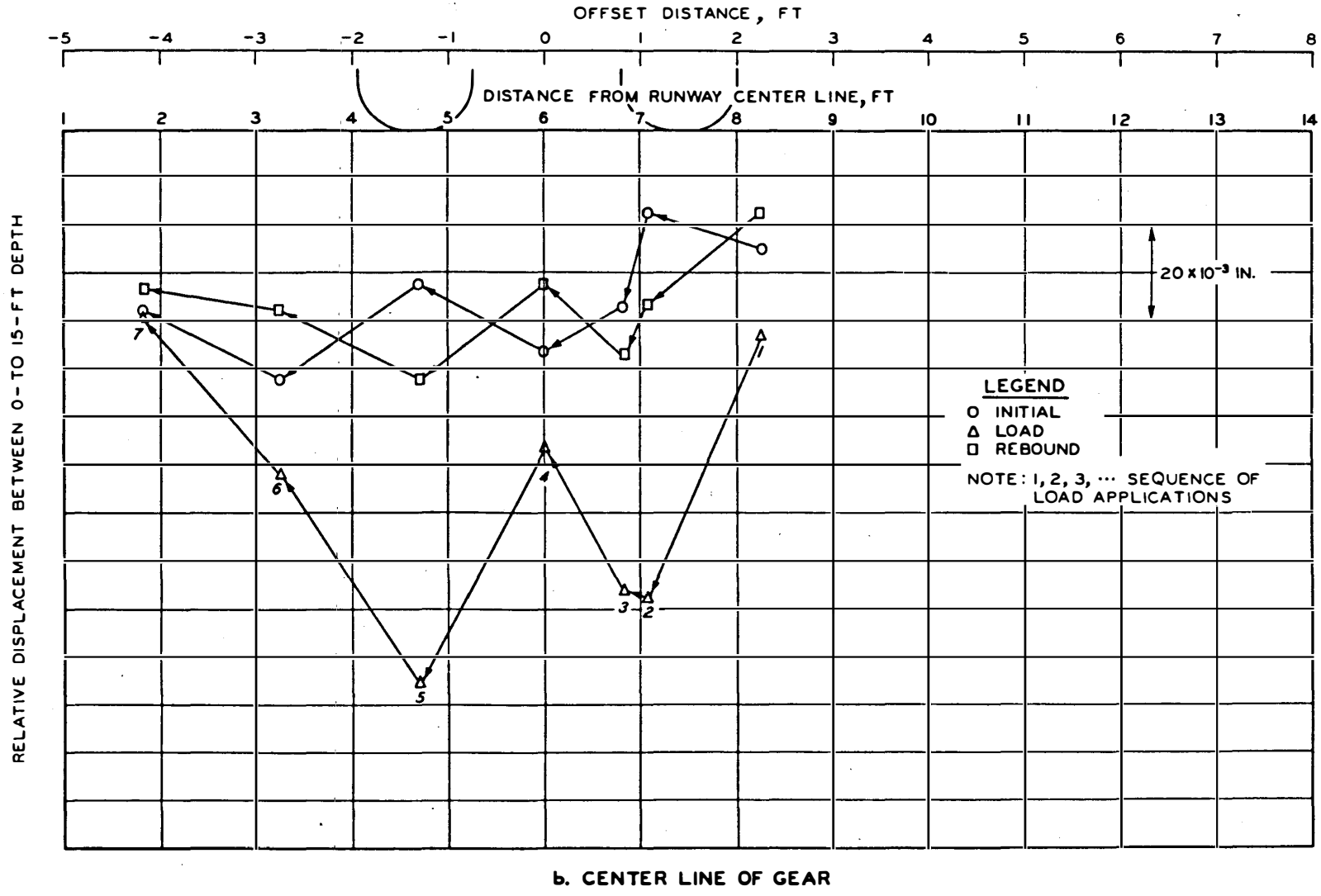

b. CENTER LINE OF GEAR

Figure 29. (Continued)

test curve of Figure 28a is superimposed on the results in Figure 29a to enable a comparison of elastic results for the static load test with those for the creep-speed taxi test. As can be seen, there is a reduction of maximum vertical elastic displacement. This reduction is believed to be a viscoelastic effect which will be discussed under "Test Results." The slight variation in the results was caused by the previously discussed variables; however, there is more variation in these results due to the offset distances being even less exactly determined for the moving aircraft (as discussed previously). For the creep-speed taxi mode, there is also a reduction in inelastic response (Figure 29b). Again, the inelastic behavior is affected by the rate of load application and decreases to zero at high speeds or rates of load application. This effect is also discussed under "Test Results."

Figure 30 shows the actual analog recordings for the creep-speed tests from which the results in Figure 29 were obtained. For each load application, the elastic responses were taken from the final no-load traces (projected back), and the difference between the initial and final no-load traces is shown. The difference between the initial and final no-load points is the inelastic response for each load application. It can easily be seen in Figure 30 that the magnitude and direction of movement of the inelastic response are controlled by the gear-to-gage offset distance. The change in direction of the inelastic response and the upward movement at the various offsets and in the immediate gage vicinity are also evident. Noticeable too are the symmetry and repetition of the elastic and inelastic responses for the load sequence. Inelastic response is symmetric and repetitive for a given symmetric or orderly load sequence. In Figure 30, the final no-load trace for each event is the initial no-load trace for the following event. One other noticeable fact shown in the figure is the odd shaped, unsymmetrical load response; this will be discussed in a following section dealing with pavement structure vertical velocity.

Figure 31 is the inelastic wave form corresponding to the creep-speed taxi tests illustrated in Figures 29 and 30. The results plotted in Figure 31 came from the inelastic response to each individual load

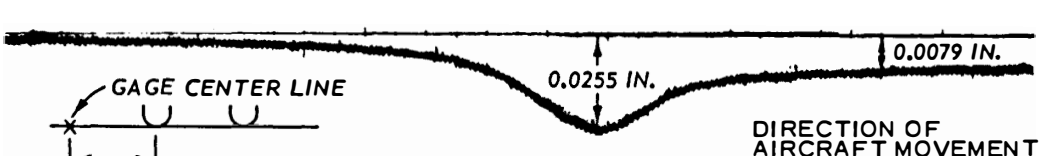

a. 10.5-IN. OFFSET

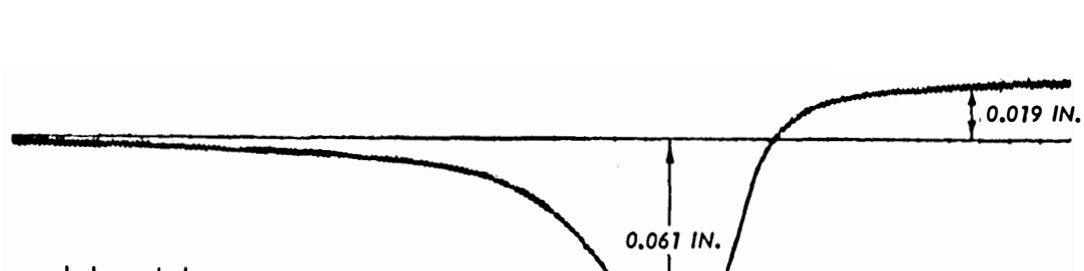

b. 0-IN. OFFSET

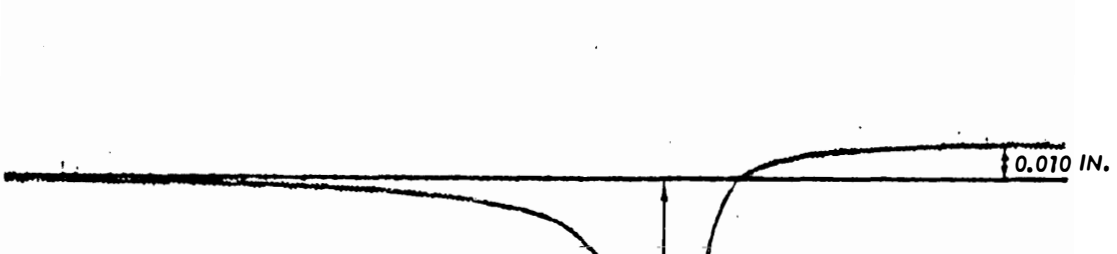

c. 4-IN. OFFSET

Figure 30. Analog recordings for creep-speed taxi tests from which results in Figure 29 were obtained

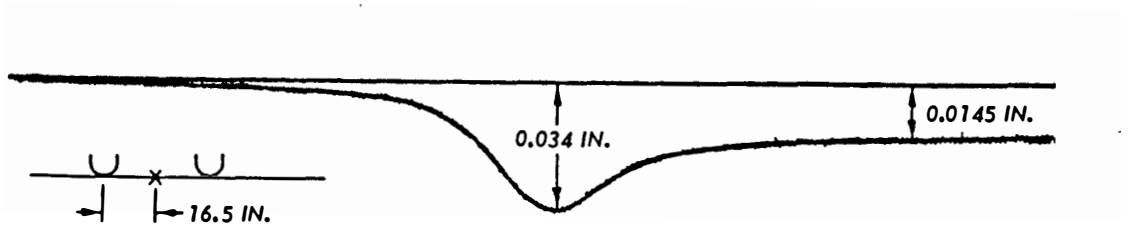

d. 16.5-IN. OFFSET

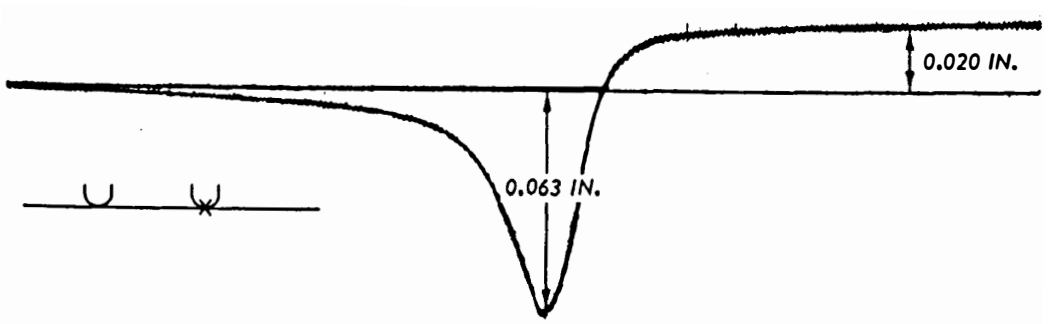

e. 0-IN. OFFSET

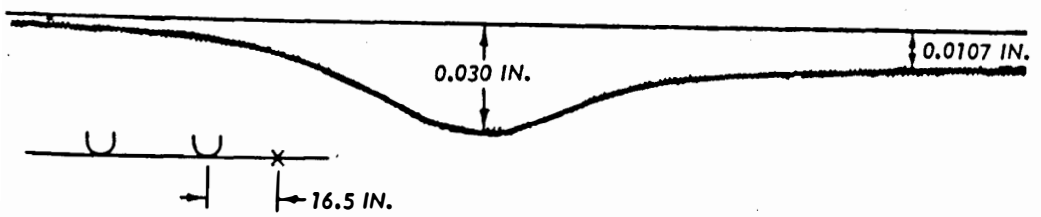

f. 16.5-IN. OFFSET

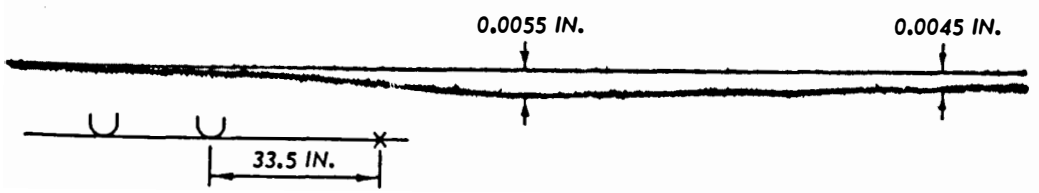

g. 33.5-IN. OFFSET

Figure 30. (Continued)

application. The symmetry of the wave form for the creep-speed taxi sequence is evident. For any load sequence and rate of application similar to those in the creep-speed taxi sequence, this is the inelastic wave form that repetitively sweeps through the pavement structure. Figure 31 shows the inelastic response per load application at any offset position; it does not give the accumulated response for a sequence of loads. If a single position is loaded sequentially, the inelastic wave form will not indicate the response since, as stated previously, inelastic response approaches zero after only a single or very few load applications.

In order to clarify the previous discussion concerning inelastic behavior and wave forms, Figure 32 has been developed. Figure 32 consists of a base sheet and a series of clear overlays with the inelastic wave form of Figure 31 on them. The overlays are numbered "1" through "7," and they correspond to the sequence of creep-speed taxies illustrated in Figures 29 and 30. Each offset position is indicated on the overlays by a point on the wave. Movements are shown for a point (indicated by an "X" on the base) on the pavement surface.

Place overlay 1 on the base and align the cross below the point on the overlay with the X on the base. Align the top line on the overlay with the side mark numbered "1" on the base. Now, the resulting figure shows the inelastic movement actually occurring at this point when the aircraft rolled past it. Place overlay 2 on top of overlay 1. Align the cross on overlay 2 with the point on the wave of overlay 1 and the top line on overlay 2 with side mark 2 on the base. The resulting figure shows the actual additional inelastic movement occurring at the point due to the aircraft rolling past at another offset position.

Continue placing overlays and aligning them as described above. The resulting figures show the actual wheel positions for the sequence of creep-speed taxies, the actual inelastic wave sequence, and the actual inelastic movement at any pavement surface point for each load application. A similar series can be constructed for the elastic phase of behavior.

Illustration, in this volume, of the total pavement structure

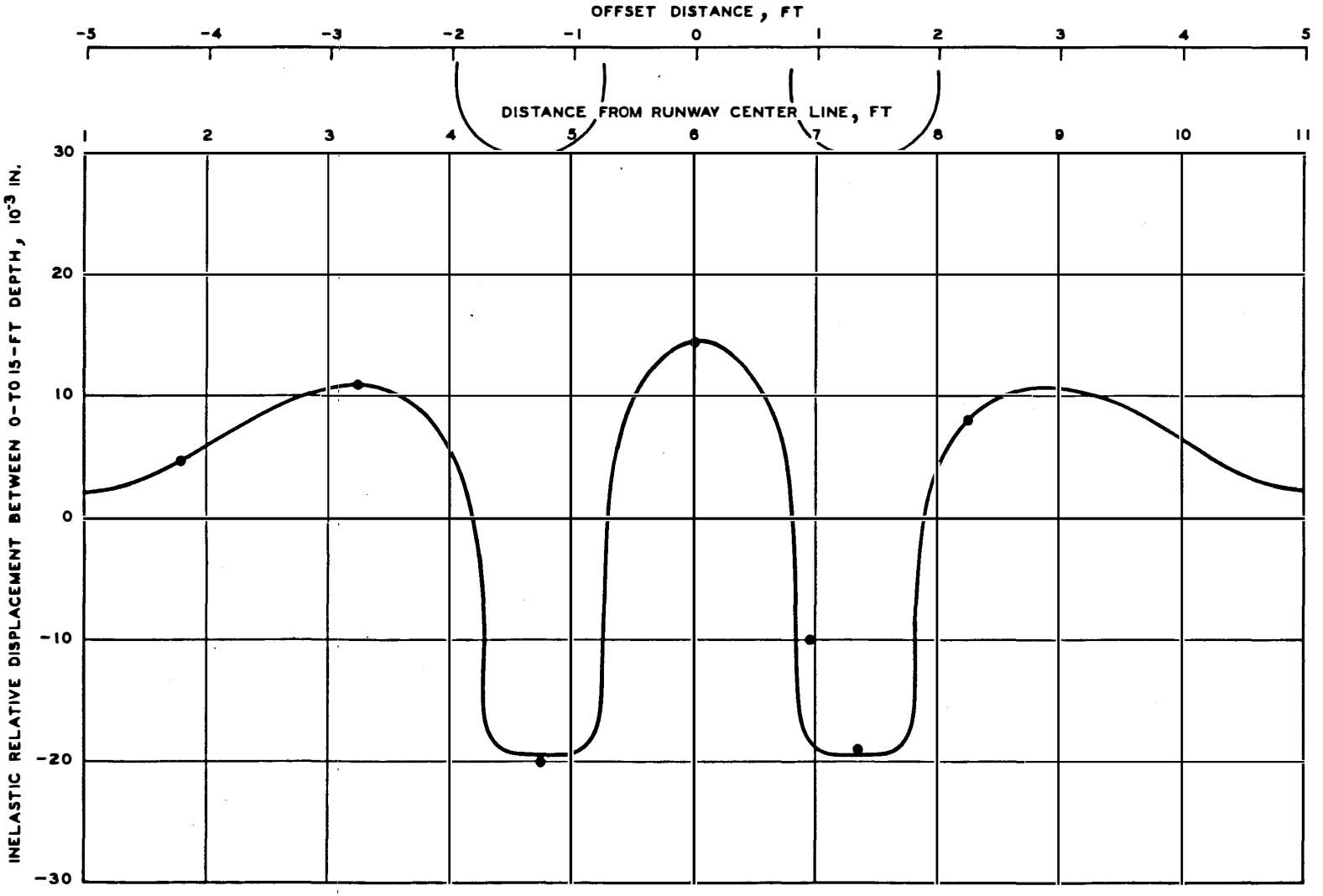

Figure 31. Inelastic wave form for creep-speed taxi tests illustrated in Figures 29 and 30

Figure 32 is in the envelope inside the back cover.

behavior for the rigid pavement tests was not felt necessary (Appendix B shows the behavior). The WES deflection gages were anchored to the concrete slabs and at a depth of 15 ft, and slab behavior under static loading was almost entirely elastic with only a negligible amount of inelastic response occurring directly beneath the aircraft wheels. However, the magnitude of the inelastic response did approach the instrument response variation and was therefore not definite. Inelastic behavior is possible in a rigid pavement structure because the slab can stay slightly bent under its own weight after a direct load application. The foundation materials of the rigid pavement test site did show inelastic behavior, and this will be discussed in the following section. Under creep-speed taxies, the slabs responded fully elastically and the possible inelastic response was of zero magnitude.

NAFEC Individual Pavement Structure Element Behavior. Figure 33 shows typical static load test results for Bison coils measuring vertical relative displacement within the flexible pavement structure for a depth of 9 to 18 in. These tests were conducted on the flexible pavement test site in 1974 with the B-727 aircraft. (Previous remarks concerning test methods and figure parts a and b also apply to this figure.) This figure is also representative of the response of rigid pavement elements (as can be seen in Appendix B) with the exception of the movement between the wheels. The rigid pavement elements do not show individual wheel effects below the concrete slab.

Of importance in this figure is the elastic expansion that occurred outside of the wheel vicinity. This behavior (as can be seen in Appendix B) occurred in both flexible and rigid pavement elements and also in all the dynamic load tests. The elastic expansion of the elements is in contrast to the total pavement structure behavior illustrated previously. Also shown in Figure 33 is the inelastic behavior common to both flexible and rigid pavement elements (as seen in Appendix B).

No static load tests were conducted to measure the movements ahead of or behind the wheels. However, the elastic characteristic shown in Figure 33, results of WES test section studies, and logic imply that elastic expansion should also occur ahead of and behind the wheels.

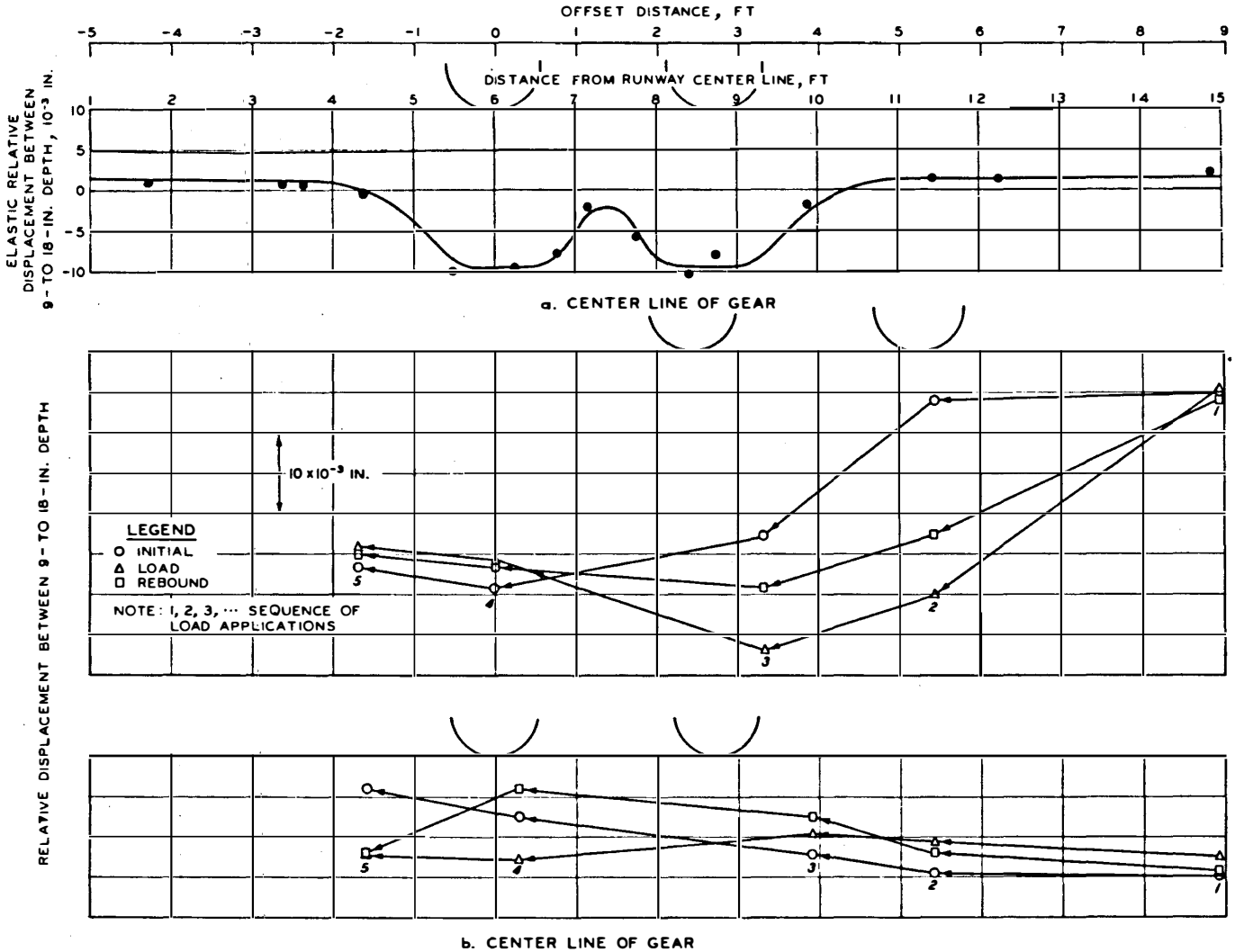

Figure 33. Typical static load test results measured with Bison coils (9- to 18-in. depth)

In the dynamic load tests, elastic expansion did occur ahead of, to the sides of, and behind the moving wheels in both pavement types (as seen in Appendix B). The measured expansion ahead of the wheels will be referred to herein as a "bow wave." Bow waves are believed to be generated by the elastic mechanism observed in the static load tests.

Once a bow wave has been generated for a moving wheel, it is probably modified by forces associated with the rolling wheel. A typical example of a bow wave is shown in Figure 20 by the first peak. Figure 34 shows computer-reproduced typical recordings of creep-speed taxi vertical responses measured by Bison coils. These came from the 1974 flexible pavement tests. Figure 34a is for the immediate vicinity of the wheels and shows the responses of the elastic bow wave, the elastic displacement beneath the wheels, and the inelastic displacement. Figure 34b is for the area outside the wheel vicinity and shows the elastic expansion and inelastic response. The elastic expansion along the wheel axis is shown here to be the largest movement; however, this is not always true. In some cases, the bow wave is larger than the expansion along the wheel axis. Outside the wheel vicinity, the bow wave and expansion are not two separate occurrences because they tend to be a common swell that may peak before or at the wheel axis. (The bow wave peak magnitudes are presented in Appendix B as part c of the figures.)

The previous discussions have dealt with two types of vertical response, those for the total pavement structure and those for the individual pavement structure elements. Both types have elastic and inelastic behavioral phases, but the two types of responses are different in that the elements show elastic expansion while the total pavement structure does not. The total pavement structure elastic displacement was in the form of a downward basin shape, while the element displacement (outside the wheel vicinity) was in the form of upward elastic expansion. The total pavement structure downward elastic movement was larger in magnitude than the sum of the element upward elastic movements; therefore, the resultant elastic movement was downward. The elastic response that was measured by the WES deflection gages was this resultant downward elastic movement. This effect will be discussed

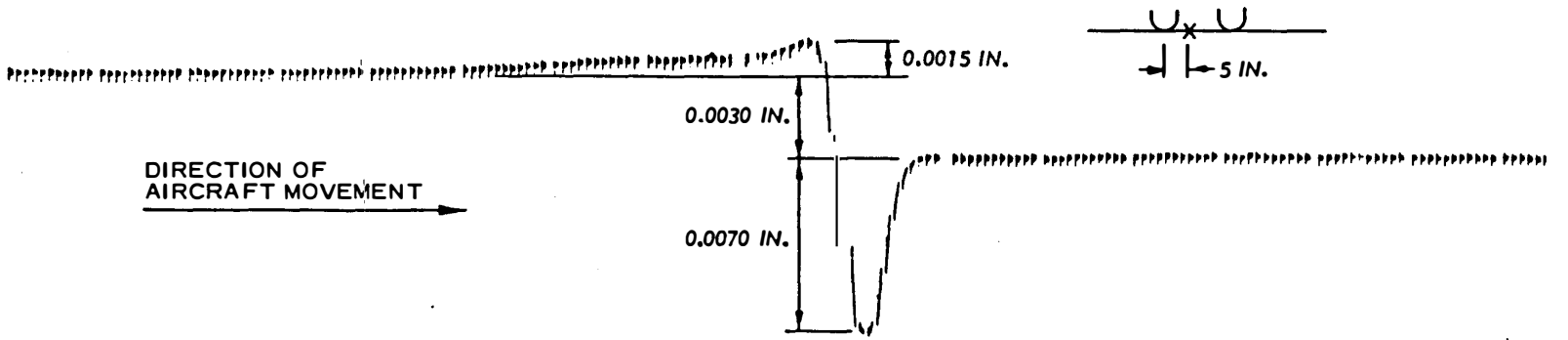

a. BENEATH WHEELS

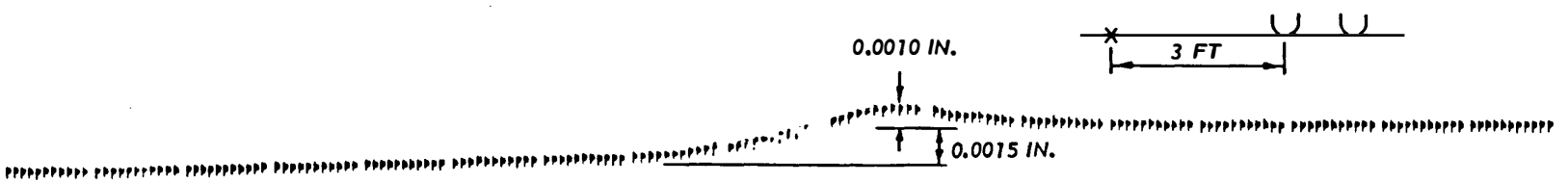

b. BENEATH AXIS OF WHEELS

Figure 34. Typical recordings for Bison coils in creep-speed taxi tests

further in the section dealing with pavement structure vertical velocity.

Horizontal longitudinal and transverse relative displacements measured by Bison coils within both pavement test sites (as seen in Appendix B) indicated effects from both total pavement structure and individual element types of vertical elastic responses. The inelastic behavior was the same as that observed for the vertical displacements. The horizontal elastic displacements showed a reversal of movement with increases in transverse offset distance, an effect that is similar to the element type of vertical elastic response. However, in the longitudinal direction, horizontal elastic displacement primarily reflected the total pavement structure downward bending with no reversal of movement between the time before the wheels reached the center line of the gages and the time at which they were directly over the gages. There was an occasional tendency for reversal which was indicated by the magnitude of the response being larger before the wheels reached the center line of the gages.

Horizontal transverse relative displacement in the top of the rigid pavement slabs was measured with the Valore strain gages. These strain gages indicated both elastic and inelastic responses as illustrated in Appendix B. The gages also indicated effects from both total pavement structure and individual element vertical elastic movements. Along the wheel axis with increases in offset distance, there was a reversal in the movement. However, there was no reversal between the time before the wheels reached the center line of the gages and the time at which they were directly over the gages. As stated previously, inelastic behavior of the slabs is possible. Because of the inelastic response in the foundation materials, a slab can stay slightly bent downward under its own weight or slightly pushed upward by its foundation.

Mathematical Model. Figures 35, 36, and 37 are computer-generated static load curves fitting the data and matching the curves shown in Figures B116, B123, and B130 which were drawn by hand. These curves and data are for static load tests in three layers of the flexible pavement structure in 1974. The data points show the elastic displacements determined by the behavioral hypothesis. These curves are presented

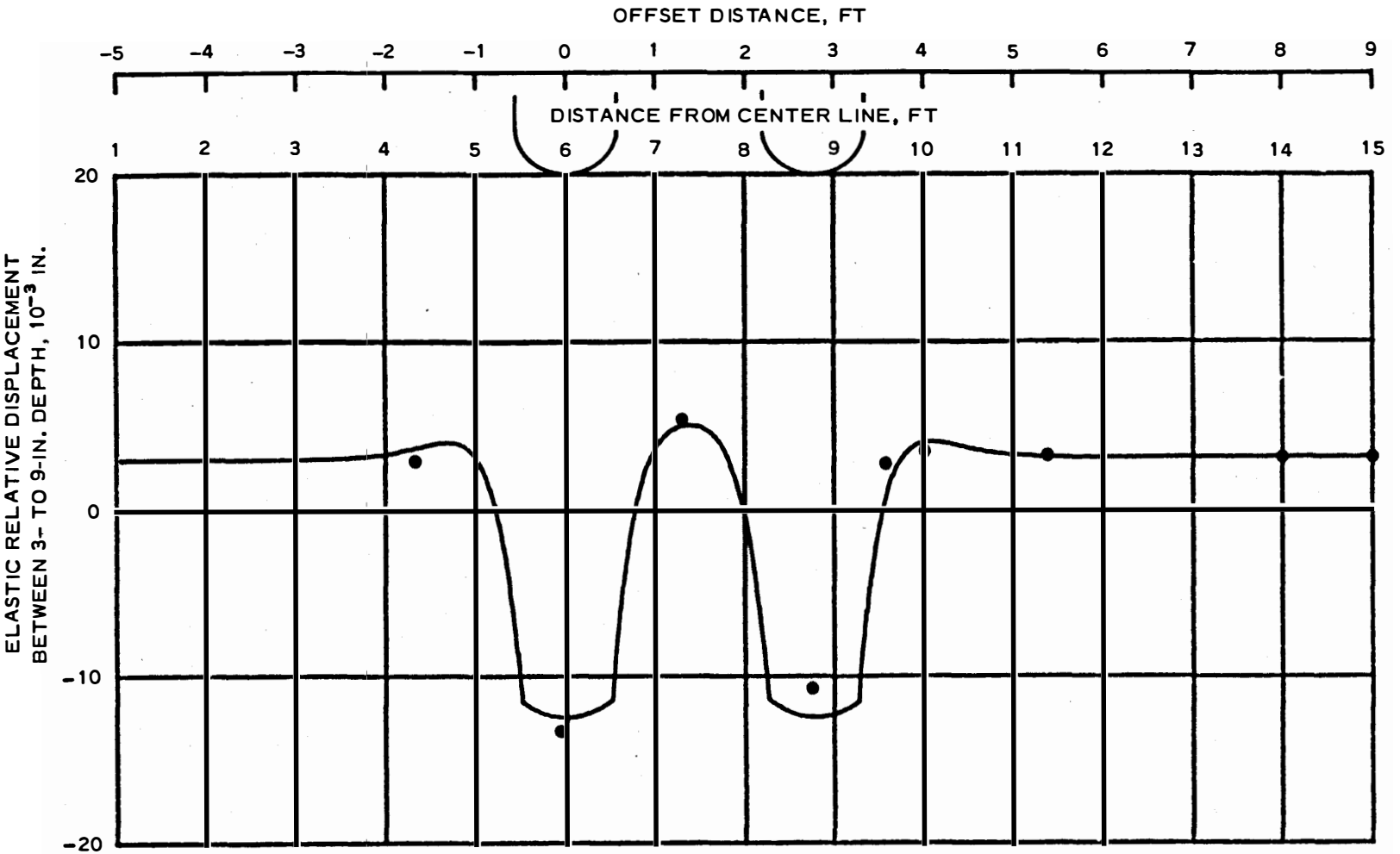

Figure 35. Computer-generated static load curve corresponding to Figure B116 (A = 84, B = 2.8, C = 90, D = 3)

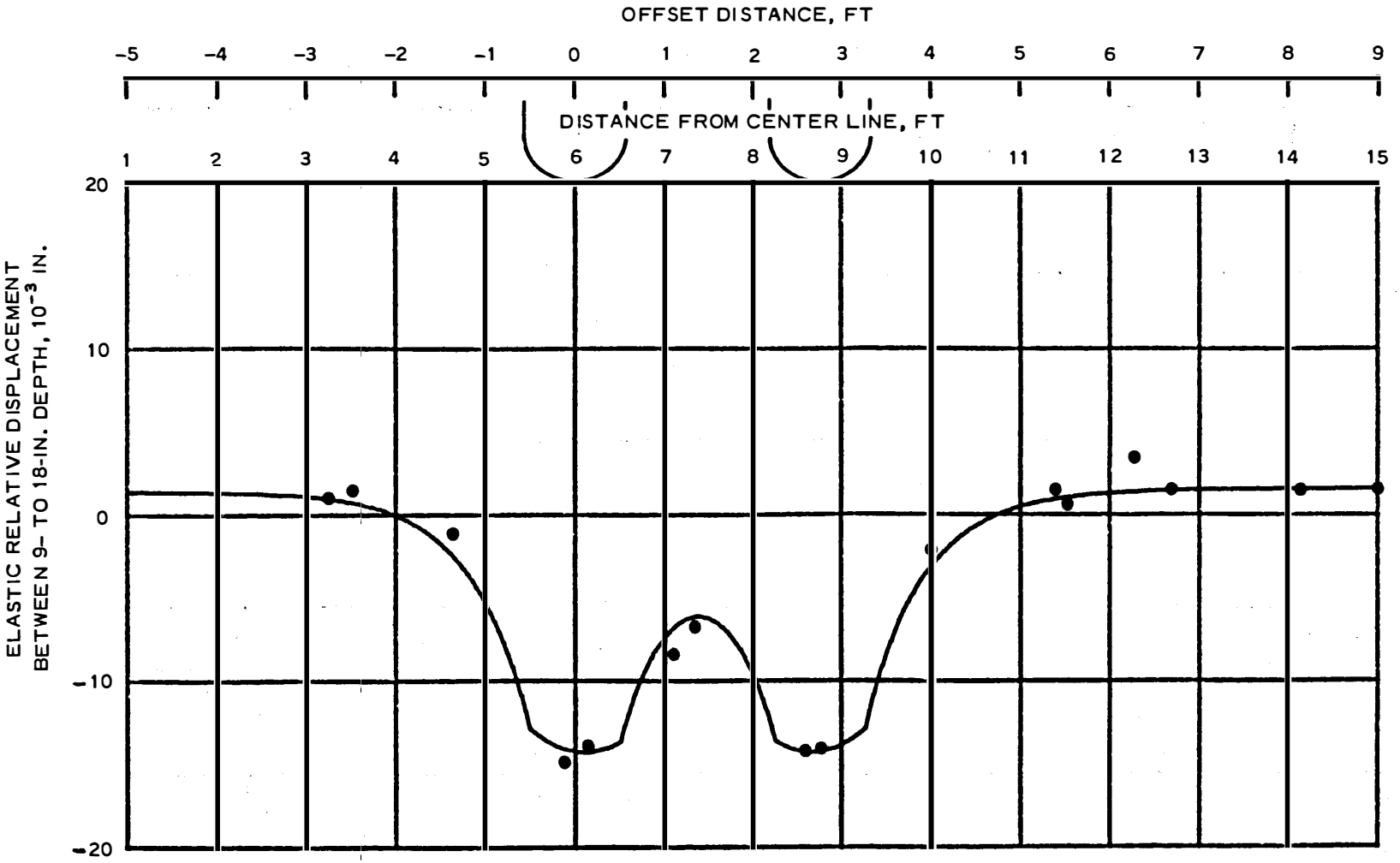

Figure 36. Computer-generated static load curve corresponding to Figure B123 (A = 30, B = 1.5, C = 0, D = 1.5)

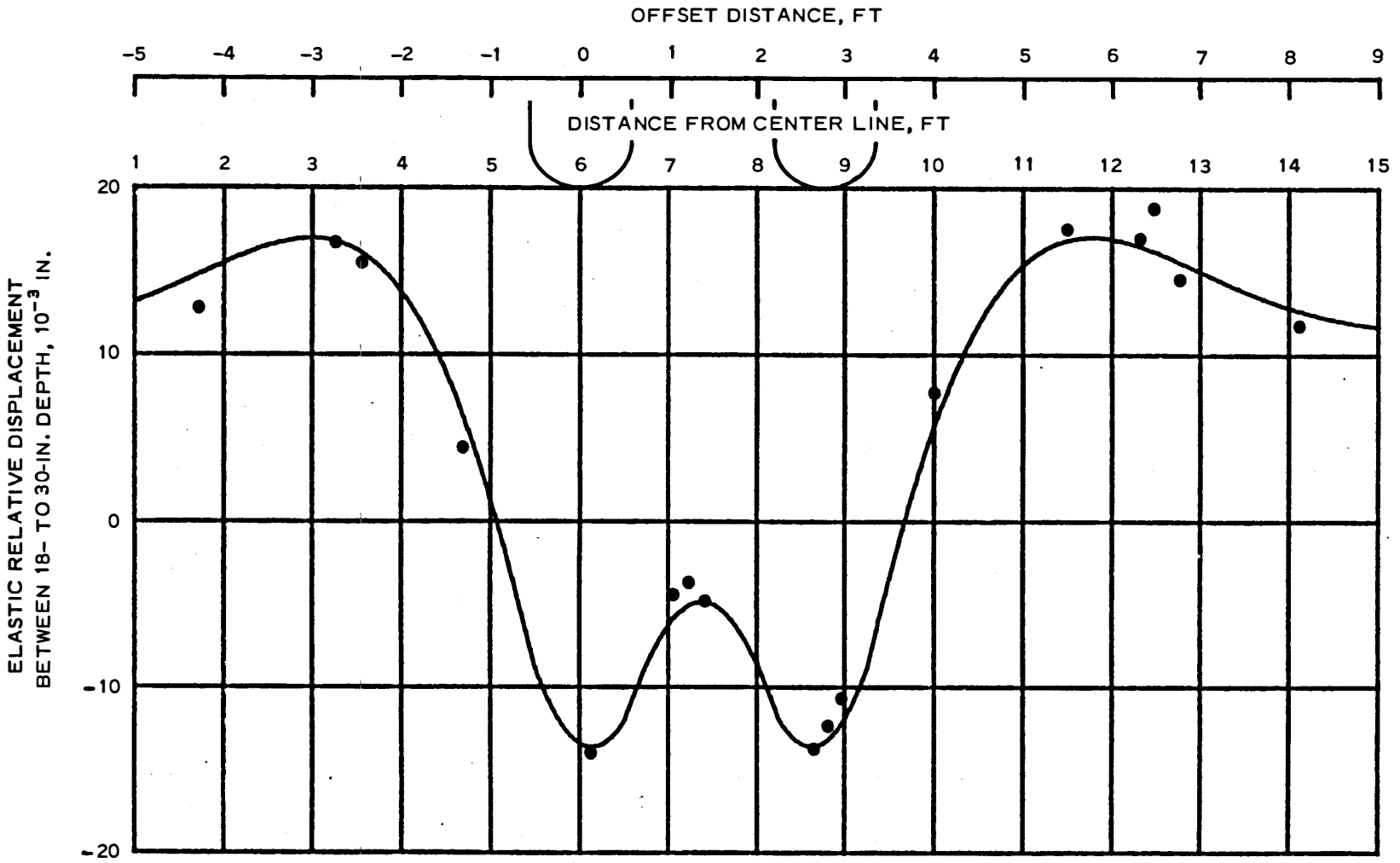

Figure 37. Computer-generated static load curve corresponding to Figure B130 (A = 36.5, B = 0.55, C = 44, D = 12.5)

to show that a mathematical model or models for duplicating the response curves and data are possible. Obviously, inelastic response curves similar to that shown in Figure 31 can also be generated by the same model that was used for these curves.

The model for the three curves was the same equation and may be a characteristic response equation. The basic equation is a decreasing amplitude oscillatory wave, and it was modified in order to make it produce symmetrical waves about a single point. For dual wheels, the responses for each wheel were calculated and added together. The modified wave equation that was used is

$$X = -Ae^{-B|Z-M|} \cos C|Z - M| - A_1 e^{-B_1|Z-M-S|} \cos C_1|Z - M - S| + D \qquad (1)$$

where

X = displacement

A, B, C, D, A_1, B_1, C_1 = constant coefficients such that $A_1 = A$, $B_1 = B$, and $C_1 = C$ if each wheel exerts the same load

Z = offset distance of the gear from the runway center line

M = offset distance of the first wheel from the runway center line

S = center-to-center wheel spacing

Figure 38 shows the form of Equation 1 for a single wheel. In the regions directly beneath the wheels, a simple second-degree curve ($ax^2 + bx + c$) was used to define the flatness shown in the curves in Figures B116, B123, and B130. The second-degree curves were tied into the wave equation curves at minus one-half and plus one-half the tire width from points at the center lines of the tires.

The coefficients A, B, C, and D varied between the three layers but were constant within each layer. These coefficients should be functions of and be capable of correlation to such variables as depth,

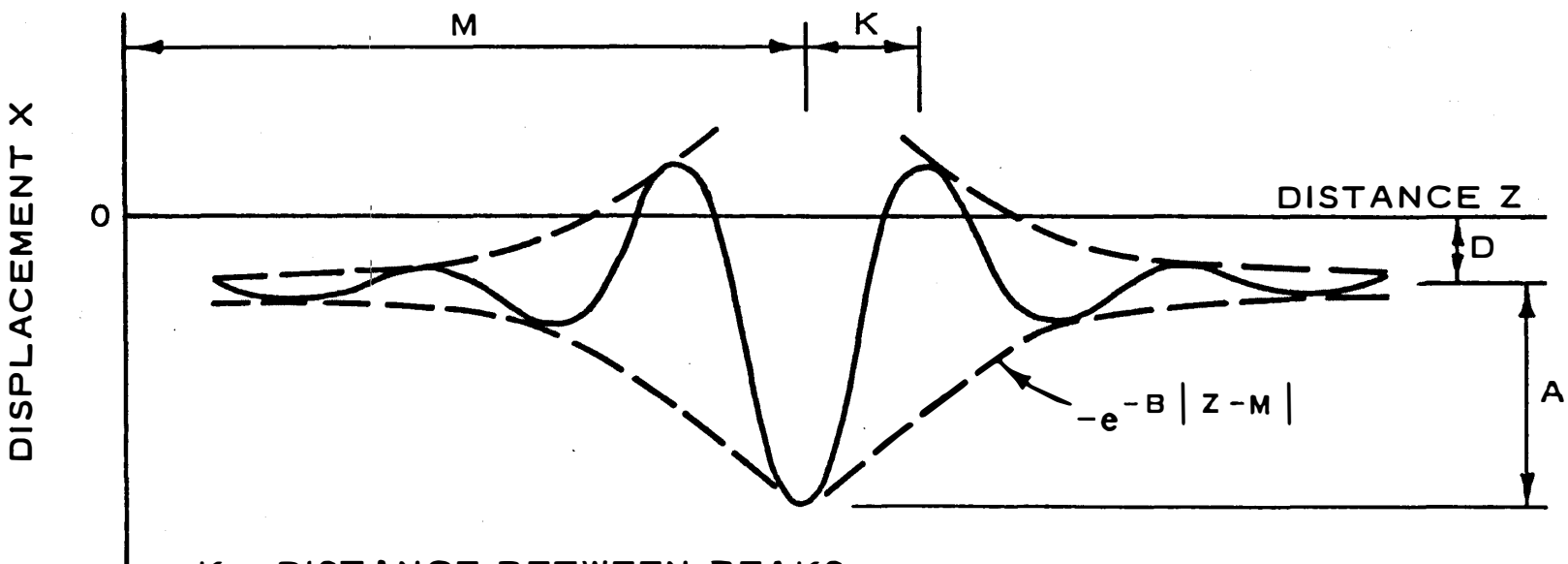

K = DISTANCE BETWEEN PEAKS

$$C = \frac{180°}{K}$$

$$X = -Ae^{-B|Z-M|}\cos C|Z-M| + D$$

Figure 38. Graphic representation of Equation 1 for a single wheel

load, number of wheels, structure strength, temperature, rate of load application, etc. If the above variables are known, all of the test results and curves can be accurately mathematically predicted.

NAFEC Pavement Structure Vertical Velocity of Motion. Figure 21 shows typical recordings of vertical velocity responses measured by a velocity gage in the dynamic load tests. These responses are representative of those for both test sites, and the velocity measurements were made in the pavement surface layers. The gages were installed at a depth of about 3 in. in the flexible pavement test site and were embedded in the bottom of the slabs in the rigid pavement test site. The traces in Figure 21 were recorded in 1972 on the flexible pavement test site. The rigid pavement structure shows a little more vibration in the signals than is shown by this figure.

As mentioned previously, simple integration of velocity data in the immediate gage vicinity yields erroneous results. For an example, simple integration of the velocity response in Figure 21a first yields an upward movement of 0.0062 in., then a downward movement of 0.0130 in., and lastly an upward movement of 0.0069 in., which brings the instrument back to its zero location. The first movement could be a bow wave, but the second and last movements should then be the downward and rebound movements that correspond to those measured by a WES deflection gage. However, the corresponding WES deflection gage response (Figure 39) is a downward and rebound movement of 0.041 in. (compared to the above 0.0130 in. and 0.0069 in.). Thus, the velocity and WES deflection gage responses do not compare favorably. Neither do the velocity peaks, zero points, or phase shifts correspond to any known motions. Due to the above results, an analysis of the motions and velocities was made which led to a possible explanation of and methodology for interpreting velocity responses.

Utilizing the methodology in computer reduction of velocity data to measurements of vertical movement was not undertaken because of the complex and time-consuming nature of such operations, as should be obvious. This section of the report, however, presents in example form the methodology for reducing velocity data in the wheel vicinity. The

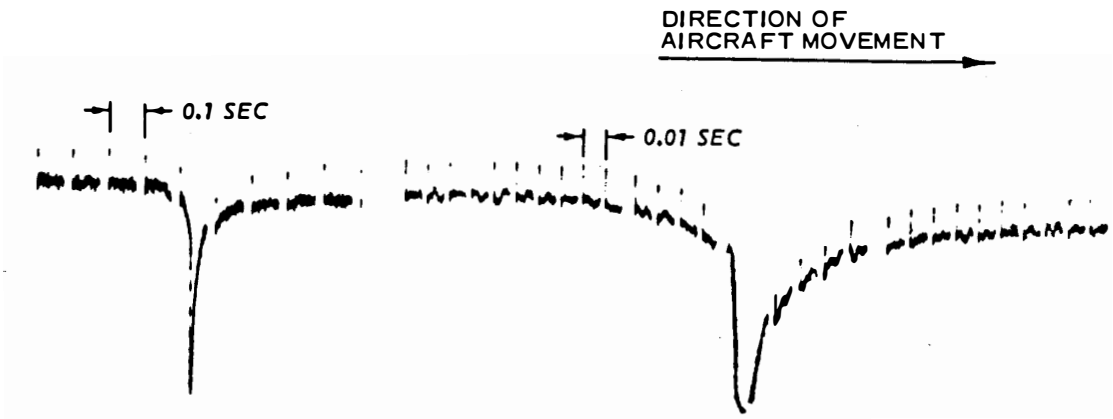

a. REAL TIME b. EXPANDED TIME

Figure 39. Recordings for WES deflection gage measuring total pavement structure relative displacement between 0- to 15-ft depth

resulting total pavement structure movement determined in this manner compares favorably with that indicated by the corresponding WES deflection gage. In addition, these results verify the presence and effects of structural element responses (bow waves) in the wheel vicinity. Velocity response outside of the wheel vicinity can be normally integrated to determine movement; however, a demonstration of this procedure was not felt necessary.

Figure 39 shows a typical computer-reproduced recording for a WES deflection gage measuring total pavement structure displacement, X. Part a shows the gage response in real time, and part b shows it in expanded time. These traces are for a taxi test at an aircraft ground speed of 166.7 ft/sec. Linearly extrapolating the time scale of 166.7 ft/sec to a time scale of 233.3 ft/sec and replotting the data in Figure 39 results in Curve 1 of Figure 40. Whether plotted at 166.7 or 233.3 ft/sec, however, the displacement is fully elastic (recovered).

If elastic response is symmetric, as indicated by the static load tests at NAFEC and at WES, the displacement shown by Curve 1 of Figure 40 should be symmetrical; however, the measured response obviously is not symmetrical. By plotting the mirror image of Curve 1 on the left-hand side in Figure 40, Curve 2 is obtained. Now, assume a bow wave is riding on Curve 2. A bow wave measured by Bison coils in the top 3 to 9 in. of the pavement structure at an aircraft ground speed of 233.3 ft/sec is plotted in Figure 41. As can be seen, the rise time that a velocity gage would detect for the bow wave is approximately 0.06 sec.

In Figure 40 further assume that the difference between Curves 1 and 2, which is Curve 3, is the peak amplitude of a total pavement structure bow wave. (Curve 3 represents the amplitude of the bow wave at distances or times before the wheels reach the center line of the gage. It is also the growth of the bow wave.) Now, at any given point (in terms of distance or time) before the wheels reach the center line of the gage, the upward change in displacement ΔX is the difference between Curves 1 and 2 (i.e., Curve 3). Assume that the rise time or time increment Δt for ΔX is the 0.06-sec rise time of the measured bow wave in the top layer of the pavement structure (Figure 41). The upward velocity $\dot{X}$

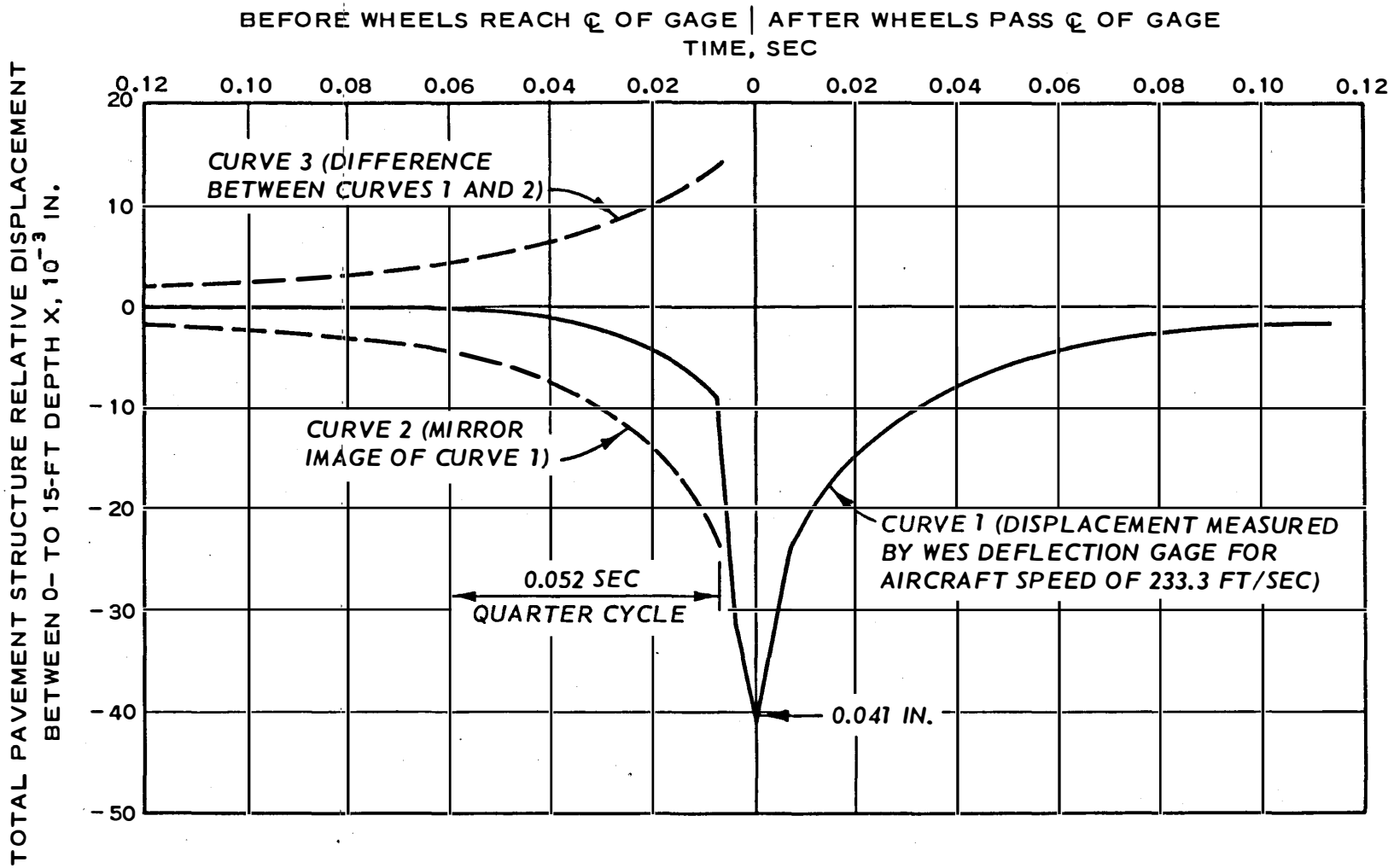

Figure 40. Plot of Figure 39 adjusted to aircraft speed of 233.3 ft/sec (Curve 1) along with assumed mirror image (Curve 2) and peak amplitude of total structure bow wave (Curve 3)

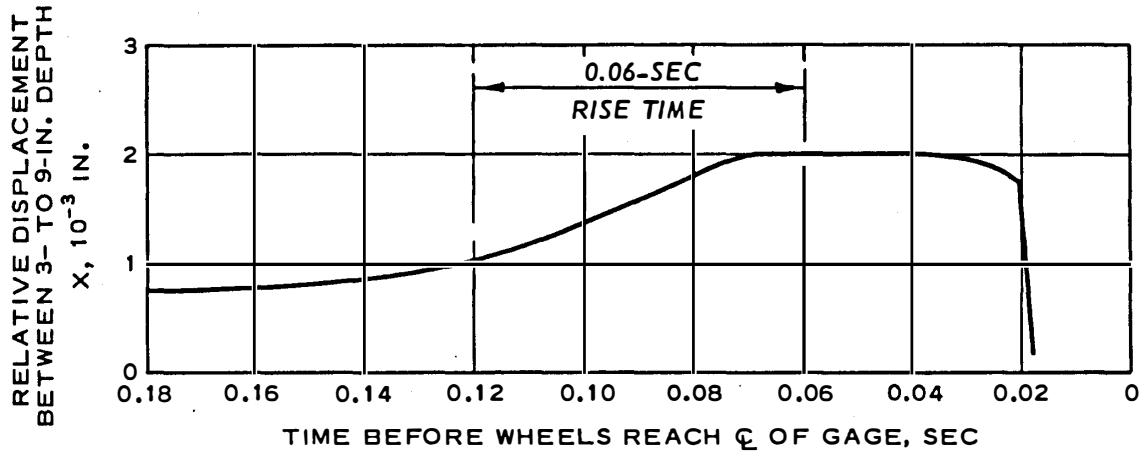

Figure 41. Bow wave measured by Bison coils (3- to 9-in. depth) at aircraft speed of 233.3 ft/sec

of the total pavement structure bow wave can now be approximated as equal to $\Delta X/\Delta t$. Before the wheels reach the center line of the gage, this total pavement structure upward bow wave velocity is larger than the total pavement structure gradual downward velocity and should be indicated by the velocity gage.

The total pavement structure displacement (Curve 1 in Figure 40) as measured by WES deflection gages is therefore the resultant of two displacements occurring at exactly the same time. At any point before the wheels reach the center line of the gage, the resultant of an upward elastic displacement and a larger downward elastic displacement would be the downward displacement shown by Curve 1. This resultant is the only displacement that a gage measuring total pavement structure displacement such as the WES deflection gage can indicate. In other words, the unsymmetrical response of Curve 1 is caused by a total pavement structure bow wave holding the pavement structure above where it would be if the bow wave did not exist.

Figure 22 shows the measured velocity of Figure 21 reprinted with an expanded time scale. The velocity data expansion for the wheel vicinity corresponds to the displacements in Figure 40 presently being discussed. Aircraft ground speed for the velocity data was 233.3 ft/sec. Figure 42 shows a plot of the measured velocity of Figure 22 before the wheels reach the center line of the gage. The upward velocity $\dot{X}$ calculated from the previously discussed $\Delta X/\Delta t$ is plotted in Figure 42 for comparison with the measured velocity. As can be seen, the agreement is excellent.

Curve 3 in Figure 40 can be obtained from the measured velocity. The measured velocity is the resultant R of the downward velocity V_2 of Curve 2 and the upward velocity V_3 of the total pavement structure bow wave, i.e.

$$R = V_2 + V_3 \qquad (2)$$

Determining V_3 from the above expression and calculating the area under the V_3 curve yields Curve 3 of Figure 40.

The previous discussion has been for the pavement structure

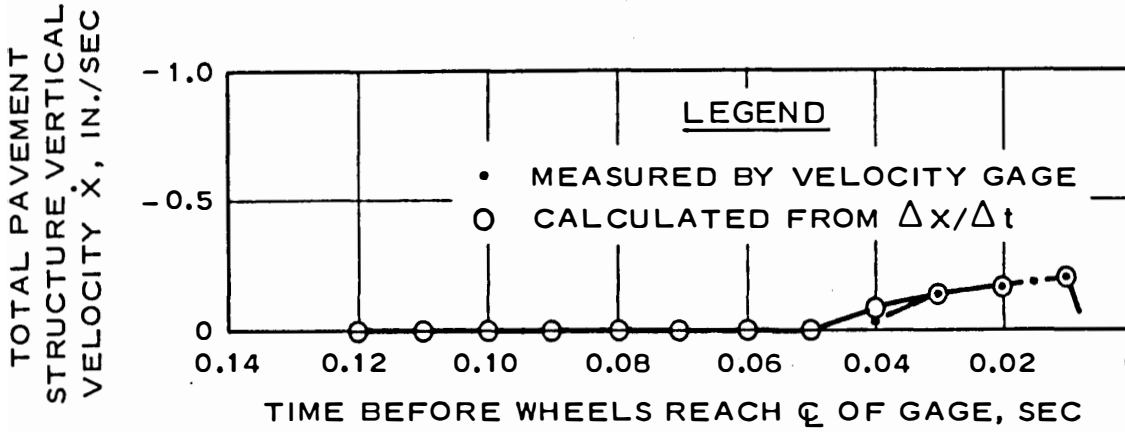

Figure 42. Comparison of measured and calculated vertical velocities before wheels reach center line of gage

behavior up to approximately 0.01 sec before the wheels reach the center line of the gage. In this region, the measured velocity curve is in phase with the displacement curve as shown below:

a. The natural undamped frequency of the velocity gage ω_n = 29.845 rad/sec.

b. The pavement structure displacement frequency corresponding to one-quarter of a cycle: one-quarter cycle = 0.052 sec and ω = 4.81 cycles/sec = 30.2 rad/sec.

c. $\omega/\omega_n = 1.01 \approx 1.0$.

d. The damping factor for the velocity gage D = 0.65.

e. The phase angle ϕ determined from velocity gage damping versus frequency ratio response curves = 0 deg = 0 rad.

f. The time of the phase shift ϕ/ω = 0 sec.

Consider the velocity gage as modeled by the simple system in Figure 43a. Figure 43b represents the movement of the mass for the first motion up to 0.01 sec before the wheels reach the center line of the gage. Figure 44 is a plot of the measured total pavement structure displacement up to the point at which the wheels reach the center line of the gage. Superimposed on Figure 44 is the acceleration $\ddot{X}$ calculated from the measured displacement. Figure 45 is a plot of the measured velocity from 0.01 sec before to the point at which the wheels reach the center line of the gage.

As shown in Figure 41, at approximately 0.02 sec before the wheels reach the center line of the gage, the bow wave peaks and is pushed downward by the wheels. At approximately 0.01 sec before, the downward acceleration exceeds the acceleration of gravity (g = 386.4 in./sec^2) as shown in Figure 44. When this occurs, the velocity gage mass is instantaneously motionless, the gage housing is moving, and the motion reference changes from the housing to the mass. (Liken this to a mass riding in an elevator that is being forced downward beyond the acceleration of gravity. When the elevator exceeds the acceleration of gravity, it is then moving faster than the mass.) This change in reference causes the velocity indicated motion to be the opposite to the actual motion, and the velocity gage responds as shown in Figure 45. Also shown in Figure 45 is the velocity gage model mass positions with time that would lead to

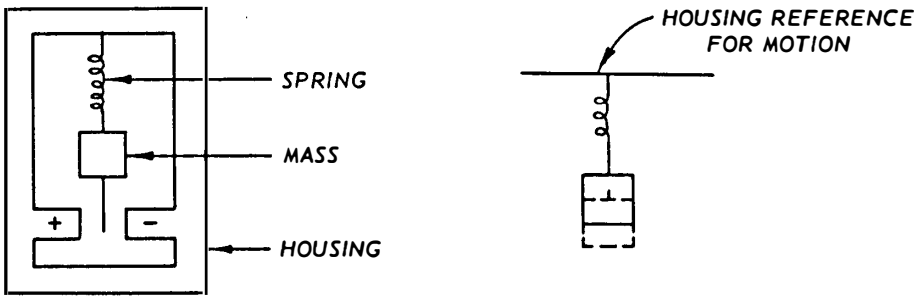

a. SPRING-MASS SYSTEM

b. MOVEMENT OF MASS FOR FIRST MOTION UP TO 0.01 SEC BEFORE WHEELS REACH CENTER LINE OF GAGE

Figure 43. Velocity gage model and movement of mass

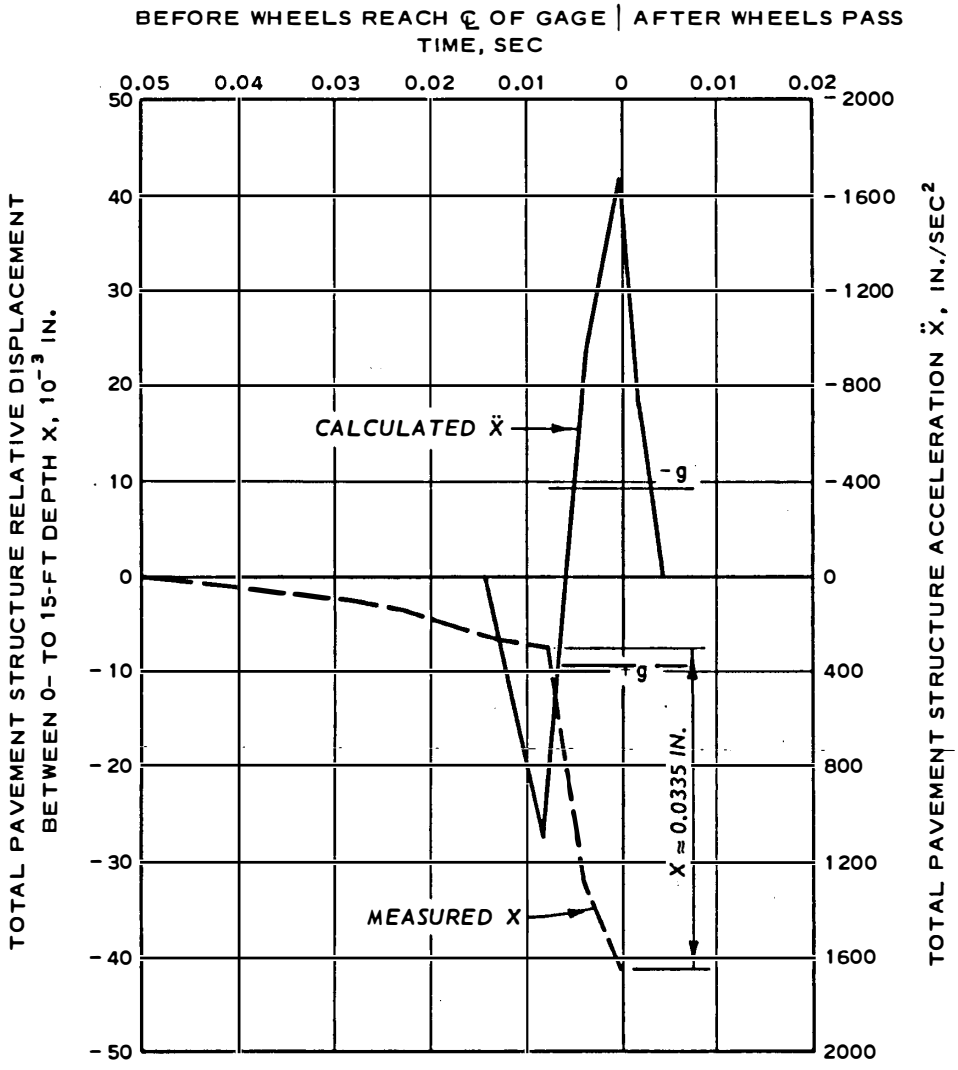

Figure 44. Measured displacement up to point at which wheels reach center line of gage (from Figure 40) and calculated acceleration

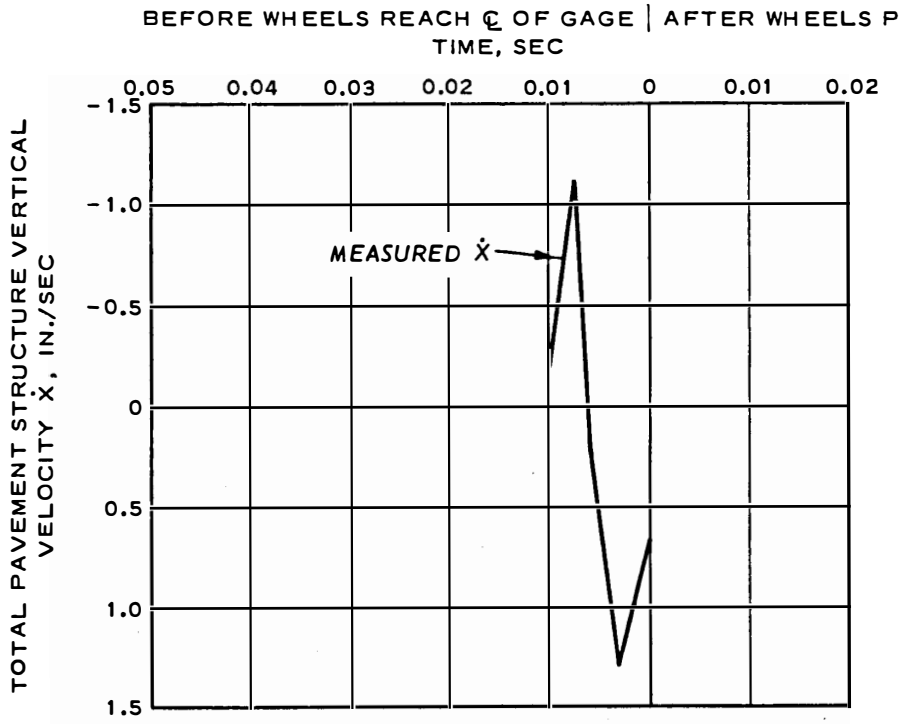

a. MEASURED VERTICAL VELOCITY

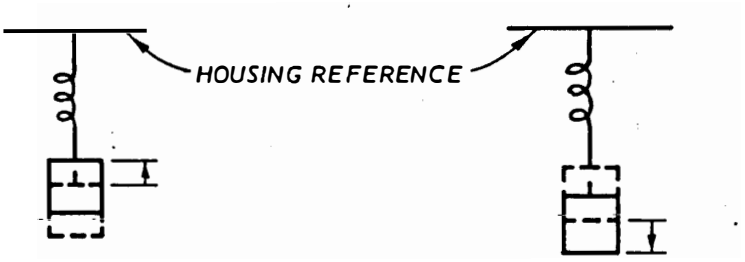

b. MASS POSITION BETWEEN 0.010 AND 0.008 SEC

c. MASS POSITION BETWEEN 0.008 AND 0.003 SEC

Figure 45. Measured vertical velocity between 0.01 sec before wheels reach center line of gage and point at which wheels reach center line of gage along with corresponding velocity gage model mass positions

the indicated velocity. After approximately 0.002 sec, the acceleration reaches a peak and the spring force causes the mass to start moving. Again, this behavior changes the reference back to the housing, and the velocity indicated motion is in the correct direction. Therefore, the indicated negative velocity after 0.01 sec must be added vectorily to the positive velocity as is shown in Figure 46.

A peak velocity is reached at approximately 0.003 sec before the wheels reach the center line of the gage. The displacement from 0.008 sec before to the point at which the wheels reach the center line of the gage is of very high frequency, and the velocity peak is leading the peak displacement by about 90 deg as it should. As can be observed in Figures 39 and 40, the displacement curve is a complex wave form containing regions of different wave behavior characteristics. These regions are more clear in the velocity response curves in Figure 22. The velocity gage responds in each region with a complete change in velocity behavior character, and these changes produce the complex velocity response curve. Now, assuming that the displacement response from 0.008 sec before to the point at which the wheels reach the center line of the gage is such a region, the velocity response in this region of Figure 46 represents approximately one-fourth of the velocity response as if this displacement cycle would be continued (not interrupted). For this region, the velocity being 90 deg out of phase with the displacement means that the velocity should be zero at the point at which the wheels reach the center line of the gage. Therefore, the displacement corresponding to the velocity for this region can be approximated by the quarter cycle velocity response and is approximately 0.0324 in. The measured deformation for this region is about 0.0335 in., as can be seen in Figure 44.

The region from the point at which the wheels reach the center line of the gage to 0.003 sec after they pass will be discussed later. As can be seen in Figure 44, at approximately 0.003 sec after the wheels pass the center line of the gage, the deceleration decreases below $-g$. When this response occurs, the motion changes to a low frequency, thereby shifting the phase from lead to lag. Figure 47 is a plot of the displacement from the point at which the wheels reach the center line of the

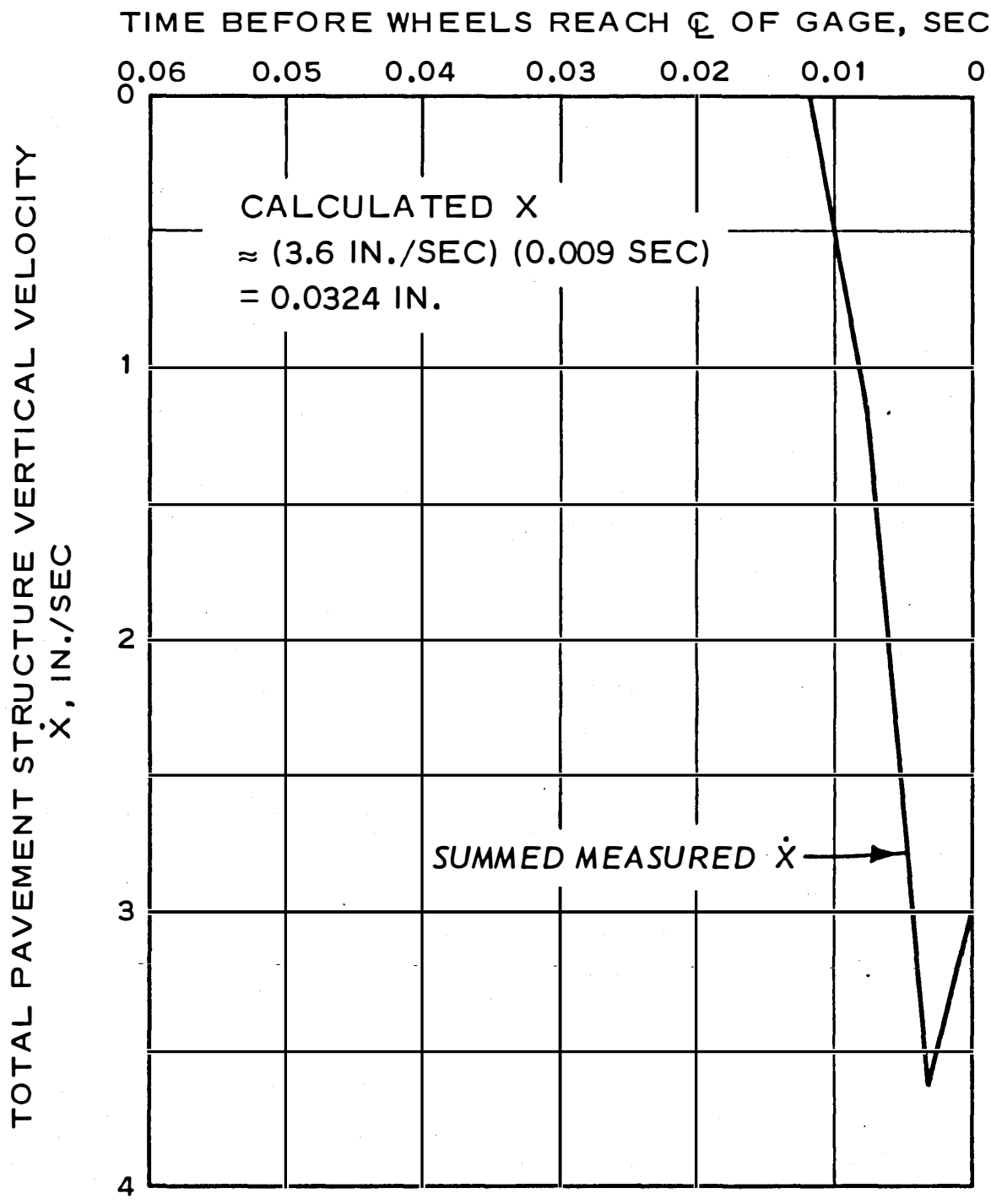

Figure 46. Summed measured vertical velocity up to point at which wheels reach center line of gage and calculated displacement

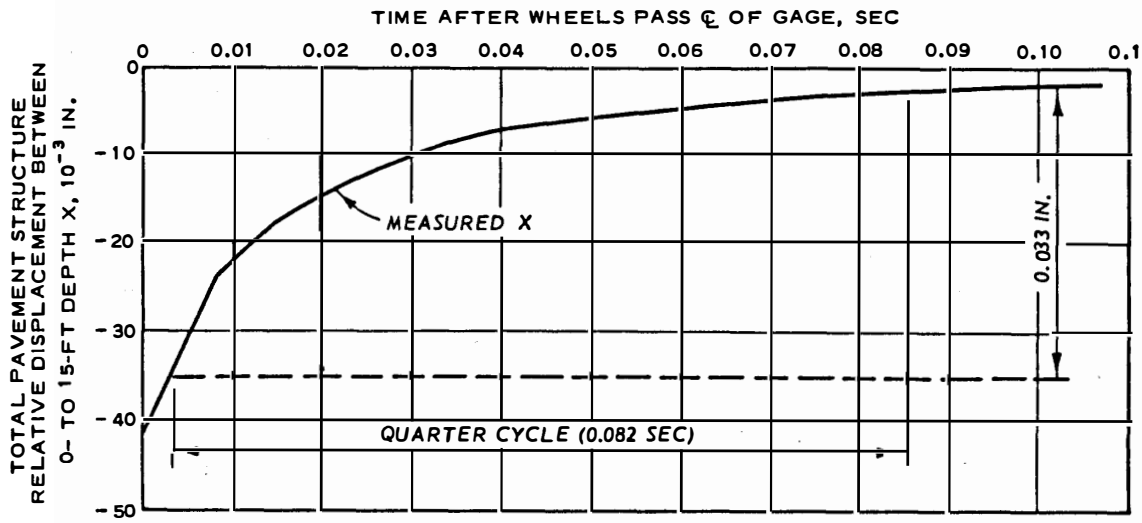

Figure 47. Measured rebound displacement (from Figure 40) between point at which wheels reach center line of gage and 0.11 sec after wheels pass center line of gage

gage to 0.11 sec after they pass, and Figure 48 is a plot of the corresponding measured vertical velocity. Assuming the displacement region between 0.003 and 0.085 sec after the wheels pass to be the last quarter of a cycle, the displacement and velocity gage response phase angle can be calculated as follows:

a. For the velocity gage: $\omega_n = 29.845$ rad/sec and $D = 0.65$.

b. For displacement: one-quarter cycle = 0.082 sec, $\omega = 3.049$ cycles/sec = 19.1560 rad/sec, and $\omega/\omega_n = 0.64185$.

c. From velocity gage damping versus frequency ratio curves, velocity is lagging the displacement by $\phi = 35$ deg = 0.61087 rad.

d. The time of the phase lag = $\phi/\omega = 0.032$ sec.

This phase lag corresponds almost exactly with the phase lag shown in Figure 48. For this region, the rebound displacement calculated from the maximum velocity change is approximately 0.03325 in. This value compares well with the measured value of 0.033 in. shown in Figure 47.

The region from the point at which the wheels reach the center line of the gage to 0.003 sec after they pass will now be discussed. In the above 0.003- to 0.085-sec region, there is approximately 0.008 in. of rebound deformation unexplained. During the process of the velocity gage changing reference systems and changing phase from lead to lag at about the point at which the wheels reach the center line of the gage, there appears to be a velocity increment missing. (Missing in the sense of being balanced out as a result of two opposed motions, balanced or damped out due to phase shifts, or being at such a high frequency as to not be registered by the gage.)

The fact that the velocity curve did not go to zero at the displacement peak ($t = 0$) can possibly be explained. The displacement curve shows an almost instantaneous change at its peak. This behavior implies that something similar to a step function or a Heaviside function is occurring. The further implication is that the displacement function does not have a continuous first derivative at $t = 0$. Therefore, the velocity gage could possibly register this behavior as an abrupt change instead of passing through zero.

Combining Figures 46 and 48 results in Figure 49. For the time

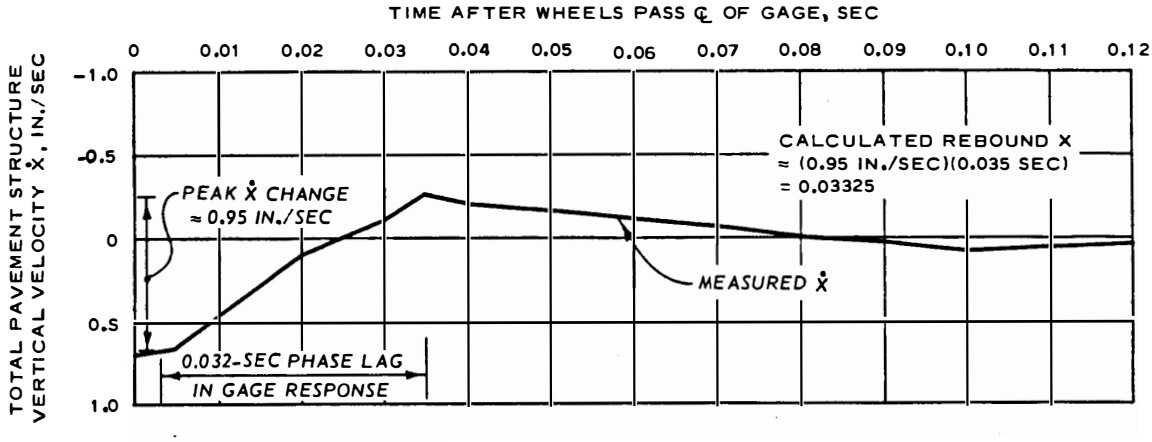

Figure 48. Measured vertical velocity between point at which wheels reach center line of gage and 0.12 sec after wheels pass center line of gage and calculated displacement

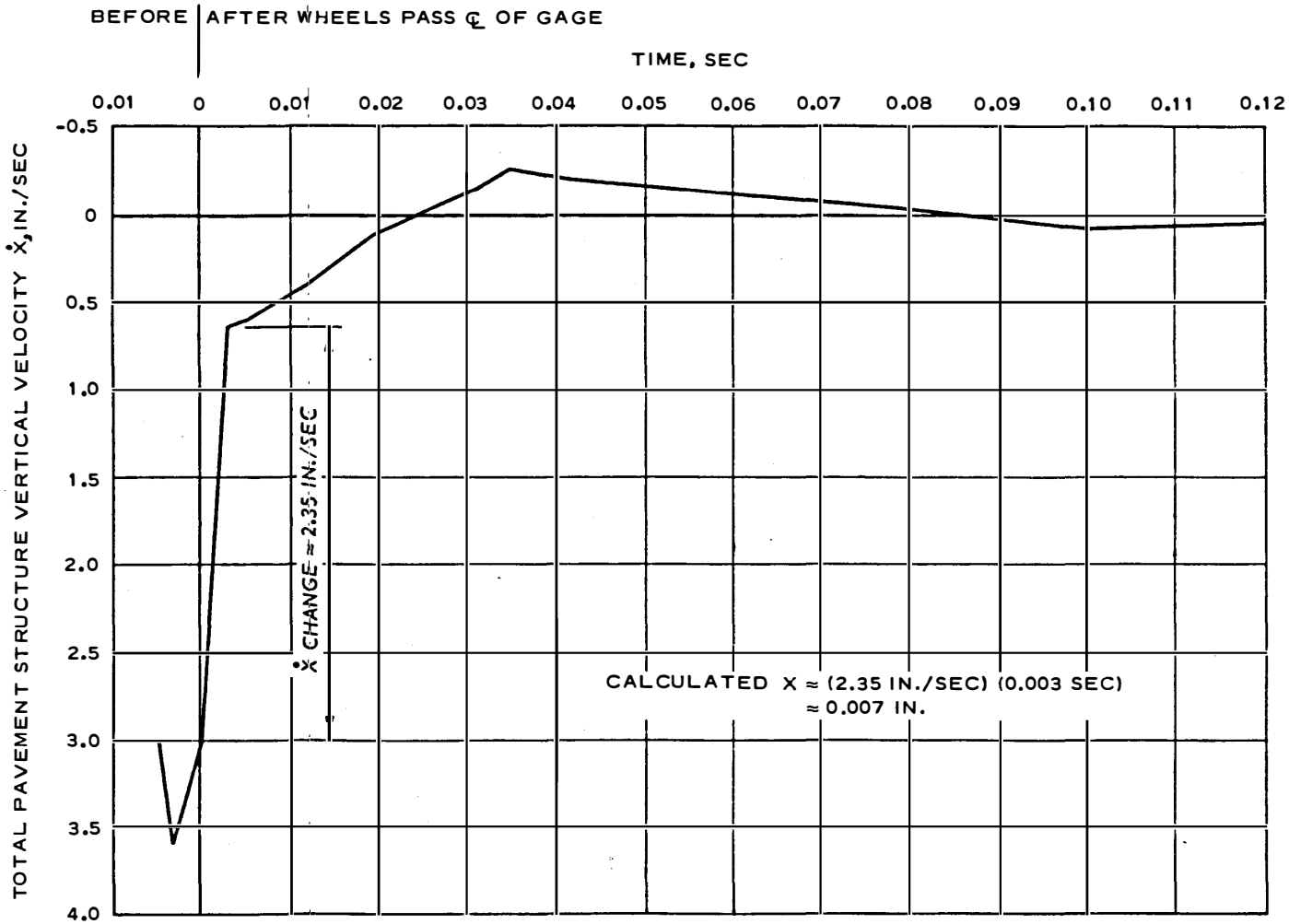

Figure 49. Measured vertical velocity (from Figures 46 and 48) between a point before wheels reach center line of gage and 0.12 sec after wheels pass center line of gage and calculated displacement

period from the point at which the wheels reach the center line of the gage to 0.003 sec after the wheels pass, the velocity change is approximately 2.3 in./sec. If this 0- to 0.003-sec region corresponds to a quarter cycle of velocity, the corresponding calculated displacement is 0.007 in. This appears to be the missing increment of rebound displacement. Adding 0.007 in. to the previous 0.03325 in. gives 0.04025 in. of rebound displacement as compared with the measured 0.041 in.

As can be observed from the example use of the above methodology, the displacement response curve is considered as being generated by several portions (quarter cycles) of different harmonic waves. The velocity gage responses indicate each of these quarter cycles by responding differently to each. By considering separately each behavioral region, the velocity data can be reduced to movements approximately equal to the measured displacements.

TEST RESULTS

The data collected in this study were reduced and interpreted according to the previous discussions. With the exception of the pavement structure vertical velocity data, the test results are presented in Appendix B. Figures B1-B276 show the displacement results for the 1972 and 1974 flexible pavement tests. Figures B277-B386 show the displacement results for the 1972 rigid pavement tests. Summary figures of these results for the maximum load points will be presented in this section of the report.

In Appendix B, three parts for each figure (a, b, c) are presented where applicable. Part a shows the elastic displacement that occurred along a line perpendicular to the longitudinal aircraft axis and directly beneath the wheel axis. The elastic responses for all recorded gages are shown in Part a; duplicate points were not plotted. Therefore, the points are representative of from one to several tests. When inelastic displacement occurred for a sequence of loadings, Part b is presented. However, if Part b is not presented, even though inelastic response did not occur for a sequence of loadings, it may have occurred for a single load application directly on a gage. Maximum inelastic responses

measured for single load applications directly on a gage are presented in the summary figures.

Part b, as previously described in the interpretation of data section, shows three responses representing the initial no-load, load, and final no-load responses beneath the wheel axis. The elastic and inelastic behavioral phases are derived from Part b. Part b shows a representative plot for the gage or gages but is not plotted for all gages. Inelastic responses for gages not shown are approximately the same as or less than those shown, depending on the load history and gage location.

Part c is presented for the individual structural elements, and it shows the bow wave peak magnitude occurring ahead of the wheel axis. The points in Part c are for all recorded gages in the structural elements. As previously discussed, no bow wave was detected by the Valore strain gages in the rigid pavement slabs. Therefore, no Part c exists for the figures showing Valore strain gage results, although they do have a Part b.

Results for all basic modes of operation are presented with the corresponding static load curves superimposed on the results of the dynamic load tests. This manner of presentation directly shows the relationship between dynamic load test and static load test results. The medium- and high-speed taxi results are plotted together because the pavement structure responses to these operations were essentially the same. (Aircraft load data were essentially the same, also.)

Not all structural element Bison coils were monitored simultaneously. More coils were placed in the pavement structures than equipment was available for simultaneous recording. This approach was purposely taken to allow flexibility in concentrating recording in certain areas if necessary and to increase the probability of acquiring the necessary data.

As stated previously, some variation in the static load and creep-speed taxi test results was caused by offset distances not being exactly determined, by variations in the pavement structure, by responses being affected by the load history, and by variations in the electronic system.

For all other operational modes, in addition to the above causes, variation in the aircraft dynamic loads was probably the major factor controlling the data spread.

In calculating the noise levels for each gage, if for a dynamic load application one-half of the noise was as large as or greater than 0.001 in. for the displacement measuring gages, the half noise level was subtracted from the data. This correction reduced the data indication to the average signal width if the computer took the data point at the top of a noise spike. For the Valore strain gages, the half noise level had to be as large as or greater than 0.000001 in./in. to be applied as a correction. No noise correction was required for static load test data because the data were taken from average signal widths.

Curves drawn through the static load test results do not represent the average of the data responses. These curves were purposely drawn through an outer boundary for the data.

The aircraft dynamic load results were presented previously (page 48) and will not be repeated here.

Flexible Pavement Structure Results. The total pavement structure responses as measured by WES deflection gages are presented in Figures B1-B52. Figures B1-B23 are for B-727 tests in 1972; Figures B24-B46 are for B-727 tests in 1974; and Figures B47-B52 are for C-880 tests in 1974. All operations for each of the three gage rows for each year are presented in sequence. No data for turning operations are presented for row 1 because the aircraft main gears did not cross this row during these operations.

The titles of the figures in Appendix B consist of a series of key identification words. A title such as

Vertical deformation, flexible, static, row 1, 0 to 15 ft, 1974

means the following:

a. The data are vertical relative displacement results.

b. The results are for the flexible pavement test site.

c. The results are for static loading.

d. The results are for gage row 1.

e. The instrument measured relative displacement between 0 and 15 ft depth and therefore was a WES deflection gage.

f. The tests were conducted in 1974 with the B-727 aircraft.

For C-880 tests, "C-880" appears before the date.

Noticeable in the B-727 results are the increases in both elastic (Part a) and inelastic (Part b) responses between the 1972 and the 1974 tests. These increases are believed due to the higher temperatures in 1974. Also noticeable is the fact that the elastic displacements of 1974 show a large decrease with increases in the rate of load application. This behavior is believed to be a viscoelastic effect in the bituminous layers. The 1972 results did not show this large decrease but rather showed elastic displacements tending to be almost constant. A few points in the 1972 results occur greater than the static elastic responses; however, it should be remembered that inelastic response is acting in addition to the static elastic phase. In other words, considering only the elastic response is not valid; the inelastic response must also be considered. In this respect, the summary curves to be presented will show better comparisons of static and dynamic load tests. It is also possible that additional static load test results could have shown the static test curves to be greater.

For the C-880 tests, all data were obtained for the rear dual wheels. As discussed in Volume I of this report,[2] only a very few dynamic load tests were conducted with the C-880; therefore, all dynamic load test results are plotted together for each gage row. Due to the limited number of C-880 static load tests, no maximum response was obtained for the WES deflection gage of row 2. Therefore, the static load curve for row 3 (Figure B49) is also used with the data for gage row 2.

Obvious in all the total pavement structure displacement results is the critical nature of offset distance determinations adjacent to the wheels. In these regions, variations in the results can be largely caused by the variations in determining actual wheel positions.

Individual pavement structure element vertical responses as

measured by Bison coils are presented in Figures B53-B258. Figures B53-B115 are for B-727 tests in 1972; Figures B116-B228 are for B-727 tests in 1974; and Figures B229-B258 are for C-880 tests in 1974. The structure element results are presented in the same manner as the total pavement structure results. Previous remarks concerning the 1972 and 1974 test results are also applicable here. The viscoelastic effects in the bituminous layers are believed to have caused the increases in elastic and inelastic responses of the soil material layers in 1974. Wheel position again can be seen to be an important variable in these results. For the structure elements, comparisons of static and dynamic load results will also be clearer in the summary curves.

In the 1972 tests, all layers were monitored during the static load tests. Figures B67 and B74 show the static load test results for all three gage rows at the 18- to 30-in. and 39- to 51-in. depths, respectively. For the 1972 dynamic load tests, recording was concentrated in the 3- to 9-in., 9- to 18-in., and 30- to 39-in. depth layers and in the horizontal coils at a depth of 9 in.

In the 1972 test results for gage row 3, only responses to static loading and creep-speed taxies are presented for the 30- to 39-in. depth. During reconstruction of runway 13-31, the subgrade in the area adjacent to row 3 became excessively wet and had to be removed. Gages at the 30-, 39-, and 51-in. depths had already been placed, and their cables had been run across the runway subgrade. The cables were therefore cut and pulled back and then spliced together later. The condition of this portion of the instrumentation along with extraneous electrical noise present in the 1972 tests made the recorded data too noisy to be used. However, extraneous electrical noise was of a lower level in the 1974 tests, and data recorded for these depths, though still noisy, were usable.

In the 1974 tests, responses of all layers were recorded under the dynamic loads but with less concentration per layer. However, no horizontal coils were recorded except for turning operations. Also for the turning operations, the 18- to 30-in. layer of row 2 was not recorded; its recording channel was used with the horizontal coils. Again,

due to the limited number of C-880 dynamic load tests, these results are presented together for each row and each layer.

As discussed in Volume I,[2] the signals of the experimental inductive probes installed at a depth of 15 ft were too weak and the extraneous electrical noise was too high for them to be usable in the 1972 tests. They were not recorded in the 1974 tests.

Pavement structure element horizontal responses measured by Bison coils are presented in Figures B259-B276. Figures B259-B274 are for B-727 tests in 1972, and Figures B275-B276 are for B-727 tests in 1974. The horizontal responses are only for the 9-in. depth of gage row 2 where the Bison coils were embedded in the bottom of the bituminous layer. Recordings were made for all operations in 1972 but for only the turning operation in 1974. Figures B259-B266 show longitudinal horizontal responses, and Figures B267-B274 show transverse horizontal responses. The 1972 longitudinal static load test curve is superimposed on the 1974 test results in Figures B275 and B276. No static load tests were recorded in 1974 for horizontal responses, and the 1972 longitudinal curve seemed to fit the data in Figures B275 and B276.

Flexible Pavement Structure Results Summarized. Figures 50-55 summarize the total pavement structure vertical responses as measured by WES deflection gages. Both the 1972 and the 1974 test results for the B-727 operations are shown in the same figures for comparison. All basic airport operating modes for which data existed at the maximum load points are represented.

The data shown are for the maximum load points of the aircraft gear. At the pavement surface and in upper layers, these maximum load points are beneath one or the other of the dual wheels. The maximum load point then migrates with depth into the geometric centroid of the gear. This behavior occurred at a depth of about 3 ft in the flexible pavement structure.

If no data points are shown for an operational mode, either no data were acquired at the maximum load point or no data were recorded on the gage or gages for that mode, and the figures in Appendix B should be checked for the results. Static and dynamic load test comparisons

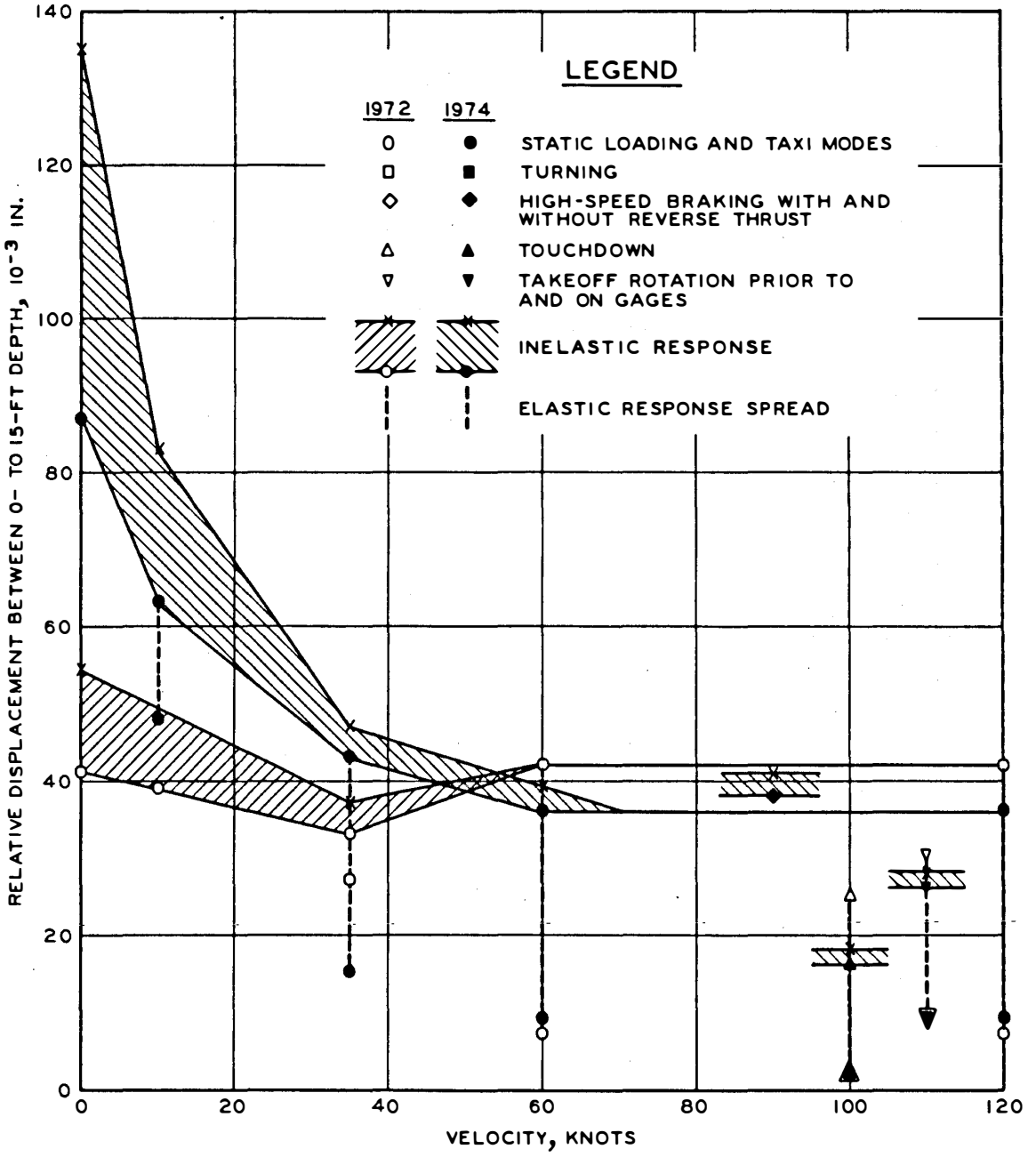

Figure 50. Maximum vertical relative displacement versus velocity, flexible, row 1, 0 to 15 ft, B-727

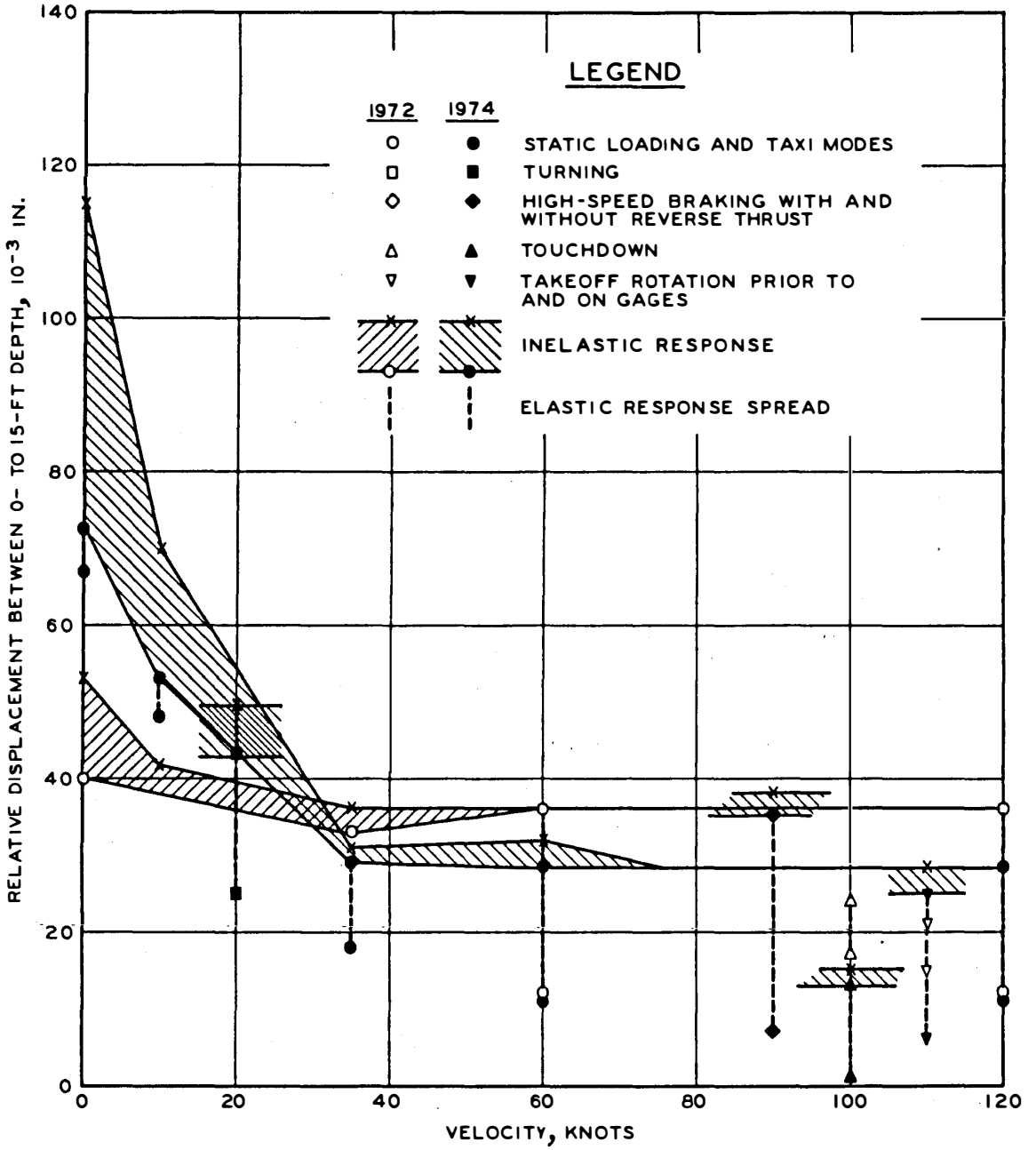

Figure 51. Maximum vertical relative displacement versus velocity, flexible, row 2, 0 to 15 ft, B-727

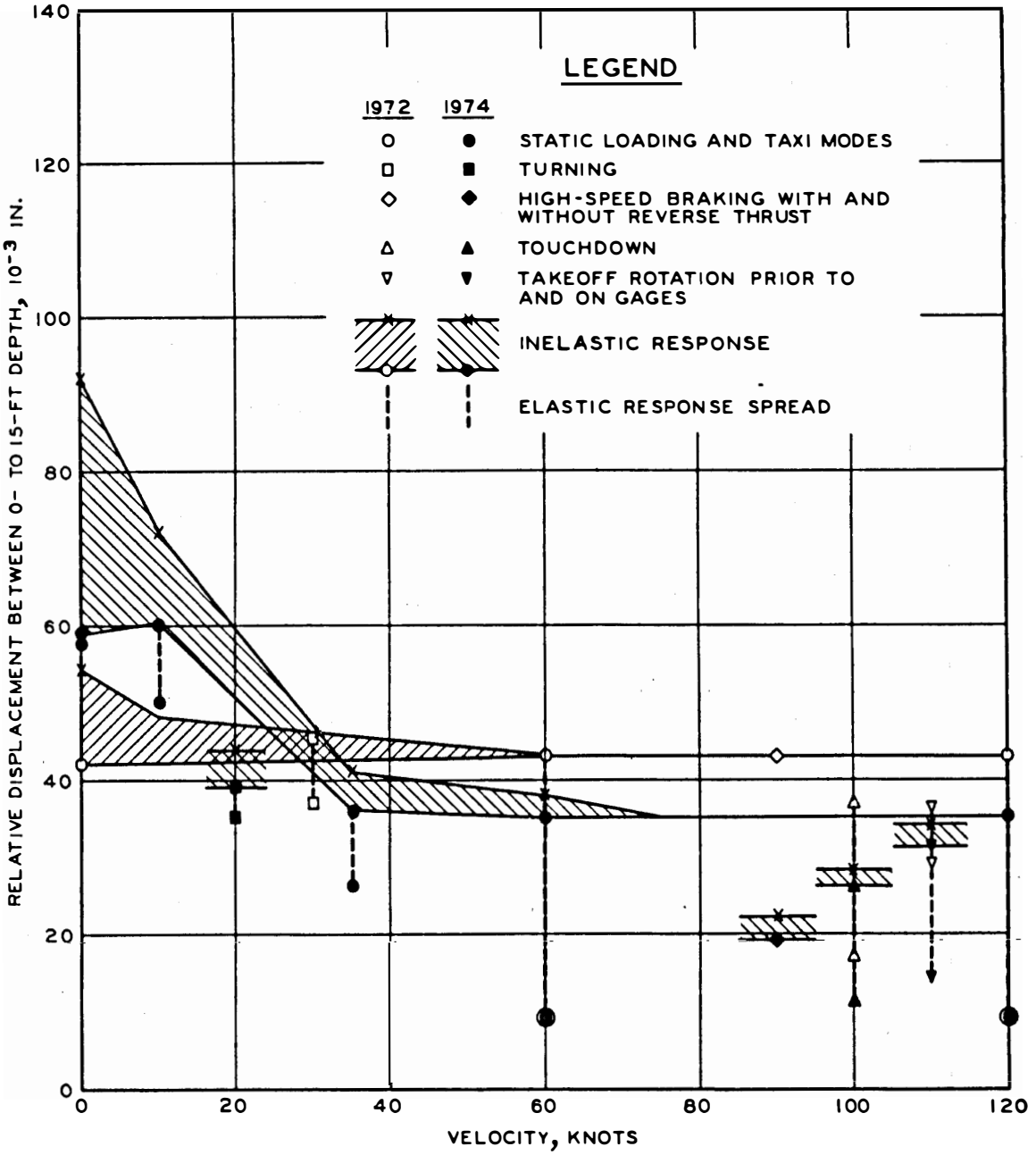

Figure 52. Maximum vertical relative displacement versus velocity, flexible, row 3, 0 to 15 ft, B-727

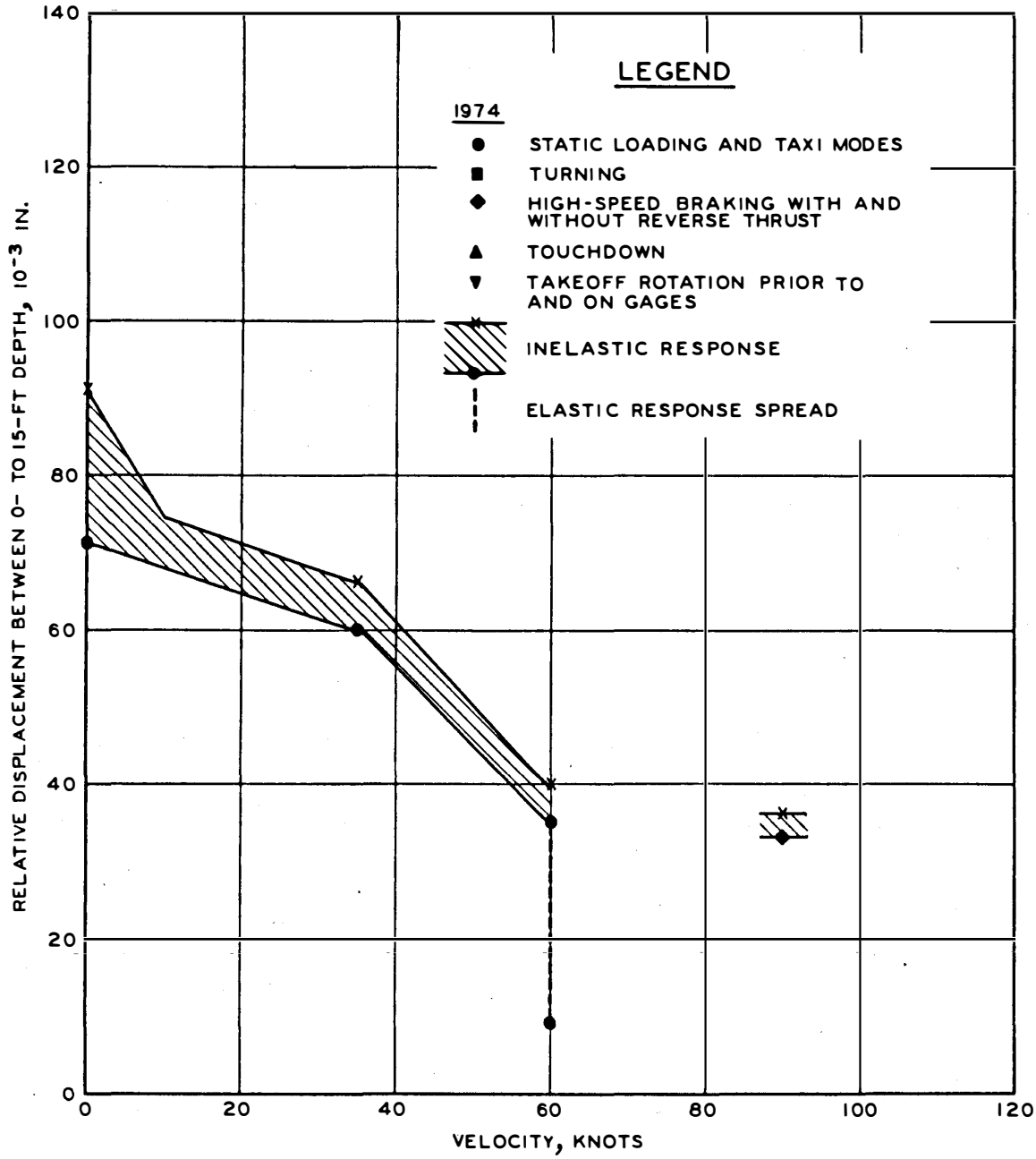

Figure 53. Maximum vertical relative displacement versus velocity, flexible, row 1, 0 to 15 ft, C-880

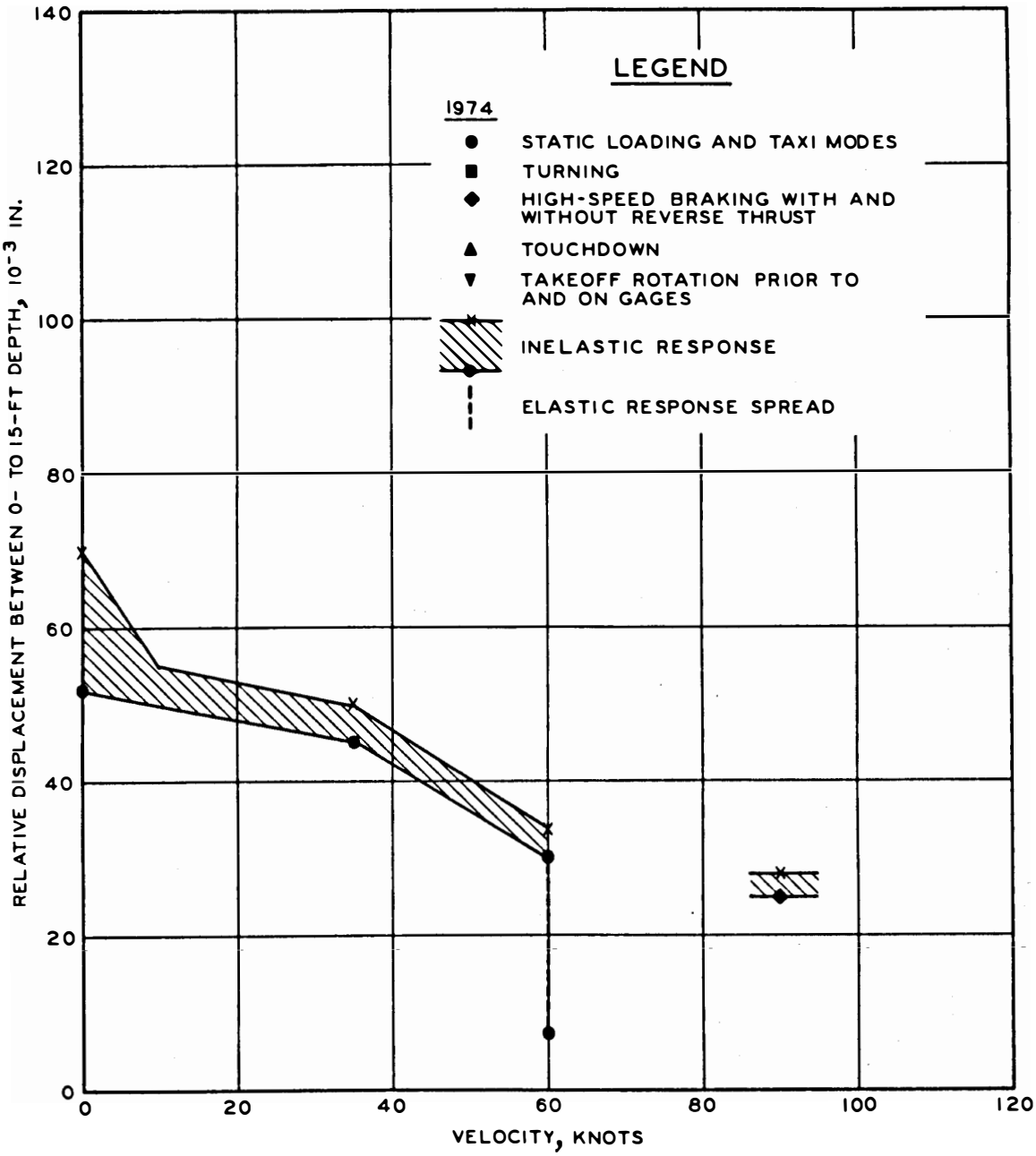

Figure 54. Maximum vertical relative displacement versus velocity, flexible, row 2, 0 to 15 ft, C-880

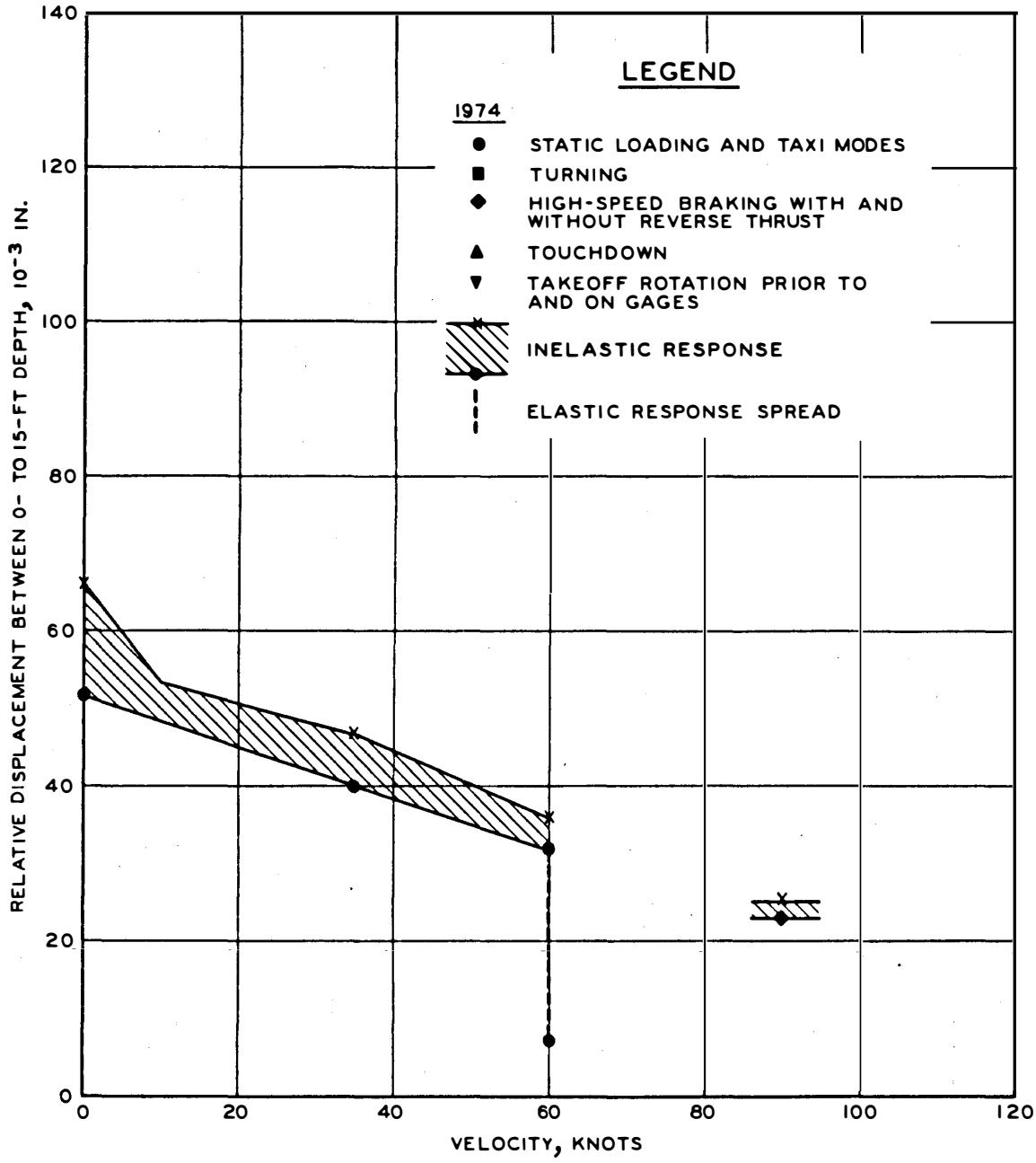

Figure 55. Maximum vertical relative displacement versus velocity, flexible, row 3, 0 to 15 ft, C-880

can be seen in the figures in Appendix B for regions outside the maximum load points. A single datum point in the summary figures indicates that only one test was recorded or no data spread existed on the gage or gages at the maximum load point.

As was the case for the aircraft load data, the data for each operational mode were grouped and are presented in the summary figures at velocity values that are representative of the specific velocity range for each mode. Creep- and low-speed taxi data are plotted at the upper ends of their velocity ranges because the majority of these tests occurred in these ranges. High-speed taxi data are plotted at the upper end of their velocity range in order to represent the highest velocities used in the tests. All other modes are plotted about the centers of their respective velocity ranges. The data points shown represent, for each operational mode, the spread of the pavement response from an upper to a lower value.

The elastic response spreads for each mode are represented by the high and low points being connected by vertical dashed lines. Only elastic high points of the taxi modes are connected across the figures. These lines show the relationship of other modes to the taxi modes and the relationship between the 1972 and the 1974 B-727 tests. Superimposed on the elastic highs are the inelastic responses (cross-hatched regions). These are the largest magnitudes of inelastic displacement measured at the gear maximum load point for a single pass over a gage row. A distributed sequence of loadings with the same gear loads as those for the data shown could result in larger inelastic displacements at a given point if the reference were considered to be the highest peak occurring in the sequence. However, no matter what the loading sequence is, the elastic movement would not be greater than what is shown for the same load ranges. Therefore, for a single pass of the aircraft, the upper boundary of the cross-hatched region represents the approximate maximum displacement that could be expected, and the lower boundary represents the maximum elastic displacement that could be expected. However, depending on the load history, the displacement could be on or anywhere between the two boundaries.

Noticeable in Figures 50-55 are the increases in inelastic responses in the 1974 tests. These are believed due to the higher temperatures and increased plasticity of the bituminous layers. The elastic responses also increased in 1974, but they decreased with increased aircraft velocities to about the 1972 test levels. The increased elastic response is believed to be due to the viscoelastic effect in the bituminous layers due to the higher temperatures. The odd behavior (response decrease about 35 knots) seen in some of the figures is believed to be due to a lack of data at the maximum load points. A comparison of Figures 23-26 and 50-55 shows that there are similar patterns in the aircraft load and pavement structure responses.

Figures 56-85 summarize the individual pavement structure element vertical responses as measured by Bison coils. Both the 1972 and the 1974 results for the B-727 operations are shown in the same figures. Previous remarks concerning data presentation in Figures 50-55 are also applicable to these figures. Noticeable in these figures are the increases in elastic and inelastic responses in 1974 and their decreases with increased velocity and depth to about the same levels as the 1972 responses. This is believed to be due to the viscoelastic effect and plastic behavior increases in the bituminous layers and not due to a temperature effect in the soil materials. In other words, the behavior in the bituminous layers was controlling the deeper material behaviors. Figures 50-85 imply that the viscoelastic response can be separated from the approximately constant elastic (without viscoelastic) response by projecting back the elastic response at high aircraft velocities.

Figures 86 and 87 summarize the flexible pavement structure horizontal responses as measured by Bison coils. The 1972 results include almost all of the operating modes, but only turning data were recorded in 1974. All previous remarks also apply to these figures, and the behavior shown is basically the same as that shown by the vertical response figures.

Rigid Pavement Structure Results. The total pavement structure responses as measured by WES deflection gages embedded in the bottom of the concrete slabs are shown in Figures B277-B297. Tests were only

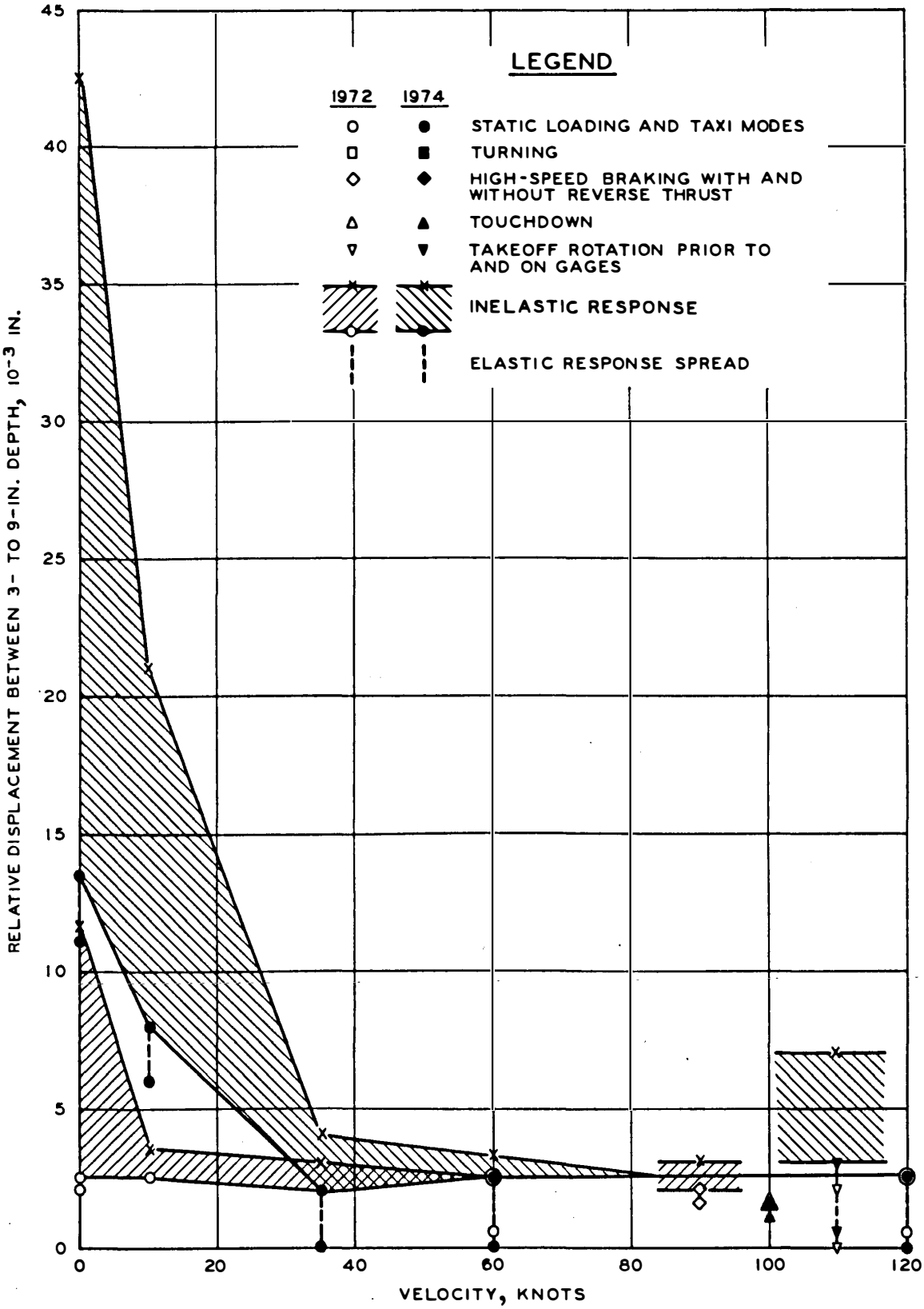

Figure 56. Maximum vertical relative displacement versus velocity, flexible, row 1, 3 to 9 in., B-727

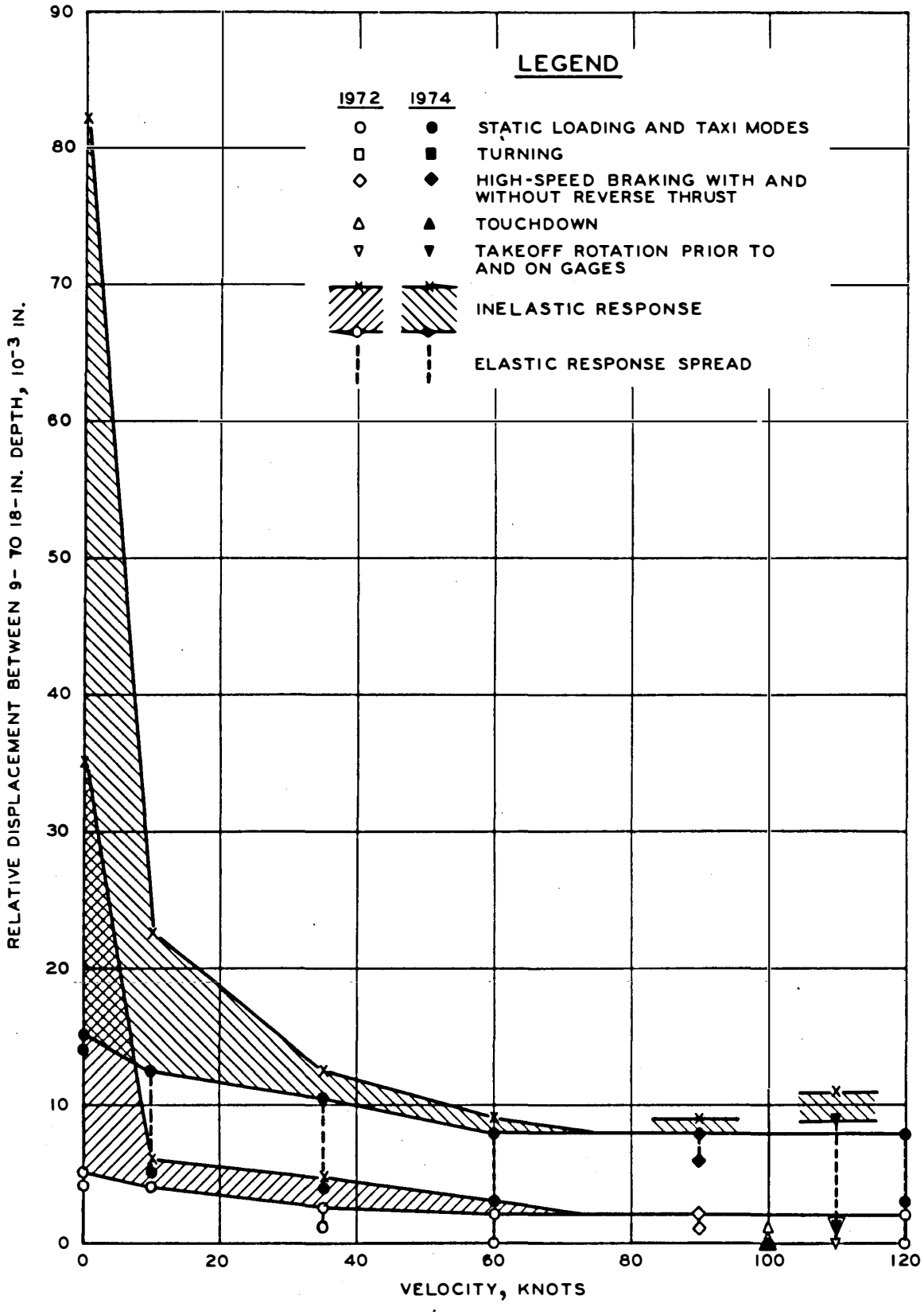

Figure 57. Maximum vertical relative displacement versus velocity, flexible, row 1, 9 to 18 in., B-727

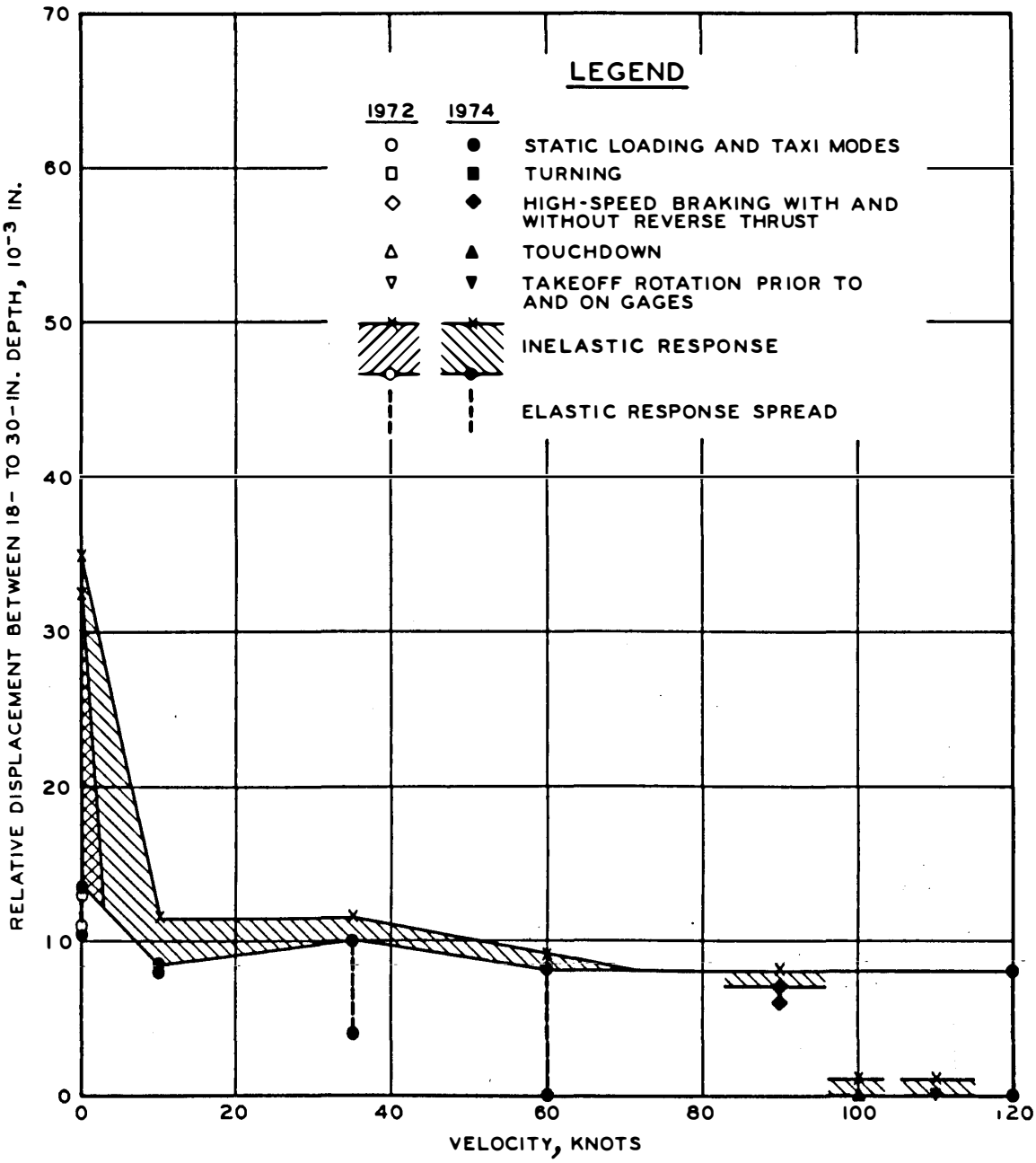

Figure 58. Maximum vertical relative displacement versus velocity, flexible, row 1, 18 to 30 in., B-727

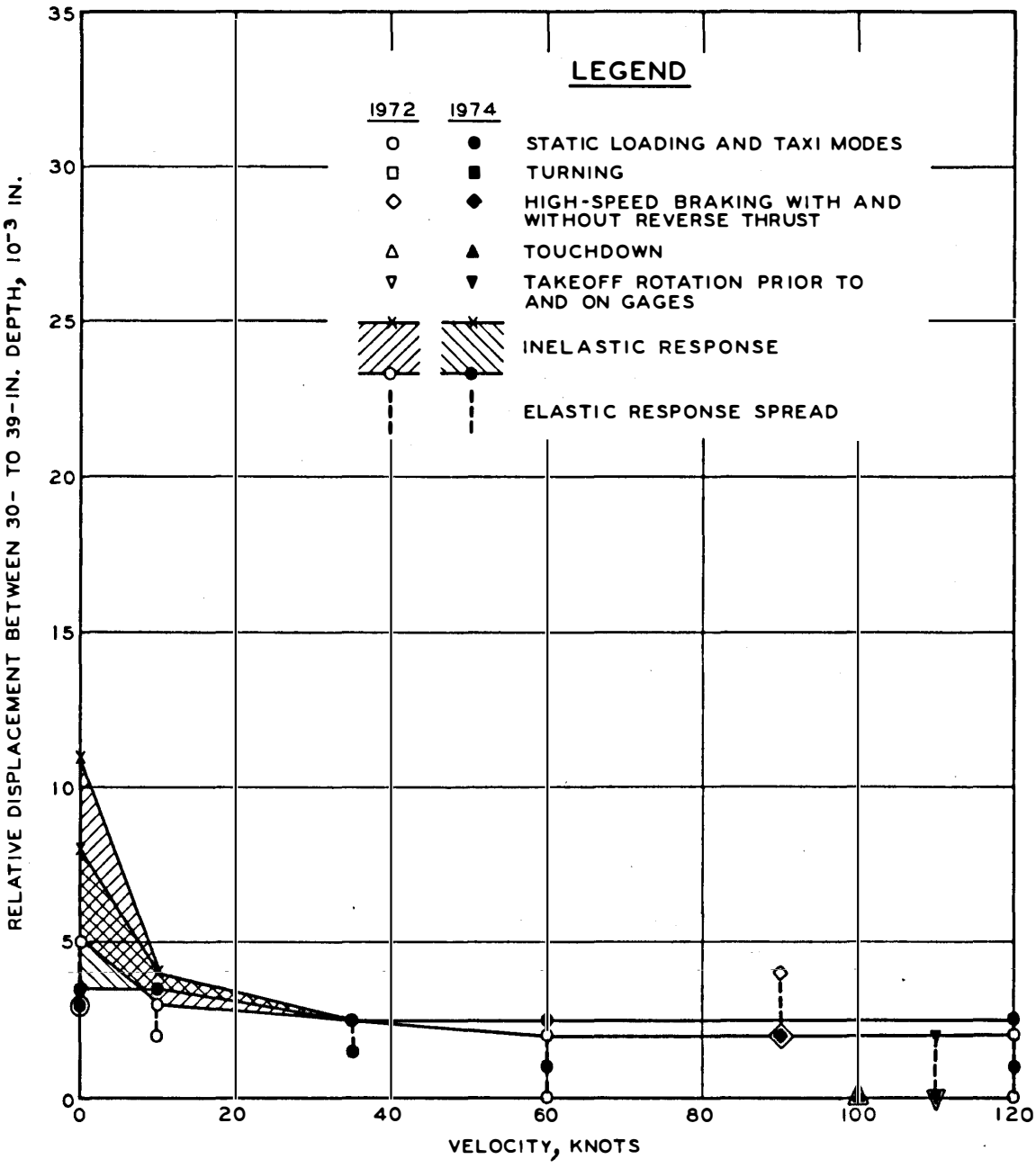

Figure 59. Maximum vertical relative displacement versus velocity, flexible, row 1, 30 to 39 in., B-727

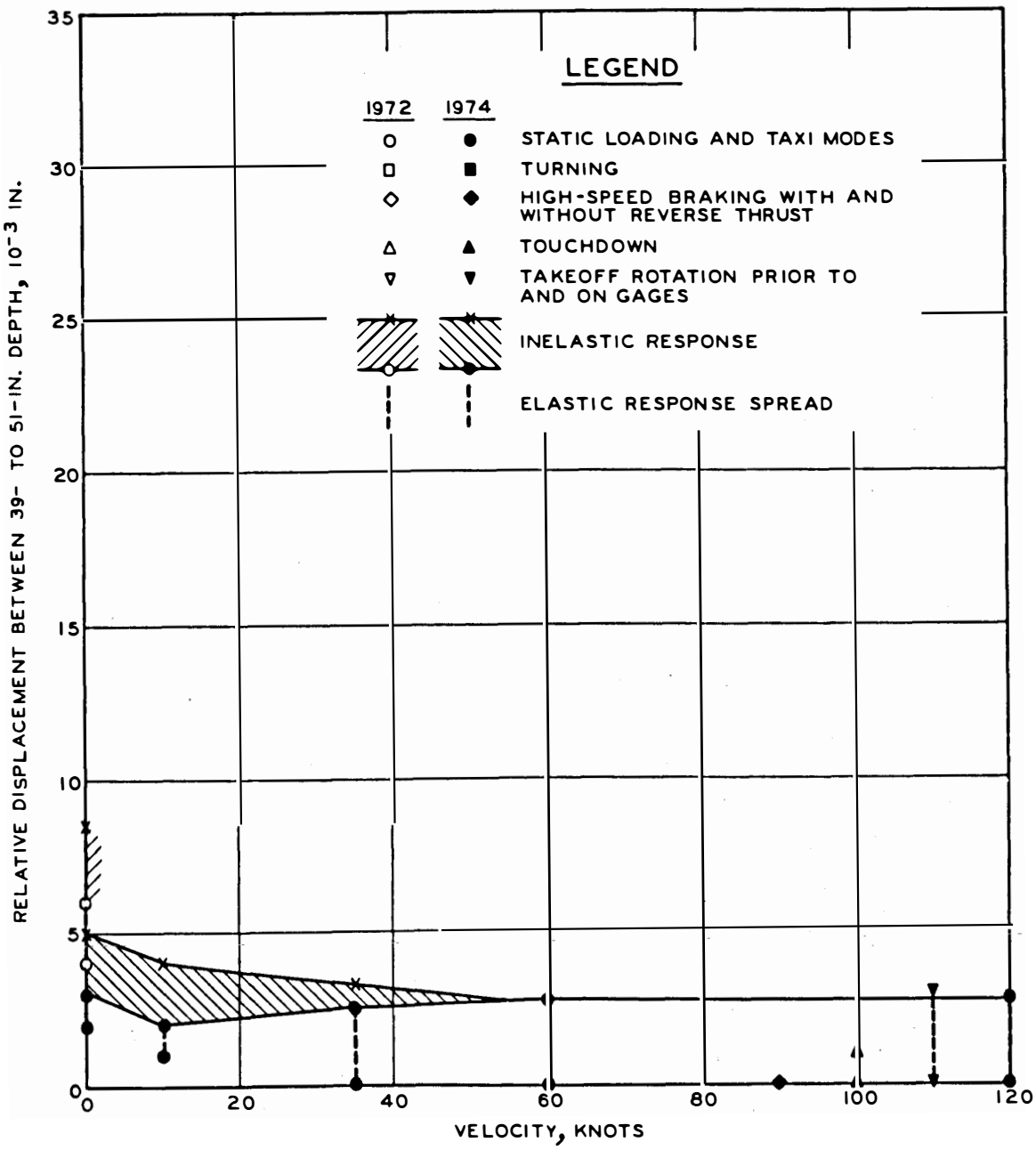

Figure 60. Maximum vertical relative displacement versus velocity, flexible, row 1, 39 to 51 in., B-727

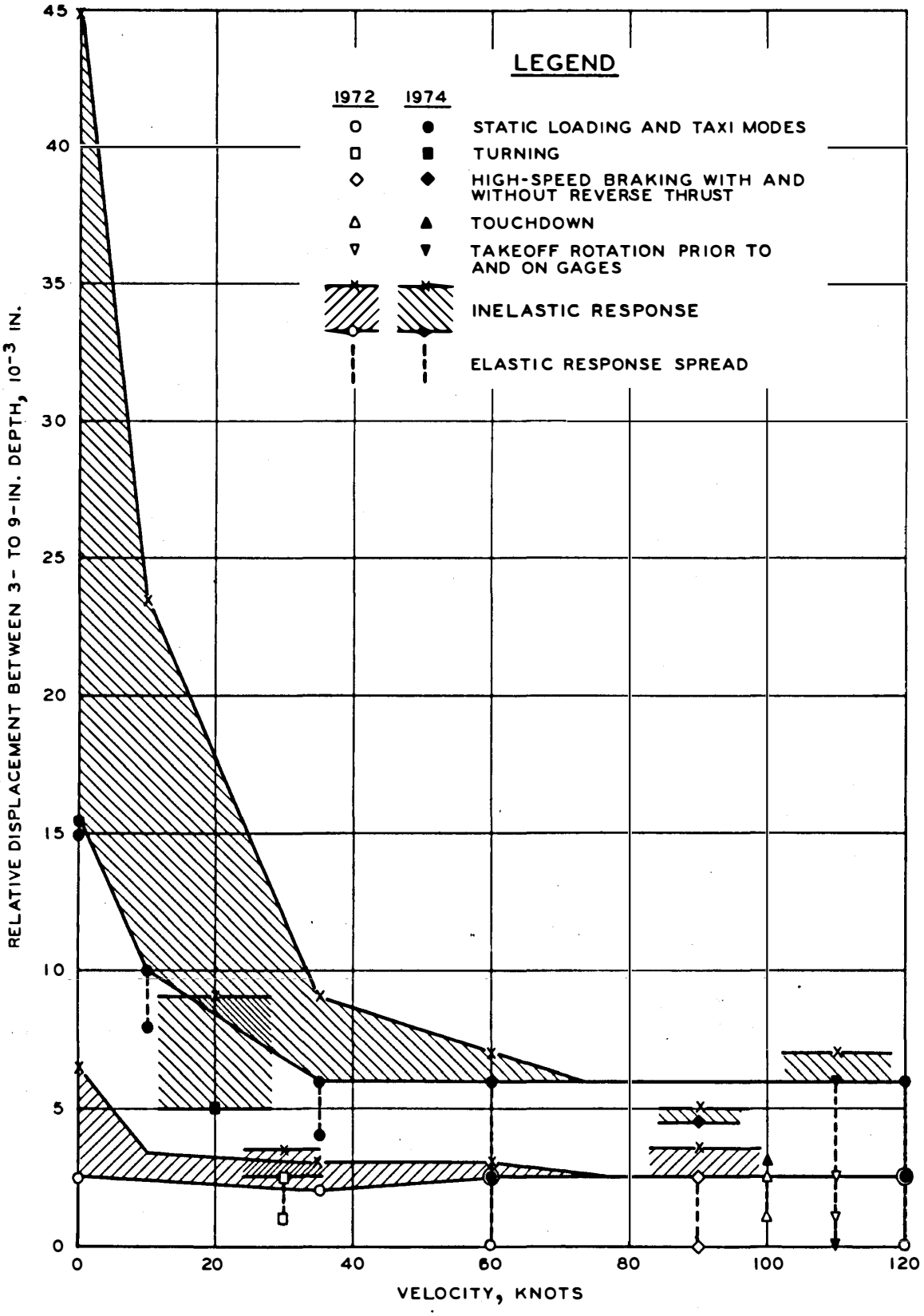

Figure 61. Maximum vertical relative displacement versus velocity, flexible, row 2, 3 to 9 in., B-727

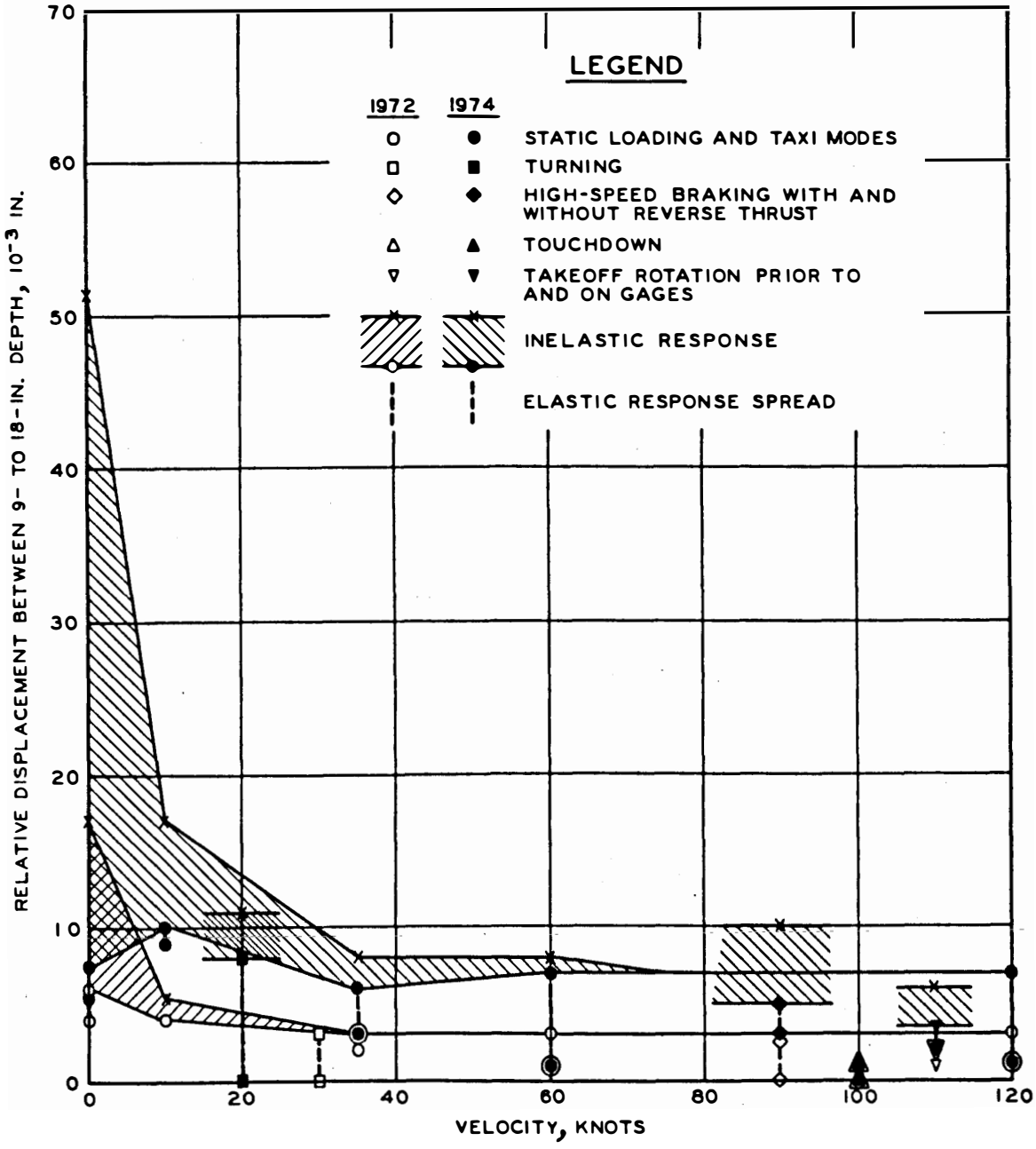

Figure 62. Maximum vertical relative displacement versus velocity, flexible, row 2, 9 to 18 in., B-727

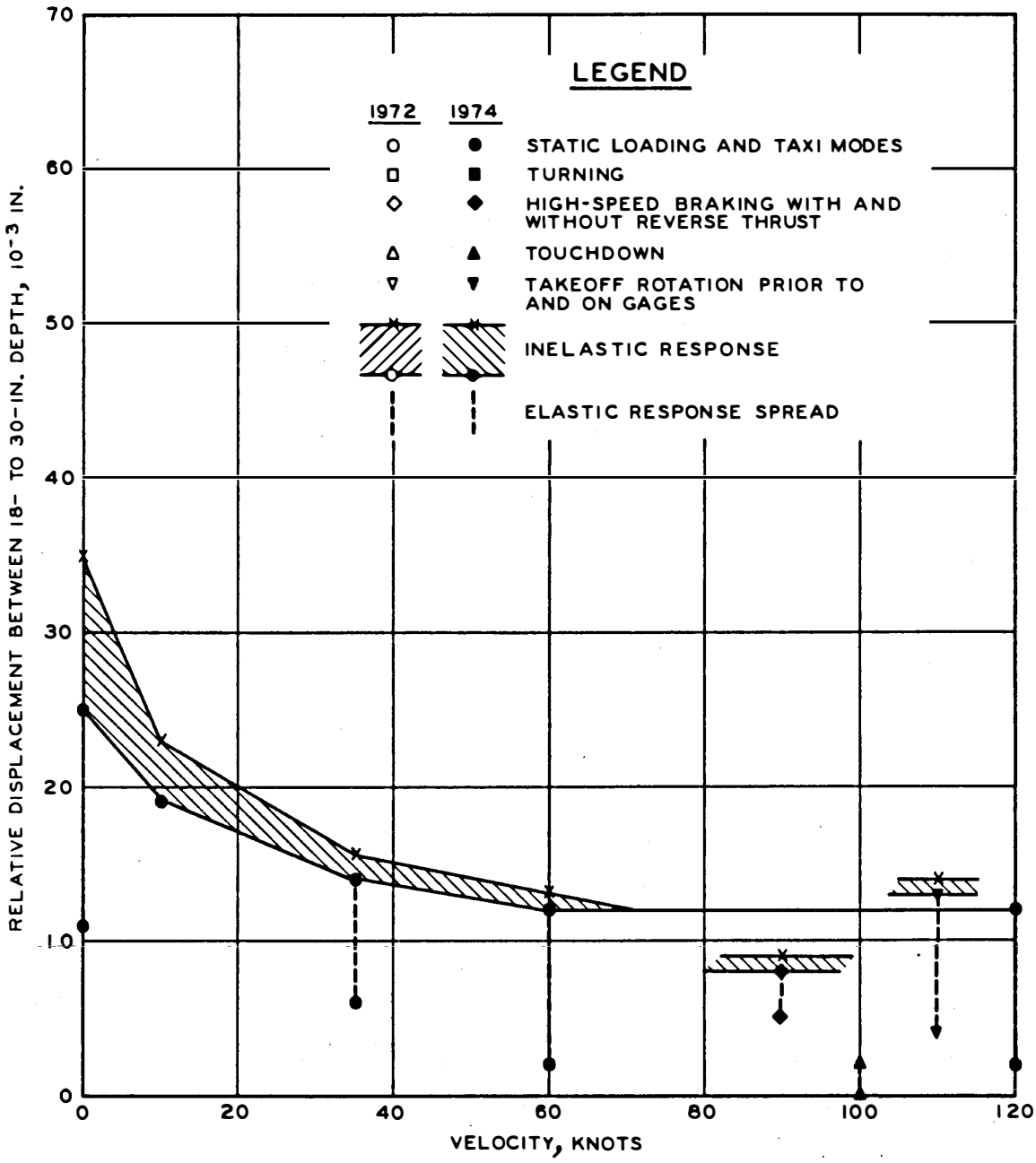

Figure 63. Maximum vertical relative displacement versus velocity, flexible, row 2, 18 to 30 in., B-727

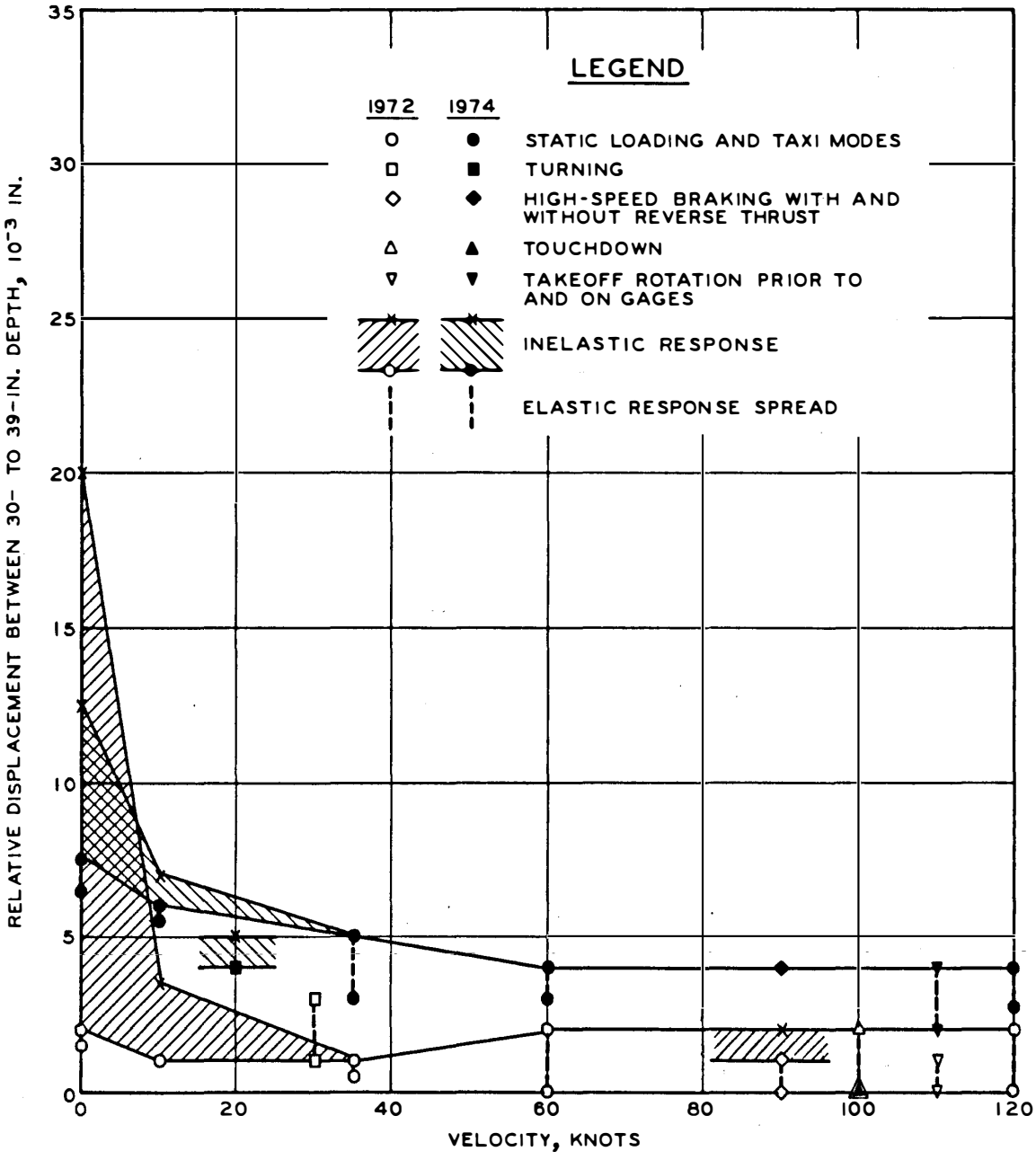

Figure 64. Maximum vertical relative displacement versus velocity, flexible, row 2, 30 to 39 in., B-727

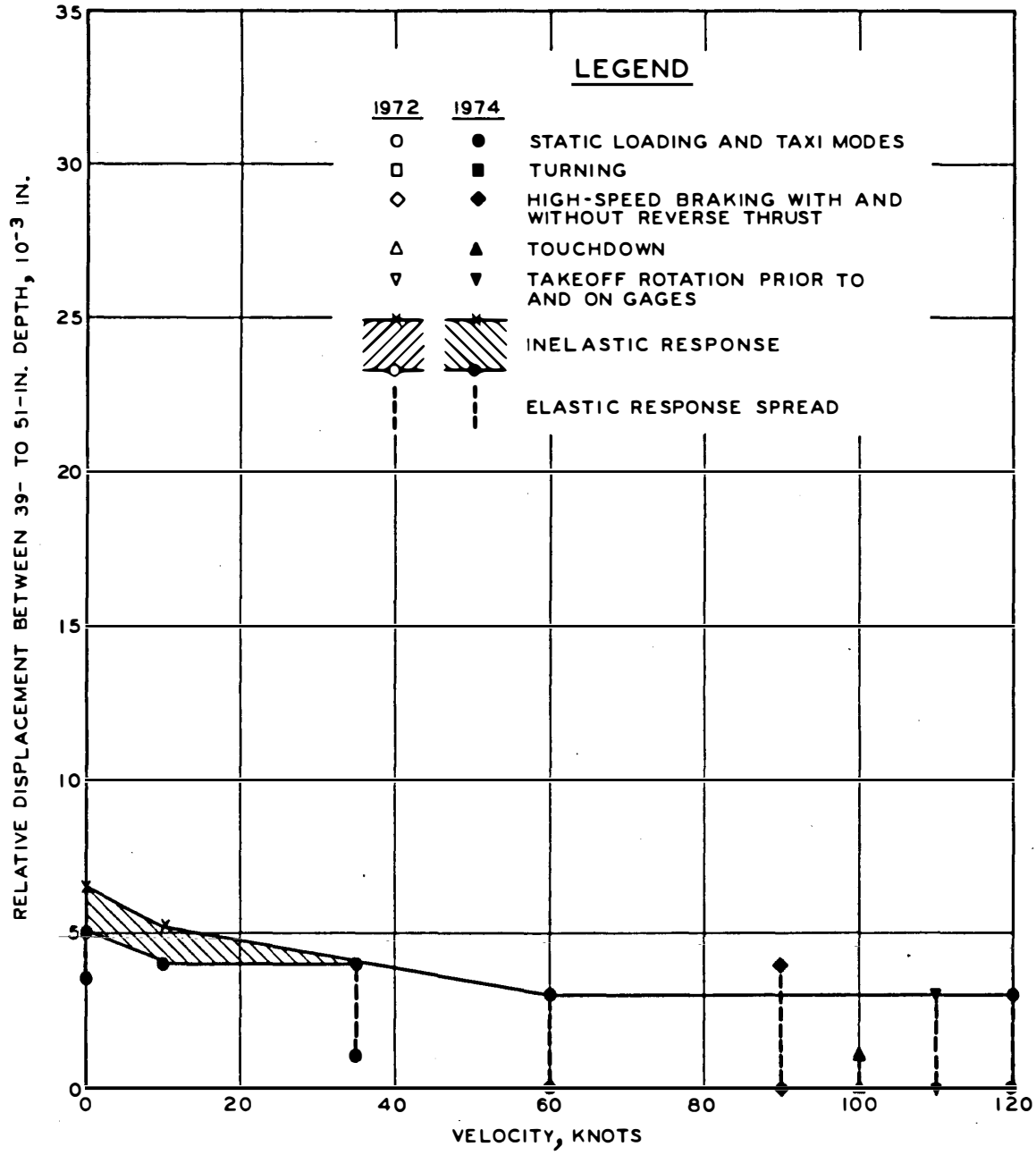

Figure 65. Maximum vertical relative displacement versus velocity, flexible, row 2, 39 to 51 in., B-727

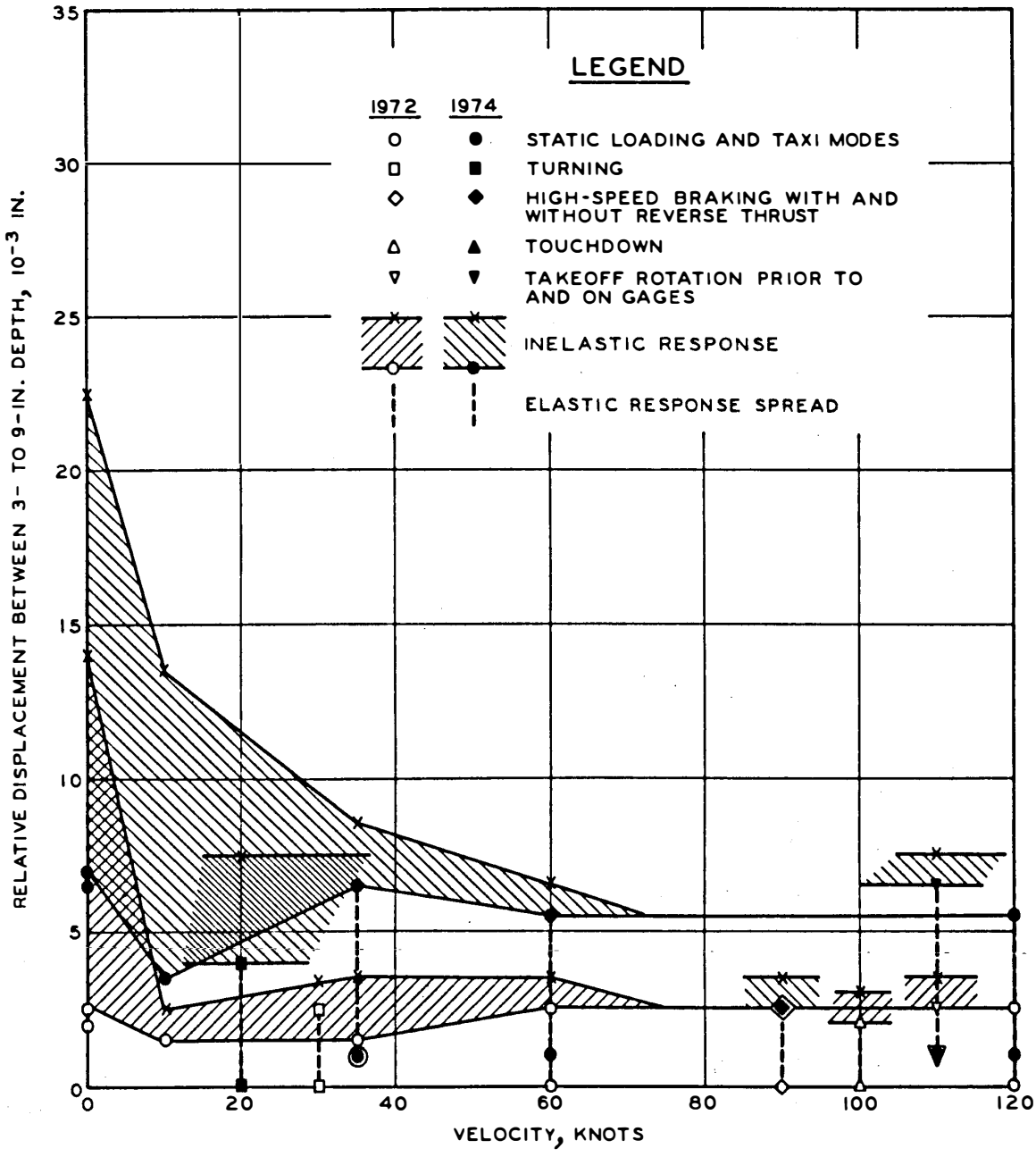

Figure 66. Maximum vertical relative displacement versus velocity, flexible, row 3, 3 to 9 in., B-727

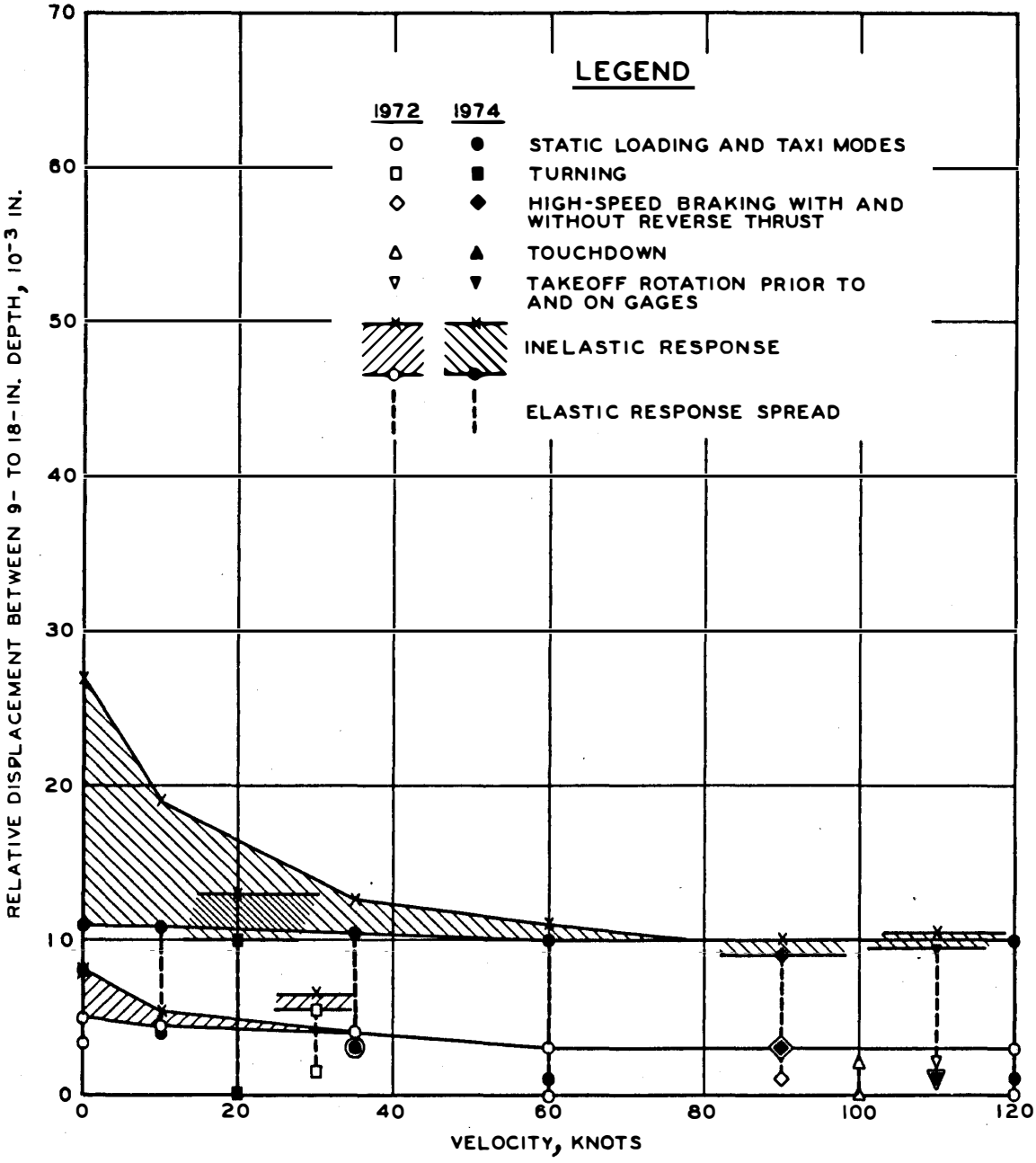

Figure 67. Maximum vertical relative displacement versus velocity, flexible, row 3, 9 to 18 in., B-727

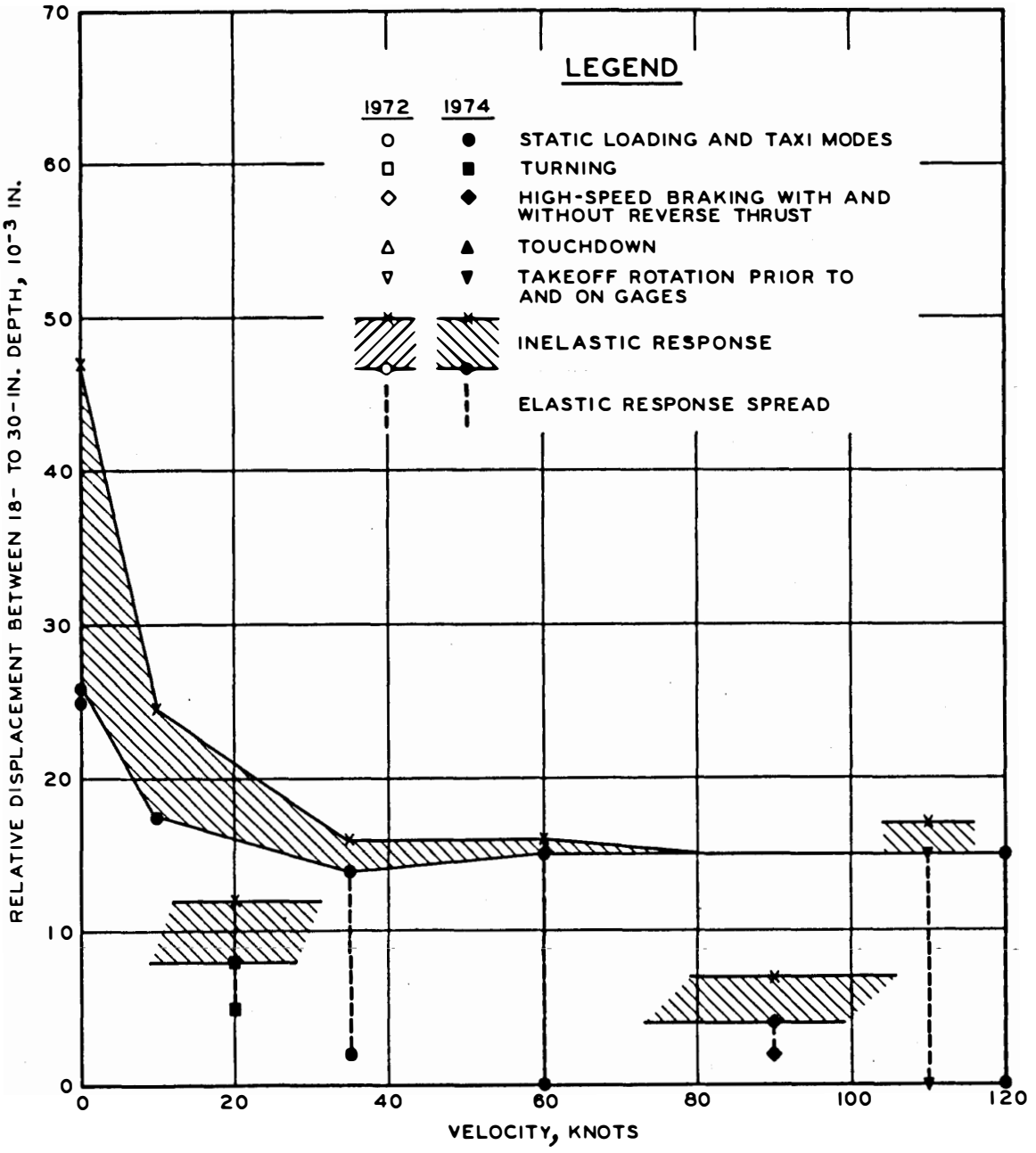

Figure 68. Maximum vertical relative displacement versus velocity, flexible, row 3, 18 to 30 in., B-727

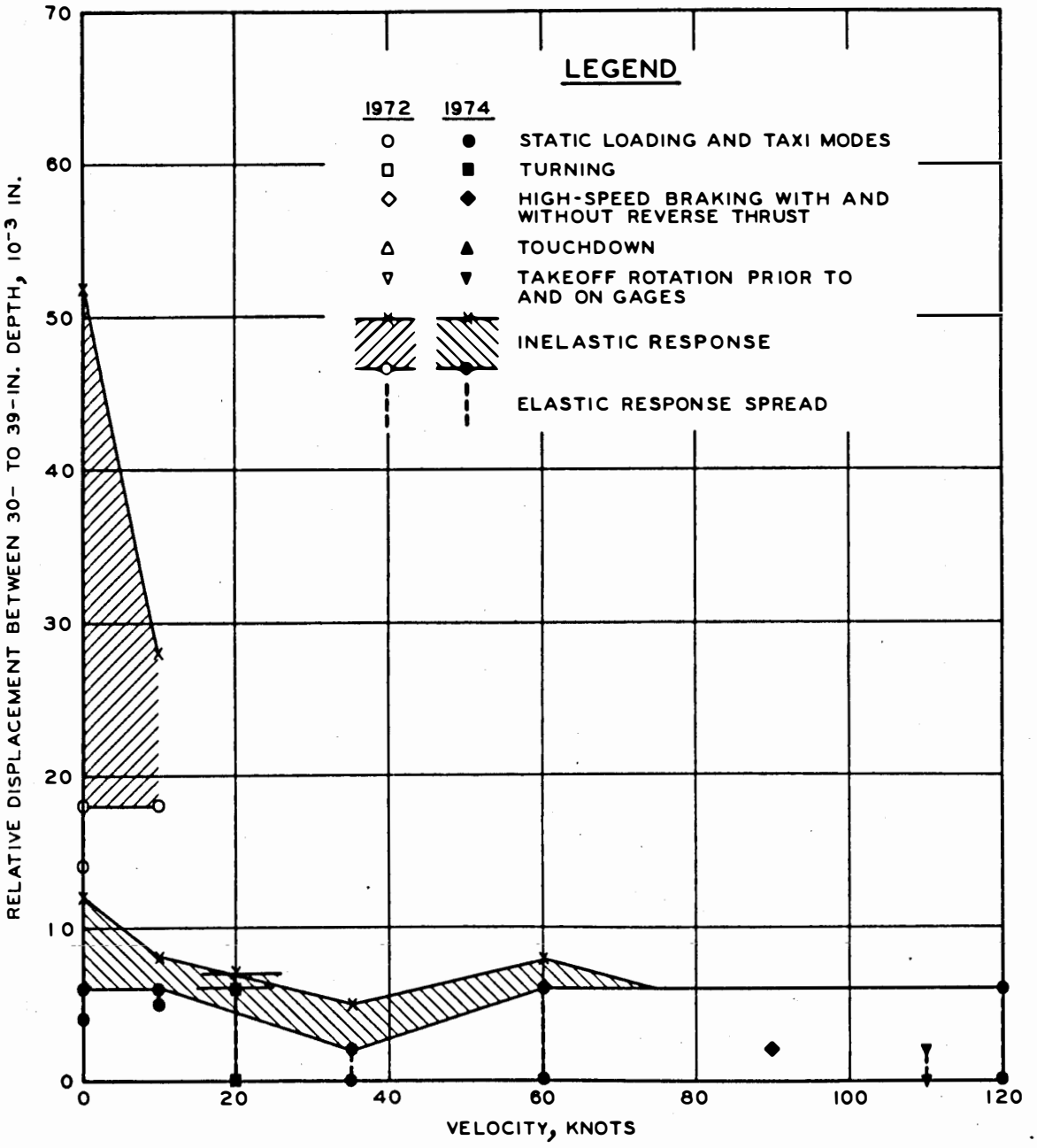

Figure 69. Maximum vertical relative displacement versus velocity, flexible, row 3, 30 to 39 in., B-727

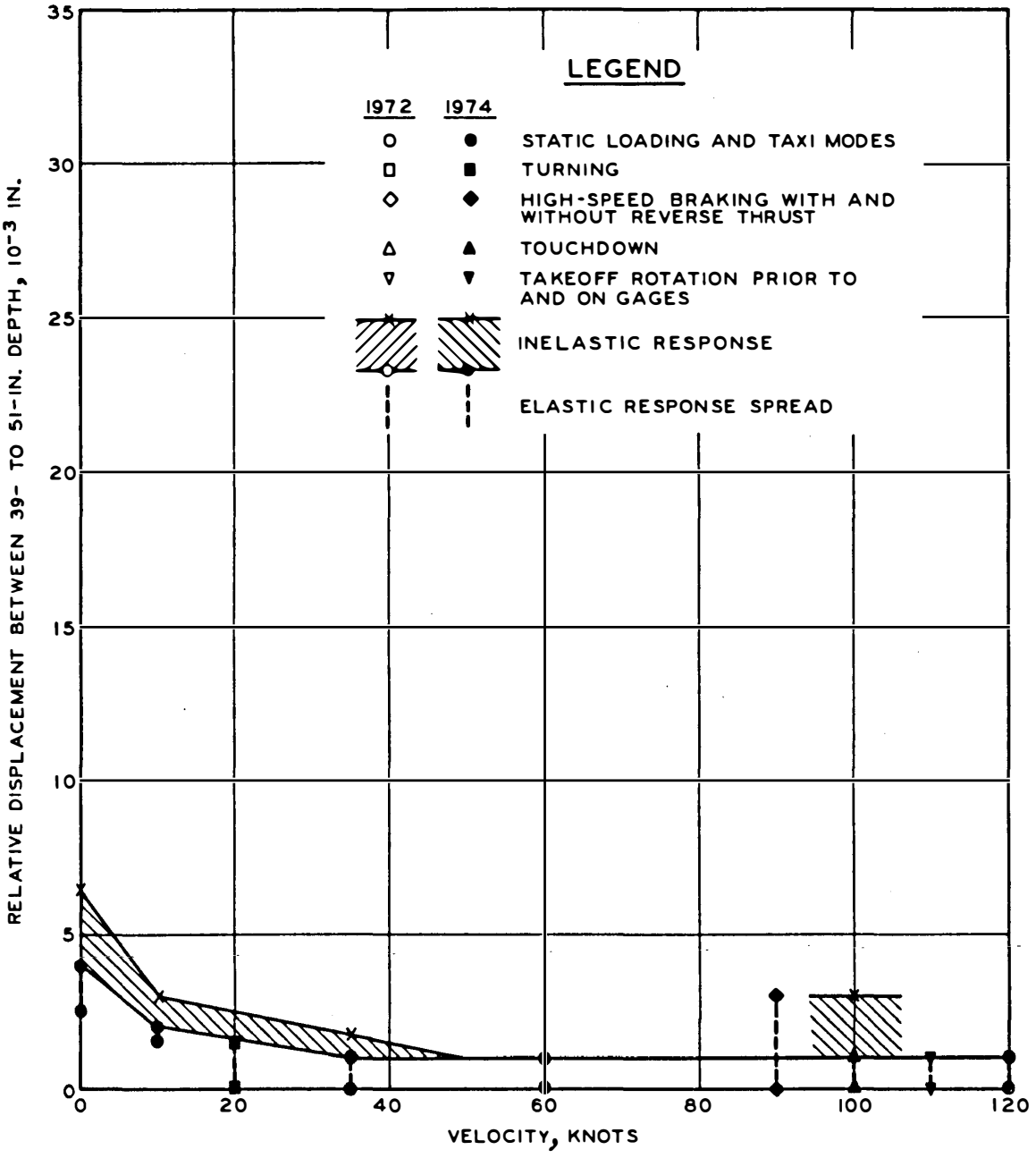

Figure 70. Maximum vertical relative displacement versus velocity, flexible, row 3, 39 to 51 in., B-727

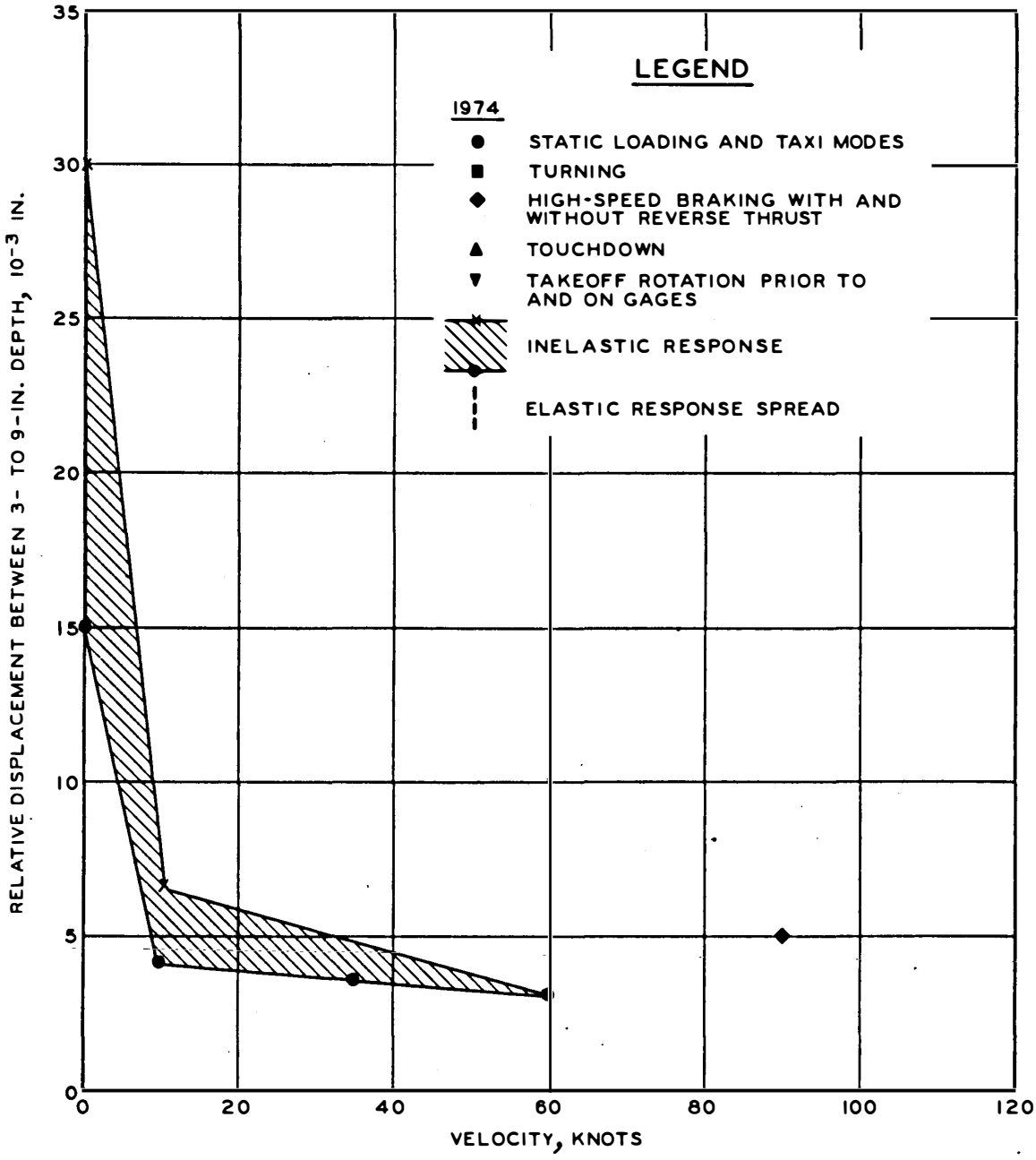

Figure 71. Maximum vertical relative displacement versus velocity, flexible, row 1, 3 to 9 in., C-880

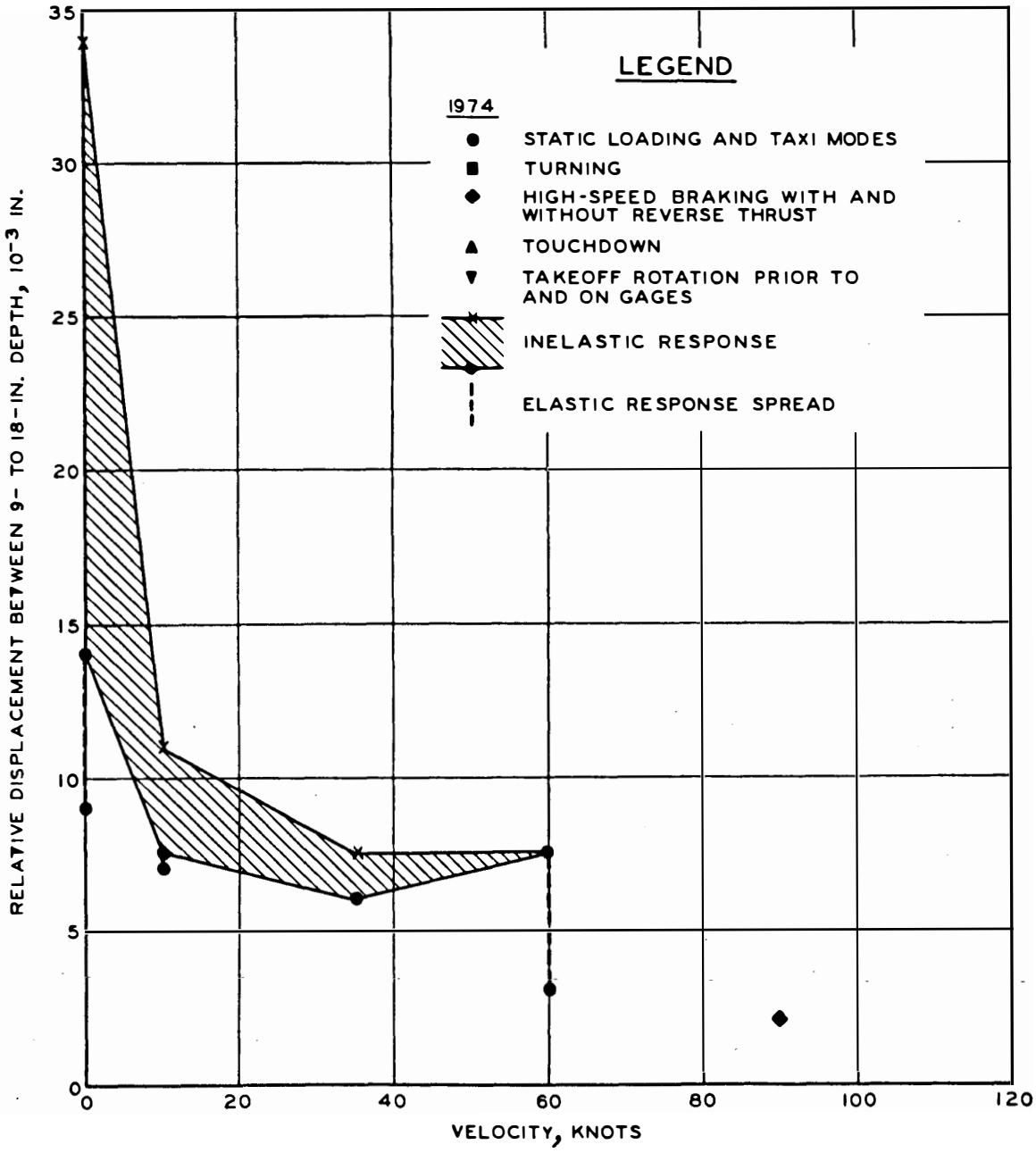

Figure 72. Maximum vertical relative displacement versus velocity, flexible, row 1, 9 to 18 in., C-880

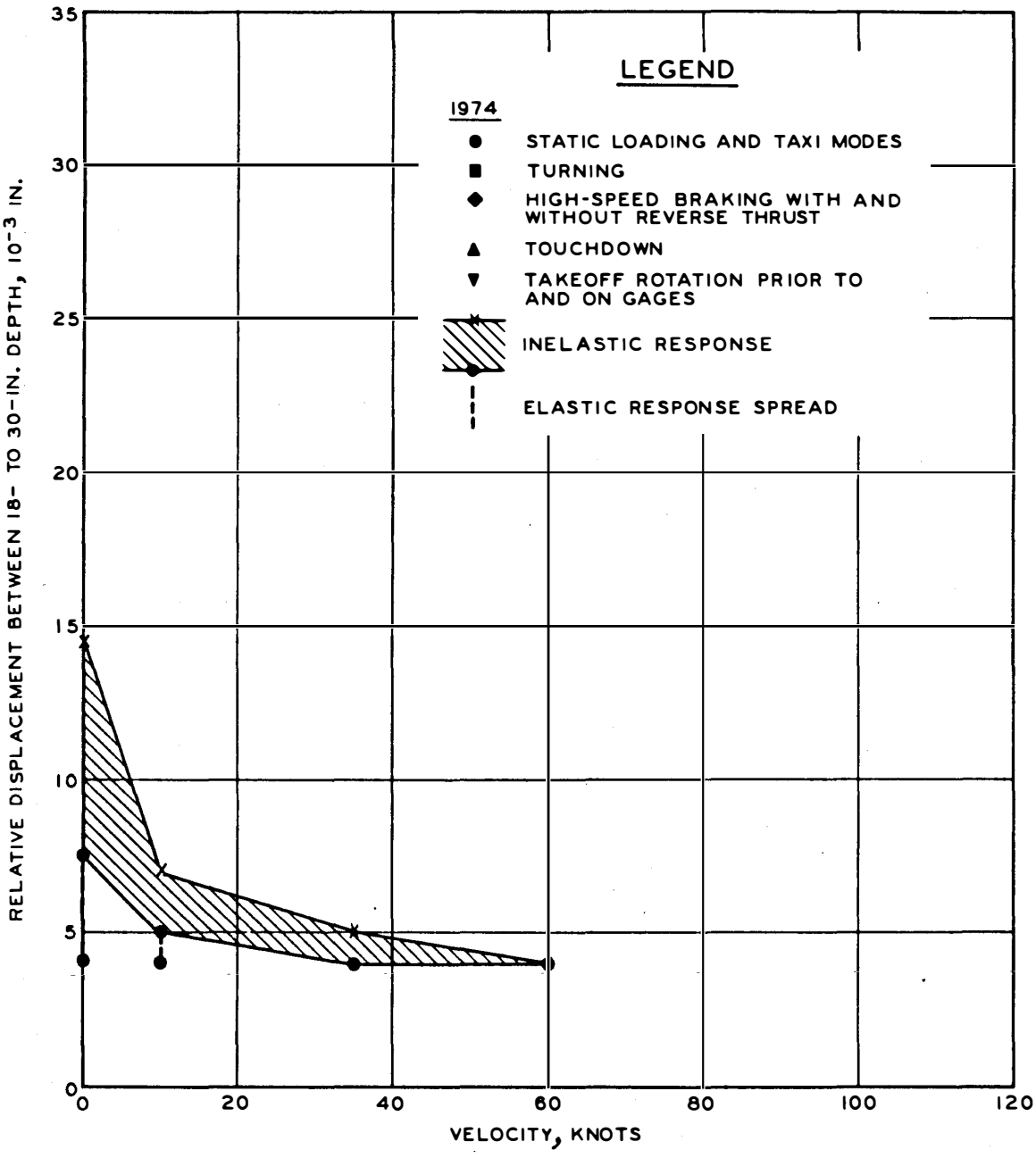

Figure 73. Maximum vertical relative displacement versus velocity, flexible, row 1, 18 to 30 in., C-880

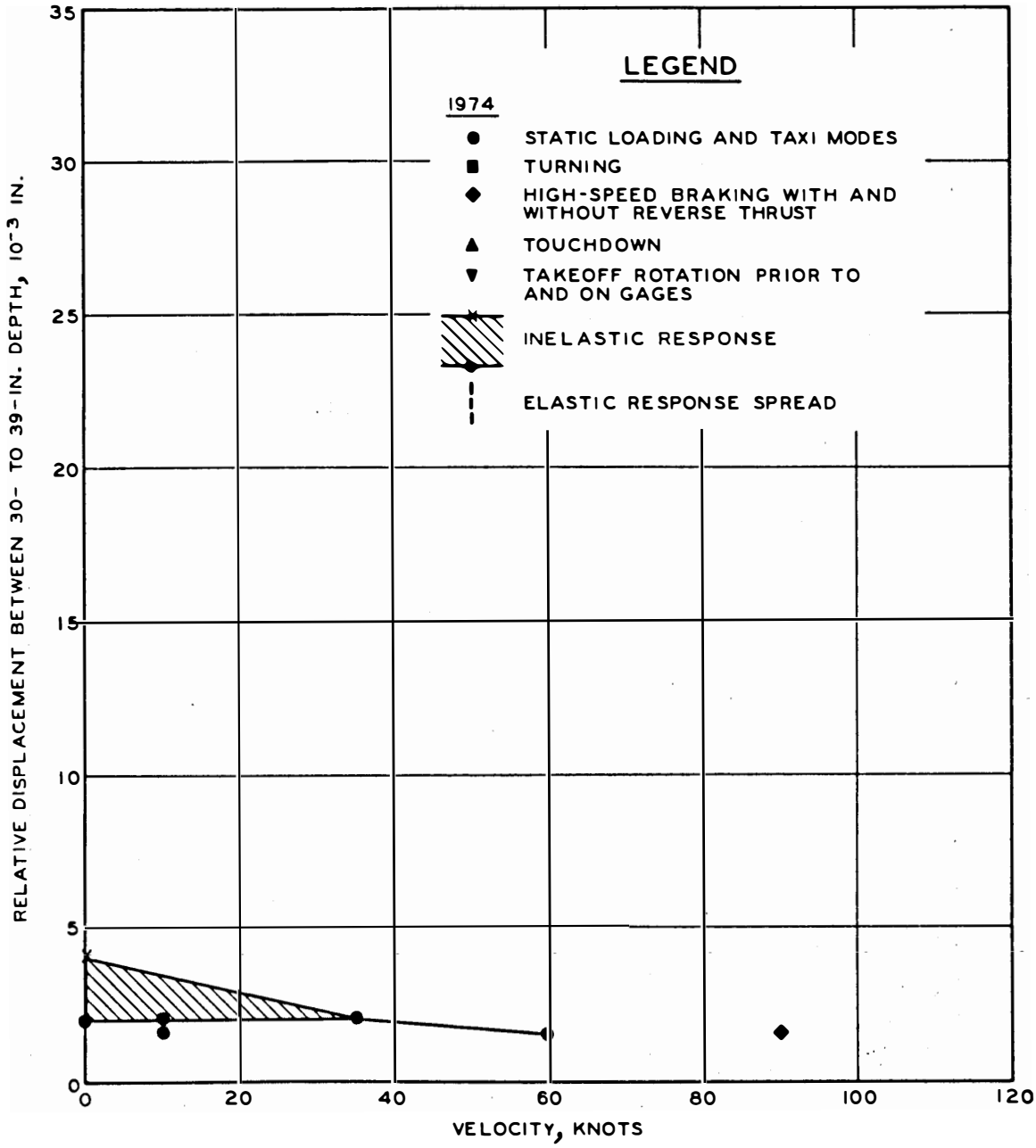

Figure 74. Maximum vertical relative displacement versus velocity, flexible, row 1, 30 to 39 in., C-880

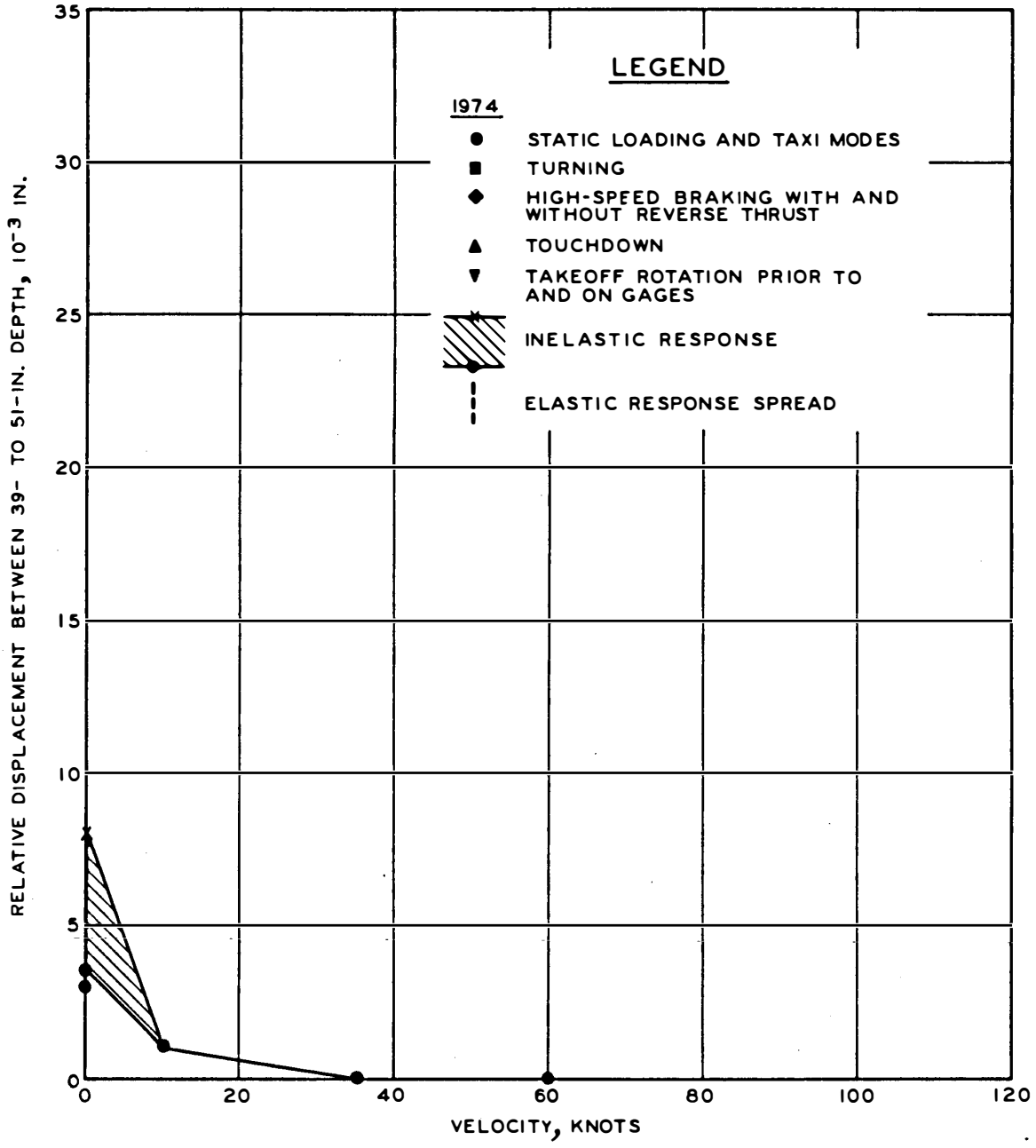

Figure 75. Maximum vertical relative displacement versus velocity, flexible, row 1, 39 to 51 in., C-880

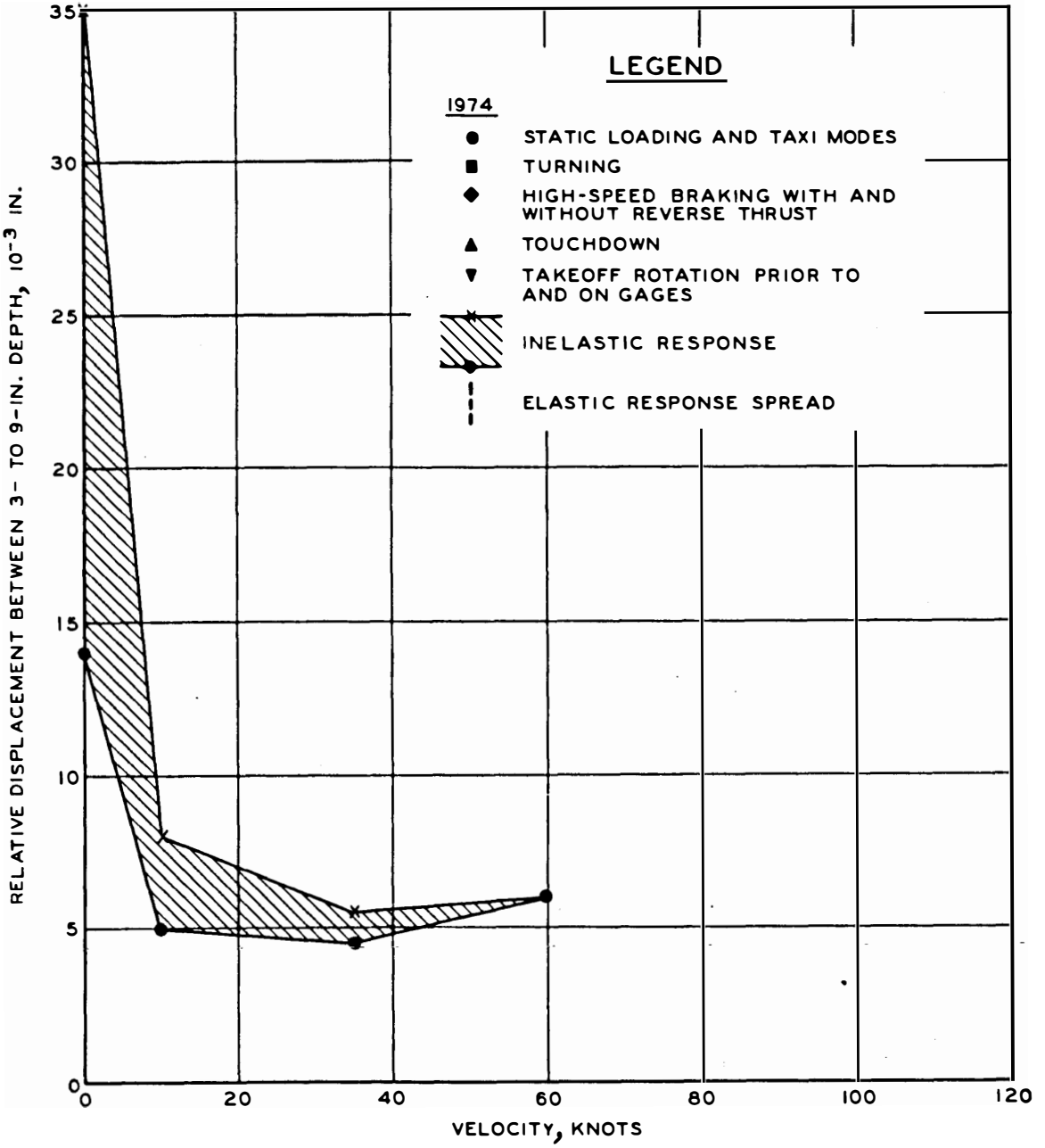

Figure 76. Maximum vertical relative displacement versus velocity, flexible, row 2, 3 to 9 in., C-880

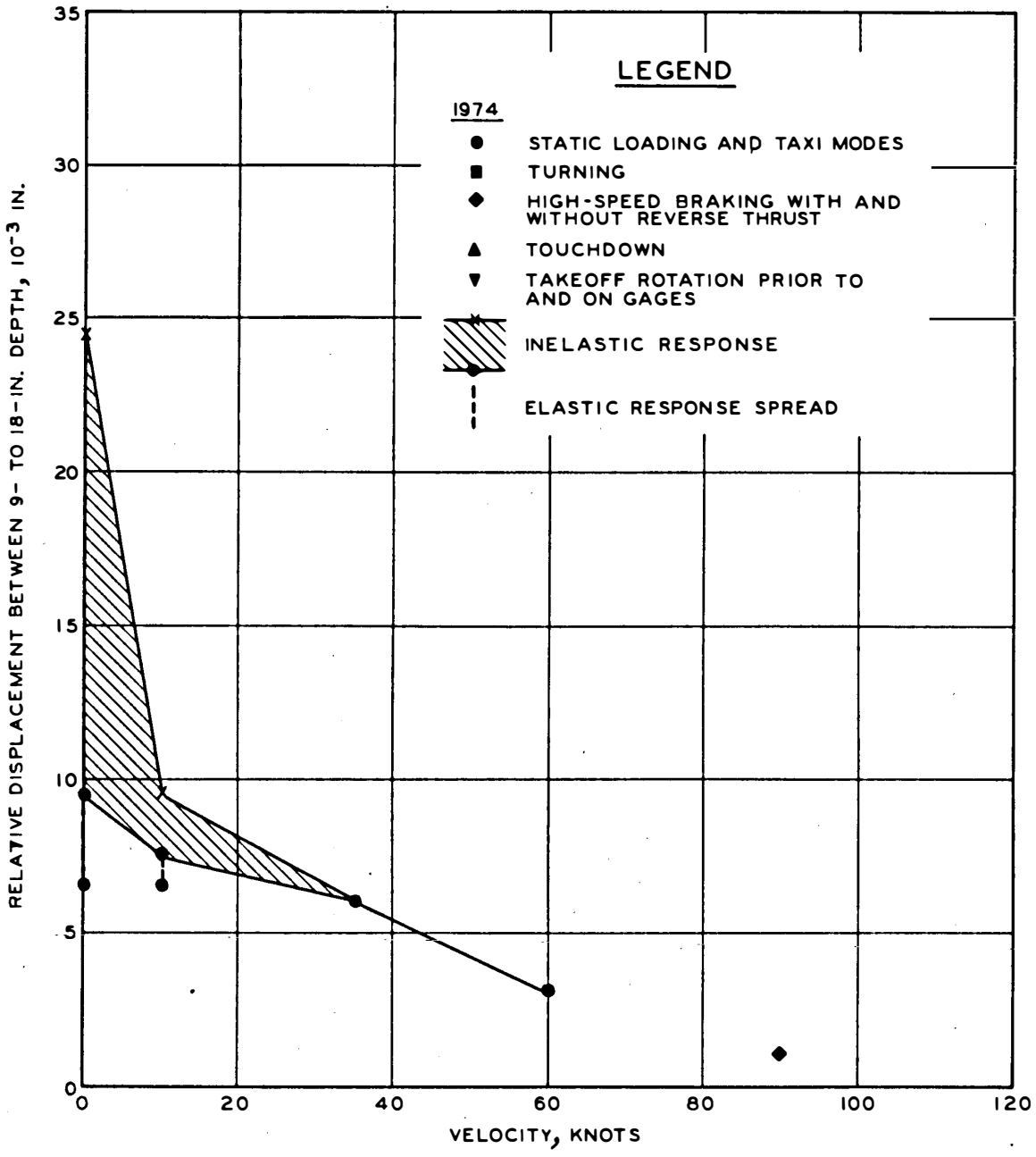

Figure 77. Maximum vertical relative displacement versus velocity, flexible, row 2, 9 to 18 in., C-880

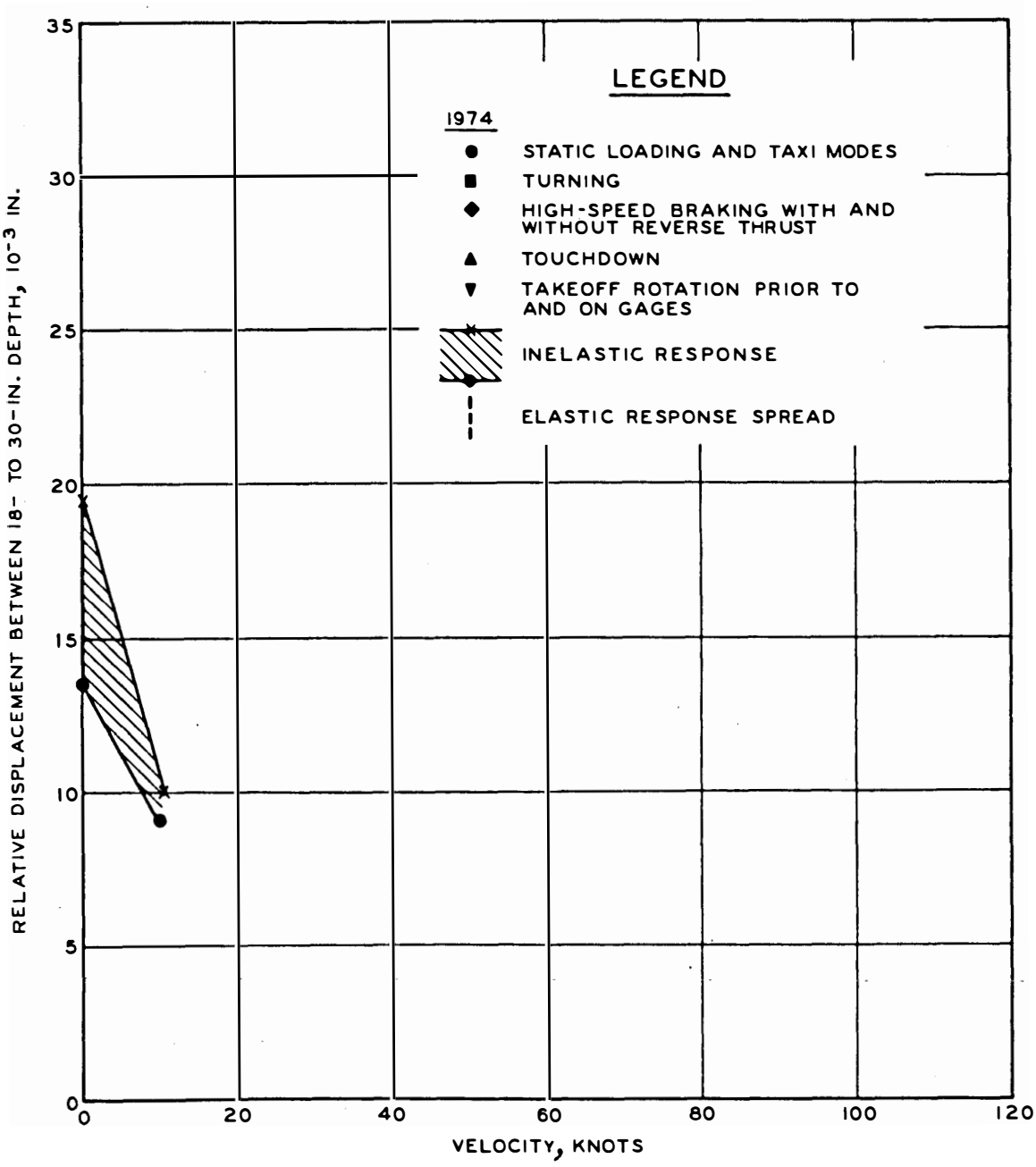

Figure 78. Maximum vertical relative displacement versus velocity, flexible, row 2, 18 to 30 in., C-880

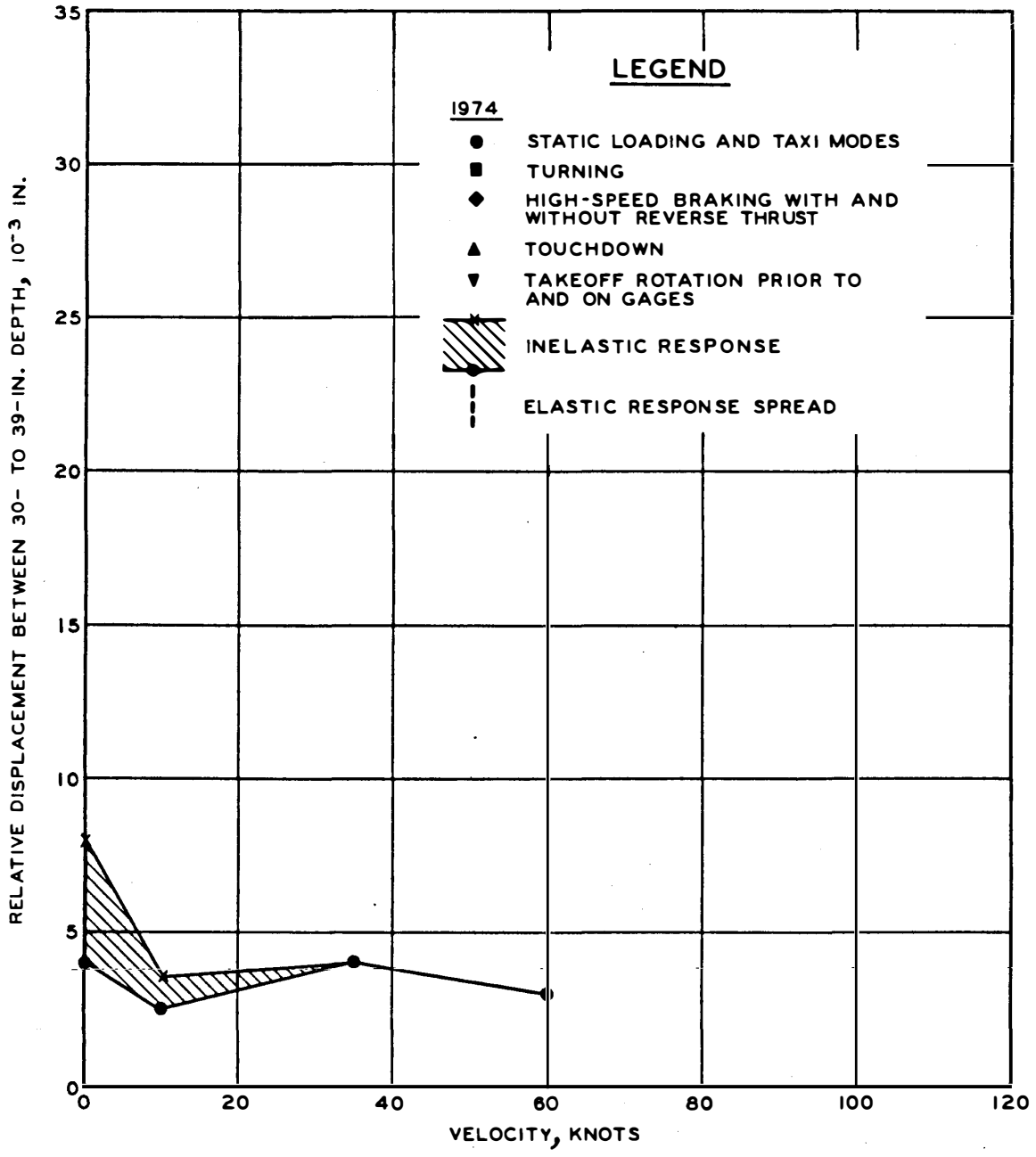

Figure 79. Maximum vertical relative displacement versus velocity, flexible, row 2, 30 to 39 in., C-880

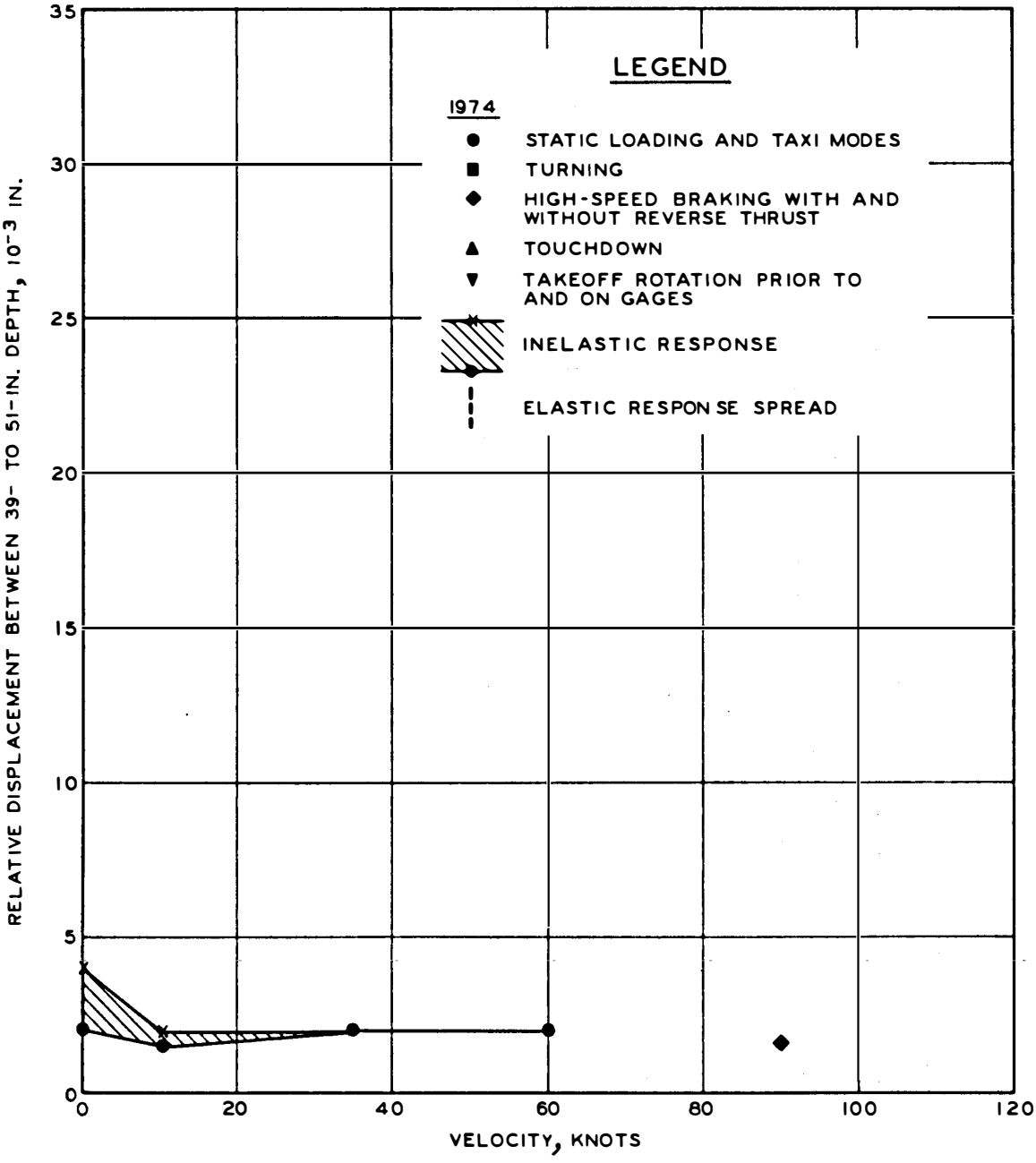

Figure 80. Maximum vertical relative displacement versus velocity, flexible, row 2, 39 to 51 in., C-880

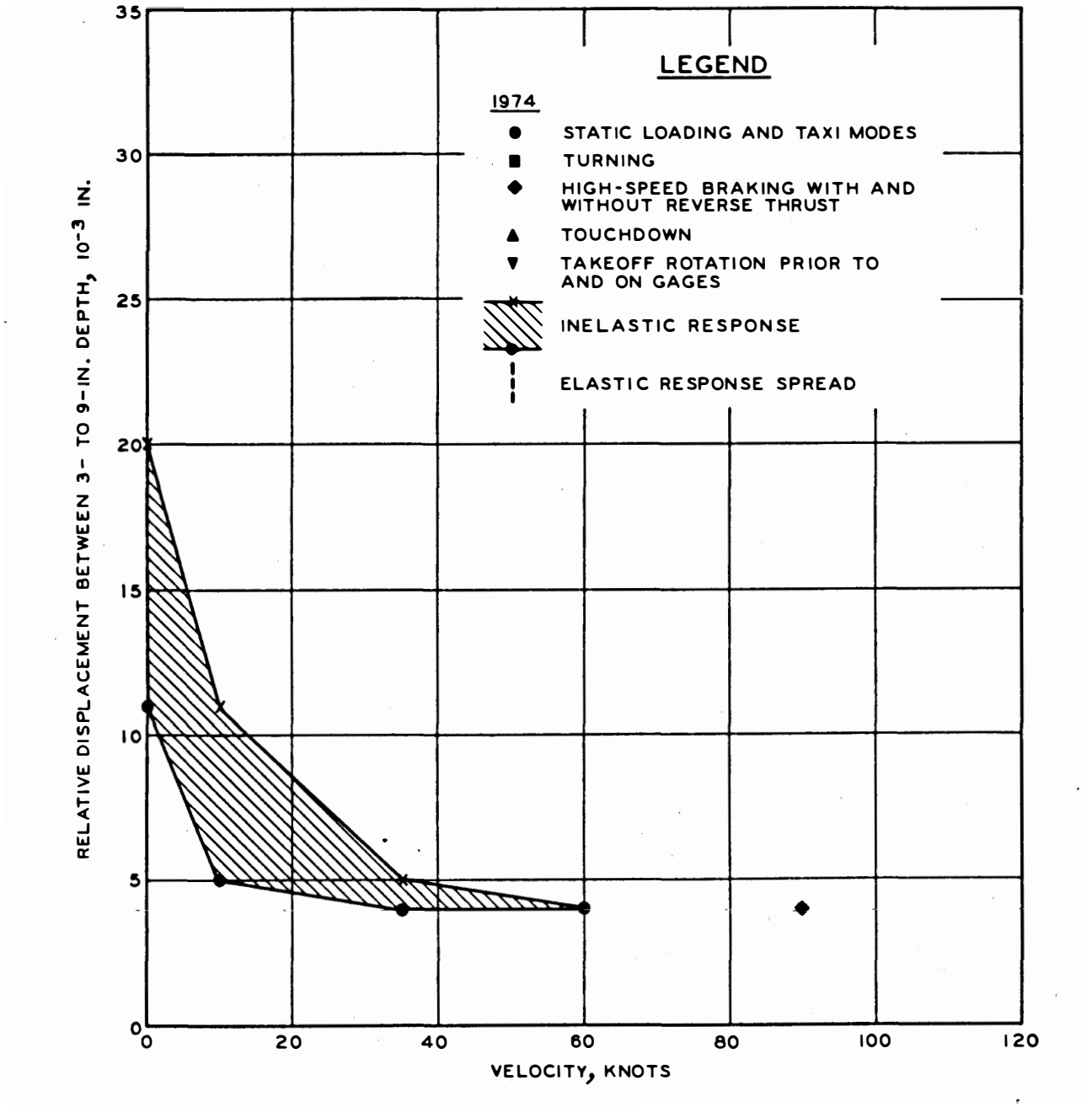

Figure 81. Maximum vertical relative displacement versus velocity, flexible, row 3, 3 to 9 in., C-880

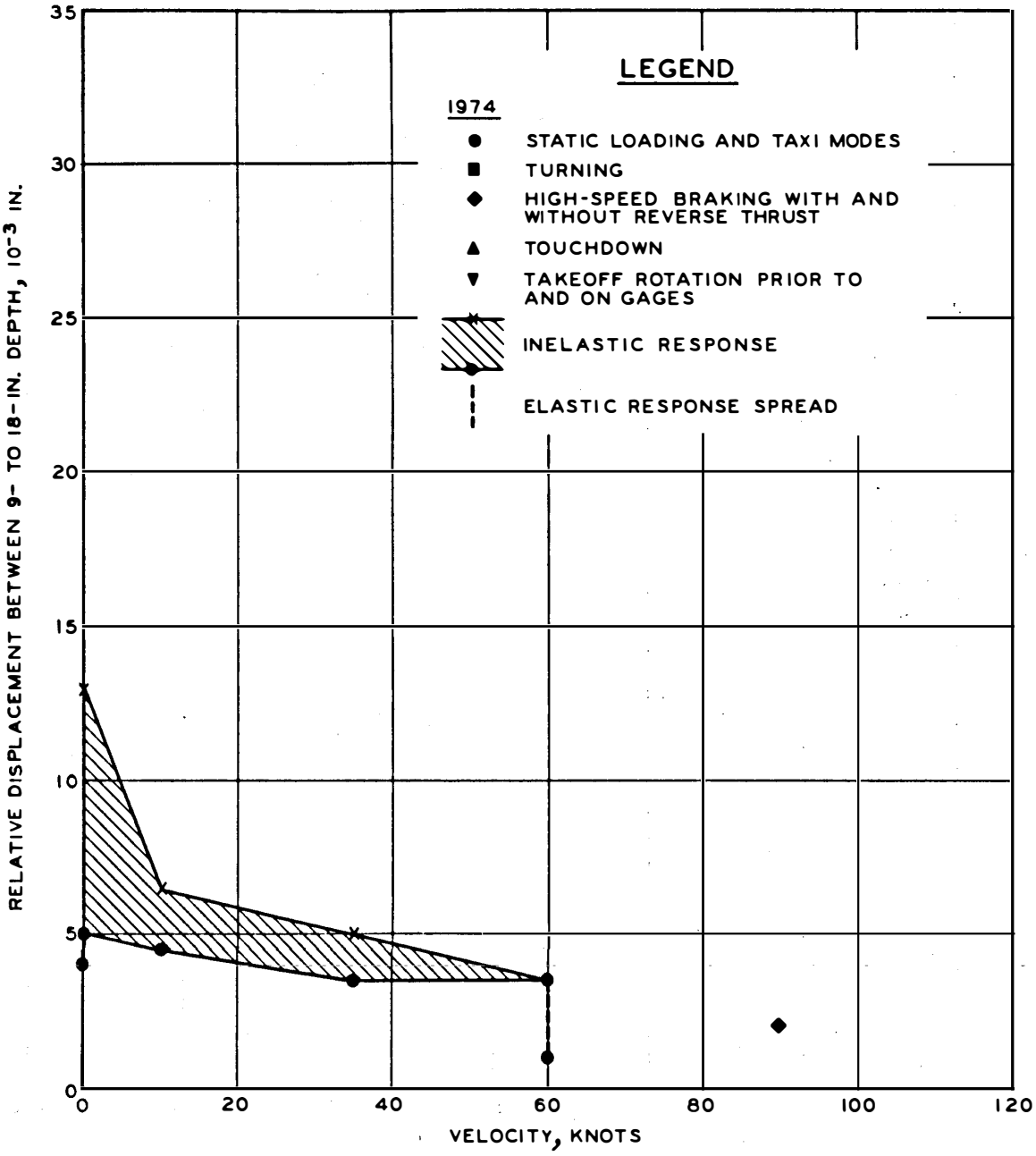

Figure 82. Maximum vertical relative displacement versus velocity, flexible, row 3, 9 to 18 in., C-880

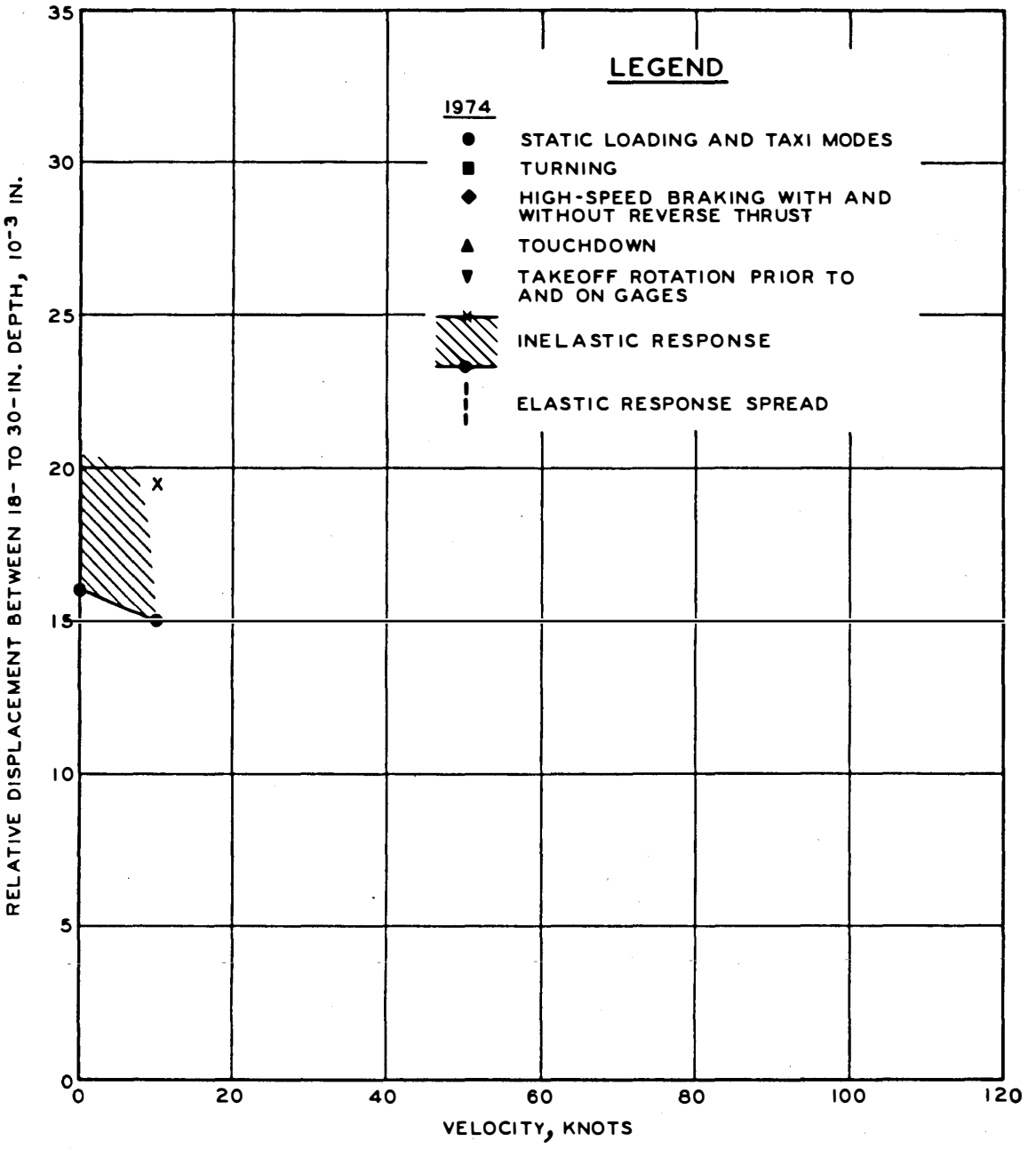

Figure 83. Maximum vertical relative displacement versus velocity, flexible, row 3, 18 to 30 in., C-880

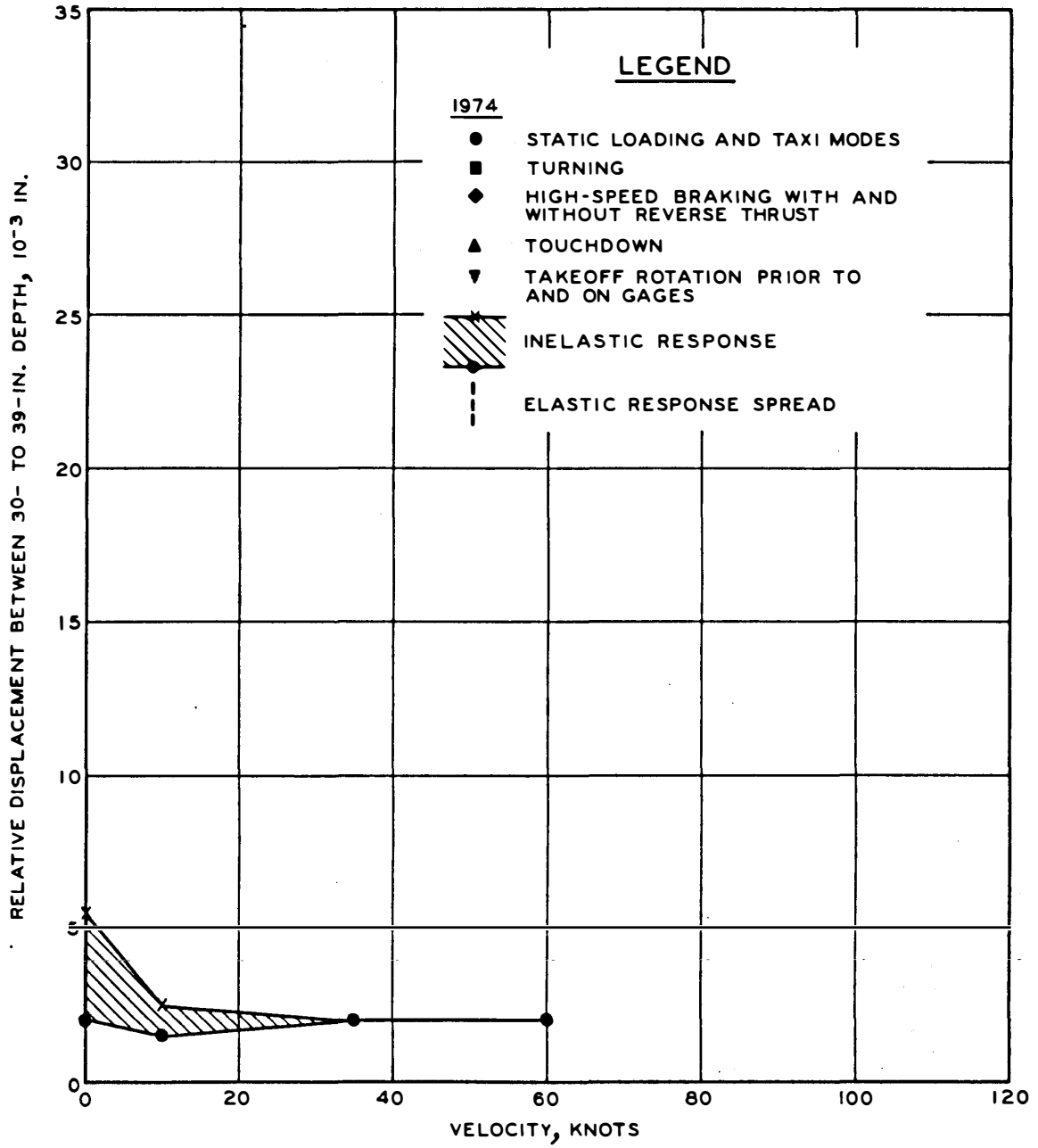

Figure 84. Maximum vertical relative displacement versus velocity, flexible, row 3, 30 to 39 in., C-880

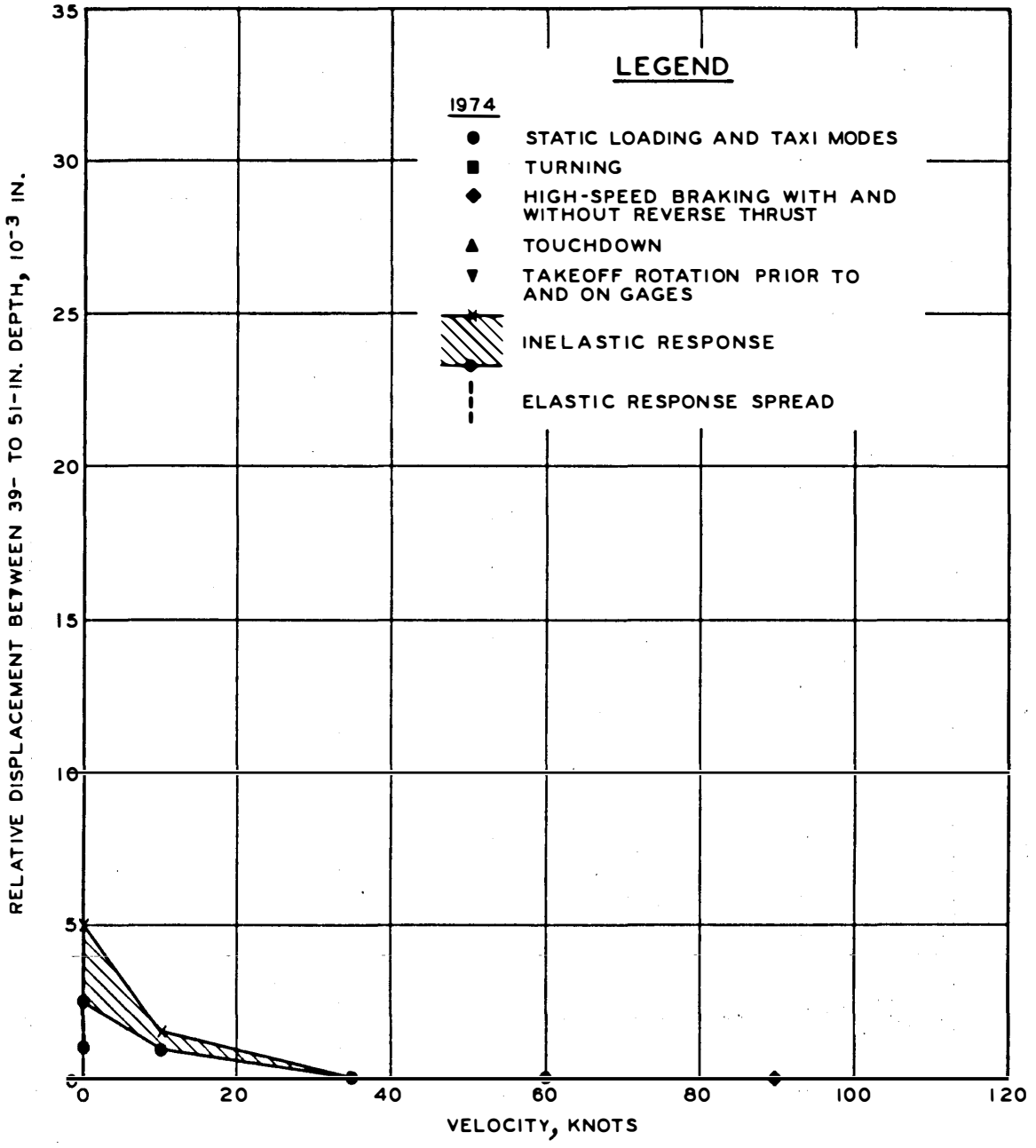

Figure 85. Maximum vertical relative displacement versus velocity, flexible, row 3, 39 to 51 in., C-880

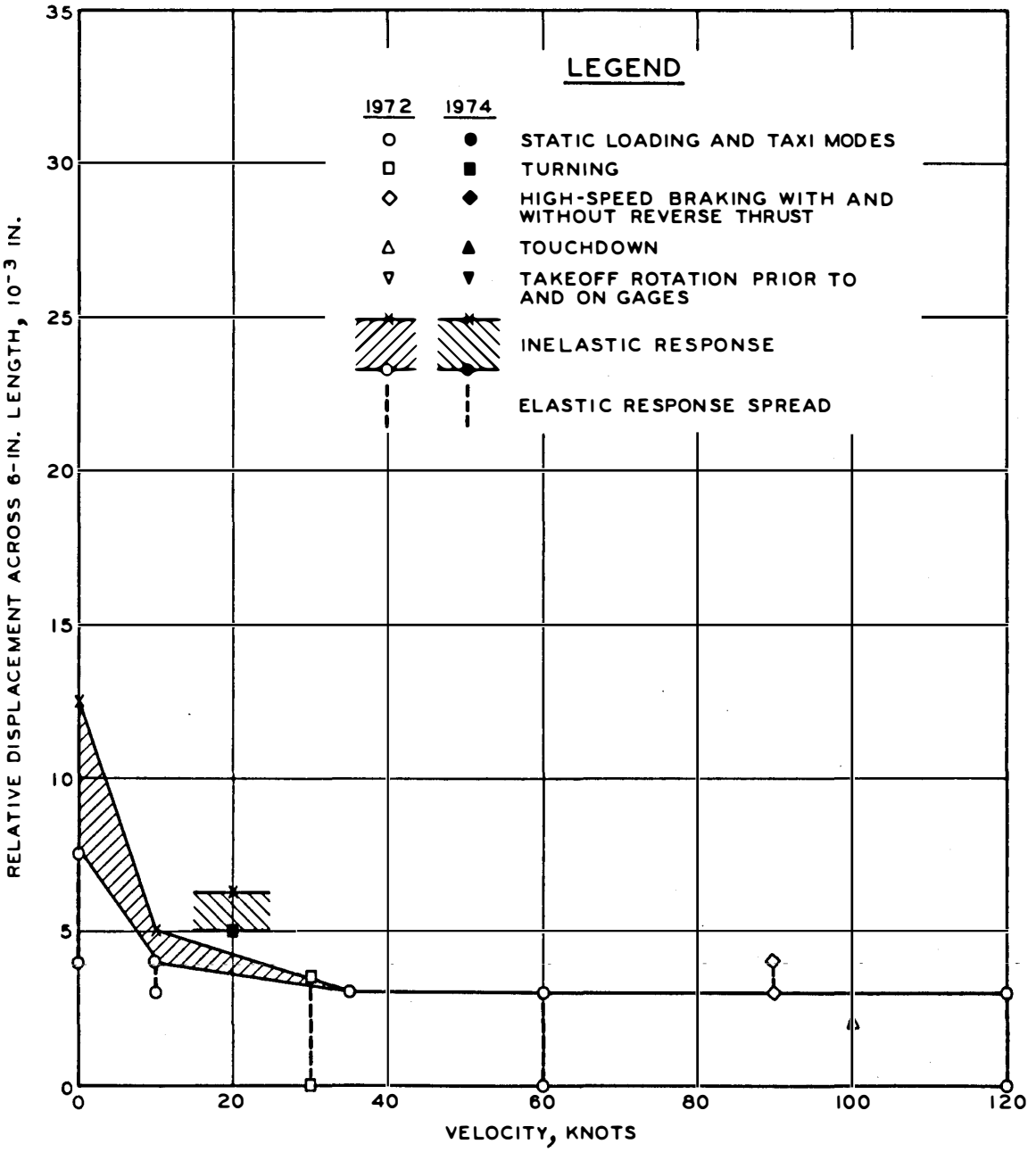

Figure 86. Maximum horizontal relative displacement (longitudinal) versus velocity, flexible, row 2, 9 in., B-727

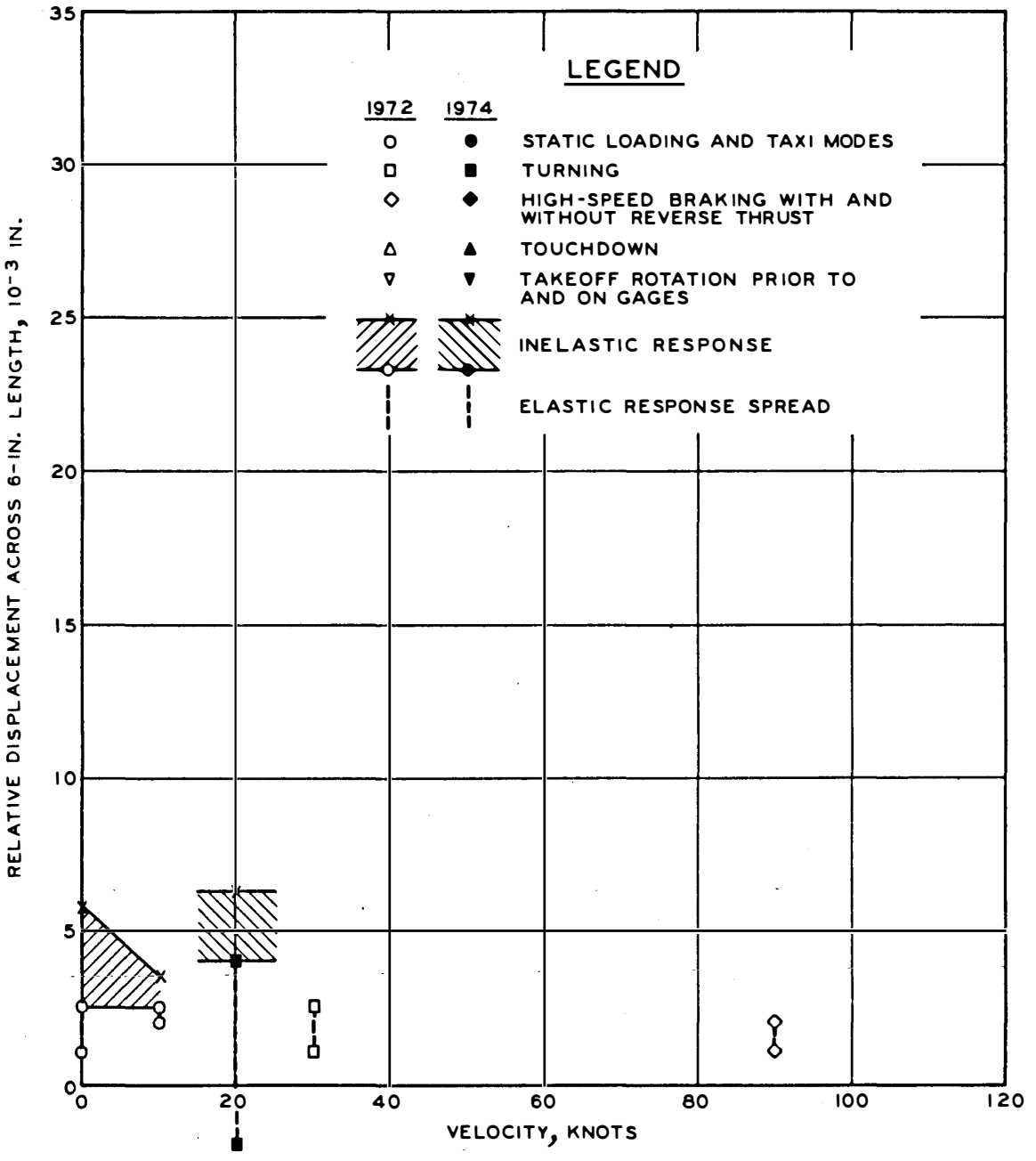

Figure 87. Maximum horizontal relative displacement (transverse) versus velocity, flexible, row 2, 9 in., B-727

conducted in 1972 with the B-727 on the rigid pavement test site. Not all operating modes are presented for gage row 1 because the deflection gage started malfunctioning after the first few dynamic load tests. Noticeable in the figures shown for row 1 are some erratic data points even in the static tests. These were early indications that the gage was starting to function improperly.

Individual pavement structure element vertical responses as measured by Bison coils are presented in Figures B298-B346. Noticeable in these figures are the inelastic and bow wave results occurring in the rigid pavement structure.

For static load tests, all layers were monitored. However, for the dynamic load tests, recording was concentrated in the 7- to 15-in. and 15- to 24-in. depths. Figure B314 shows static load test results for the 24- to 36-in. depth for all three gage rows. The static to low-speed taxi test results for the rigid pavement structure seem to have more variation than did those for the flexible pavement structure. This could have been caused by the foundation materials being in a looser state (less dense) due to the reconstruction in these areas. The experimental inductive probes were not recorded for the same reasons as discussed for the flexible pavement test site.

Pavement structure element horizontal responses are presented in Figures B347-B363. Horizontal behavior responses were previously discussed in the interpretation of data section. Figure B347 shows the static load test horizontal transverse displacement measured by Bison coils embedded in the bottom of the concrete slab at gage row 2. If inelastic behavior was present in the bottom of the slab, it was within the recorded noise level of the coils. (Extraneous noise was very high in 1972.) Figures B348-B363 show the longitudinal and transverse horizontal responses measured by Bison coils at a depth of 15 in. in gage row 2. All operating modes are presented.

Figures B364-B386 show the transverse displacements measured by the Valore strain gages in the top of each slab for each gage row. The behavior measured by the Valore strain gages was discussed in the interpretation of data section. Noticeable in these figures are the inelastic

responses in the static load tests. Also noticeable are the critical offset distance regions adjacent to the wheels. As discussed for the flexible pavement structure displacements, offset distance variations in these regions could cause large erroneous variations to appear in the data.

Rigid Pavement Structure Results Summarized. Figures 88-90 summarize results for the total pavement structure vertical responses as measured by WES deflection gages embedded in the bottom of the concrete slabs. Previous remarks concerning the elastic and inelastic responses are also applicable here. There was a small amount of inelastic behavior, but the figures show that the concrete slabs acted primarily as elastic plates. The odd behavior (response decrease about 20 knots) shown in some of these and following figures is possibly caused by lack of maximum load point data.

Figures 91-96 summarize the individual pavement structure element vertical responses as measured by Bison coils. Of interest in these figures are the inelastic responses of the foundation materials of the rigid pavement structure even though the concrete slabs responded almost entirely elastically.

Figures 97-101 summarize the rigid pavement structure horizontal responses as measured by Bison coils at a depth of 15 in. and the responses measured by Valore strain gages at the surface of the concrete slabs. Figures 97 and 98 show the longitudinal and transverse horizontal displacements in the foundation materials. The horizontal responses show about the same static to dynamic load comparisons as were noted for the vertical deformations. Noticeable in Figures 97-101 are the inelastic responses of the rigid pavement structure. The odd behavior (response decrease) shown for the creep- and low-speed taxi modes is believed due to a lack of data at the maximum load points, as can be seen in Appendix B.

INTERPRETATION OF PAVEMENT STRUCTURE PRESSURES

BEHAVIOR

Vertical pressures measured by the pressure cells at various depths

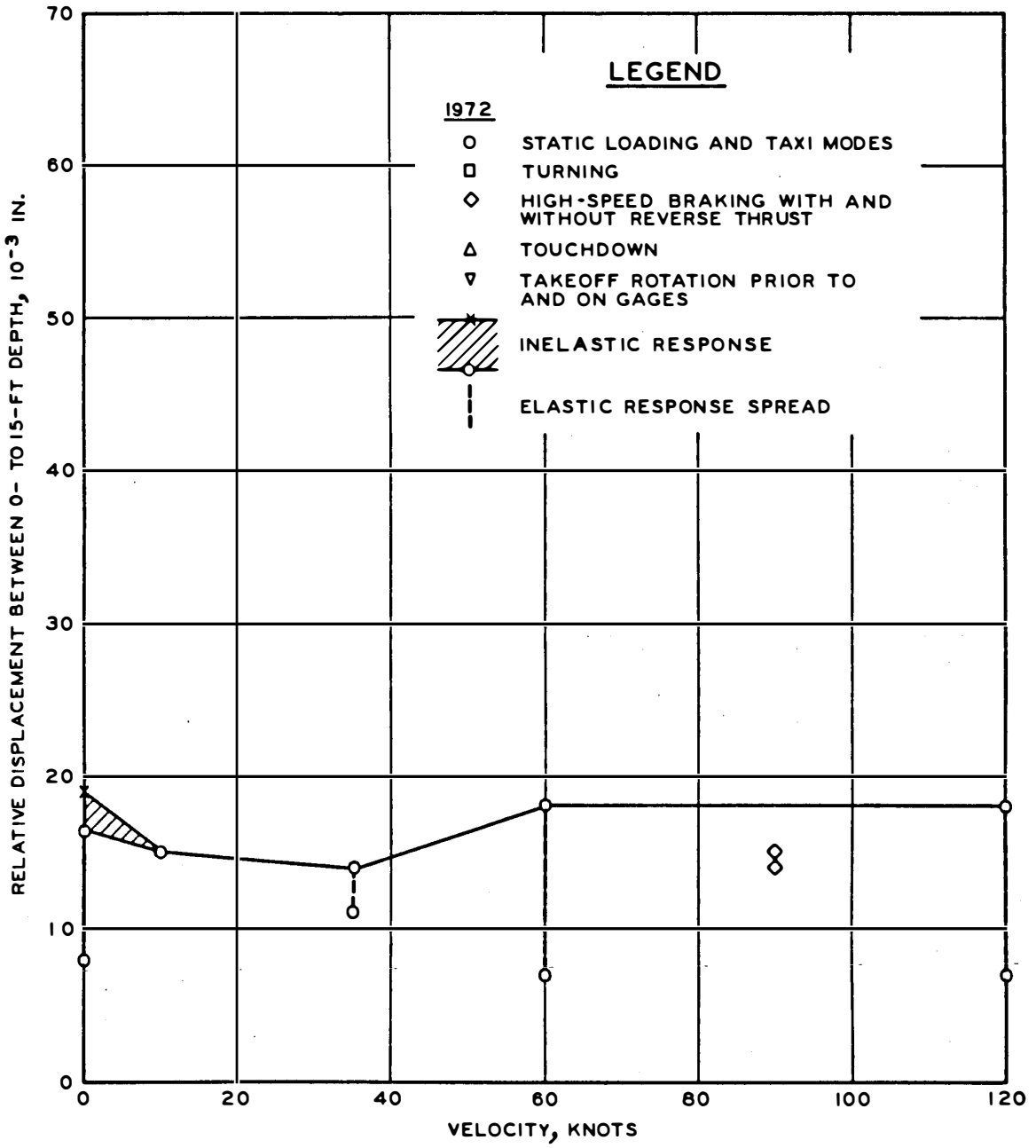

Figure 88. Maximum vertical relative displacement versus velocity, rigid, row 1, 0 to 15 ft, B-727

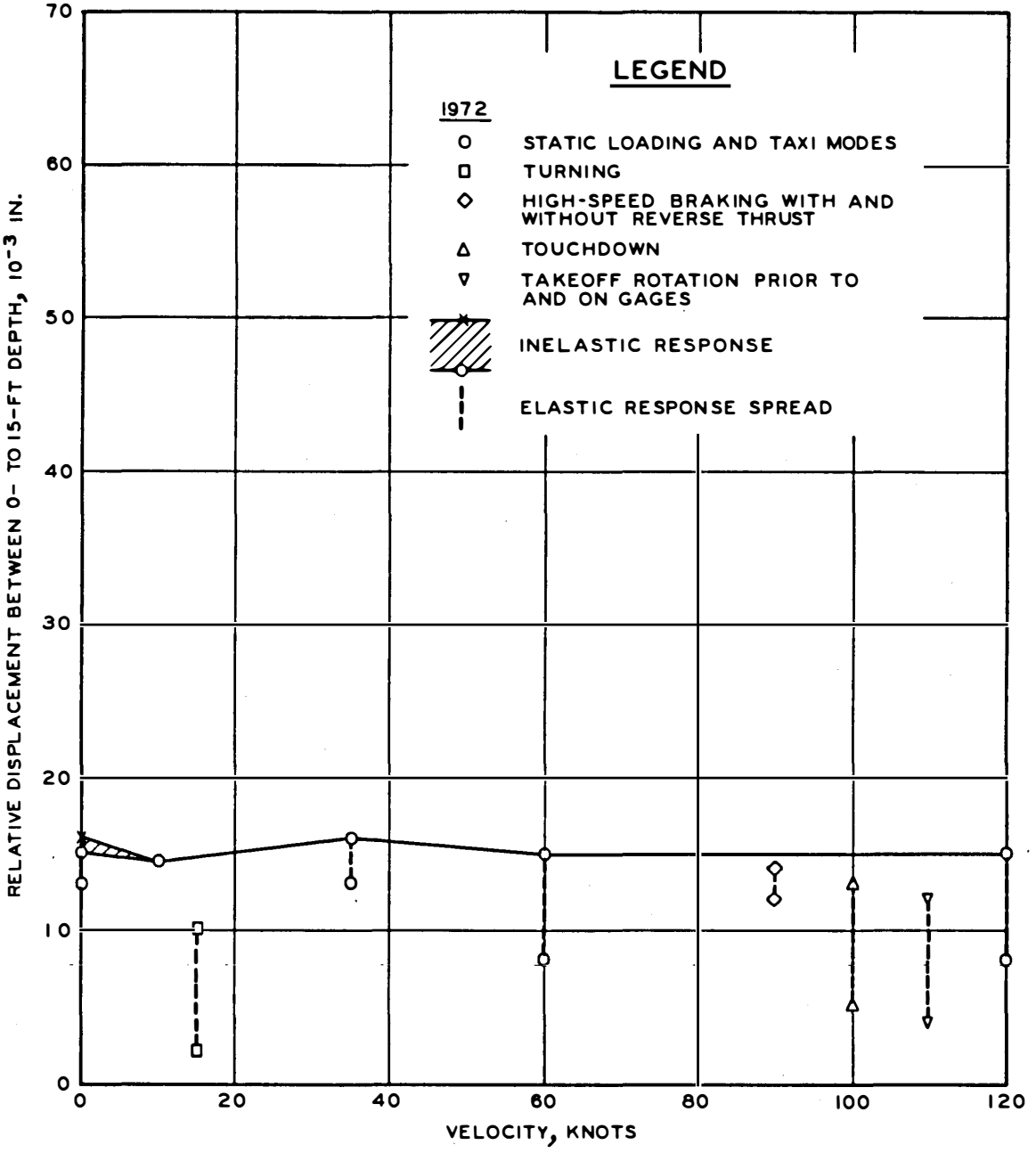

Figure 89. Maximum vertical relative displacement versus velocity, rigid, row 2, 0 to 15 ft, B-727

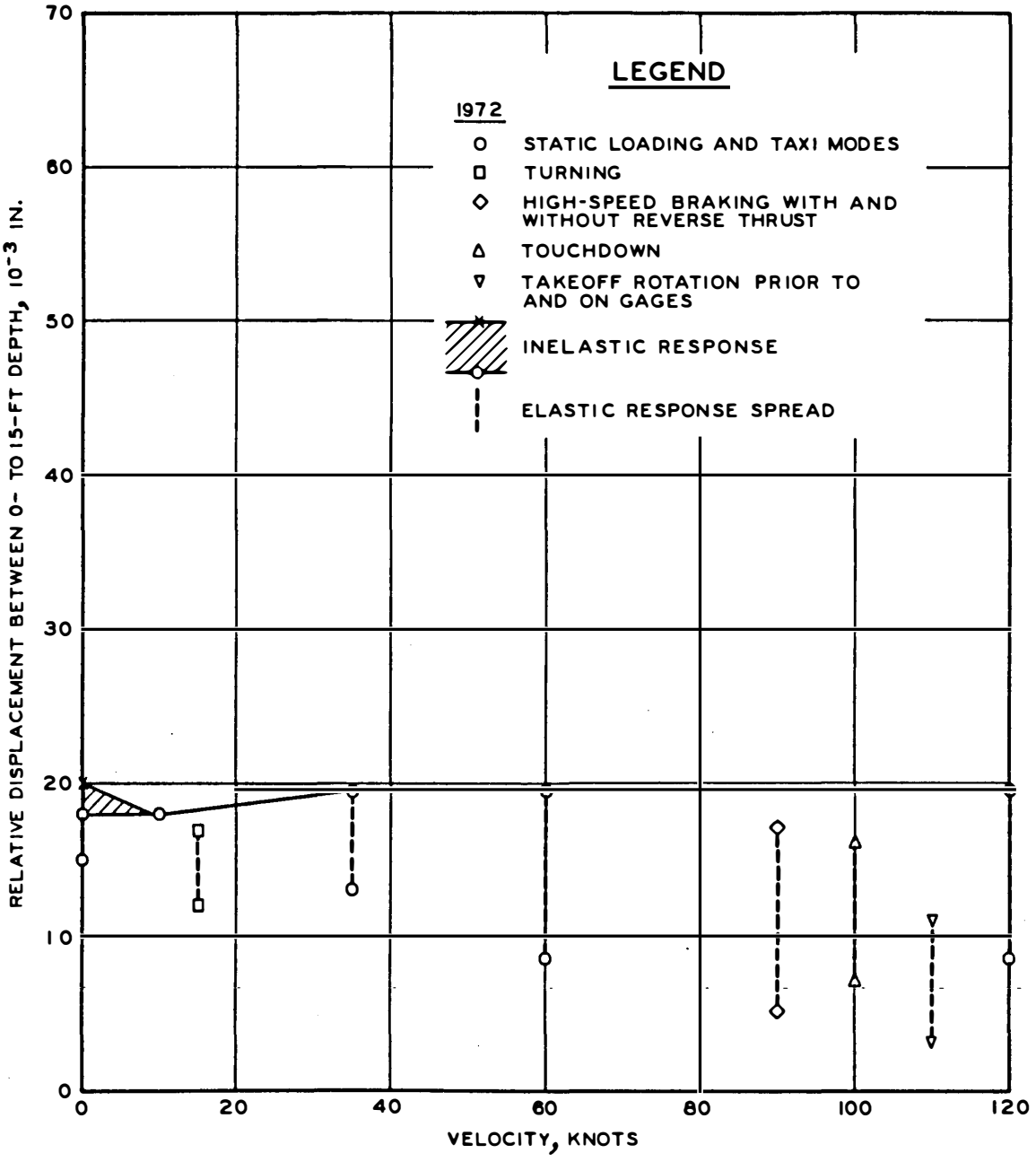

Figure 90. Maximum vertical relative displacement versus velocity, rigid, row 3, 0 to 15 ft, B-727

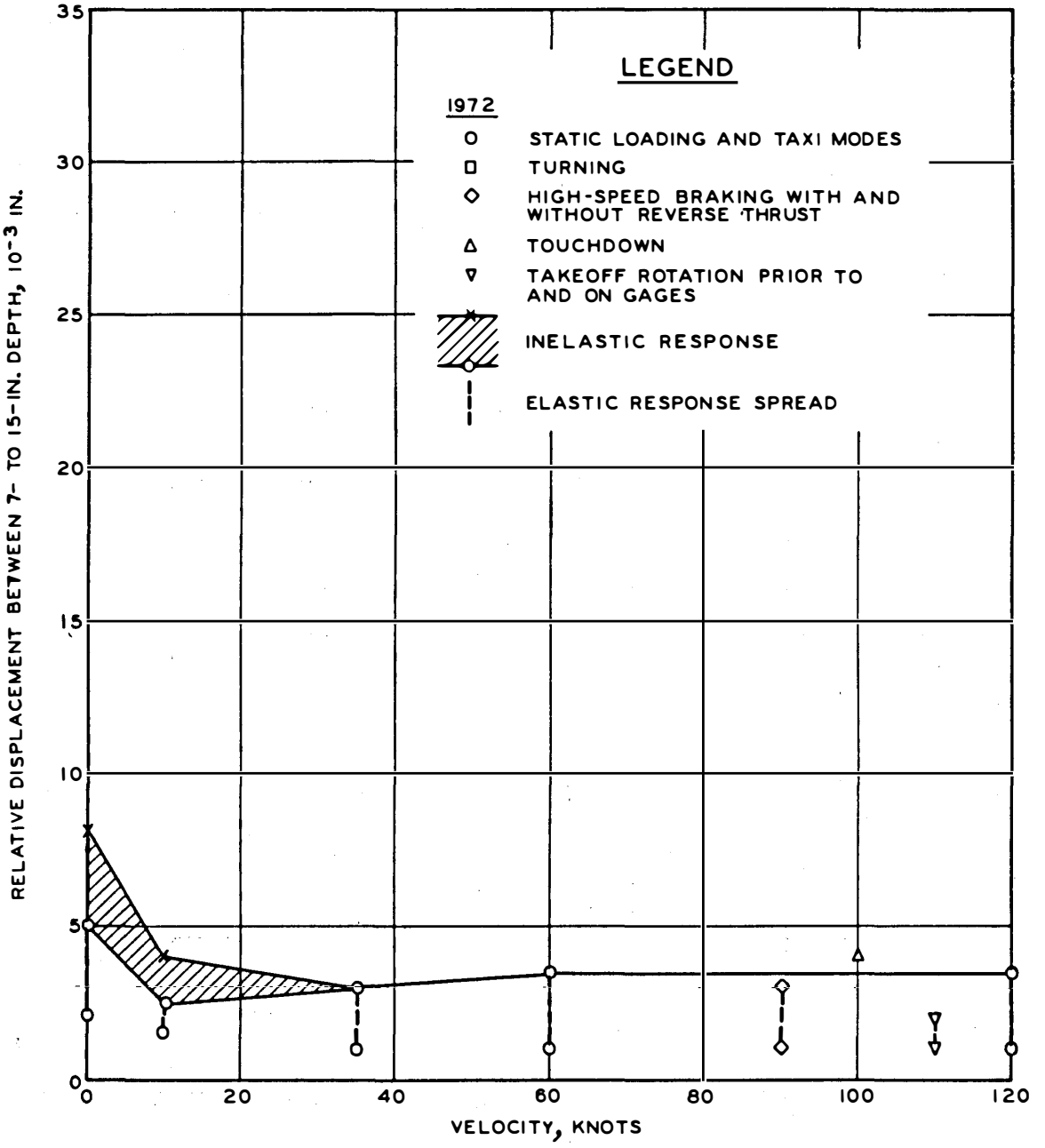

Figure 91. Maximum vertical relative displacement versus velocity, rigid, row 1, 7 to 15 in., B-727

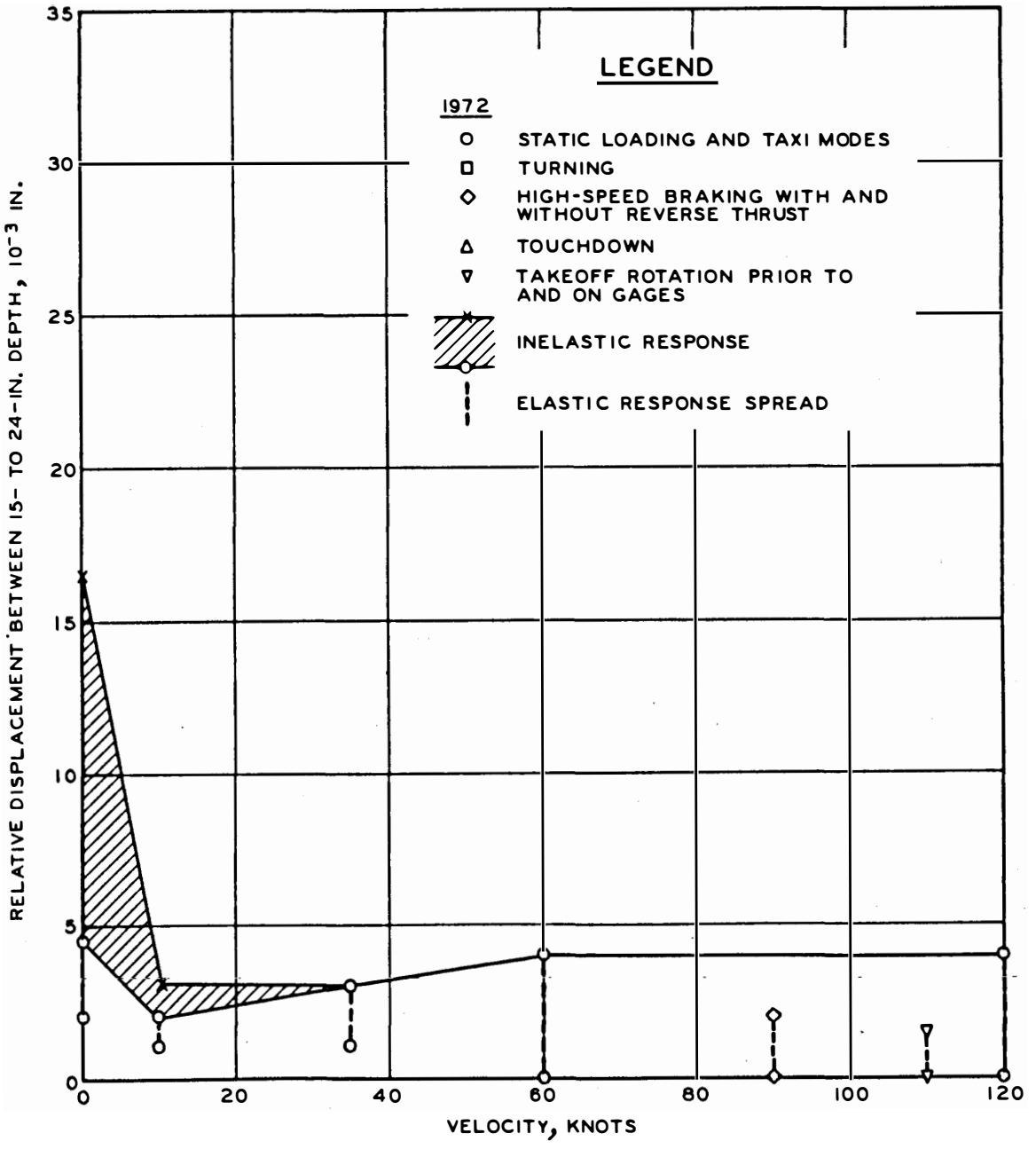

Figure 92. Maximum vertical relative displacement versus velocity, rigid, row 1, 15 to 24 in., B-727

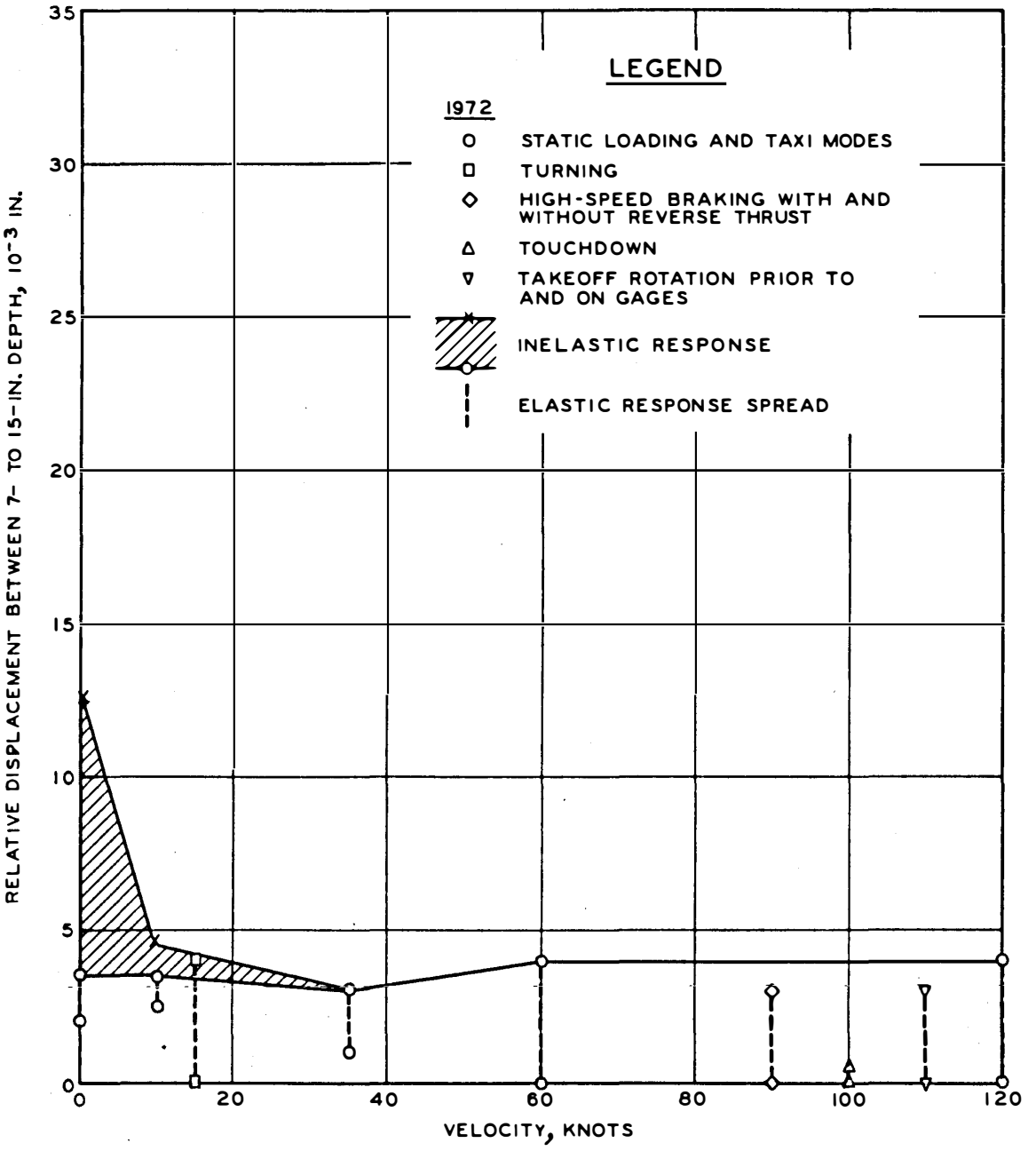

Figure 93. Maximum vertical relative displacement versus velocity, rigid, row 2, 7 to 15 in., B-727

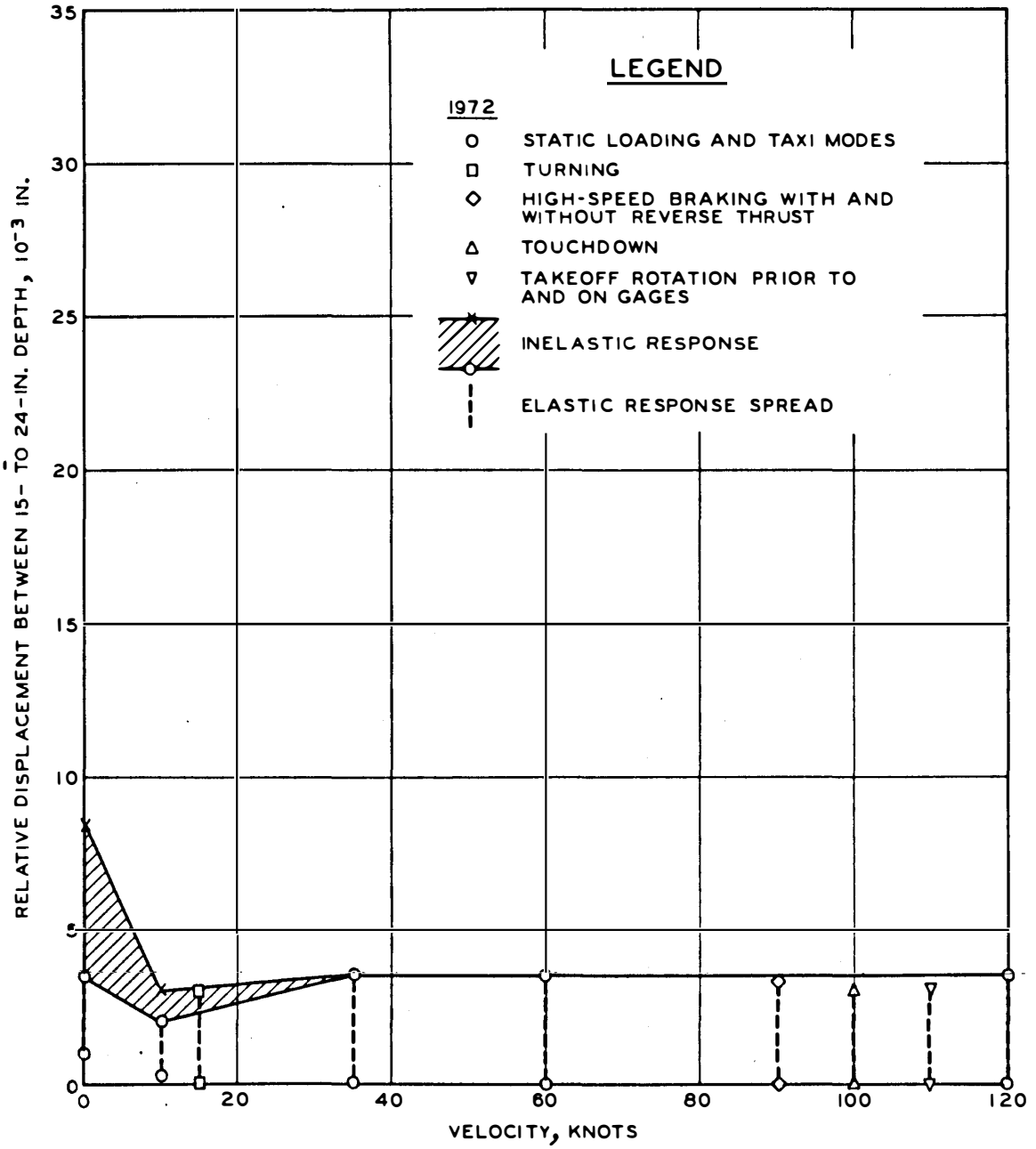

Figure 94. Maximum vertical relative displacement versus velocity, rigid, row 2, 15 to 24 in., B-727

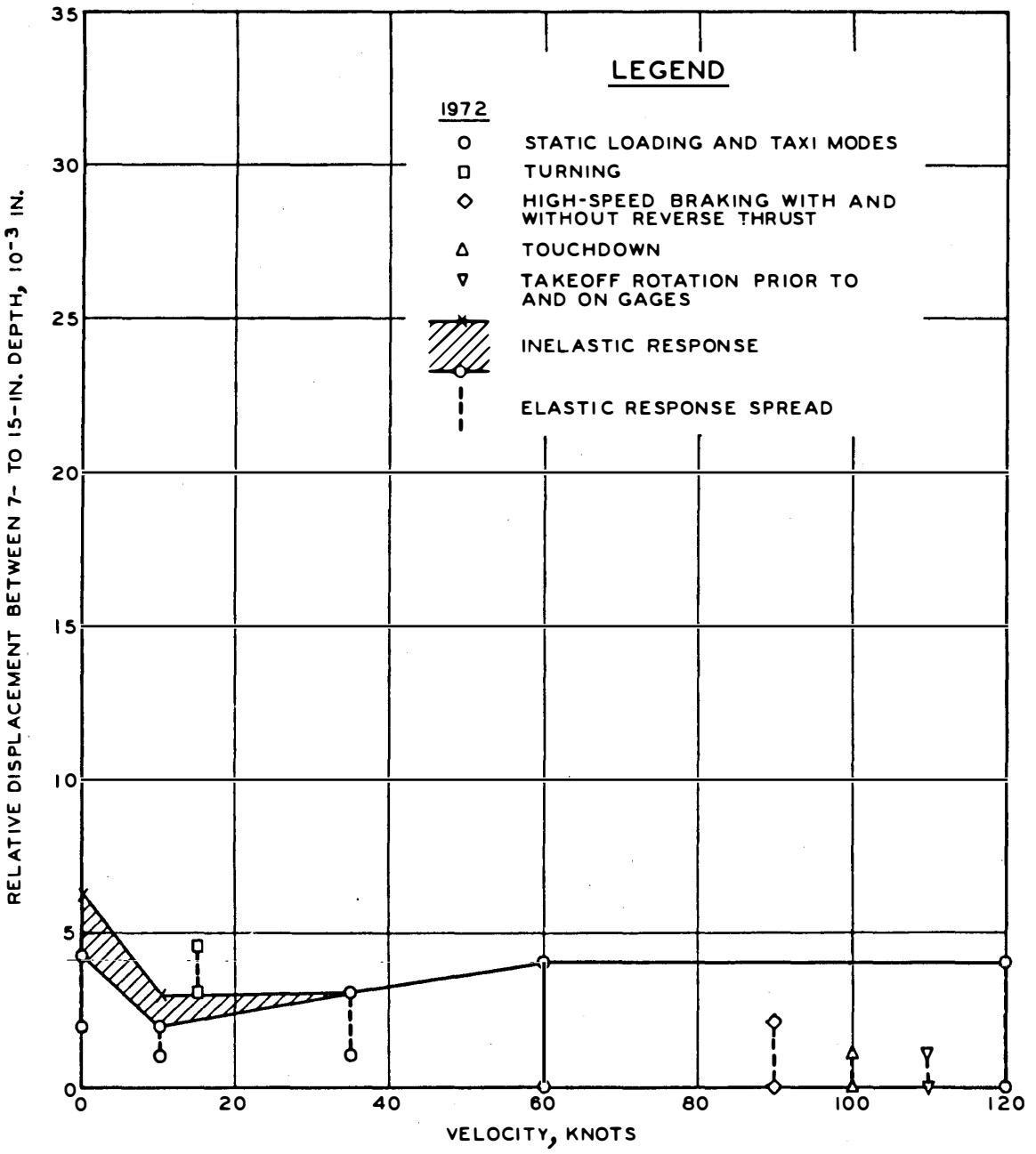

Figure 95. Maximum vertical relative displacement versus velocity, rigid, row 3, 7 to 15 in., B-727

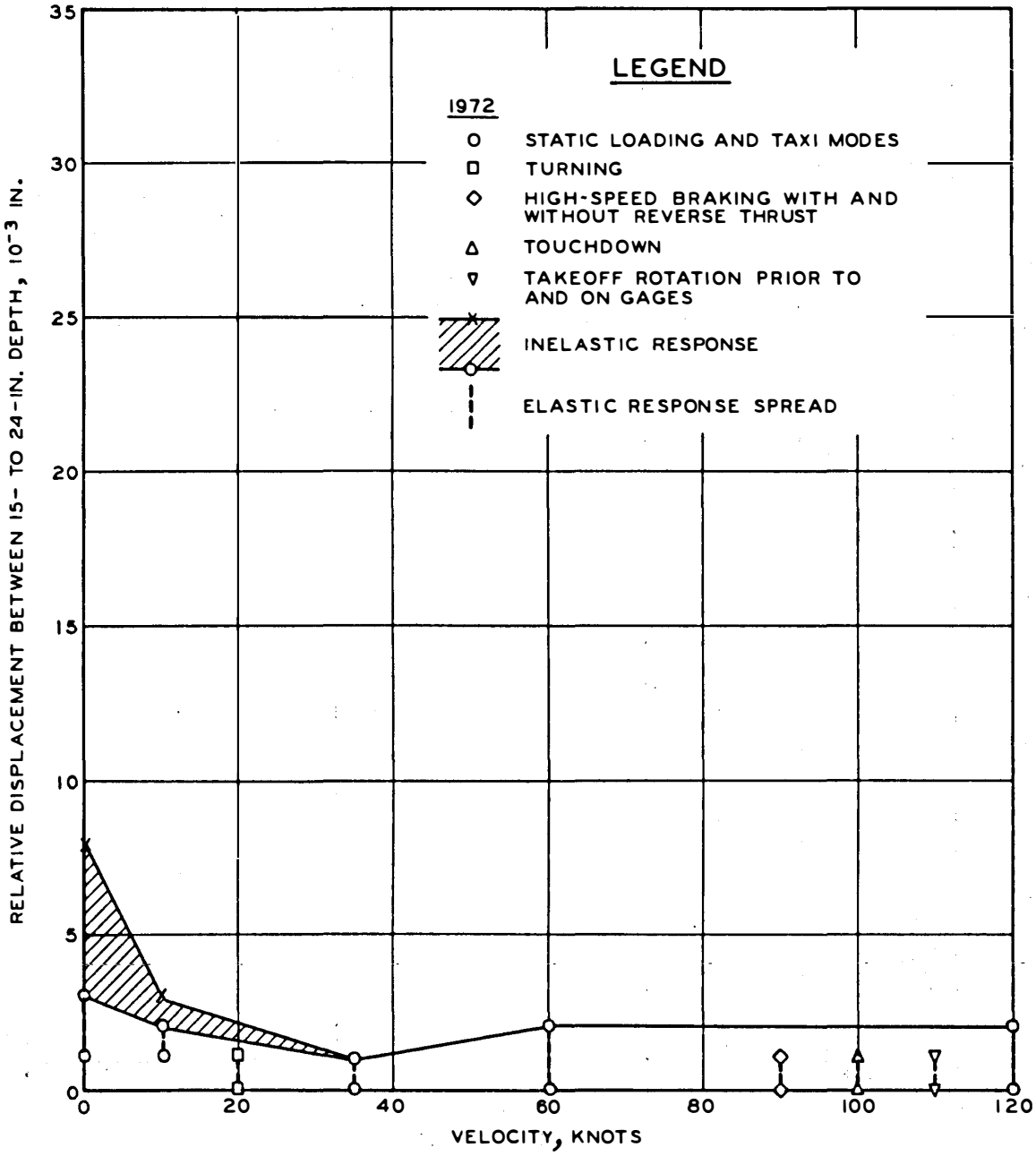

Figure 96. Maximum vertical relative displacement versus velocity, rigid, row 3, 15 to 24 in., B-727

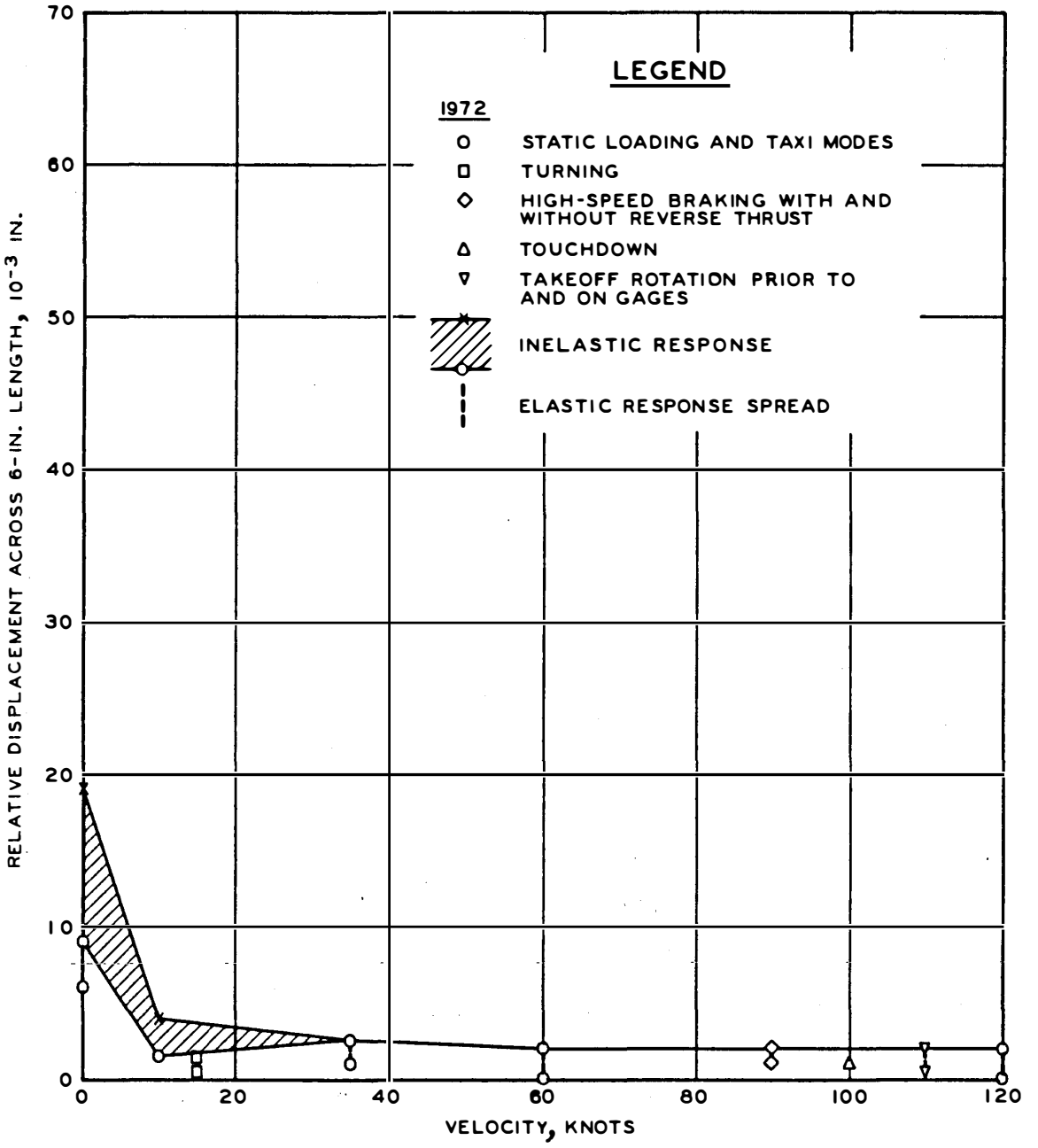

Figure 97. Maximum horizontal relative displacement (longitudinal) versus velocity, rigid, row 2, 15 in., B-727

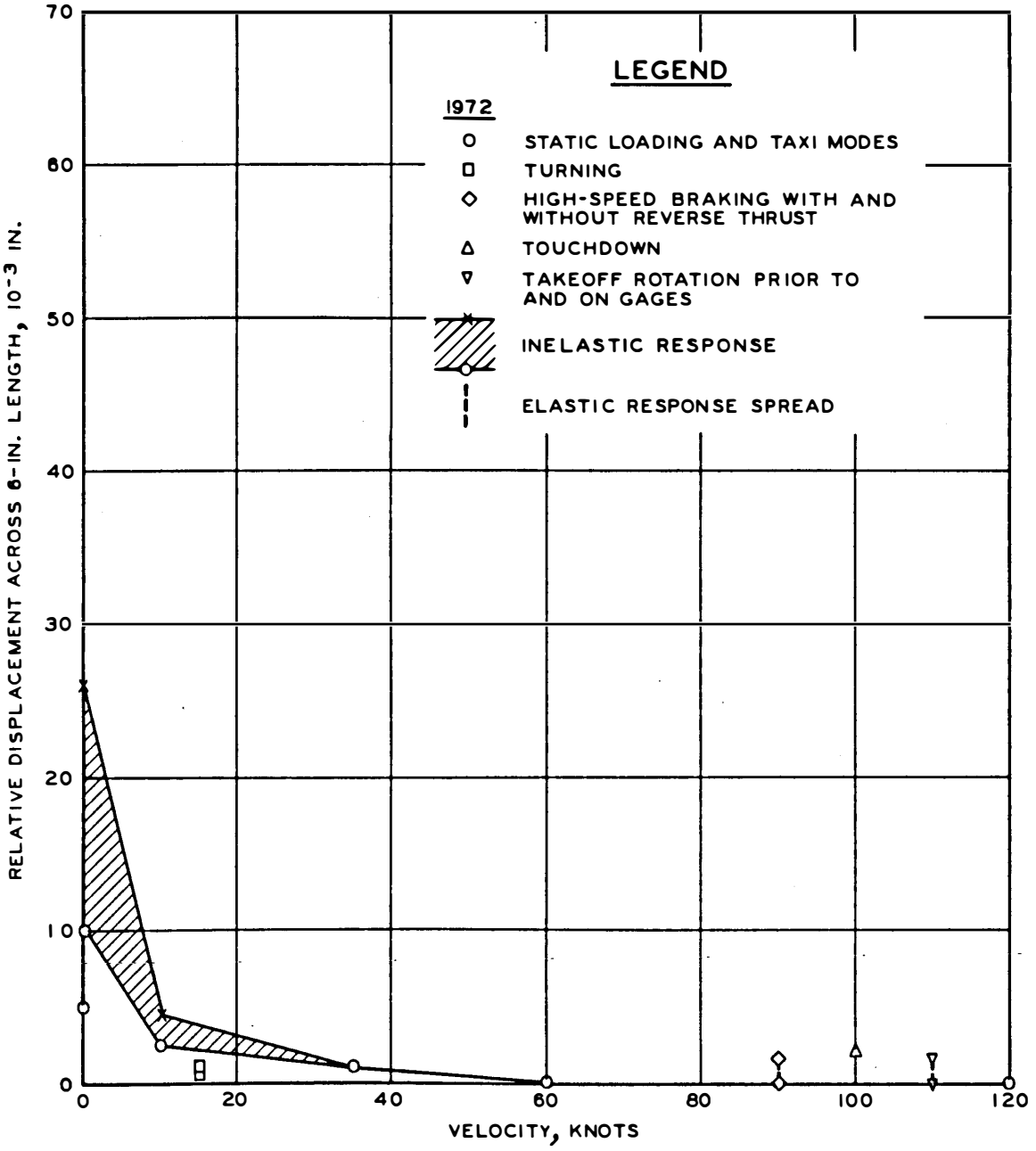

Figure 98. Maximum horizontal relative displacement (transverse) versus velocity, rigid, row 2, 15 in., B-727

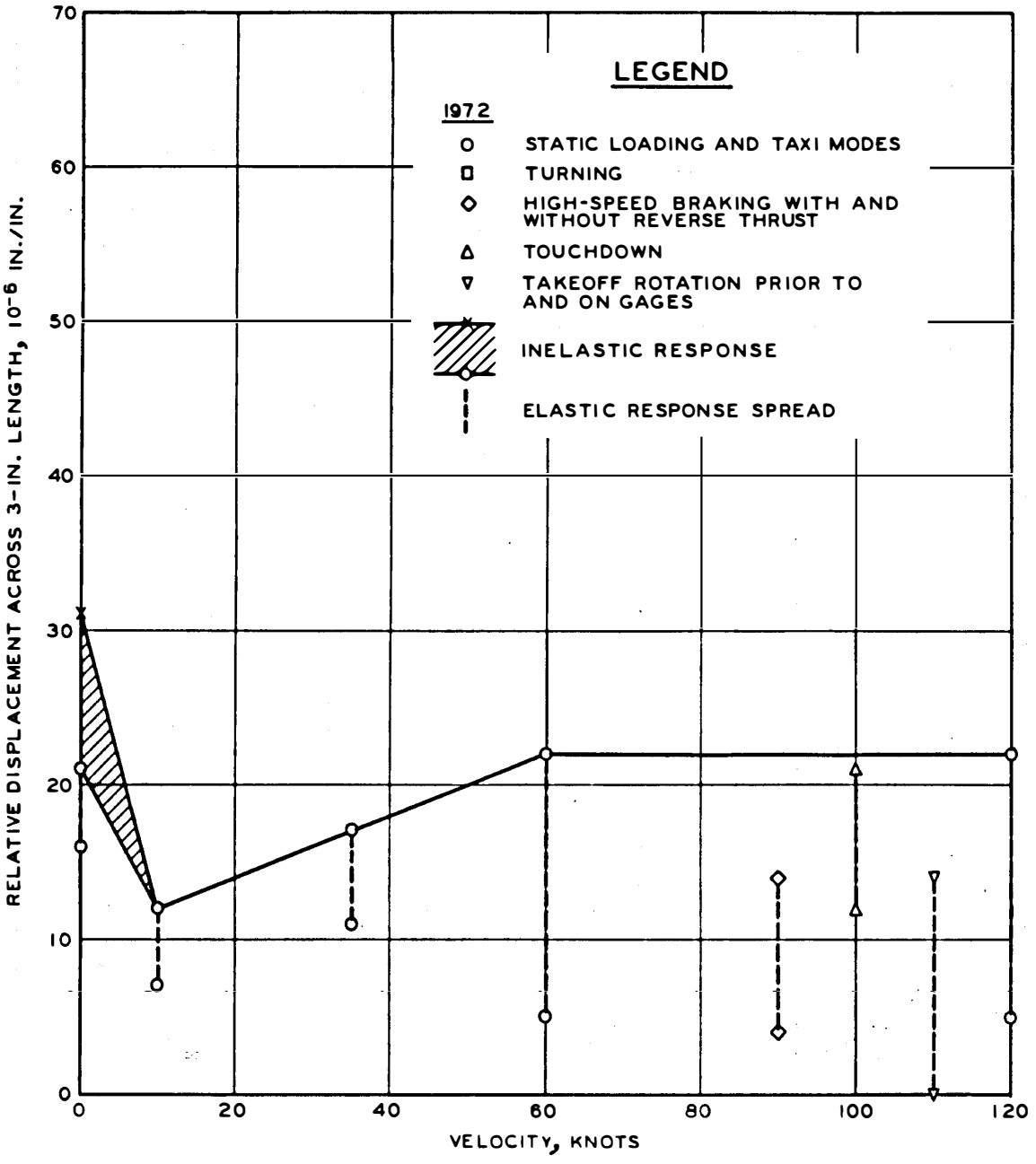

Figure 99. Maximum horizontal relative displacement (transverse) versus velocity, rigid, row 1, surface, B-727

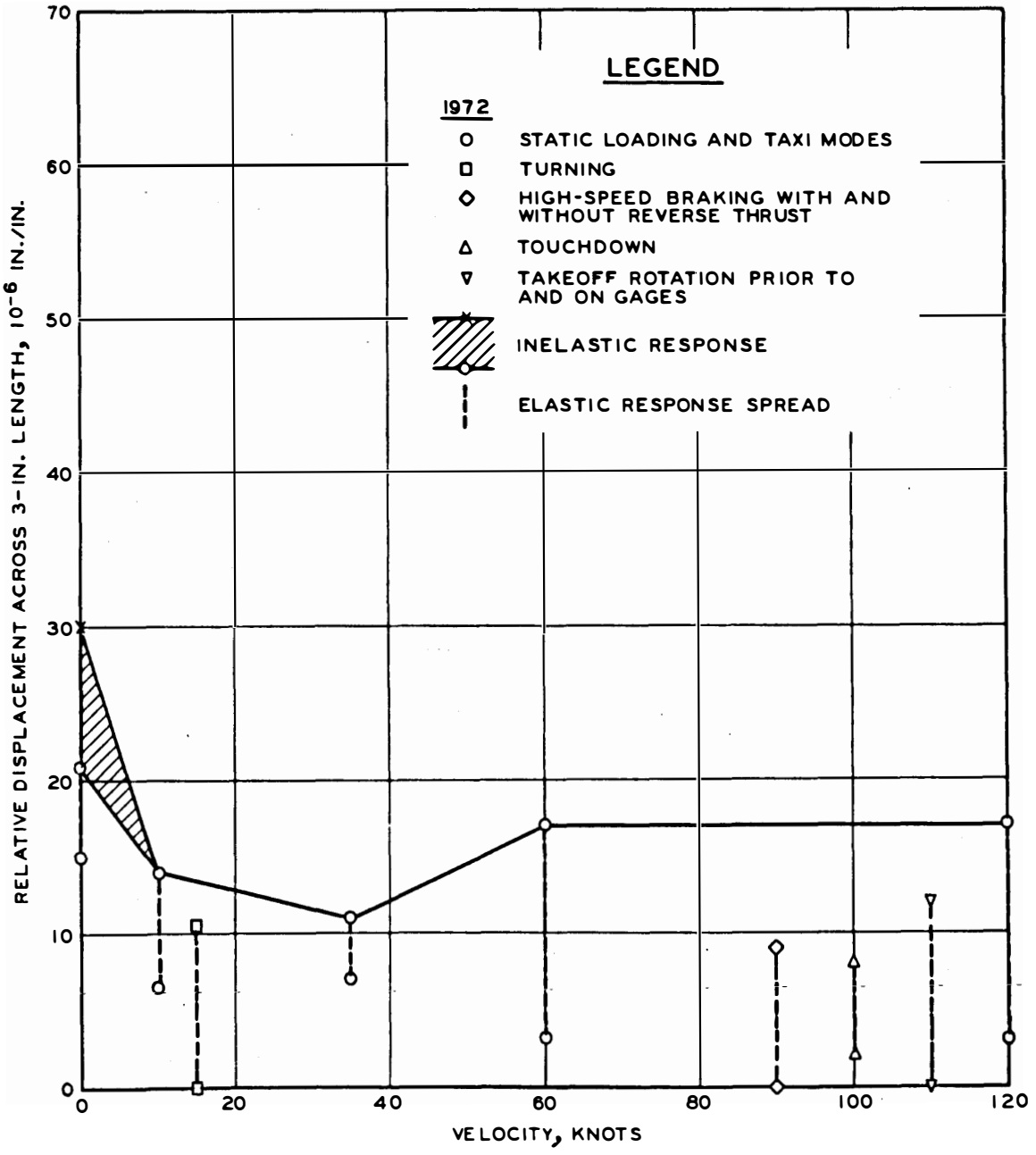

Figure 100. Maximum horizontal relative displacement (transverse) versus velocity, rigid, row 2, surface, B-727

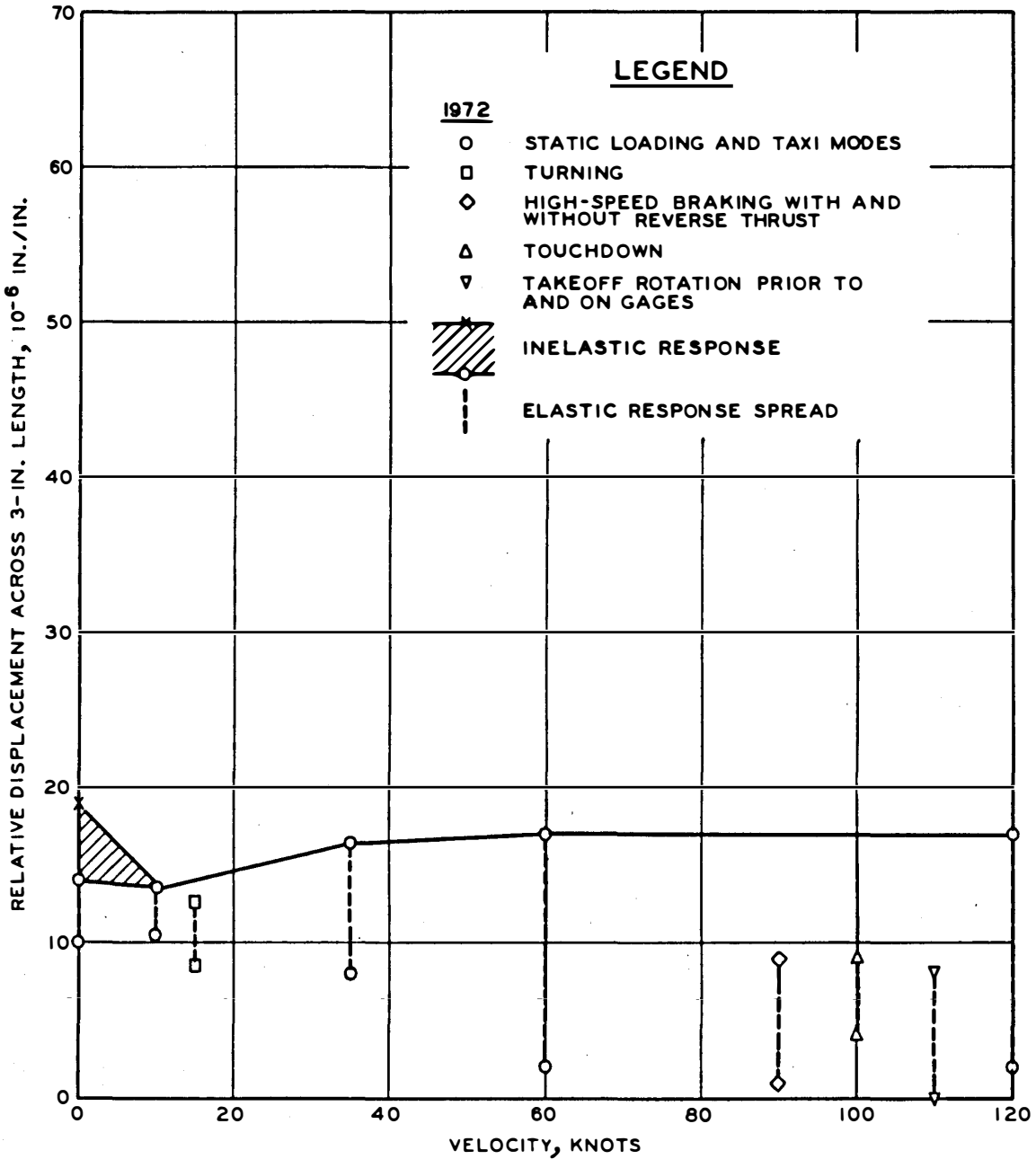

Figure 101. Maximum horizontal relative displacement (transverse) versus velocity, rigid, row 3, surface, B-727

in both pavement structures did not have complex behavioral patterns. They showed no distinct residual pressures acting for either static or dynamic load conditions. Inelastic displacement did not seem to have an effect on the pressure cells. They appeared to be carried with or ride within the pulsating pavement structures. Any differences between the initial and final no-load responses were within the noise and variation levels of the instruments.

Load response was computed from the initial no-load signal levels. As was the case for the displacement measuring instruments, one-half of the noise level was subtracted for the dynamic load tests. Also as for the displacement results, the static load test curves were not drawn through the average results but rather through an outer boundary. The static load test curves are superimposed on the dynamic load test results to allow comparisons of the vertical pressures.

The vertical pressure results are presented in Figures B387-B621. The order and logic of presentation are the same as previously discussed for the displacement results. Flexible pavement test results for 1972 and 1974 are presented in Figures B387-B561. The 1972 rigid pavement test results are presented in Figures B562-B621. The previously discussed variables affecting displacement results also apply to these results.

The pressure cells did not directly indicate the elastic expansion of the structure elements. However, some did show a tendency of a slight rise ahead of the wheels. At offset distances outside of the immediate gage vicinity, some pressure cells actually registered pressure releases (not an upward or tension pressure) under load. This behavior is consistent with the previously discussed structure element behavior.

TEST RESULTS

Flexible Pavement Structure Results. Vertical pressure results for the B-727 1972 tests are presented in Figures B387-B486. Figures B487-B561 present the B-727 1974 results. Very noticeable in these figures are the critical offset regions adjacent to the wheels. These patterns are similar to those for the displacements, and the previous

displacement discussions are applicable here.

Flexible Pavement Structure Results Summarized. Figures 102-116 summarize the flexible pavement structure vertical pressure results. Both the 1972 and 1974 results are shown in the same figures for comparisons. Noticeable in these figures are the sharp initial decreases in elastic pressures with increases in velocity and the increased pressure magnitudes of 1974. However, also noticeable are the decreases with increases in depth of the 1974 pressure magnitudes to about the same level as 1972 results at the 30- and 39-in. depths. This behavior is fairly consistent with that of the structure element displacements.

Rigid Pavement Structure Results. Vertical pressure results for the B-727 1972 tests are presented in Figures B562-B621. Noticeable in these figures is the fact that the maximum pressures occur beneath the gear center for all depths.

Rigid Pavement Structure Results Summarized. Figures 117-125 summarize the rigid pavement structure vertical pressure results. Noticeable in these figures are the nearly constant vertical pressures. This behavior is fairly consistent with the displacment results.

EVALUATION OF PAVEMENT STRUCTURE
MAJOR MEASURING INSTRUMENTS

Accuracy applies to the ability of the instrumentation to properly reflect the existing conditions in and behavior of the material within which the measuring instrument is buried. Accuracy is the degree to which the results from instruments as installed compare with what the results would be if the instruments had not been in the material. Therefore, accuracy is a measure of the disturbance of the conditions and behavior caused by the presence of an instrument in the material. Accuracy, as stated above, is difficult to evaluate because the only known value is that of the material responding with the instrument present; how the system would behave without the instrument is unknown. If the actual behavior or response were a known fact, then there would be no need to instrument the material to measure the responses. Thus, it is evident that accuracy cannot be evaluated; only an indication of

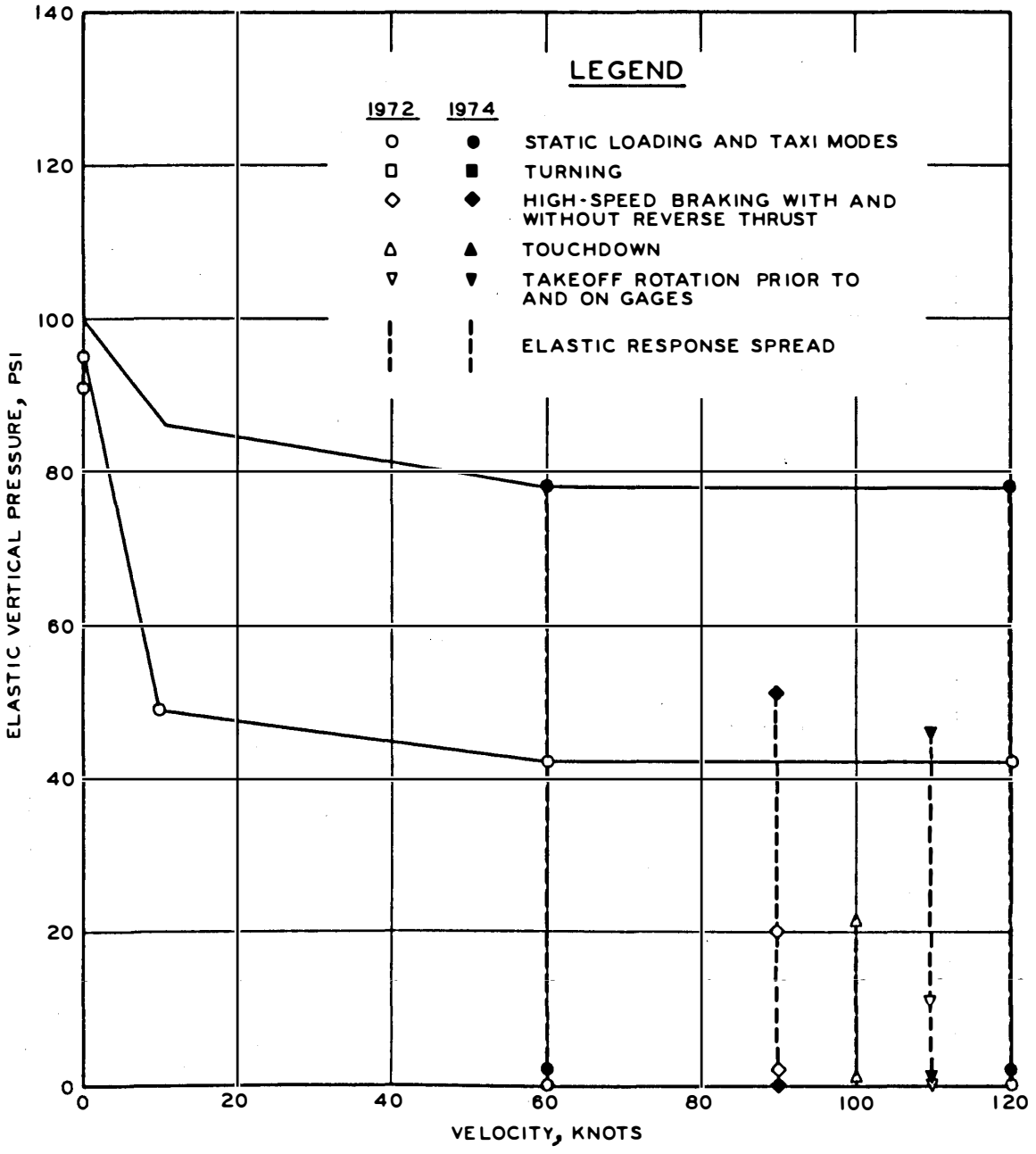

Figure 102. Maximum vertical elastic pressure versus velocity, flexible, row 1, 3 in., B-727

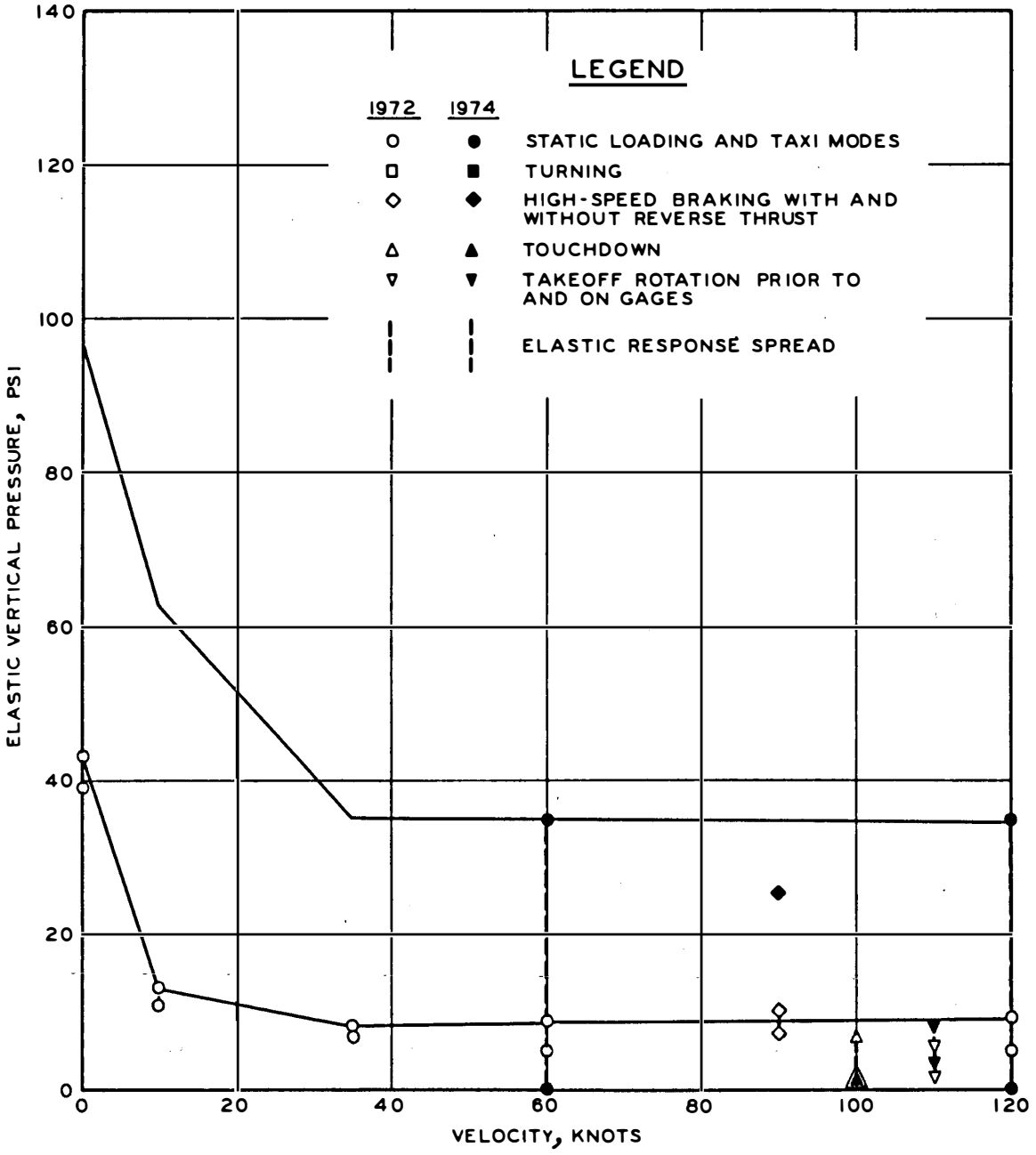

Figure 103. Maximum vertical elastic pressure versus velocity, flexible, row 1, 9 in., B-727

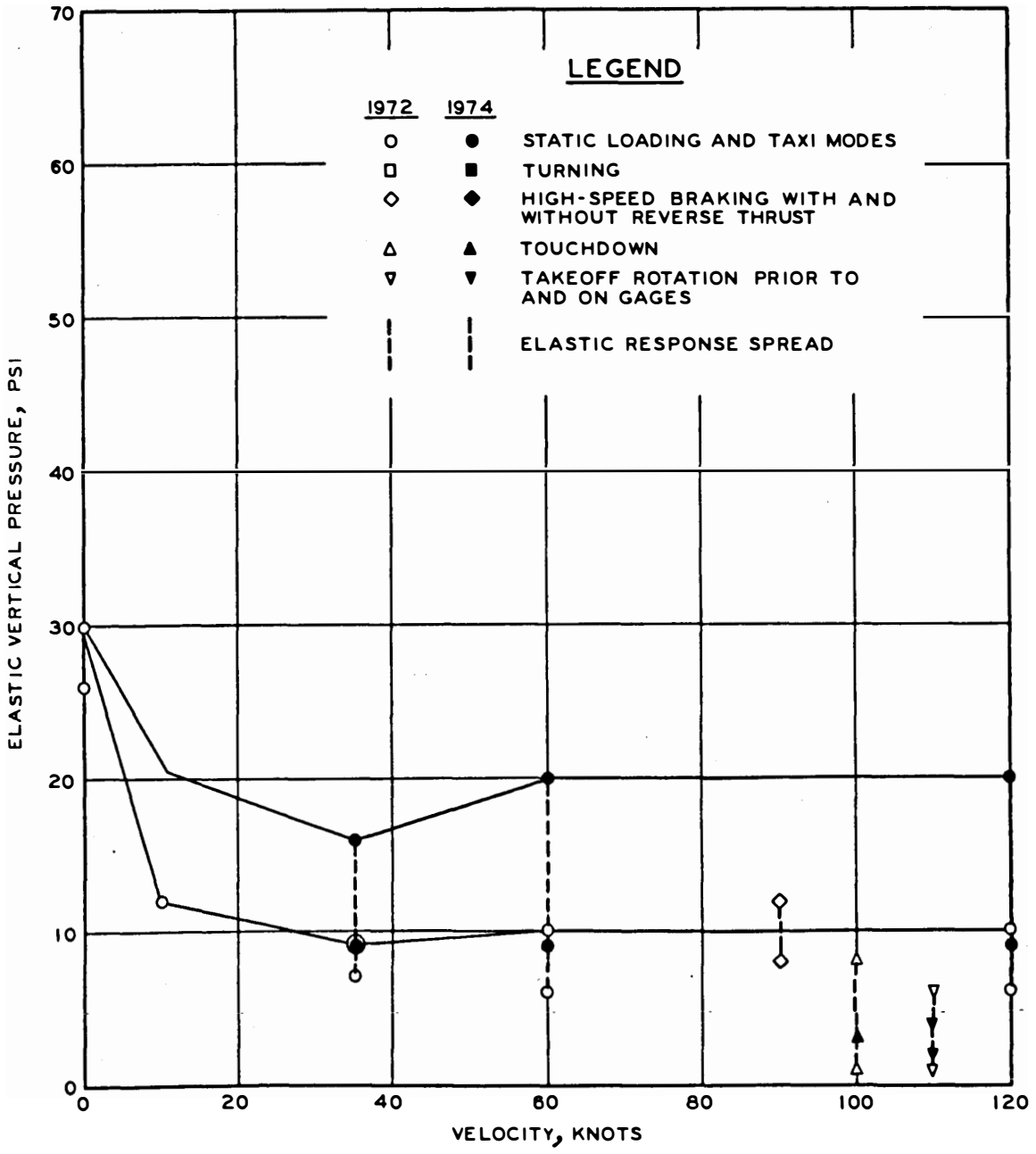

Figure 104. Maximum vertical elastic pressure versus velocity, flexible, row 1, 18 in., B-727

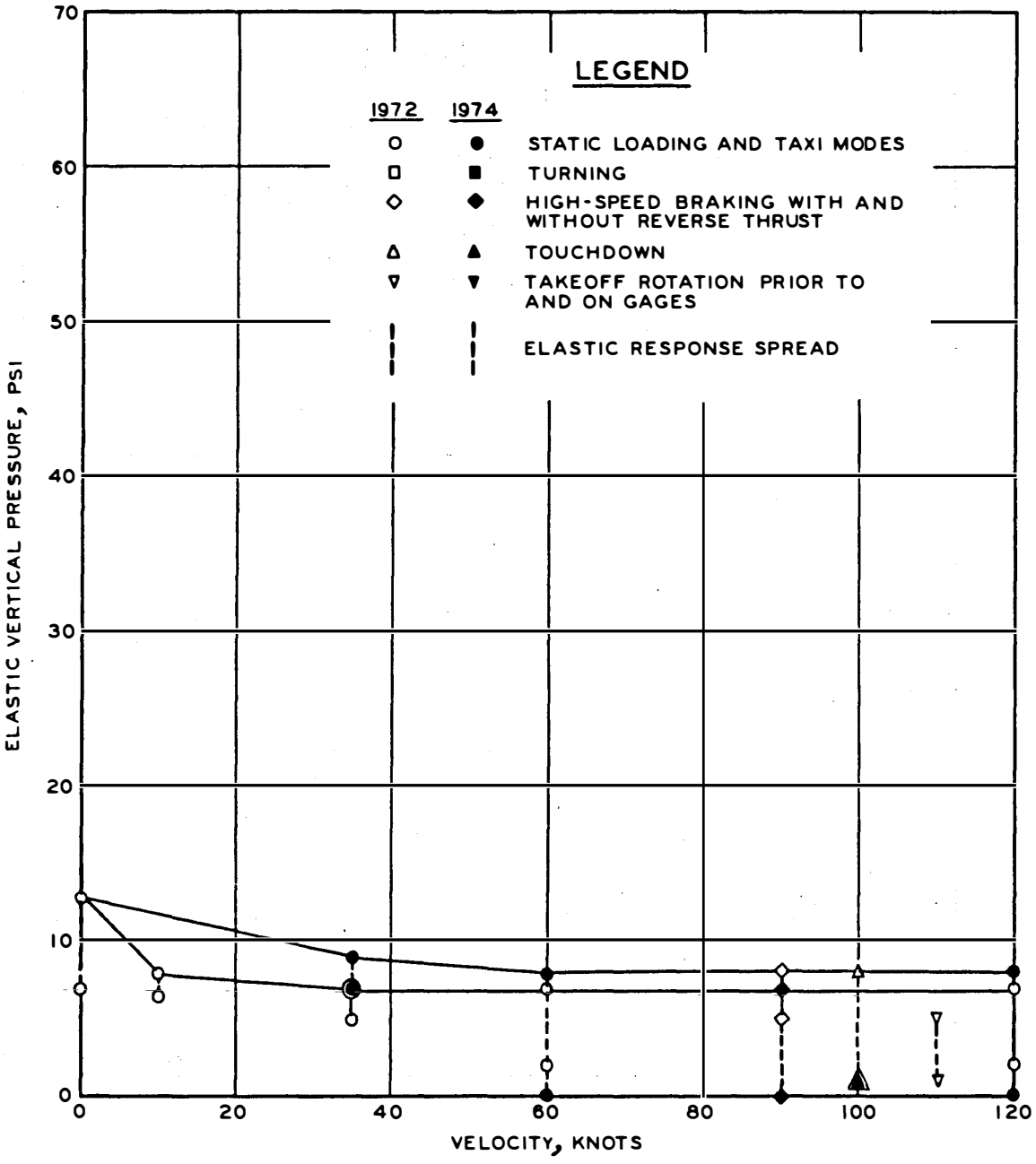

Figure 105. Maximum vertical elastic pressure versus velocity, flexible, row 1, 30 in., B-727

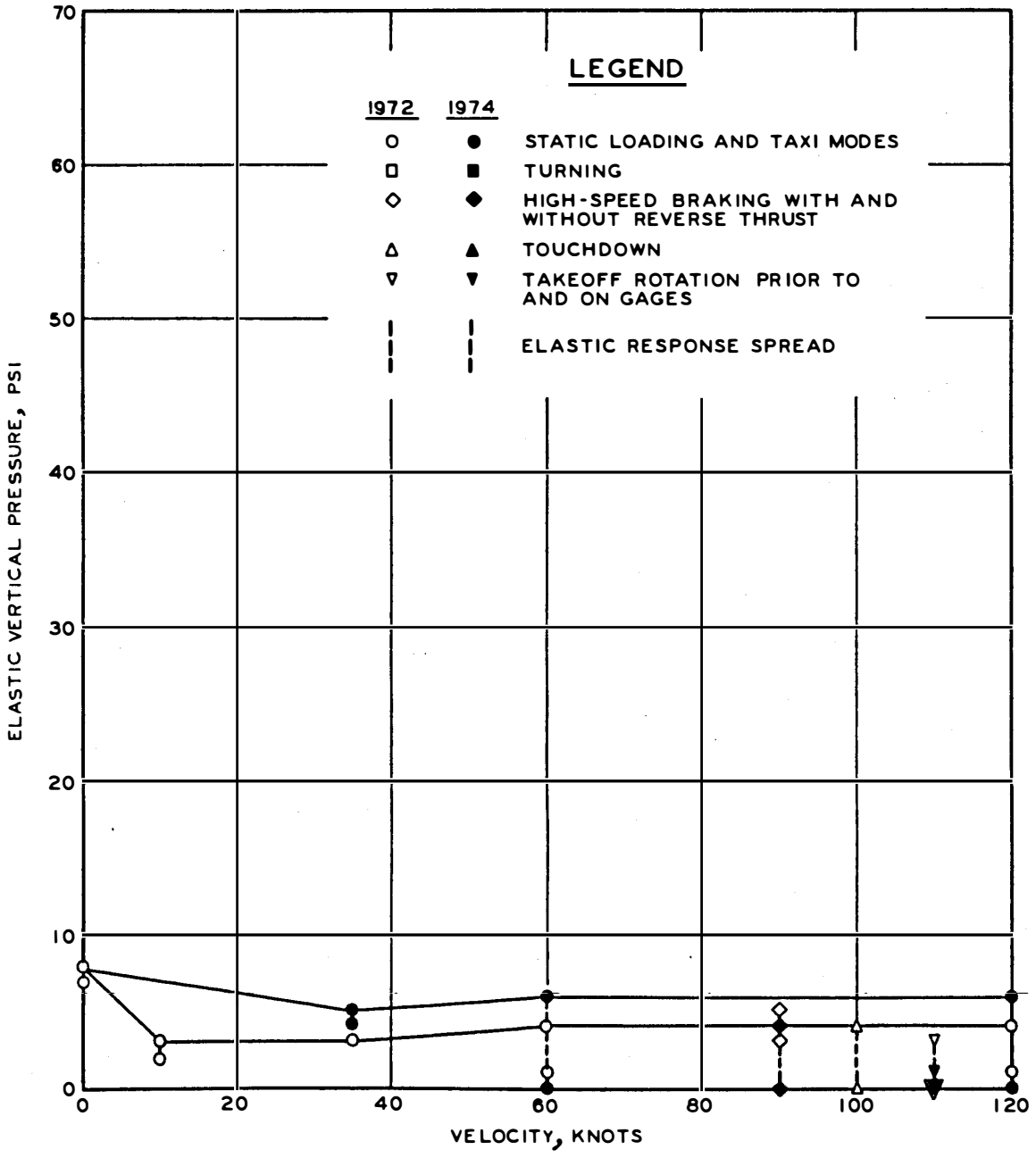

Figure 106. Maximum vertical elastic pressure versus velocity, flexible, row 1, 39 in., B-727

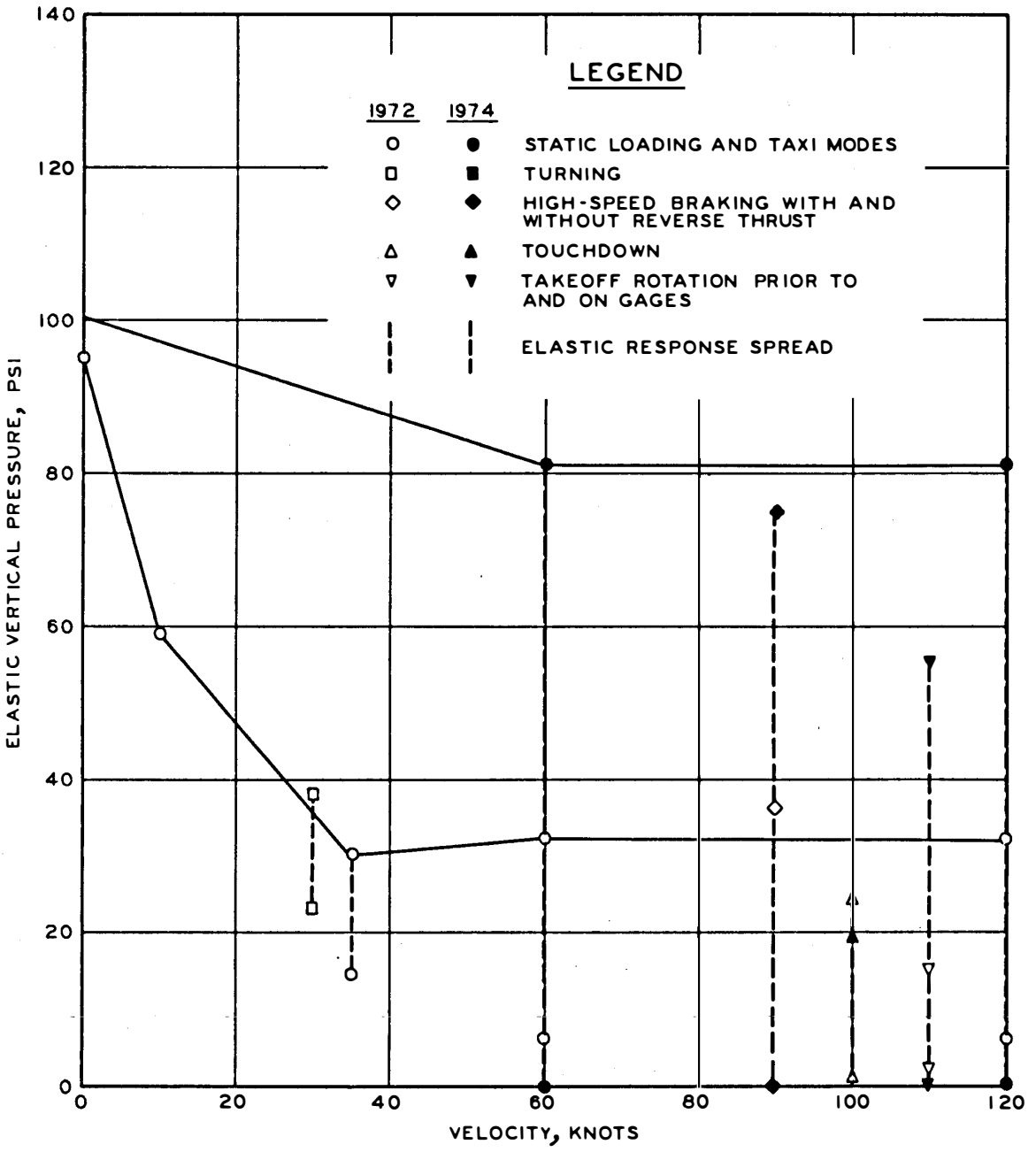

Figure 107. Maximum vertical elastic pressure versus velocity, flexible, row 2, 3 in., B-727

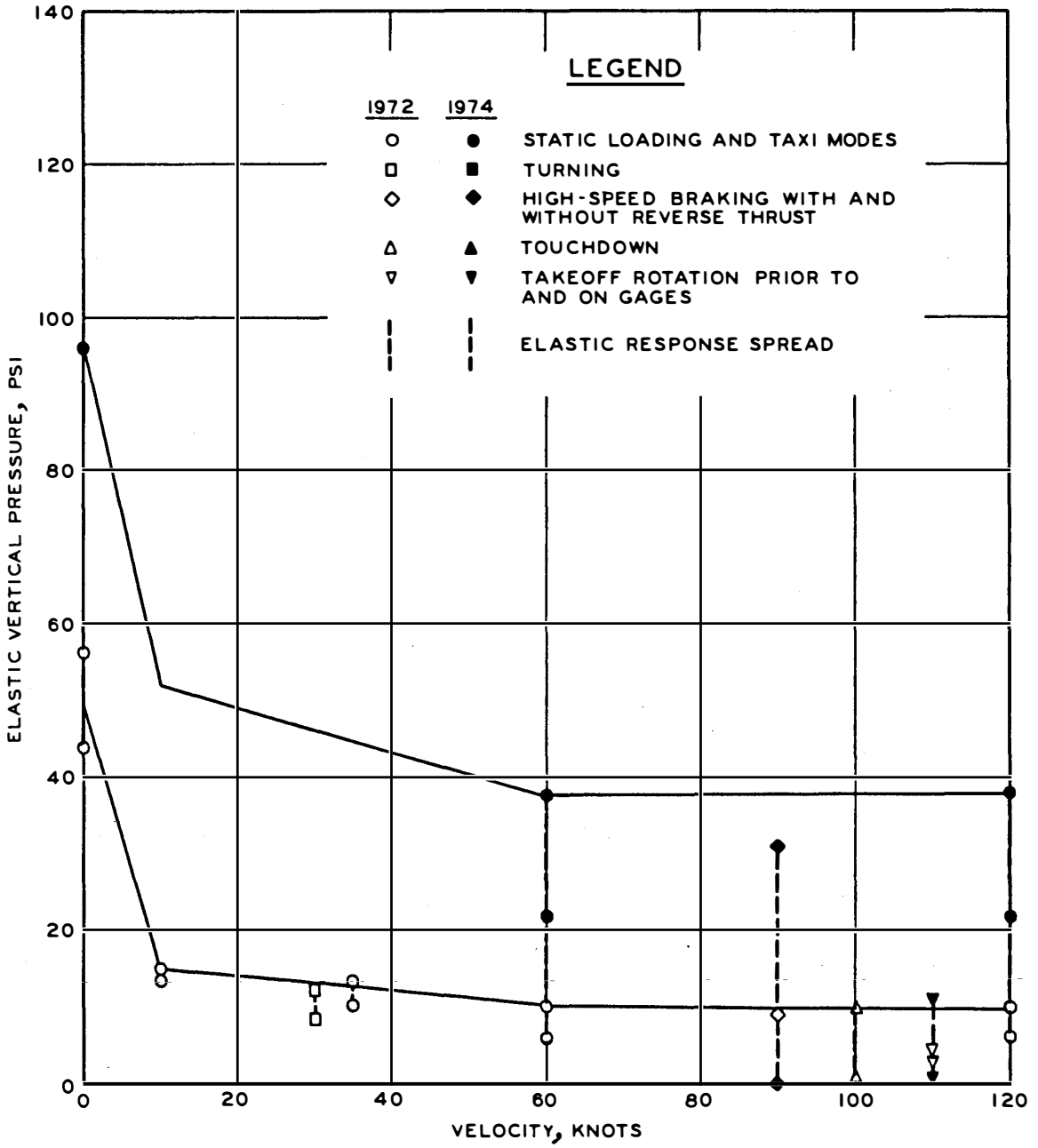

Figure 108. Maximum vertical elastic pressure versus velocity, flexible, row 2, 9 in., B-727

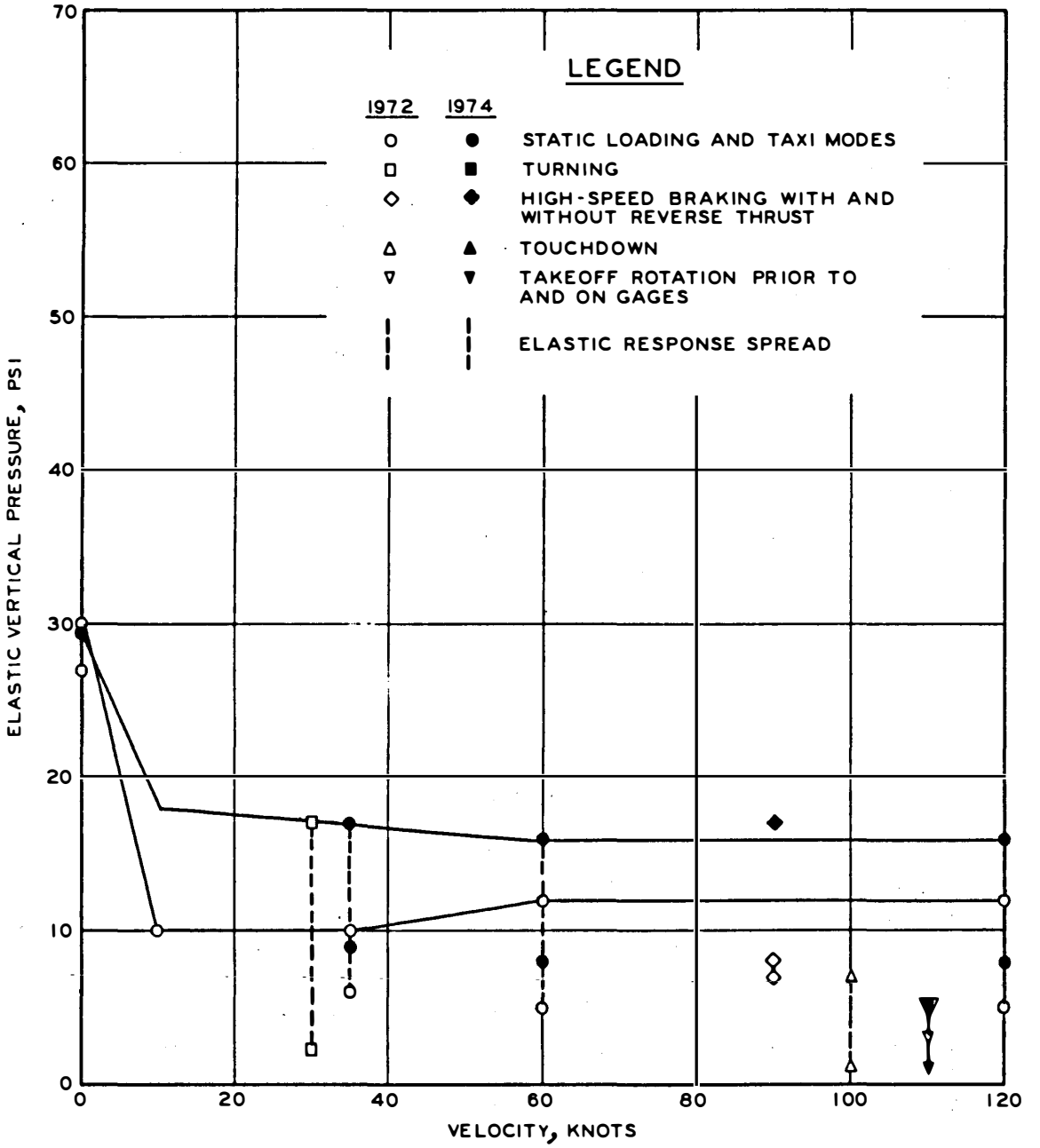

Figure 109. Maximum vertical elastic pressure versus velocity, flexible, row 2, 18 in., B-727

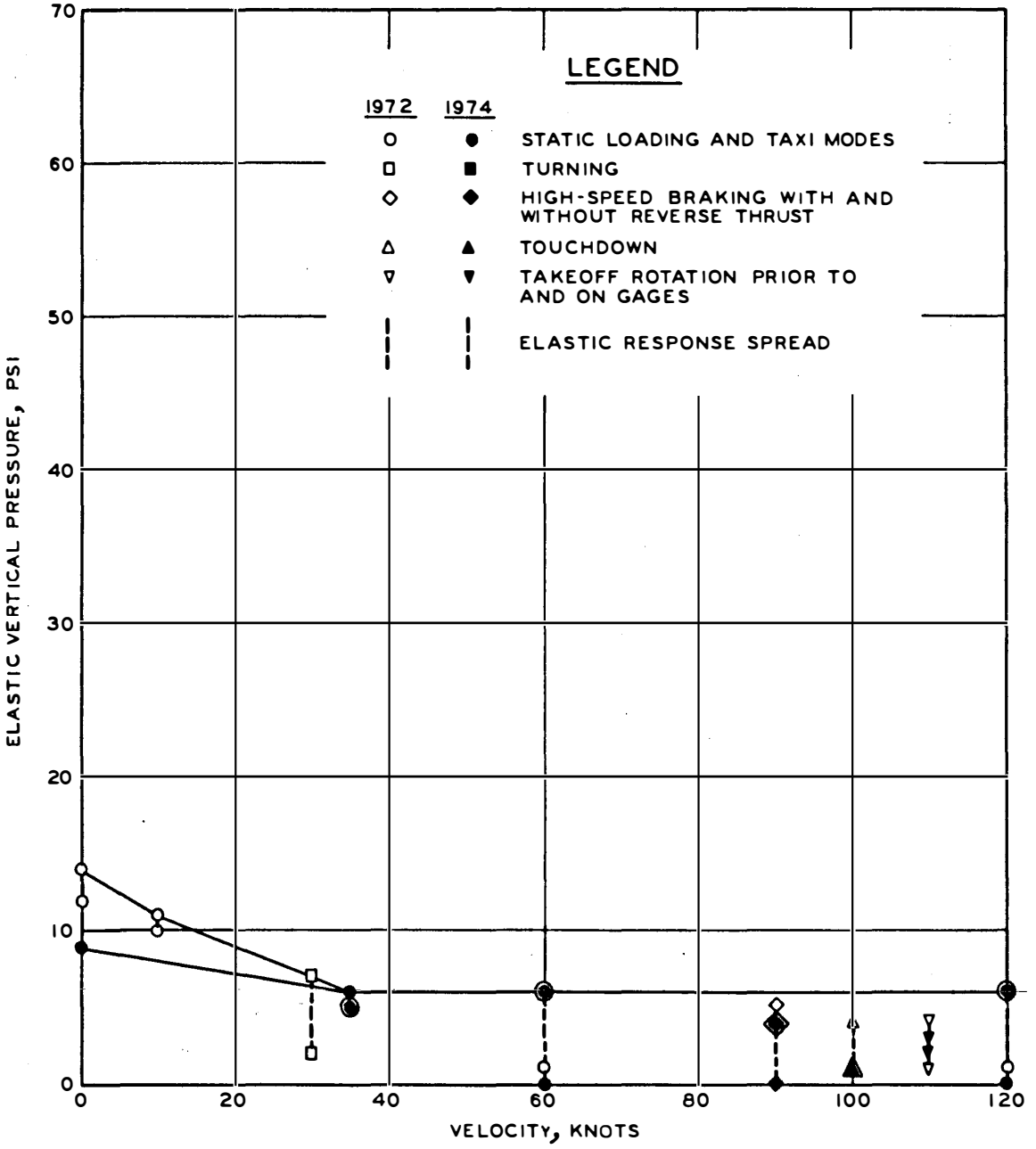

Figure 110. Maximum vertical elastic pressure versus velocity, flexible, row 2, 30 in., B-727

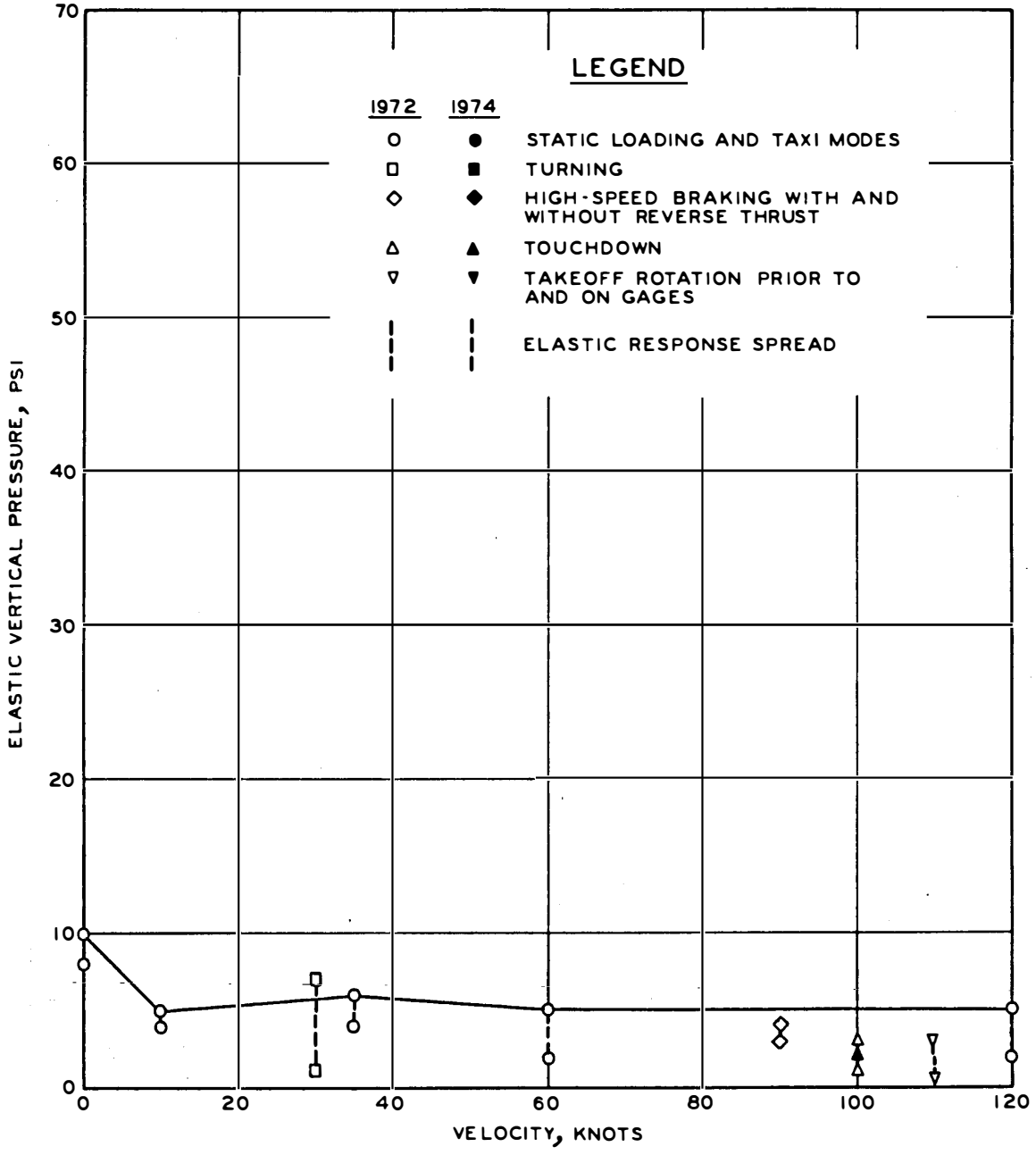

Figure 111. Maximum vertical elastic pressure versus velocity, flexible, row 2, 39 in., B-727

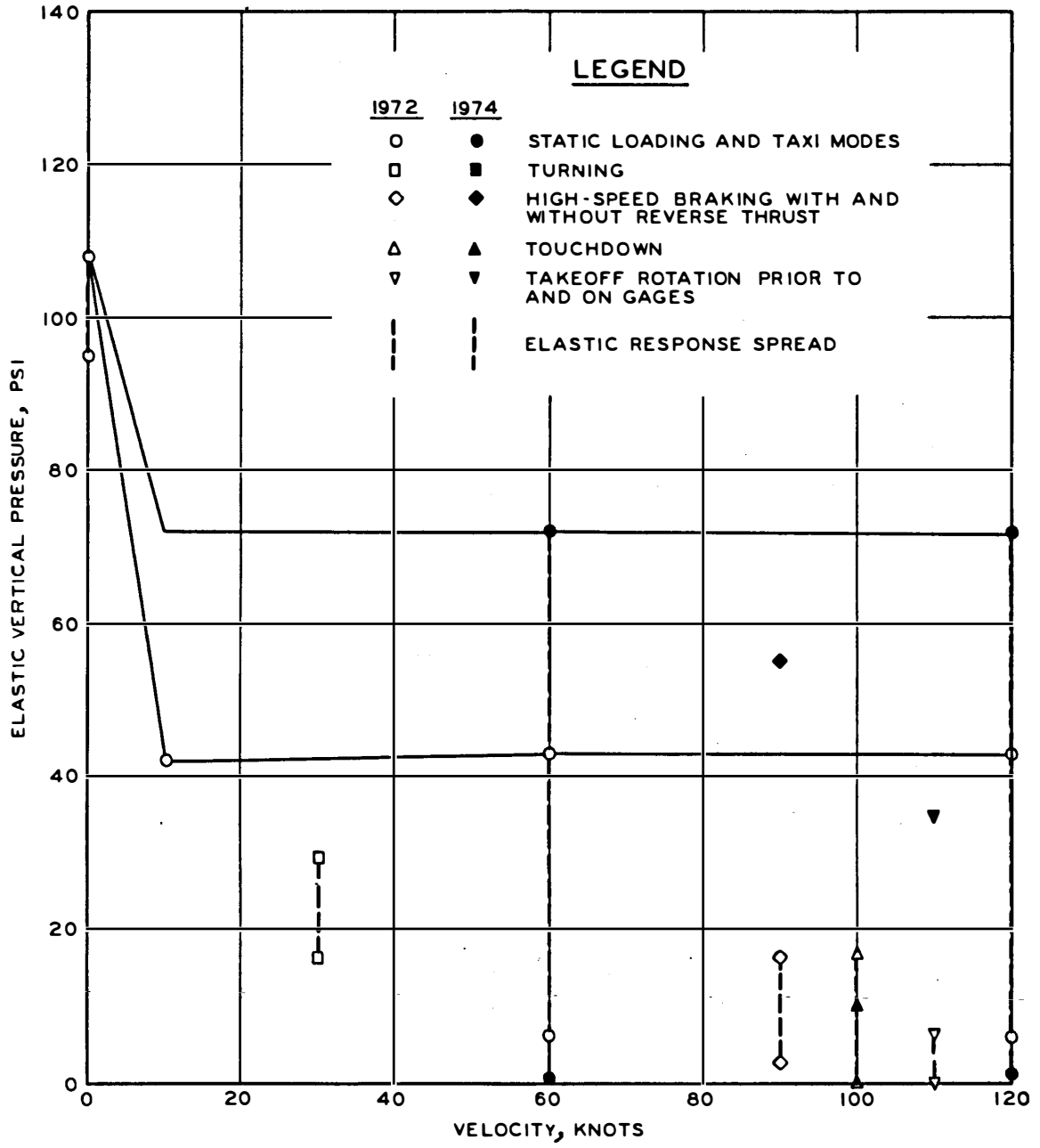

Figure 112. Maximum vertical elastic pressure versus velocity, flexible, row 3, 3 in., B-727

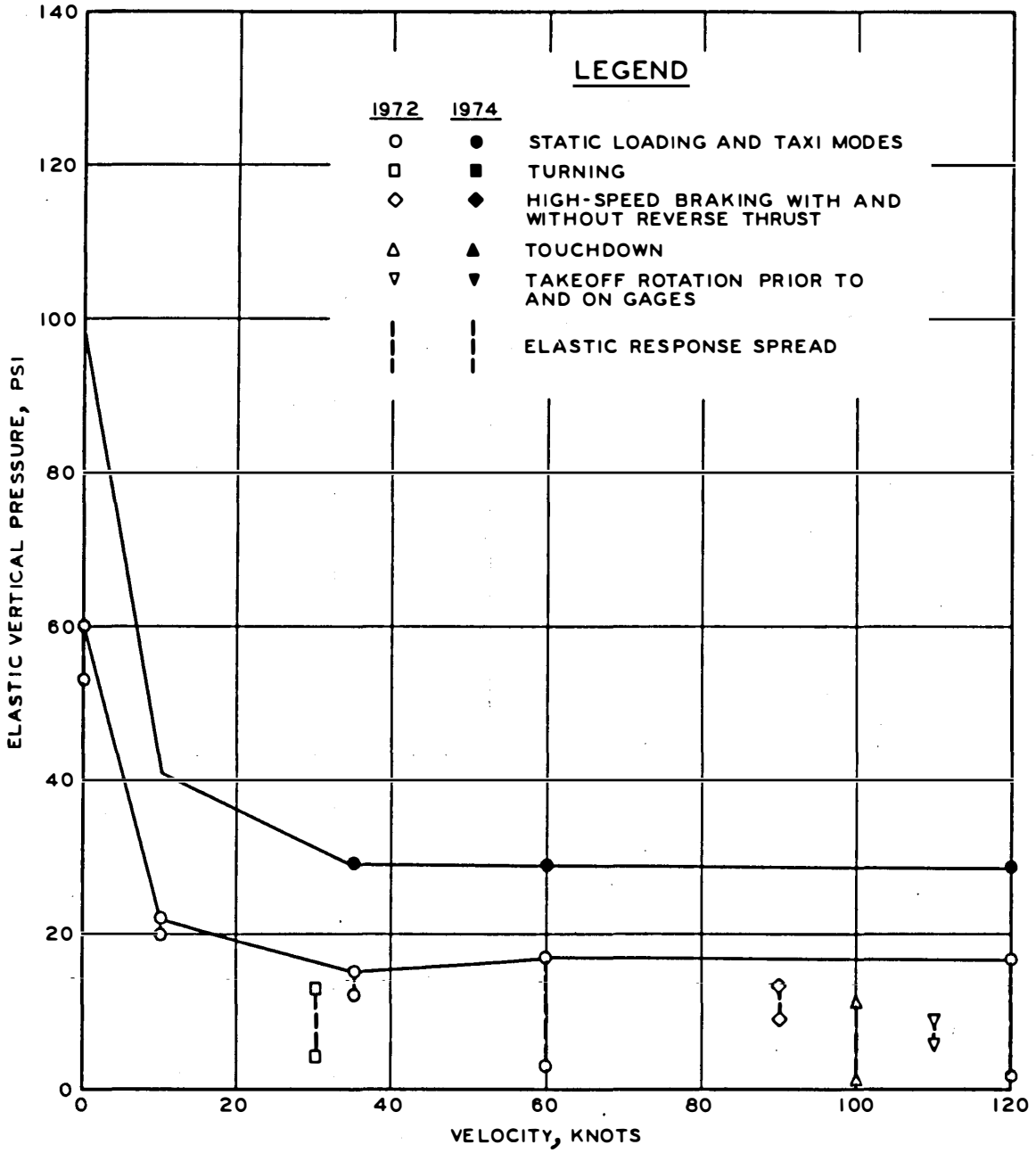

Figure 113. Maximum vertical elastic pressure versus velocity, flexible, row 3, 9 in., B-727

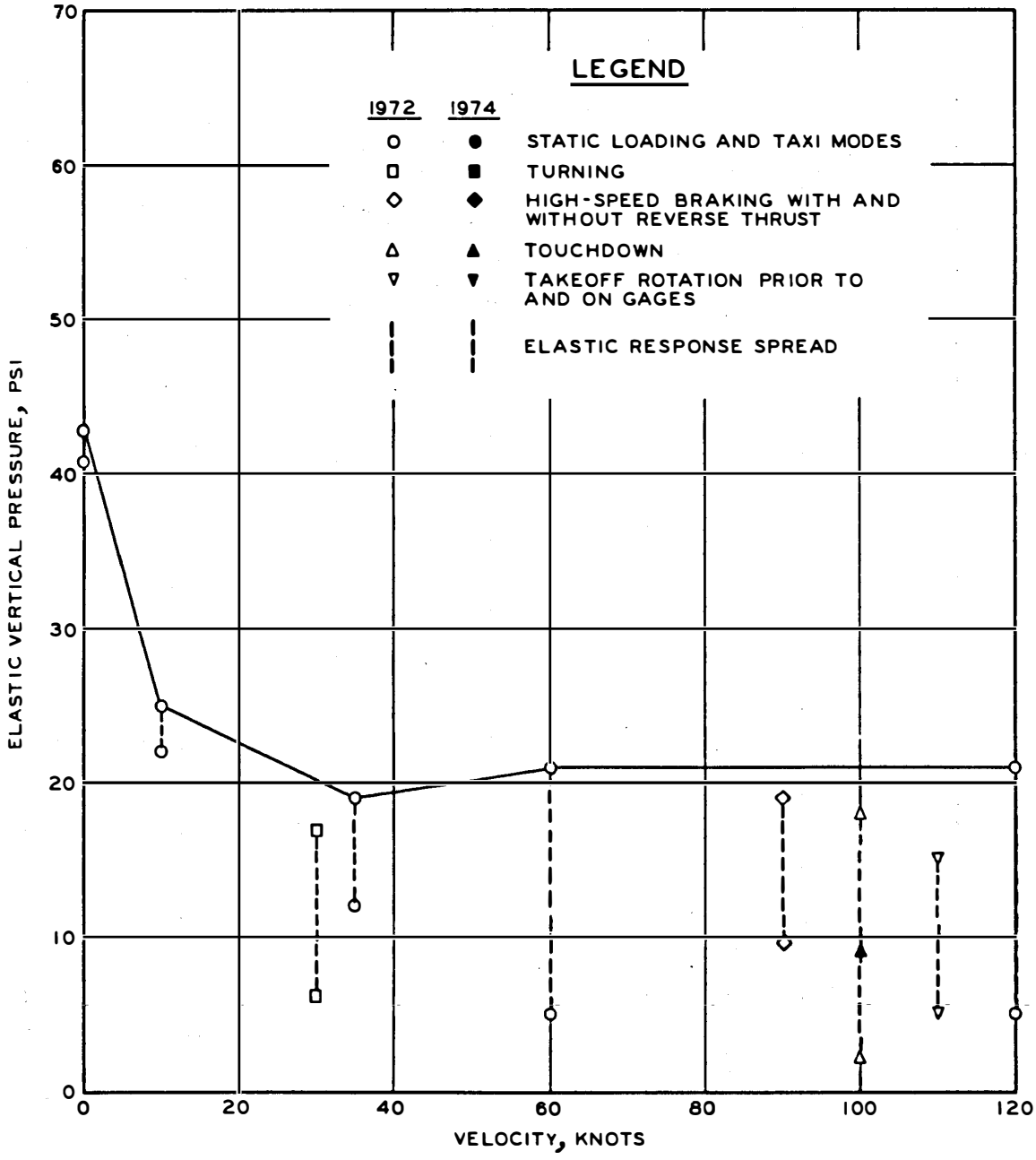

Figure 114. Maximum vertical elastic pressure versus velocity, flexible, row 3, 18 in., B-727

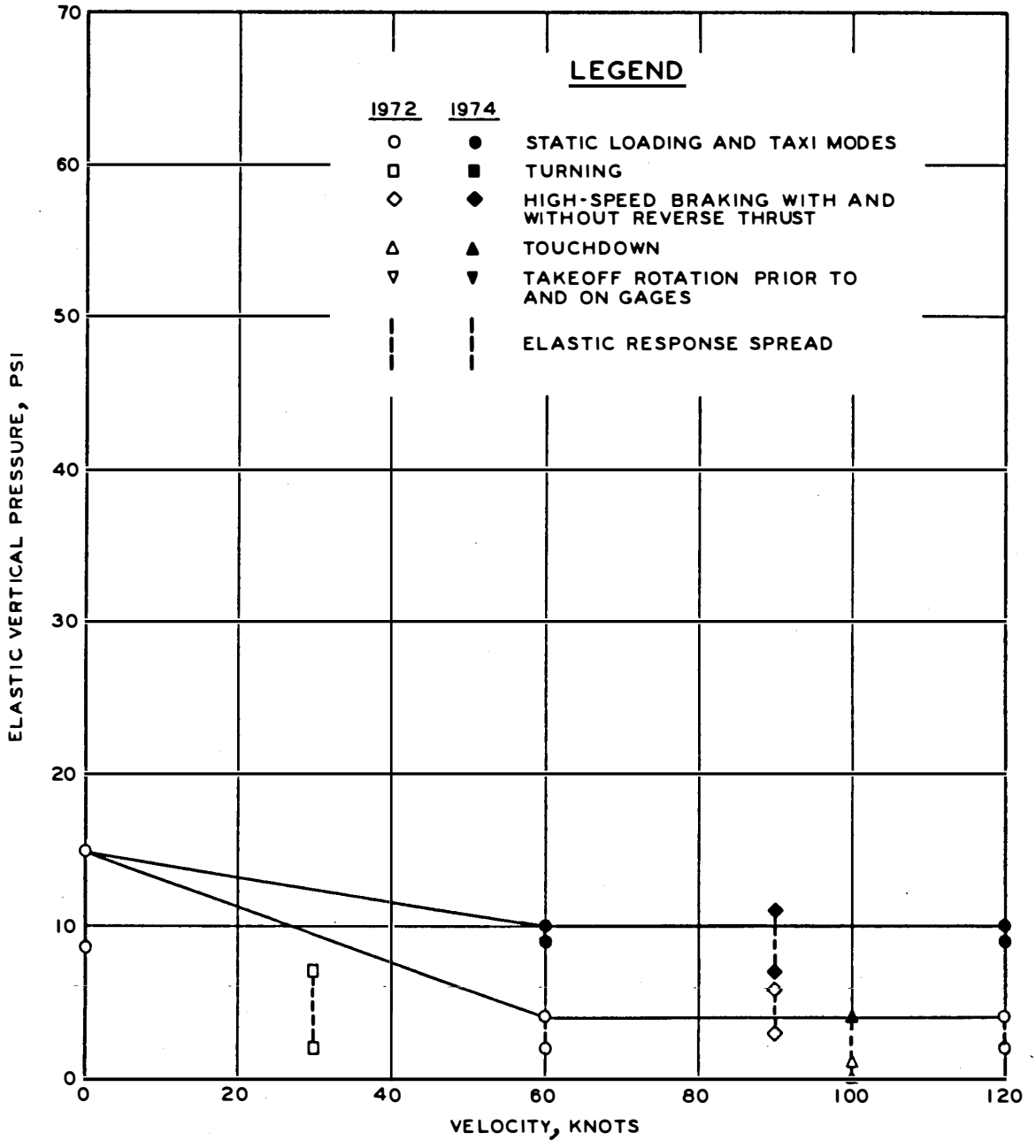

Figure 115. Maximum vertical elastic pressure versus velocity, flexible, row 3, 30 in., B-727

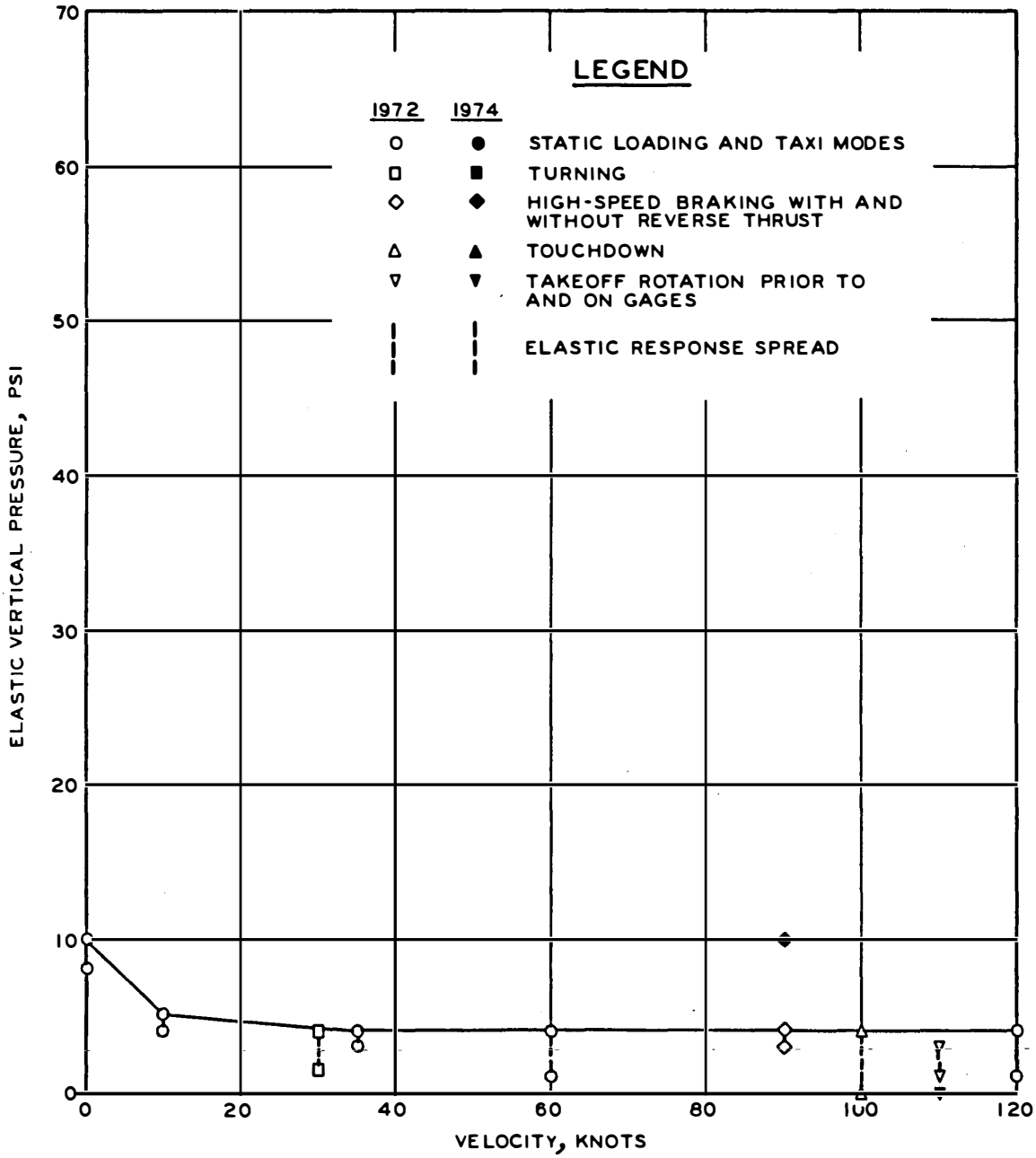

Figure 116. Maximum vertical elastic pressure versus velocity, flexible, row 3, 39 in., B-727

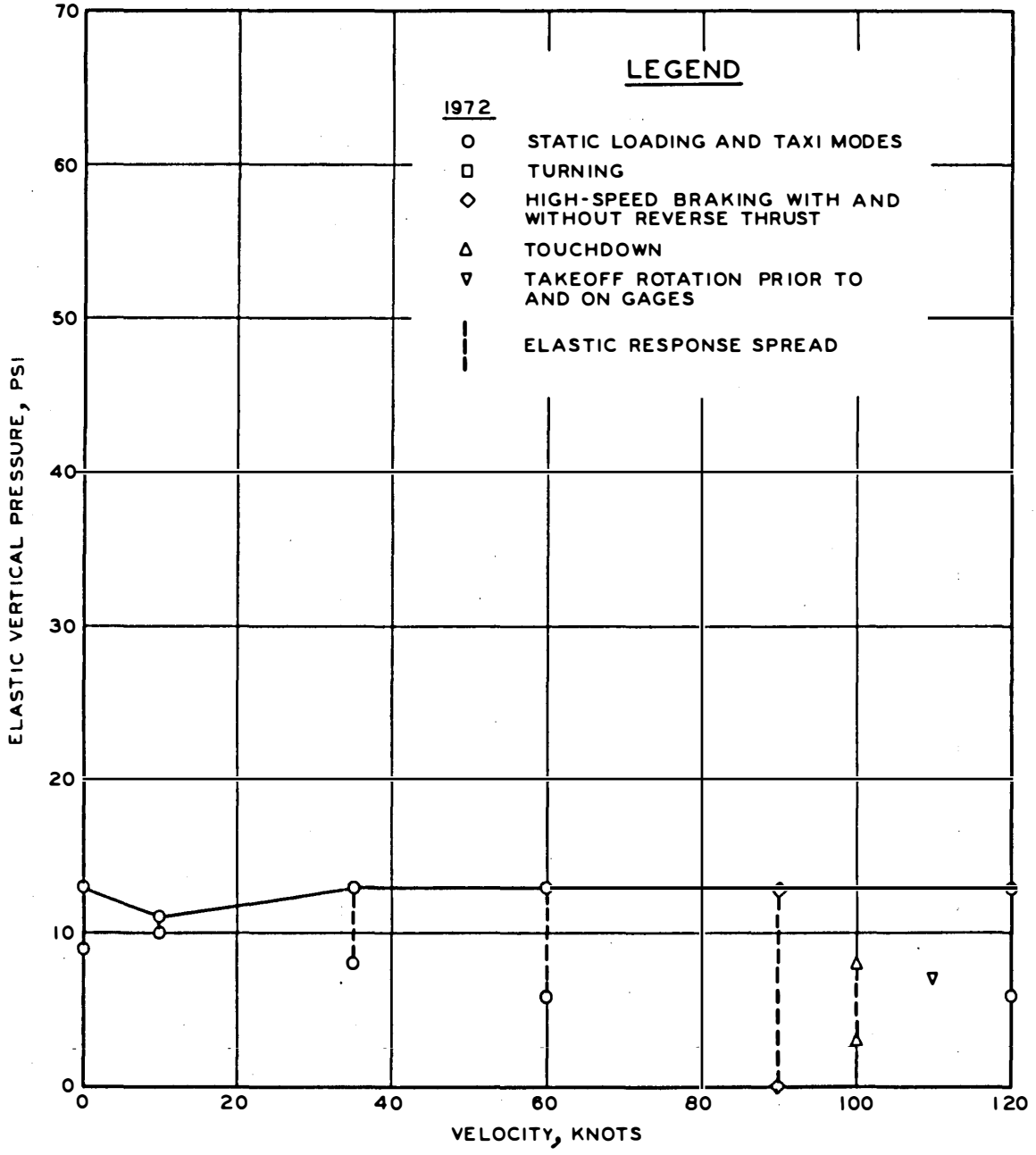

Figure 117. Maximum vertical elastic pressure versus velocity, rigid, row 1, 7 in., B-727

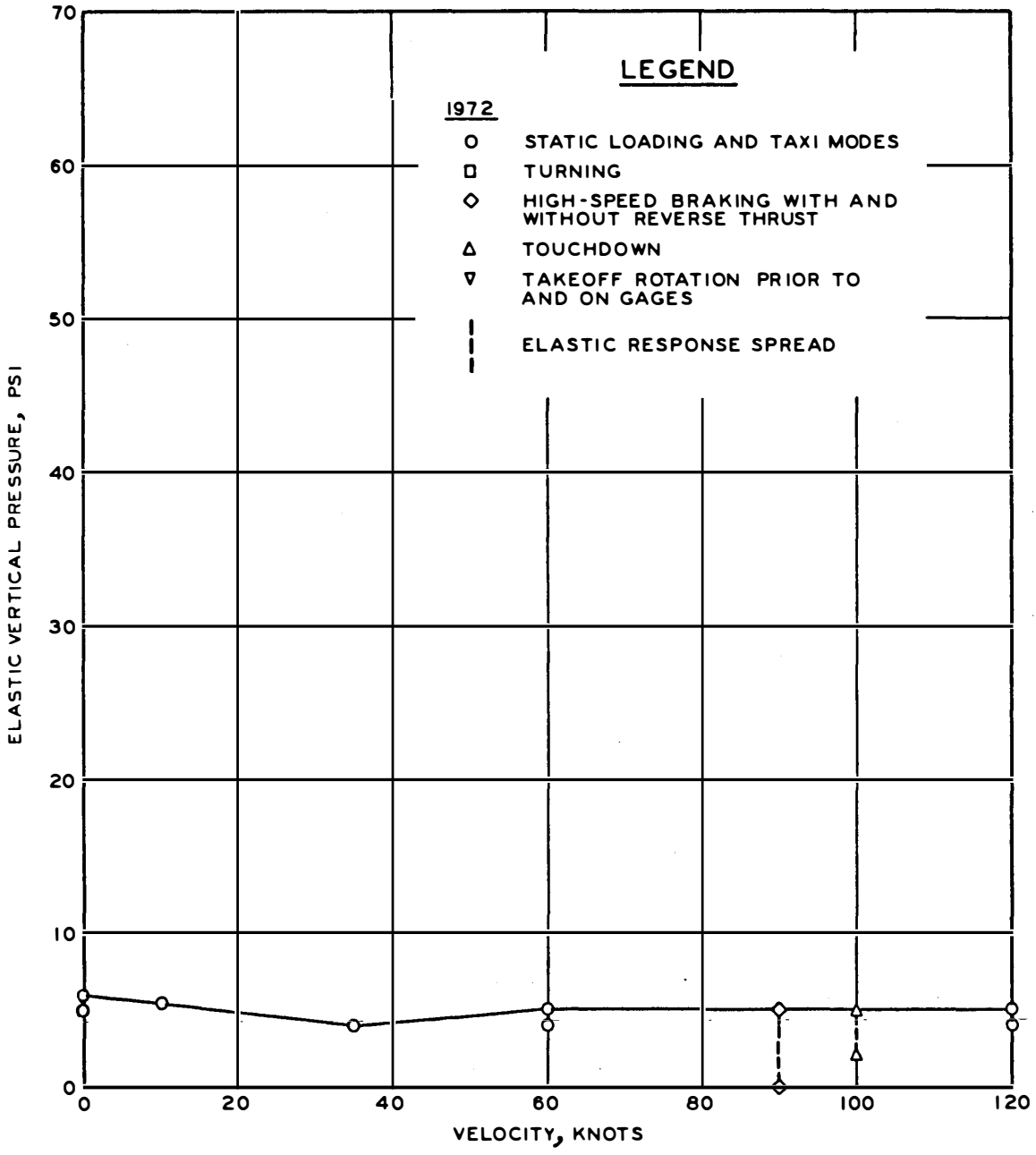

Figure 118. Maximum vertical elastic pressure versus velocity, rigid, row 1, 15 in., B-727

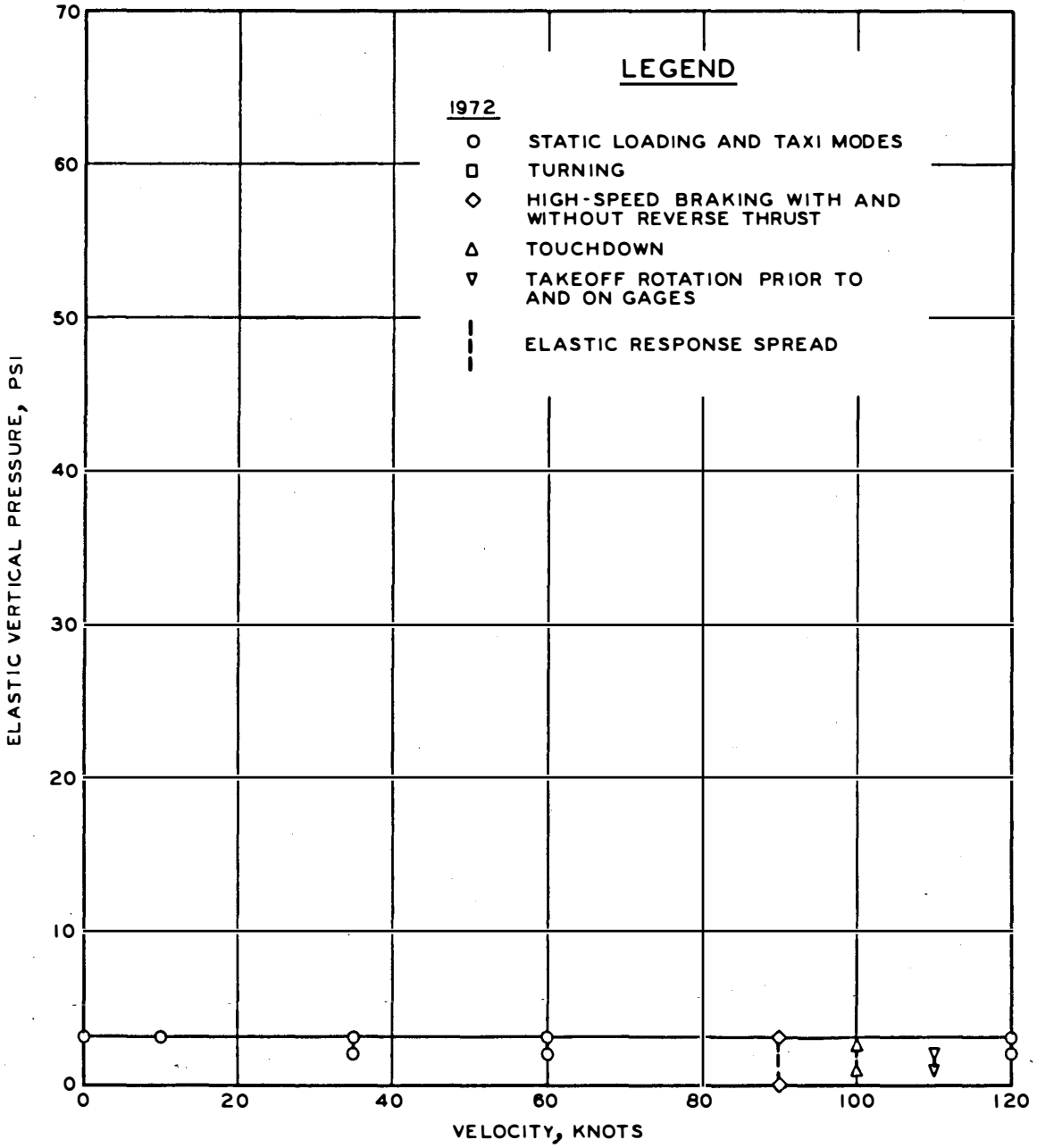

Figure 119. Maximum vertical elastic pressure versus velocity, rigid, row 1, 24 in., B-727

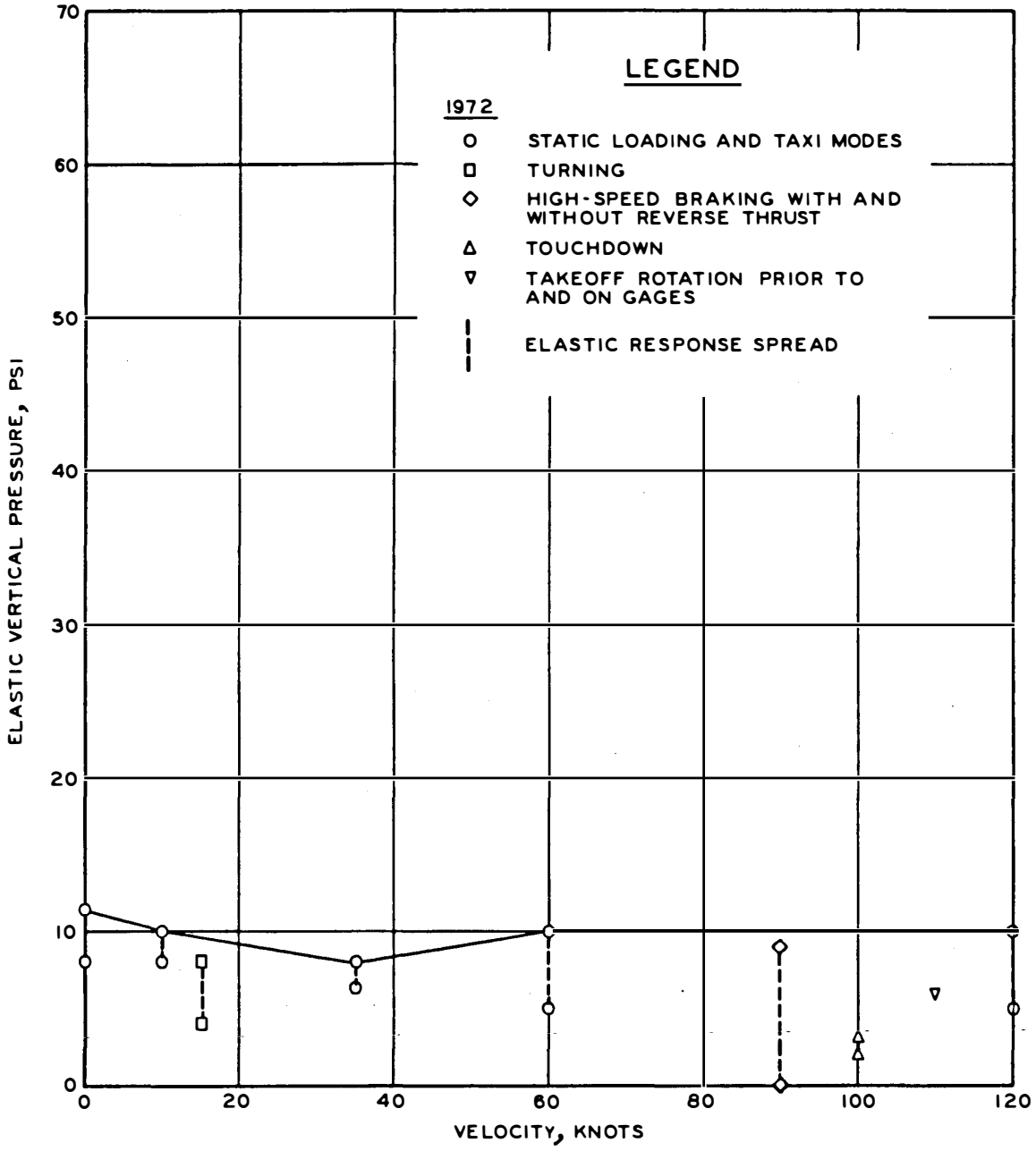

Figure 120. Maximum vertical elastic pressure versus velocity, rigid, row 2, 7 in., B-727

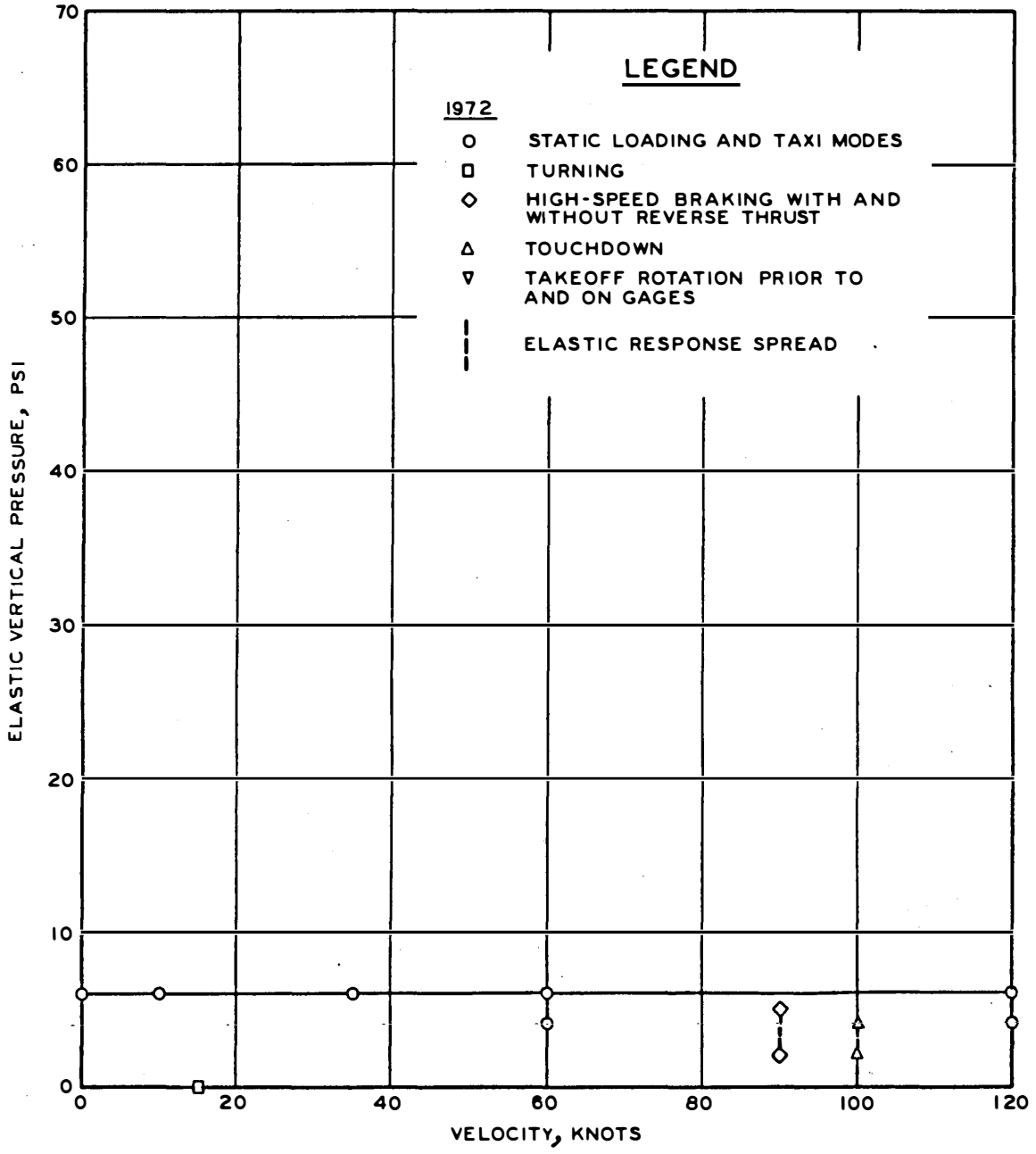

Figure 121. Maximum vertical elastic pressure versus velocity, rigid, row 2, 15 in., B-727

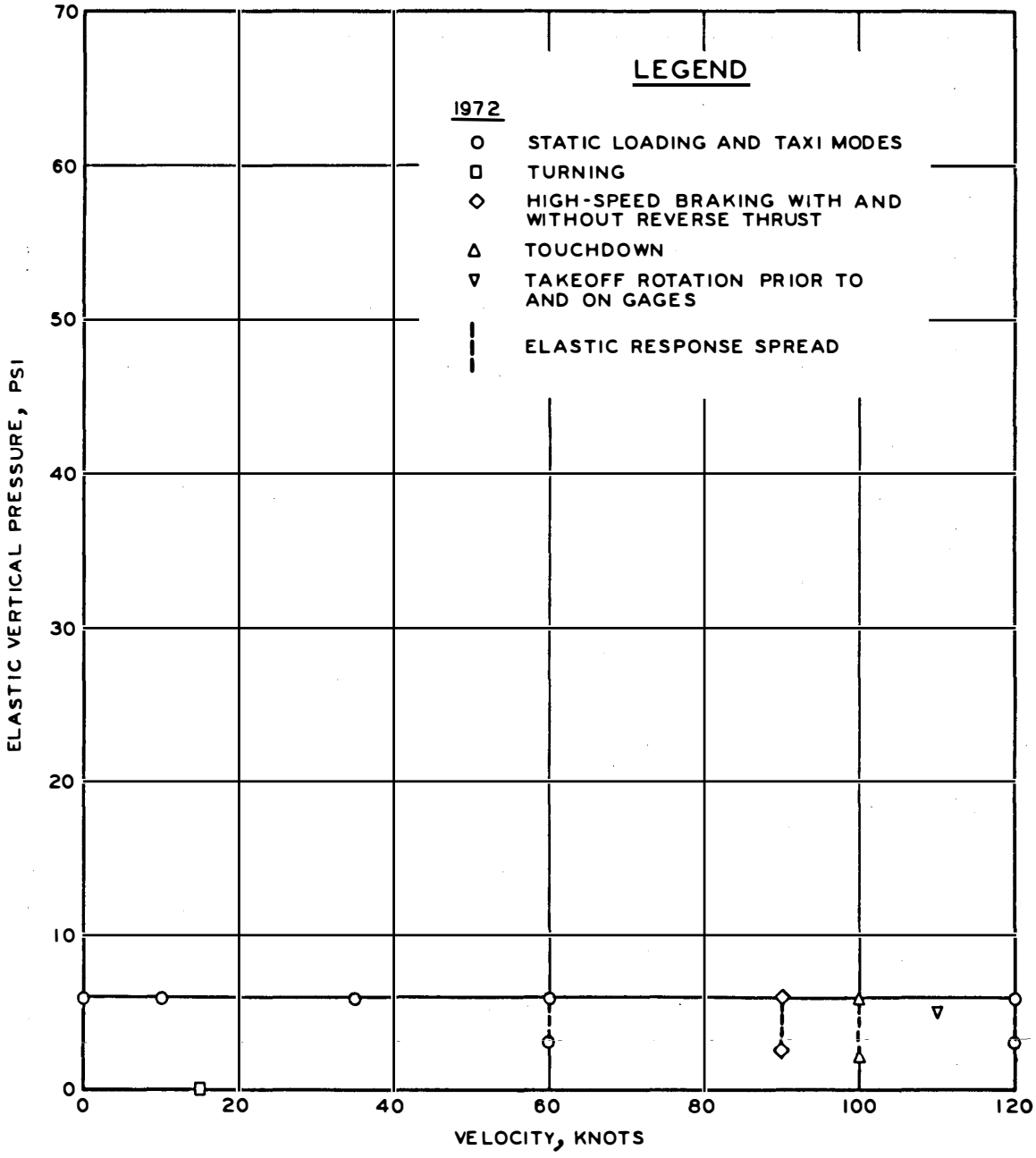

Figure 122. Maximum vertical elastic pressure versus velocity, rigid, row 2, 24 in., B-727

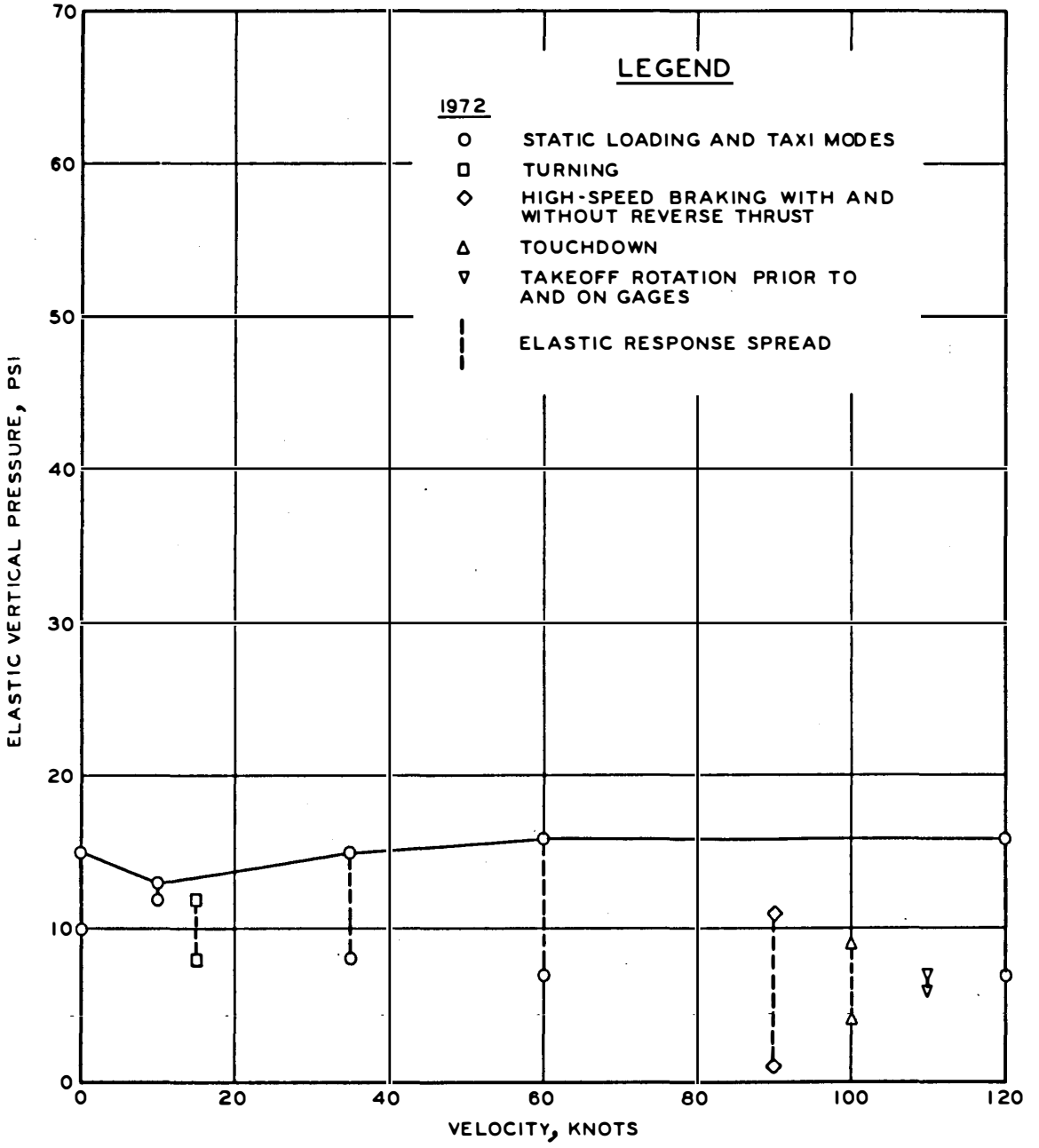

Figure 123. Maximum vertical elastic pressure versus velocity, rigid, row 3, 7 in., B-727

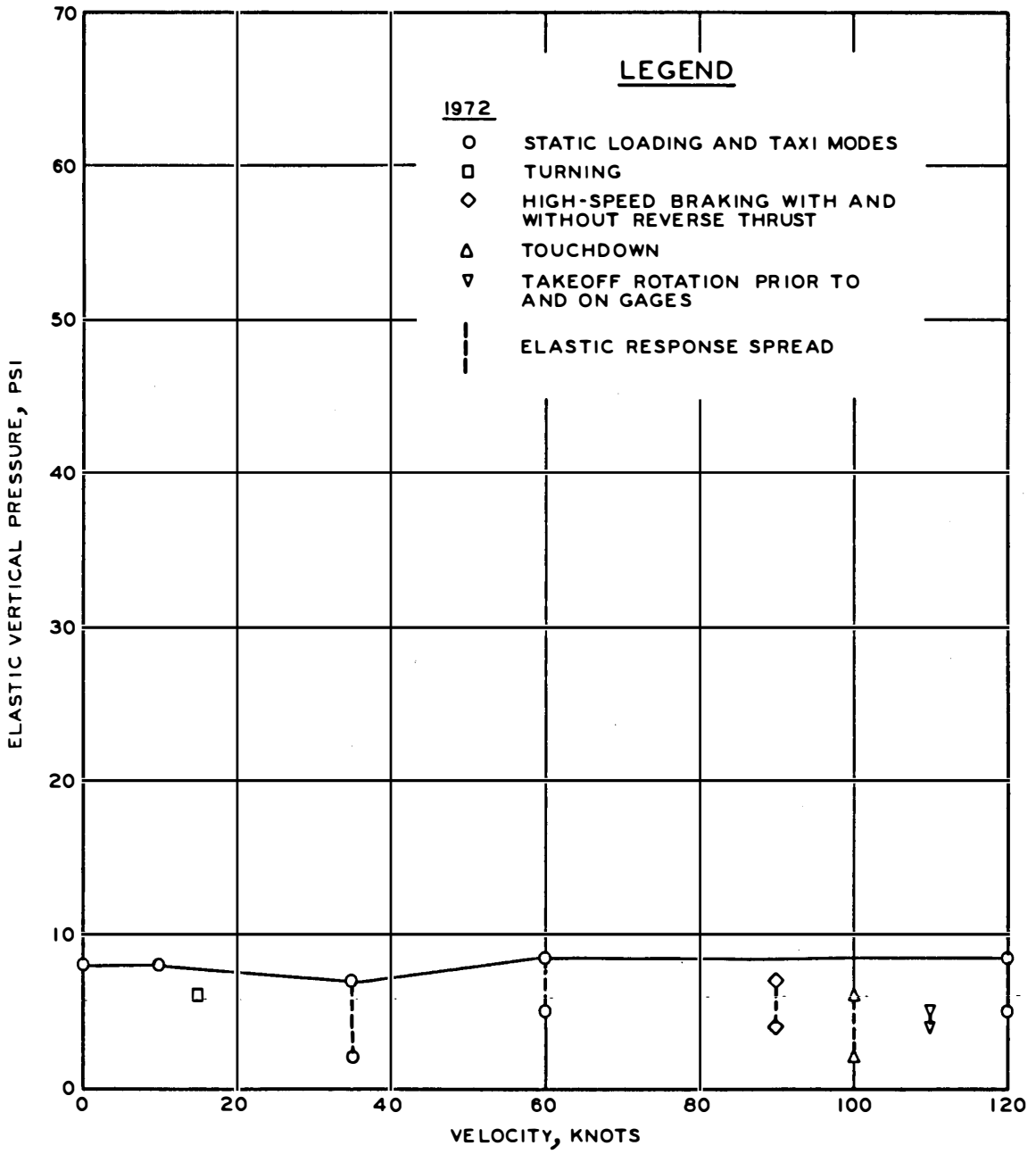

Figure 124. Maximum vertical elastic pressure versus velocity, rigid, row 3, 15 in., B-727

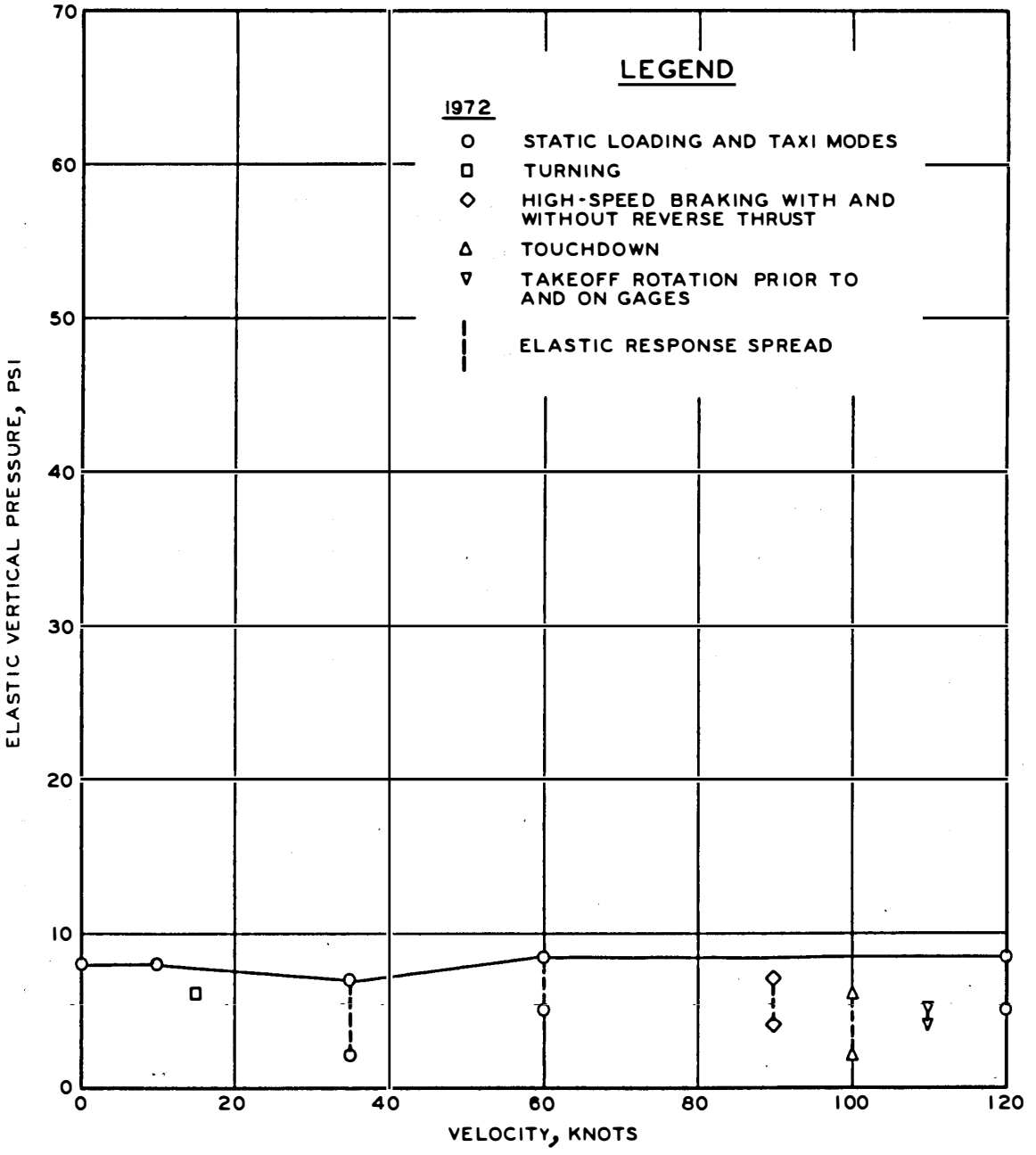

Figure 125. Maximum vertical elastic pressure versus velocity, rigid, row 3, 24 in., B-727

accuracy can be evaluated based on theoretical and other concepts.

Consistency is difficult to separate from accuracy. Several factors that affect the accuracy of an instrument are also factors that determine the consistency of measurements from the instrument. No specific tests were conducted in order to determine the consistency of the instrumentation registrations; therefore, the indications of consistency must be taken from the actual test data. The results to be presented in the following paragraphs are combinations of all the factors determining accuracy and governing field performance that added together dictate the consistency of the behavior of the instruments under actual field use. Also (but probably not the least of these factors) added to the above are the error sources of the complete system of power supply, gage, amplifier, and indicator or recorder.

SE SOIL PRESSURE CELLS

A soil pressure cell constructed of metal or some similar rigid material, and necessarily constructed to obey Hooke's law in its compressibility, can be expected to alter the stress distribution in soil, resulting in a concentration of stress in the vicinity of the cell in the same manner that a large stone will concentrate stresses in a sand or plastic soil mass. Theoretically, a very thin compressible (but not flexible) plate will distort the stress pattern in the soil very slightly. This fact suggests a cylindrical cell that is thin in proportion to its diameter. The probable existence of anomalous local stress variations, due to a lack of complete homogeneity in the soil, indicates the need for a large pressure response area in a pressure cell. The concentration of stress by a pressure cell would be expected to depend greatly on its compressibility; therefore, if its compressibility were less than that of the soil, indicated pressures would probably be higher than true stresses. In reverse, if the cell compressibility were higher than that of the soil, arching action (at least in granular soils) might be expected to withhold an appreciable portion of the normal stress from the cell. As a result, indicated pressures would probably be lower than true stresses.

A few factors affecting the accuracy of all soil pressure cells under field conditions are error parameters of effects such as eccentric loading, unmatching compressibility, and the technique of cell installation. The modulus of the soil in which the cell is embedded may be either larger or smaller than the modulus of the cell, thereby causing a distortion of the stress pattern in the immediate vicinity of the pressure cell and possibly causing a source of error. Another limitation of soil pressure cells is the stability with time, which is determined by cell design and craftsmanship. Such possible changes are resistance changes in the gage wires, imperfect temperature compensation, and variations of the elastic constants of the cell material.

Performance parameters or sources of error associated with the recording devices or other indicating means for the gages and cells should also be considered in their effect on accuracy. These associated equipment effects influence both the degree of accuracy and the consistency and reproducibility of instrument indications.

Small errors can be introduced in direct reading equipment from variations in the equipment and also from human ability in precisely reading the indicators. In the recording equipment, small errors enter from variations in the recorders and in the associated signal amplifiers, which have the function of increasing the magnitude of the signal from an instrument circuit without distorting or warping the signal.

The primary performance parameters to be considered in all types of indicators and recording equipment are frequency response, relative phase shift of input components of different frequency, sensitivity, and stability. Such factors as variable sensitivity, shifting reference levels, temperature drift, and sensitivity to vibration or noise (disturbances which are carried along with the desired information) may cause problems. The degree of sensitivity, especially with respect to vibration or noise, decreases with increases in amplification required for the instrument response signal; therefore, the accuracy and consistency decrease with increases in amplification and consequently noise level.

The development and laboratory tests of SE soil pressure cells

are fully described in Reference 11. SE soil pressure cells are small, thin, symmetrical, wafer-shaped gages having an aspect ratio greater than 5 and a diameter-to-deflection ratio greater than 2000. Laboratory tests showed that the gages are suitable for short-term static and dynamic measurements and that they have a stress range of 1 to 2000 psi. The linear range exceeds 1800 psi. The gages have very low acceleration sensitivity and hysteresis and have excellent dynamic response of rise time less than 6 μsec and undamped natural frequency greater than 40 kHz.

SE soil pressure cell performance for the NAFEC dynamic load tests will have to be judged primarily by the static load test results. The gages showed generally good responses with average consistency about ±1 psi.

WES DEFLECTION GAGES

Most of the discussion of theory and error parameters that was previously discussed in regard to the soil pressure cells is also applicable to the WES deflection gages and their effect on material behavior by being present. A major consideration is whether the gage movements are actually representative of the body at the point of measurement. The gage movements are considered to be representative of the material mass if careful installation methods are used. Linear variable differential transformers (LVDT's) are mounted within the WES deflection gage housings. An indication of accuracy must be based on the LVDT specifications and laboratory calibration tests. Also, the field performance and factors in the field affecting the gage must be considered. Distortions in the material caused by the gage should be limited to a small area around the gage and should not affect movement a few feet or more below the gage, which is the movement that the gage is actually measuring (between the gage plate and the reference flange at a deep depth).

Factors that could cause errors in the field are improper installation of the gage and assembly and changes of stability with time. Resistance changes in the gage wire with time, temperature effects, or variations of the elastic constants of the gage and assembly materials with time could result in error parameters.

Laboratory tests and calibrations of the LVDT elements used in the WES deflection gages have yielded a resolution of 0.0002 in. with a digital voltmeter as the displacement monitor, a repeatability of ±0.001 in., and an accuracy of ±0.002 in. or better, considering the possible error parameters that could exist in the laboratory calibration tests including those of the associated equipment.

Consistency of these gages was reported in Ledbetter et al.[8] The gages performed well for both static and slowly moving loads. The degree of consistency varied from ±0.001 in. for the same gage and duplicate gages under single-wheel 30,000-lb test loads to ±0.002 in. for the same and duplicate gages under 12-wheel 30,000-lb-per-wheel test loads. This degree of consistency decreased slightly with increases in load and number of wheels. Similar results are believed to have existed in the NAFEC static and dynamic load tests based on the indicated static load results.

BISON COILS

Consistency of Bison coils has been found in laboratory tests to be better than ±0.0001 in. However, all of the previous discussion concerning field condition effects is also applicable to these gages. The NAFEC static and dynamic load test results generally showed consistency of about ±0.001 in. with resolution much better. The Bison coils performed satisfactorily.

LOSS OF INSTRUMENTS

The complete loss of instrumentation was negligible, and only a few gages had unusable responses. Prior to the 1972 tests on the flexible pavement test site, two SE soil pressure cells at the 30-in. depth on gage row 3 stopped responding. This loss may have been due to moisture entering the housing or the sensing elements losing bond. During the dynamic load tests of 1972, another SE soil pressure cell stopped responding at the 30-in. depth of gage row 1 in the flexible pavement test site. The probable cause for this loss is believed to be the same as that for the previous soil pressure cells. In the 1972 flexible pavement tests, due to extraneous noise as previously described under "Test Results," Bison coil responses for the 30- to 39-in. and 39- to 51-in.

depths of gage row 3 during dynamic load tests were not usable, but they were usable in the 1974 tests. Due to extraneous noise in 1972, the experimental induction probes were not usable. Between the 1972 and 1974 tests, 10 more SE soil pressure cells were lost.

For the rigid pavement tests, one WES deflection gage became erratic and not usable during the dynamic load tests. This loss could have been caused by a faulty connection or by moisture in the housing. The inductive probes were not usable in the rigid pavement tests due to the extraneous noise.

CONCLUSIONS

Based on the measurements of the nonconditioned (page 61) flexible and rigid pavement structure responses under aircraft static and dynamic load tests, the following conclusions are believed justified.

INSTRUMENTATION

In general, all instrumentation performed satisfactorily.

INTERPRETATION OF DATA

a. Elastic (including viscoelastic) and inelastic phases of material behavior were found acting in the displacements of both flexible and rigid pavements.

b. In order to be able to fully interpret and analyze the nonconditioned (page 61) pavement structure response data, the elastic and inelastic phases had to be separated (they occur simultaneously) and treated independently in the investigation of static and dynamic load test results. Instrument responses could not be completely analyzed unless the inelastic behavior was fully recognized and utilized.

c. Two different types of displacement responses were identified as acting in both flexible and rigid pavements. The two types are total pavement structure response as assumed to be referenced to infinity (inertial reference) and individual pavement structure element response referenced internally to each element (noninertial reference). Each type of response exhibited both elastic and inelastic material behavioral phases.

d. Bow waves in front of the wheels and elastic vertical expansions behind and adjacent to the wheels were found to occur within the structural elements (noninertial reference) of both pavement structures under moving aircraft operations.

e. The three different types of displacement and motion measuring instruments (WES deflection gages, Bison coils, and velocity gages) were compatible and complemented each other in their indications of pavement structure responses.

f. The vertical pressure data for both flexible and rigid pavements were found to be totally recovered, elastic (corresponding to the elastic phase of behavior), upon removal or passage of a load. No residual pressures appeared to be acting; therefore, the inelastic behavior did not seem to induce residual vertical pressures. The pressure cells

appeared to be carried with or ride within the pulsating structures.

TEST RESULTS

a. B-727 aircraft dynamic load tests in 1972 (cold weather) and 1974 (warm weather) on the nonconditioned (page 61) flexible pavement structure and in 1972 on the nonconditioned rigid pavement structure at NAFEC showed that no basic aircraft ground operating mode induced pavement responses (elastic plus inelastic) greater than those occurring for static load conditions even though the aircraft dynamic loads were as large as 1.2 times the static load. Elastic response alone generally indicates this also to be true. The pavement surfaces were relatively smooth in the test site areas.

b. However, extrapolation of the test results indicates that for stiff pavement structures, such as the rigid pavement and the flexible pavement in cold weather, unusual conditions of large dynamic loading that could result from rougher surfaces than at NAFEC, holes or bumps, etc., could possibly cause responses larger than those that would occur under static loading. This behavior is possible because of the inelastic behavior being of low magnitude for the stiff pavements and the elastic response being essentially of a constant magnitude with a changing rate of load application. The larger than static load response that could occur should be entirely elastic and should not be detrimental to the pavement structure except by contributing to an increase in elastic fatigue damage.

c. Based upon gradually reduced elastic response but primarily upon reduced inelastic response with high speeds, indications are that thickness can be reduced in the interior of runways.

d. Measured aircraft loads during turns showed that high horizontal loads are applied to the pavement surfaces. Due to the high loads and to prevent excessive deterioration in turn areas, the pavement surface in exit areas of flexible pavement runways should be strengthened or be stronger than the main runway. Airports, such as the Baltimore Friendship International have experienced pavement distress in turn areas (Witczak[12]).

e. Test results showed inelastic behavior to be highly dependent on temperature, rate of load application, and load history (magnitude of load and lateral position of aircraft).

f. Inelastic displacements larger than the elastic displacements were measured within the velocity range of static load to low-speed taxi.

g. Test results showed elastic behavior to be almost constant

for stiff pavement structures (rigid pavements and flexible pavements in cold weather) and the probable viscoelastic effects to be more pronounced at high temperatures in bituminous materials.

h. The flexible pavement structure layer at a depth of 39 to 51 in. slightly responded (less than 10 percent of surface response) to the various modes of aircraft operation. The rigid pavement structure layer at a depth of 15 to 24 in. responded (about 30 percent of surface response) to the various modes of aircraft operation. These were the deepest layers monitored during dynamic load tests for both pavement structures.

i. Elastic and inelastic displacement behavior and response can be accurately mathematically modeled (page 83).

j. The elastic and inelastic displacement behavioral phases directly associate the behavior of WES pavement test sections under simulated aircraft loads and wheel configurations and distributed (nonconditioning, page 61) traffic to actual pavement behavior under actual aircraft operations (NAFEC tests). This connection means that any further investigation of dynamic load effects can probably be conducted on pavement structure test sections of limited size.

k. Inelastic behavior occurred in both the nonconditioned flexible and rigid pavement structures and may possibly be a common characteristic that links or ties together the performance of all pavement types. In fact, it may be the major controlling factor or mechanism for pavement performance and life because it can be the primary movement for static and low-speed operations.

RECOMMENDATIONS

Based on the study of pavement responses to aircraft dynamic loads, the following recommendations are made:

a. A vast amount of valuable data were collected, but an analysis of the data beyond the objectives of this report has not been made. There is a wealth of information to be gained, and the analysis and study of the data and results should be continued. Specific areas of study should be the elastic and inelastic displacement phases with emphasis on further defining and understanding the inelastic behavior and its importance to pavement structure performance.

b. Development of a mathematical model or models of the elastic and inelastic behavioral phases should continue with emphasis on correlating and defining the functions of the constant coefficients for the model presented. These coefficients should be functions of variables such as depth, load, number

of wheels, structure strength, temperature, rate of load application, etc.

c. Constitutive relations based on the measured results for the pavement structures should be investigated.

d. Results pertaining to longitudinal moving wheel displacement basin responses should be investigated with emphasis on developing a mathematical model or models, based on the measured results, for purposes of simulating rolling aircraft wheels on a pavement structure.

If satisfactory results concerning the above items are obtained, a solid foundation should exist upon which to base theoretical models concerning pavement structure design, behavior, and performance under any type of loading conditions.

REFERENCES

1. Wignot, J. E. et al., "Aircraft Dynamic Wheel Load Effects on Airport Pavements," Report No. FAA-RD-70-19, May 1970, Federal Aviation Administration, Washington, D. C.

2. Horn, W. J. and Ledbetter, R. H., "Pavement Response to Aircraft Dynamic Loads; Volume I: Instrumentation Systems and Testing Program," Report No. FAA-RD-74-39-I, June 1975, Federal Aviation Administration, Washington, D. C.

3. Ledbetter, R. H., "Pavement Response to Aircraft Dynamic Loads; Vol III: Compendium," Report No. FAA-RD-74-39-III, November 1975, Federal Aviation Administration, Washington, D. C.

4. Department of Defense, "Unified Soil Classification System for Roads, Airfields, Embankments, and Foundations," Military Standard No. MIL-STD-619B, Jun 1968, Washington, D. C.

5. Federal Aviation Administration, "Airport Pavement Design and Evaluation," Advisory Circular AC 150/5320-6B, May 1974, Washington, D. C.

6. New Jersey State Highway Department, "Standard Specifications for Road and Bridge Construction," 1961, Trenton, N. J.

7. Federal Aviation Administration, "Standards for Specifying Construction of Airports," Advisory Circular AC 150/5370-1A, May 1965, Washington, D. C.

8. Ledbetter, R. H. et al., "Multiple-Wheel Heavy Gear Load Pavement Tests; Presentation and Initial Analysis of Stress-Strain-Deflection and Vibratory Measurements; Instrumentation," Technical Report S-71-17, Vol IIIB, Nov 1971, U. S. Army Engineer Waterways Experiment Station, CE, Vicksburg, Miss.

9. Chou, Y. T. and Ledbetter, R. H., "The Behavior of Flexible Airfield Pavements Under Loads--Theory and Experiments," Miscellaneous Paper S-73-66, Jul 1973, U. S. Army Engineer Waterways Experiment Station, CE, Vicksburg, Miss.

10. Ahlvin, R. G., Chou, Y. T., and Hutchinson, R. L., "The Principle of Superposition in Pavement Analysis," Highway Research Record No. 466, Highway Research Board, Washington, D. C.

11. Ingram, J. K., "Development of a Free-Field Soil Stress Gage for Static and Dynamic Measurements," Technical Report No. 1-814, Feb 1968, U. S. Army Engineer Waterways Experiment Station, CE, Vicksburg, Miss.

12. Witczak, M. W., "A Comparison of Layered Theory Design Approaches to Observed Asphalt Airfield Pavement Performance," Jul 1973, Asphalt Institute, College Park, Md.